# The Role of GFI1 in regulating the metabolism of Acute Myeloid Leukemic cells

Inaugural-Dissertation

for

the doctoral degree

Dr. rer. nat.

from the Faculty of Biology

University of Duisburg-Essen

Germany

Submitted by

Pradeep Kumar Patnana

Born in Cheepurupalli, India

November 2021

The experiments underlying the present work were conducted at the Department of Haematology, at the University Hospital Essen and Medizinische Klinik A, University Hospital Münster.

1. Examiner: Apl. Prof Dr. Cyrus Khandanpour
2. Examiner: Prof. Dr. Ralf Küppers

Chair of the Board of Examiners: Prof. Dr. med. Katharina Fleischhauer

Date of the oral examination: 16.02.2022



**DOI:** 10.17185/duepublico/75456
**URN:** urn:nbn:de:hbz:465-20230731-092419-1

# Table of Contents

## List of Abbreviations

| | | |
|---|---|---|
| 2-DG | - | 2-Deoxy Glucose |
| 3'UTR | - | Three prime Untranslated Region |
| ABL1 | - | Abelson murine leukemia, Tyrosine-protein kinase ABL1 gene |
| ADP | - | Adenosine Diphosphate |
| AF9 | - | Gene MLLT3 (Mixed-Lineage Leukemia Translocated to Chromosome 3 Protein) |
| AKG | - | Alpha- Ketoglutarate |
| AKT | - | Protein kinase B gene |
| AKT | - | Other name for protein kinase B |
| ALL | - | Acute lymphoblastic leukemia |
| ALL1 | - | Leukemia, acute lymphocytic, susceptibility to, 1 gene |
| AML | - | Acute Myeloid Leukemia |
| AML1 | - | acute myeloid leukemia 1 or RUNX1 gene |
| AML-ETO | - | Fusion protein of AML1 and ETO |
| AML-ETO9a | - | an Alternatively Spliced Form of AML1-ETO |
| AMP | - | Adenosine Monophosphate |
| AMPK | - | AMP-activated protein kinase |
| ANOVA | - | Analysis of variance |
| APC | - | Allophycocyanin |
| APL | - | Acute Promyelocytic Leukemia |
| APS | - | Ammonium Persulfate |
| ATACseq | - | Assay for Transposase-Accessible Chromatin using sequencing |
| ATP | - | AdenosineTriphosphate |
| ATRA | - | All-Trans Retinoic Acid |
| BCA | - | Bicinchoninic Acid |
| BCR | - | breakpoint cluster region gene |
| BCR-ABL1 | - | Fusion protein of BCR and ABL1 genes |
| BM | - | Bone Marrow |
| BSA | - | Bovine Serum Albumin |
| CBF | - | Core Binding Factor |
| CBFB | - | Core Binding Factor Subunit Beta |
| CD | - | Cluster of differentiation receptors |
| CDS | - | Protein Coding Sequence |
| CEBPA | - | CCAAT enhancer-binding protein alpha |
| CFU | - | Colony Forming Units |
| CHIPseq | - | Chromatin Immunoprecipitation sequencing |
| CLP | - | Common Lymphoid Progenitor |
| CML | - | Chronic Myeloid Leukemia |
| CMP | - | Common Myeloid Progenitor |
| CO2 | - | Carbon Dioxide |
| CPT-1 | - | Carnitine Palmitoyltransferase-1 gene |
| CSF1 | - | Colony-Stimulating Factor 1 |
| CSFR1 | - | Colony stimulating factor 1 receptor |
| $C_T$ | - | Cycle Threshold |

| | | |
|---|---|---|
| DAPI | - | 4′,6-diamidino-2-phenylindole |
| DEG | - | Differentially Expressed Genes |
| DEK | - | DEK proto-oncogene |
| DEPC | - | Diethyl Pyrocarbonate |
| DES | - | Differential gene expression |
| DMEM | - | Dulbecco's Modified Eagle Medium |
| DMSO | - | Dimethyl sulfoxide |
| DNA | - | Deoxyribonucleic acid |
| DPBS | - | Dulbecco's Phosphate-Buffered Saline |
| DS | - | Down syndrome |
| ECAR | - | Extracellular Acidification Rate |
| EDTA | - | Ethylenediaminetetraacetic acid |
| ELL | - | Elongation Factor for RNA Polymerase II gene |
| ELN | - | European LeukemiaNet |
| ENL | - | Other name for gene MLLT1 |
| ENO1 | - | Enolase 1 |
| ETC | - | Electron Transport Chain |
| ETO | - | Eight Twenty One, Protein coded by gene RUNX1T1 |
| ETP | - | Early T cell Precursors |
| EVI | - | Ecotropic Virus Integration site 1 |
| FAB | - | French–American–British |
| FABP | - | Fatty Acid Binding Protein |
| FACS | - | Fluorescence Activated Cell Sorting |
| FAD | - | Flavin Adenine Dinucleotide |
| FADH2 | - | reduced FAD |
| FAO | - | Fatty Acid Oxidation |
| FATP | - | Fatty Acid Transport Proteins |
| FBS | - | Fetal Bovine Serum |
| FCCP | - | Carbonyl cyanide-p-trifluoromethoxyphenylhydrazone |
| FCS | - | Fetal Calf Serum |
| FILNC1 | - | FOXO Induced Long Non-Coding RNA 1 |
| FL2 | - | Fluorescence Channel 2 |
| FLT3 | - | fms like tyrosine kinase 3 |
| FOXO | - | Forkhead Transcriptional Factors |
| GAPDH | - | Glyceraldehyde 3-phosphate dehydrogenase |
| GATA2 | - | GATA-binding factor 2 |
| GFI1 | - | Growth Factor Independence 1 (Human) |
| Gfi1 | - | Growth Factor Independence 1 (Mouse) |
| GFI136N | - | 36N mutant variant of GFI1 |
| GFI136S | - | 36S wildtype of GFI1 |
| GFI1B | - | Growth Factor Independence 1b |
| GFP | - | Green fluorescent protein |
| GLS | - | Glutaminase |
| GLUT | - | Glucose Transporter |
| GMP | - | Granulocyte Monocyte Progenitor |
| GO | - | Gene Ontology |

| | | |
|---|---|---|
| GSEA | - | Gene Set Enrichment Analysis |
| Gy | - | Gray |
| H2O2 | - | Hydrogen Peroxide |
| HAT | - | Histone Acetyltransferase |
| HBS | - | HEPES Buffered Saline |
| HCL | - | Hydrochloric acid |
| HDAC | - | Histone Deacetylases |
| HEK | - | Human Embryonic Kidney |
| HEPES | - | 4-(2-hydroxyethyl)-1-piperazineethanesulfonic acid |
| HF | - | High Fidelity |
| HK | - | Hexokinase |
| HOX | - | Homeobox genes |
| HPRT | - | Hypoxanthine-guanine phosphoribosyltransferase |
| HRP | - | Horseradish peroxidase |
| HSC | - | Hematopoietic stem cells |
| IC50 | - | Half-maximal inhibitory concentration |
| IgG | - | Immunoglobulin G |
| IGV | - | Integrative Genomics Viewer |
| IL | - | Interleukin |
| ILC2 | - | Innate type 2 lymphoid cells |
| IMDM | - | Iscove's Modified Dulbecco's Medium |
| INT | - | p-Iodonitrotetrazolium Violet |
| IRES | - | Internal ribosome entry site |
| ITD | - | Internal Tandem Duplication |
| K3EDTA | - | tri-potassium EDTA |
| KD | - | Knock-down |
| kDa | - | Kilo Daltons |
| KI | - | Knock-In |
| KMT2A | - | Lysine Methyltransferase 2A |
| KO | - | Knock-out |
| KRAS | - | Kirsten Rat Sarcoma virus |
| LB | - | Lysogeny Broth |
| LDH | - | Lactate dehydrogenase |
| LIC | - | Leukemia Initiating Cells |
| Lin- | - | Lineage depleted cells |
| LMPP | - | Lymphoid Primed Multipotent Progenitors |
| LSC | - | Leukemic Stem Cells |
| LSD1 | - | Lysine-specific demethylase 1 |
| LT-HSCs | - | Long Term-HSCs |
| MACS | - | Matrix Composed of Superparamagnetic spheres |
| MAX | - | MYC-associated factor X |
| MCSV | - | Murine stem cell virus |
| MCT | - | Monocarboxylate transporter proteins |
| MDB | - | Membrane Desalting Buffer |
| MDS | - | Myelodysplastic Syndrome |
| MEP | - | Megakaryocyte/Erythrocyte Progenitors |

| | | |
|---|---|---|
| MFI | - | Median Fluorescence Intensity |
| mIL3 | - | mouse Interleukin 3 |
| mIL6 | - | mouse Interleukin 6 |
| MLL | - | Mixed-Lineage Leukemia |
| MLLT3 | - | Myeloid/Lymphoid Or Mixed-Lineage Leukemia Translocated To Chromosome 3 |
| MMP | - | Mitochondrial Membrane Potential |
| MN | - | Myeloid Neoplams |
| MPC | - | Mitochondrial Pyruvate Carrier |
| MPN | - | Myeloproliferative Neoplasms |
| MPP | - | Multipotent Progenitor cells |
| MRC | - | Myelodysplasia Related Changes |
| mTOR | - | mammalian Target of Rapamycin |
| mTORC1 | - | mTOR Complex 1 |
| MTT | - | (3-(4,5-dimethylthiazol-2-yl)-2,5-diphenyltetrazolium bromide |
| MW | - | Molecular Weight |
| MXD | - | MAX dimerization proteins |
| MYC | - | Myelocytomatosis |
| MYH11 | - | Myosin Heavy Chain 11 |
| $Na_2HPO_4$ | - | Disodium phosphate |
| NADH | - | Nicotinamide adenine dinucleotide |
| NE | - | Nuclear Extraction |
| NK | - | Natural Killer |
| NOS | - | Nonspecified |
| NP40 | - | onyl phenoxypolyethoxylethanol |
| NPM1 | - | Nucleophosmin 1 |
| NTP | - | Nucleoside triphosphate |
| NUP98 | - | Nucleoporin 98 |
| OCR | - | Oxygen Counsption Rate |
| OS | - | overall survival |
| OXPHOPS | - | Oxidativephosphorylation |
| PAGE | - | Polyacrylamide gel Electrophoresis |
| PB | - | Peripheral blood |
| PBS | - | Phosphate Buffered Saline |
| PCR | - | Polymerase chain reaction |
| PDL | - | Poly-D-lysine hydrobromide |
| PE | - | Phycoerythrin |
| PEI | - | Polyethylenimine |
| PerCp cy5.5 | - | Peridinin Chlorophyll Protein-Cyanine5.5 |
| PFKM | - | phosphofructokinase |
| PI3K | - | Phosphoinositide 3-kinase |
| PI3K-AKT | - | Fusion of PI3K and AKT genes |
| PLT | - | Platelets |
| PML | - | Promyelocytic Leukemia |
| PML-RARA | - | Fusion of PML and RARA genes |
| PMSF | - | Phenylmethylsulfonyl Fluoride |

| | | |
|---|---|---|
| PRMT1 | - | Protein Arginine Methyltransferase 1 |
| PVDF | - | Polyvinylidene Fluoride |
| RARA | - | Retinoic acid receptor alpha |
| RIPA | - | Radioimmunoprecipitation assay buffer |
| RNA | - | Ribonucleic Acid |
| RNAi | - | RNA interference |
| ROS | - | Reactive Oxygen Species |
| RPM | - | Revolutions Per Minute |
| RPMI | - | Roswell Park Memorial Institute |
| RT | - | Room Temperature |
| RT-PCR | - | Real-Time PCR |
| RUNX1 | - | Runt-related transcription factor 1 |
| RUNX1T1 | - | RUNX1 Partner Transcriptional Co-Repressor 1 |
| SCF | - | Stemcell Factor |
| SCM | - | Stemcell Media |
| SCR | - | Scrambled |
| SD | - | Standard Deviation |
| SDS | - | Sodium Dodecyl Sulfate |
| SEM | - | Standard Error of Mean |
| shRNA | - | Short hairpin RNA |
| siRNA | - | Small interfering RNA |
| SKP2 | - | S-Phase Kinase Associated Protein 2 |
| SNP | - | Single Nucleotide Polymorphisms |
| SPL | - | Spleen |
| TAE | - | Tris base, acetic acid and EDTA |
| TBS | - | Tris-buffered saline |
| TC | - | Tissue Culture |
| TCA | - | Tricarboxylic Acid |
| TEMED | - | Tetramethylethylenediamine |
| TG | - | Tris-Glycine |
| TKD | - | Tyrosine Kinase Domain |
| TMRE | - | Tetramethylrhodamine methyl ester perchlorate |
| TRM | - | Treatment-Related Mortality |
| UCP | - | Uncoupling Protein |
| UV | - | Ultra-violet |
| VCP | - | Valosin Containing Protein |
| VDAC | - | Voltage-dependent anion channel |
| WBC | - | White Blood Cells |
| WHO | - | World Health Organisation |
| WT | - | Wild Type |
| ZF | - | Zinc-Finger |

**List of tables**

**List of figures**

# 1. Introduction

## 1.1. Hematopoiesis and HSCs

Hematopoiesis is the development process of mature blood cells originating from multipotent hematopoietic stem cells (HSCs) during embryonic development and in the bone marrow microenvironment. HSCs reside at the top of the hierarchy of hematopoietic development. Due to the short life span of mature blood cells, HSCs are required to regenerate the mature cells through a series of various intermediate progenitor cells. HSCs can reconstitute the entire blood system, which is therapeutic in various haematological malignancies (Orkin & Zon, 2008).

HSCs are characterized by two distinct properties - self-renewal and differentiation. The self-renewal property helps maintain the number of HSCs throughout life, whereas differentiation leads to the production of functional blood cells, which accounts for the multipotency of HSCs (Orkin, 2000). HSCs depend on the microenvironment (niche) to maintain self-renewal property (Boulais & Frenette, 2015).

HSCs are categorized into two subtypes based on reconstitution potential: long-term (LT)- HSCs and short-term (ST)- HSCs. In the early step of cellular reprogramming, LT-HSCs differentiate into ST-HSC, which in turn differentiate into heterogeneous multipotent progenitor cells (MPP). MPPs lose self-renewal capacity but retain full differentiation potential. MPPs further differentiate into oligopotent common myeloid progenitor (CMP) and lymphoid-primed multipotent progenitors (LMPPs), which carry the potential to give myeloid and lymphoid lineages, respectively. CMPs segregate into megakaryocyte/erythrocyte progenitors (MEPs) and granulocyte/macrophage progenitors (GMPs). MEPs differentiate into megakaryocytes and erythrocytes through a series of intermediate cellular subtypes, whereas GMPs differentiate into granulocytes and monocytes. LMPPs differentiate into Common Lymphoid Progenitors (CLPs) in lymphoid lineage development and further differentiate to produce T cells, B Cells, NK cells, and dendritic cells (Cheng, Zheng, & Cheng, 2020).

The differentiation and reprogramming of HSCs are regulated by the expression levels of several transcriptional factors and signalling pathways initiated by various cytokines during mature blood cell development (Orkin & Zon, 2008; Zhu & Emerson, 2002). Deregulated expression or improper functionality of these transcriptional factors' leads to various haematological malignancies such as myelodysplastic syndrome and leukemia development (Gery & Koeffler, 2007).

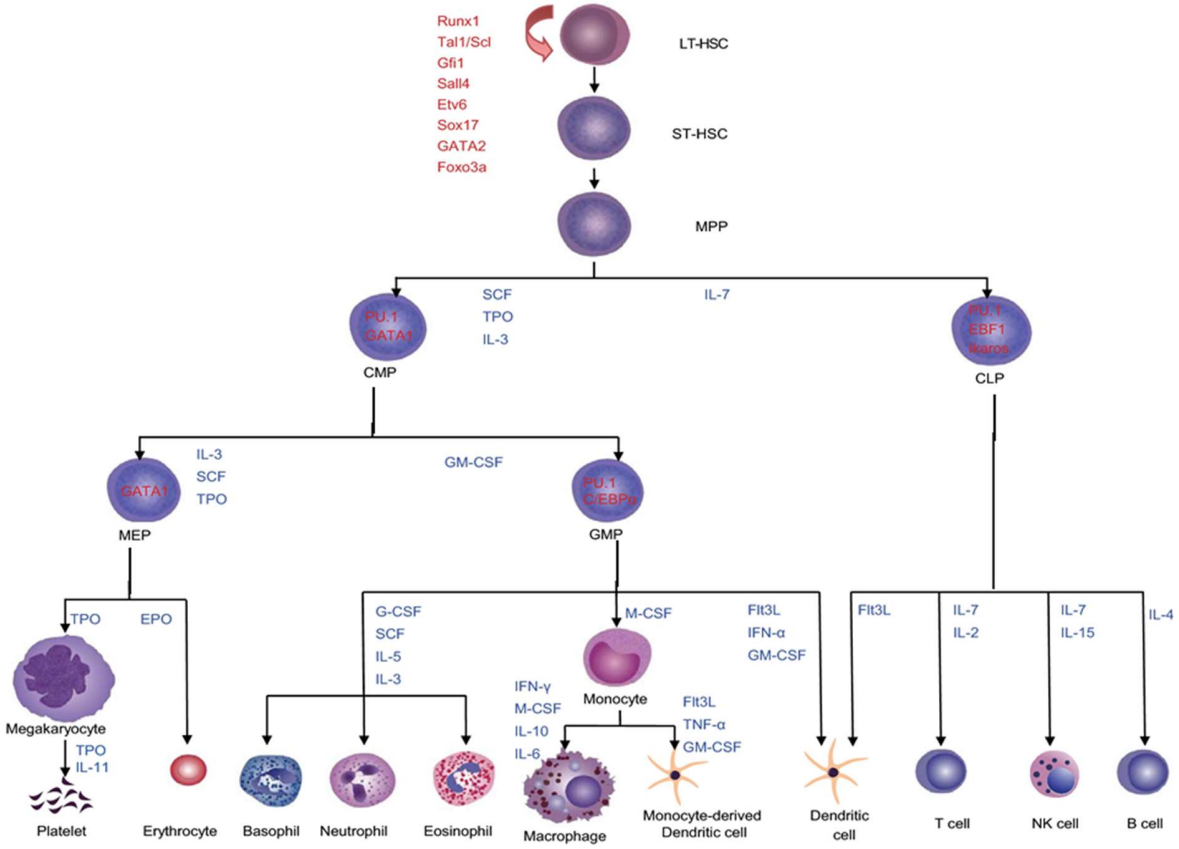


**Figure 1: Schematic representation of hematopoiesis**

The figure describes the process of hematopoiesis from the hematopoietic stem cells (HSCs) into the diverse daughter cells of the myeloid and lymphoid lineages. Various cytokines and the transcriptional factors that promote the differentiation direction of the specific lineages are represented (Cheng et al., 2020).

### 1.2. Myelodysplastic syndrome

Myelodysplastic syndrome (MDS), is a heterogeneous group of clonal haematological disorders resulting from ineffective hematopoiesis, which can progress to other haematological cancers such as Acute Myeloid Leukemia

(AML) and rarely Acute Lymphoblastic Leukemia (ALL) (Greenberg, 2011; Mohammad, 2018). The main symptoms of MDS include anaemia, thrombocytopenia, and secondary infections. Among the known causative factors, chemotherapy-related MDS is quite discernible. MDS has an incidence rate of 4.9 per 100,000 persons/ year with a fivefold increase in risk between age 60 and ≥80. It is most commonly diagnosed in older people (≥70 years of age), making the treatment quite challenging and hence a poor prognosis (Klepin, 2016; Mohammad, 2018). MDS blasts show hypermethylation of genes associated with apoptosis, differentiation, and DNA repair (Estey & Dohner, 2006). Hence DNA methyltransferase inhibitors such as Azacitidine and Decitabine have therapeutic potential in MDS treatment (Dohner et al., 2010). Accumulation of secondary mutations in MDS patients promotes AML development in nearly one-third of patients (Barzi & Sekeres, 2010). The presence of blast cells (early progenitors) < 20% is considered as MDS, whereas blasts >20% are considered as AML (DiNardo et al., 2016).

### 1.3. Acute Myeloid Leukemia

Leukemia is an abnormal condition of immature or abnormal leukocytes, leading to reduced blood cell synthesis, cytopenia. Acute Myeloid Leukemia (AML) is one of the most predominant, accounting for one-third of all leukemias, and is the most common acute leukemias in adults and males. The incidence of AML of total leukemic cases increased to 23.1% in 2017 compared to 18.0% in 1990 calculated worldwide (Dong, Shi, et al., 2020).

The incidence rate of AML increases with age from 1.3 to 12.2 cases per 100000 population from less than 65 years to more than 65 years, respectively (De Kouchkovsky & Abdul-Hay, 2016; Saultz & Garzon, 2016). AML accounts for 1.1% of new cancer cases and 1.8% of cancer deaths in 2020, with a 5-year relative survival of 28.7% calculated during 2010-2016 (SEER Cancer Stat Facts). AML is associated with a poor prognosis due to high relapse rates and an overall 40-45% survival rate in younger patients and less than 10% in adults (Grove & Vassiliou, 2014).

AML is characterized by clonal expansion of myeloid precursors due to genetic alterations, leading to abnormal accumulation of ≥ 20% of immature

myeloblasts in blood and bone marrow. The major causative factors of AML development include genetic modifications due to unknown factors. In contrast, a small fraction of patients developed AML due to prior chemotherapy and occupational exposure to benzene and formaldehyde chemicals (Yi et al., 2020). The pathophysiology of AML includes abnormal proliferation and impaired differentiation of myeloid progenitors. The molecular pathogenesis of AML includes genetic mutations (in > 97% of AML patients), chromosomal translocations leading to the formation of the chimeric protein, and alteration of epigenetically regulating genes. The two-hit model explains the pathogenesis, in which a combination of mutations or genetic alterations is responsible for AML development. According to this model, a conjunction of two classes of mutations promotes AML progression; class I mutations induce proliferation and promote cell survival through constitutive signal transduction. Class II mutations hinder differentiation by deregulated transcriptional factors. Besides, the concept of class III mutations has been introduced in recent times, which induces epigenetic and chromatin changes. The interactions of frequent mutations in AML is represented in Figure 2 (Naoe & Kiyoi, 2013).

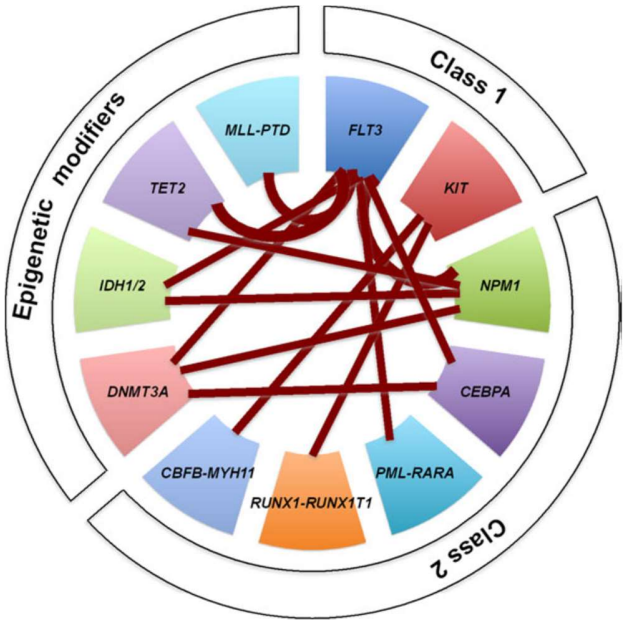


**Figure 2: Classification of gene mutations in AML.**

Most common gene mutations overlapped with class I, Class II, and epigenetic modifiers associated with AML development (Naoe & Kiyoi, 2013)

### 1.3.1. Classification of AML

AML was initially classified in 1976 by several French, American, and British leukemic experts (FAB system) and later by World Health Organisation (WHO) by considering additional features. The classical FAB system is still standard. Based on morphological and cytochemical characteristics and differentiation status, the FAB system classified AML into M0 to M7 (Table 1) (Angelescu, Berbec, Colita, Barbu, & Lupu, 2012; Palanisamy, 2010; Segeren & van 't Veer, 1996)

**Table 1: FAB classification of AML (Angelescu et al., 2012)**

| FAB subtype | AML description | % of AML Patients |
|---|---|---|
| M0 | Myeloblastic leukemia minimally differentiated | 5 |
| M1 | Myeloblastic leukemia without maturation | 15 |
| M2 | Myeloblastic leukemia with maturation | 25 |
| M3 | Acute promyelocytic leukemia- microgranular variant | 10 |
| M4 | Myelomonocytic leukemia | 20 |
| M4Eo | Myelomonocytic leukemia with bone marrow eosinophilia | 5 |
| M5 | Monocytic leukemia- Poorly differentiated (5a) and differentiated (5b) | 10 |
| M6 | Erytroleukemia | 5 |
| M7 | Megakaryoblastic leukemia | 5 |

In 2001, the world health organization (WHO) introduced another classification system by integrating genetic abnormalities, diagnosis, and therapy management. With the latest revised edition of WHO released in 2017 by accommodating additional morphological, prognostic, immunophenotypic, and clinical data, AML has been classified into six types (Table 2). At the same time, AML with recurrent genetic abnormalities is further classified into 11 subtypes based on chromosomal translocations (Table 2) (Arber et al., 2016; De Kouchkovsky & Abdul-Hay, 2016; Hwang, 2020; Pelcovits & Niroula, 2020).

**Table 2: WHO classification of AML (Arber et al., 2016; Hwang, 2020).**

| | |
|---|---|
| AML with recurrent genetic abnormalities | • AML with t(8;21)(q22q22.1); RUNX1-RUNX1T1<br>• AML with inv(16)(p13.1q22) or t(16;16)(p13.1;q22); CBFB-MYH11<br>• APL with PML-RARA<br>• AML with t(9;11)(p21.3;q23.3); KMT2A-MLLT3<br>• AML with t(6;9)(p23;q34.1); DEK-NUP214<br>• AML with inv(3)(q21.3q26.2) or t(3;3)(q21.3;q26.2); GATA2, MECOM<br>• AML (megakaryoblastic) with t(1;22)(p13.3;q13.1); RBM15-MKL1<br>• Provisional entity: AML with BCR-ABL1<br>• AML with mutated NPM1<br>• AML with biallelic mutation of CEBPA<br>• Provisional entity: AML with mutated RUNX1 |
| AML with myelodysplasia- related changes (MRC) | |
| Therapy-related myeloid neoplasms (t-MN) | |
| AML, not otherwise specified (NOS) | |
| Myeloid sarcoma | |
| Myeloid proliferations related to Down syndrome (DS) | |

Contemplating chromosomal translocations and cytogenetic abnormalities as prognostic markers, European LeukemiaNet (ELN) further classified AML into favourable, intermediate, and adverse risk groups (Pelcovits & Niroula, 2020). The prognostic assessment is beneficial for reducing treatment-related mortality (TRM) and presume the treatment strategy (De Kouchkovsky & Abdul-Hay, 2016; Saultz & Garzon, 2016). Independent of these prognostic factors, patients above 60 years are considered poor prognoses, curtailing the remission rate and shortening overall survival (OS).

### 1.3.2. Frequent translocations in AML

Cytogenetic analysis indicates that more than 75% of AML patients show chromosomal aberrations such as translocations with high prognostic value (Mrozek, Heinonen, de la Chapelle, & Bloomfield, 1997; Palanisamy, 2010). De novo adult AML cases display 25-30% of translocations (Slovak et al., 2000). Most of the balanced translocations of AML accord a fusion product with oncogenic potential and proliferative advantage. t(8;21) was the first reciprocal

translocation identified, accounting for up to 6% of adult AML patients (Byrd et al., 2002). t(8;21) yield a fusion product RUNX1-RUNXT1 (AML1-ETO) and is exceedingly associated with FAB M2 AML and characteristic of core-binding factor (CBF) AML (Mrozek & Bloomfield, 2008; Peterson et al., 2007).

Mixed-lineage leukemia 1 (*MLL1*) rearranged leukemias (*MLLr*) amount for 10% of leukemias and more common in adult AML (Krivtsov & Armstrong, 2007; Muntean & Hess, 2012) and 35-50% of infant AML. Up to 70% of therapy-related leukemias haul MLL fusions (Blanco et al., 2001). MLL is a histone methyltransferase (Histone H3 Lysine 4- H3K4) and positively regulates gene expression of target genes such as *HOX* and *EVI-1*(Krivtsov & Armstrong, 2007). *MLL1* fuses with >80 partner genes through its N terminus and induces leukemia development through the HOX gene cluster's upregulation (Krivtsov & Armstrong, 2007; Milne et al., 2002; Zeisig et al., 2004). The most common fusion proteins or partners include *AF4* [t(4,11)], *AF6* [t(6,11)], *AF9* [t(9,11)], *AF10* [t(10,11)], *ENL* [t(11,19)] and *ELL* [t(11,19) (Meyer et al., 2013; Muntean & Hess, 2012). *AF4* (ALL1 fused gene from chromosome 4) stimulates ALL development in 50% of infant ALL cases. (Meyer et al., 2013). *MLL-ENL* is associated with lymphoid and myeloid leukemias, whereas *MLL-AF9* is ubiquitous in myeloid leukemias (Drynan et al., 2005). *MLL-AF9* contributes to a major fraction (up to 29%) of *MLL* translocations in AML (Winters & Bernt, 2017). A cohort investigation shows that >70% of *MLL* translocations in pediatric and adult AML are *MLL-AF9* (Meyer et al., 2013). 2-5% of total AML patients display *MLL-AF9* fusion and 25% of *de novo* AML in children with the median survival of 4 years (Huret, Minor, Dorkeld, Dessen, & Bernheim, 2000). Hence *MLL-AF9* induced AML development model is used extensively in the current investigation.

### 1.3.3. Transcriptional factors in AML

Transcriptional factors are the proteins that bind and regulate the expression of the promoter or enhancer regions of target genes through chromatin modifications (Thoms, Beck, & Pimanda, 2019). They play an essential role in the stemness, differentiation, and maturation of HSCs and progenitor cell lineage determination. Deregulated or altered expression of these

transcriptional factors resulting from mutations or translocations leads to haematological malignancies such as AML. Various transcriptional factors such as GFI1, C/EBPα, PU.1, RUNX1, p53, and c-MYC regulate hematopoiesis, dysregulation of which induce AML development (Assi, Bonifer, & Cockerill, 2019; Takei & Kobayashi, 2019; Thoms et al., 2019).

### 1.3.4. Growth Factor Independence 1 (GFI1)

GFI1 is a transcriptional repressor protein that plays an essential role in differentiating myeloid and lymphoid progenitors and regulating hematopoiesis. It also has a role in developing the inner ear (Matern et al., 2020; Wallis et al., 2003).

#### 1.3.4.1. Structure and function of GFI1

GFI1 is localized mainly in the nucleus and has three domains: a c terminal, six C2H2-type zinc finger domains, an intermediate domain, and an N terminal conserved SNAG domain. Through its zinc finger domains 3,4, and 5, GFI1 binds to its target genes at a consensus sequence motif [taAATCac(t/a) gca]. Zinc finger domains 1,2,6 meditate interaction with other proteins (Lee et al., 2010; Zweidler-Mckay, Grimes, Flubacher, & Tsichlis, 1996). The SNAG domain is essential for recruiting other proteins for histone modification (Saleque, Kim, Rooke, & Orkin, 2007). Proteins involved in RNA splicing, protein modifications, and transcriptional regulation bind to the intermediate domain (Figure 3). A paralogue of *GFI1* known as *GFI1B* shows 89% structural similarity in SNAG and zinc finger domains and only 39% similarity in the intermediate domain (Figure 3).

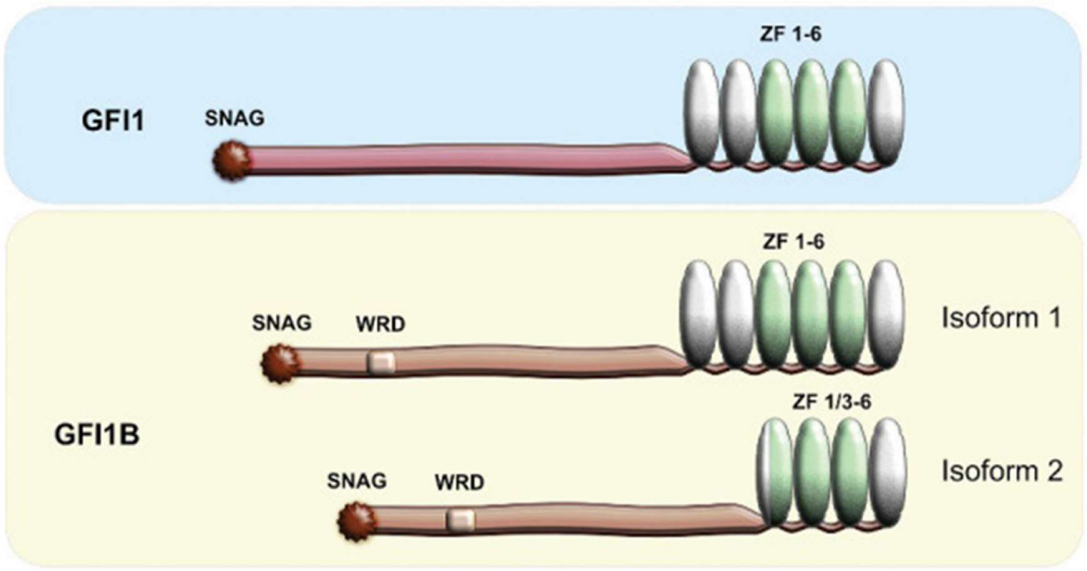


**Figure 3: Structure of GFI1 and GFI1B proteins**

The figure shows the structural homology between GFI1 and GFI1B proteins, with the homologous C-terminal DNA binding C2H2 zinc finger domains (ZF 1-6) and N-terminal SNAG domains, while the intermediate domains vary between GFI1 and GFI1B. The GFI1B has two isoforms. The green colour zinc finger domains represent the DNA binding domains, whereas the other domains interact with other proteins (Beauchemin & Moroy, 2020).

GFI1 represses the expression of target genes through epigenetic modifications. GFI1 binds to the promoter of target genes and recruits histone methyltransferases (G9A), histone demethylases (LSD1), and histone deacetylases (HDAC), thereby modifying the chromatin structure and hence transcriptional repression. LSD1 binds to the SNAG domain, while G9A and HDAC bind to the intermediate domain of GFI1 (Figure 4). The binding of HDAC and G9A impel deacetylation of lysine 9 of histone 3 (H3K9) and demethylation of lysine 4 of histone 3 (H3K4), respectively, and promotes gene silencing of the target gene (Saleque et al., 2007).

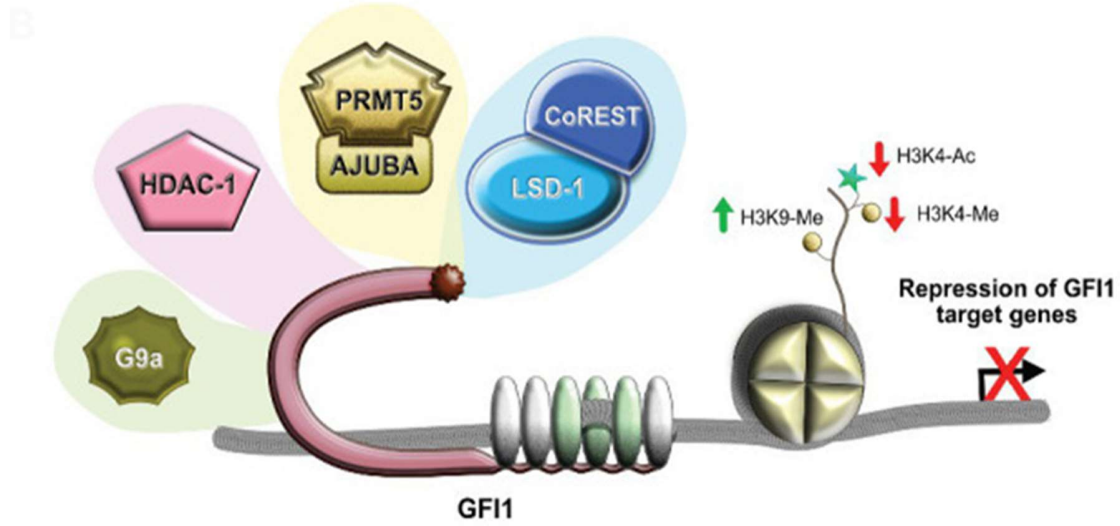


**Figure 4: Function of GFI1**

GFI1 binds to the target gene through the zinc finger domains, while the SNAG and intermediate domains recruit DNA modifying proteins to promote gene silencing by chromatin modification. GFI1 promotes H3K9 methylation and decreases H3K4 acetylation and methylation of the target genes (Beauchemin & Moroy, 2020).

In addition to its canonical function, GFI1 has also been shown to regulate DNA damage and repair mechanisms through its interaction with arginine methyltransferase (PRMT1) and regulating methylation of DNA repair proteins MRE11 and 53BP1 (Vadnais et al., 2018). GFI1 also inactivates the tumour suppressor protein P53 by forming a tripartite complex with LSD1 and demethylating its C-terminal lysine residue (J. Huang et al., 2007; Khandanpour & Moroy, 2013; Khandanpour et al., 2013).

1.3.4.2. Gene targets of GFI1

Chromatin immunoprecipitation sequencing (CHIPseq) analysis shows GFI1 binds to the promoter of various genes such as *Hoxa9*, *Pbx1*, *Meis1*, *CSF1*, *CSFR1, Id2, PU.1* that play a role in myeloid differentiation (Horman et al., 2009; H. Li, Ji, Klarmann, & Keller, 2010; Phelan, Shroyer, Cook, Gebelein, & Grimes, 2010; van der Meer, Jansen, & van der Reijden, 2010). GFI1 counteracts PU.1 by repressing the expression of PU.1 directly and also through protein-protein interaction (Dahl, Iyer, Owens, Cuylear, & Simon, 2007; Spooner, Cheng, Pujadas, Laslo, & Singh, 2009). GFI1 also inactivates the

tumour suppressor protein p53 by recruiting LSD1 and demethylating its active lysine residue (Khandanpour & Moroy, 2013; Khandanpour et al., 2013)

#### 1.3.4.3. Regulation of *GFI1* expression

The expression of *GFI1* and *GFI1b* are mutually exclusive due to cross-regulation (Vassen, Okayama, & Moroy, 2007) and cell dependence during hematopoiesis. HSCs express a low level of GFI1 compared to *Gfi1b* (Khandanpour, Sharif-Askari, et al., 2010) and GFI1 expression maintains the self-renewal capacity of HSCs (Zeng, Yucel, Kosan, Klein-Hitpass, & Moroy, 2004). The expression of GFI1 escalates during the differentiation to MPPs (Khandanpour, Sharif-Askari, et al., 2010). *Gfi1* also shows high expression in lymphoid progenitors such as CLPs, ETPs (early T cell precursors), GMPs, monocytes, granulocytes, and B cells progenitors (Yucel, Kosan, Heyd, & Moroy, 2004). GFI1 is not significantly detected in megakaryocyte progenitors where GFI1b levels are high (Vassen et al., 2007). GFI1 shows autoregulation, and the expression of GFI1 is well regulated by other transcriptional factors such as GFI1b (Vassen, Fiolka, Mahlmann, & Moroy, 2005), Ajuba (Montoya-Durango et al., 2008), and Ikaros (Spooner et al., 2009).

#### 1.3.4.4. Role of GFI1 in AML development

A low level of *GFI1* (knockdown of *GFI1* expression - *GFI1 KD*) is associated with a poor prognosis in AML and promotes onco-fusion gene expression (*MLL-AF9* and *NUP98-HOXD13*) steered AML development in mouse models (Hones et al., 2016). The deficiency of *GFI1* alone does not promote leukemia development. Accumulation of secondary mutations such as *Kras* mutation (Horman et al., 2009) or altered gene expression such as increased *Bcl-2* (Khandanpour et al., 2011) and reduced *Gfi1* expression promotes AML development. *GFI1 KD* mice show an increase in H3K9 acetylation of GFI1 target genes (Hones et al., 2016). Loss of *Gfi1* (knockout - *Gfi1* KO) in mice impairs the self-renewal capacity of HSCs (Zeng et al., 2004). Knock-out of *Gfi1* in mice displays severe neutropenia and accumulates GMPs and myelomonocytic progenitor cells (Hock et al., 2003).

#### 1.3.4.5. GFI1 36N variant in AML

GFI136N is a single nucleotide polymorphism (SNP) variant of GFI1 associated with poor treatment outcomes and prognosis. It is characterized by the replacement of asparagine (N) at position 36 instead of naturally existing serine (S) amino acid (GFI136S) (Khandanpour, Thiede, et al., 2010) at the intermediate domain of the protein. The presence of the *GFI136N* variant leads to a higher proliferative capacity of myeloid precursors. The GFI136N variant has reduced binding efficiency to its target genes, and it can not efficiently induce the epigenetic changes of its target genes such as *Hoxa9* (Khandanpour et al., 2012). At the same time, the cells expressing the *GFI136N* variant show increased H3K9 acetylation of GFI1 target genes, thereby promoting transcription (Botezatu, Michel, Helness, et al., 2016; Botezatu, Michel, Makishima, et al., 2016). AML patients carrying *GFI136N* mutation showed a higher risk of AML development for 2-3 fold and a low survival rate. The presence of a single variant allele is not enough to induce leukemia development in murine models and patients (Khandanpour, Thiede, et al., 2010). The GFI136N variant hastens myeloproliferative disease in the presence of oncogenic mutations such as KRAS and facilitates AML development in the presence of other oncofusion proteins (Khandanpour et al., 2012). Akin to *GFI1-36N*, mice expressing *GFI1- KD* display increased *H3K9* acetylation of GFI1 target genes (Botezatu, Michel, Helness, et al., 2016).

#### 1.3.4.6. Absent or low level of *GFI1* in AML development

*GFI1* deficient cells show increased apoptosis due to active p53 (Khandanpour et al., 2013). Loss of *Gfi1* causes neutropenia and accumulation of monocytes and granulocytic precursors (Hock et al., 2003). Loss of *Gfi1* accelerates the MDS development in the presence of additional mutations such as those in the *Kras* gene (Horman et al., 2009).

Analysis from the AML patients cohort study indicates that a low expression level of *GFI1* is associated with poor survival of MDS and AML patients. A low level of *GFI1* and the expression of *MLL-AF9* or *NUP98-HOXD13* translocations accelerates the development and progression of AML in mice (Hones et al., 2016). A low level of *GFI1* is also associated with poor outcomes

in CML (Kok et al., 2013). Leukemic mouse models with a reduced level of *GFI1* (*GFI1 KD*) and a variant of *GFI1* (*GFI136N*) were more sensitive to histone acetyltransferase inhibitors (HATi) compared to wild type *GFI1* (*GFI1-36S*) (Botezatu, Michel, Helness, et al., 2016; Hones et al., 2016).

#### 1.3.4.7.GFI1 and AML1-ETO9a interactions

In the current study, along with *MLL-AF9*, we used *AML1-ETO9a* induced leukemic cells for metabolic experiments. Based on previous reports, it has been shown that *GFI1* is essential for *AML1-ETO9a* induced leukemia development, and GFI1 is the direct target of the fusion product. *GFI1* is essential for *AML1-ETO9a* induced leukemia development. Either loss or reduced expression of *GFI1* impedes *AML1-ETO9a* induced leukemia development and prevents leukemic development in murine models (Marneth et al., 2018).

### 1.3.5. Growth Factor Independence 1b (GFI1b)

GFI1b is a closely related protein of GFI1, with conserved DNA binding and zinc finger SNAG domains, but they differ in the intermediate domain. The structural homology between GFI1 and GFI1b proteins is shown in Figure 3. The expression and localisation of GFI1 and GFI1b are cellular and compartment dependant, and they repress the expression of each other. GFI1b is essential for the stemness of HSCs and plays a role in the differentiation of erythroid and megakaryocyte lineages and platelets development (Khandanpour, Sharif-Askari, et al., 2010; Randrianarison-Huetz et al., 2010). Loss of *GFI1b* affects the development of mice at the embryonic stage due to defects in the erythroid and platelet development (Saleque, Cameron, & Orkin, 2002). Loss of a single or both alleles of *GFI1b* promotes the development of AML by increasing the number of leukemic stem cells (LSCs) (Thivakaran et al., 2018).

## 1.4. Metabolism and metabolic changes in cancers

### 1.4.1. Overview

Cancer is characterized by metabolic deregulation in addition to genetic alterations. Hence, studying and investigating the various metabolic pathways in cancers is essential. The metabolic pathways are characterized by the consumption of various nutrients by the cells and the intracellular conversion of the nutrients into micromolecules and energy. These small molecules and the energy generated is utilized for cell division and are very important in cancer cell proliferation. The essential metabolic pathways in cancers are shown below.

#### 1.4.1.1. Glycolysis

Glucose is one of the primary sources of cellular energy. The process of metabolizing glucose into pyruvate or lactate is known as glycolysis. The presence of oxygen leads to aerobic reactions and gives two pyruvate molecules from a glucose molecule. During aerobic glycolysis, two ATP and two NADH molecules are produced. The pyruvate enters into the TCA cycle to further oxidize into $CO_2$ and H2O to yield further ATP. Anaerobic glycolysis in the absence of oxygen gives two lactate and two ATP molecules. The condition of excess production of lactate due to lack of oxygen is known as lactic acidosis, a risk factor in cancer patients (Akram, 2013; Held-Warmkessel & Dell, 2014). At the same time, the reverse process of generating glucose from pyruvate is known as gluconeogenesis. The glycolysis pathway is shown in Figure 5.

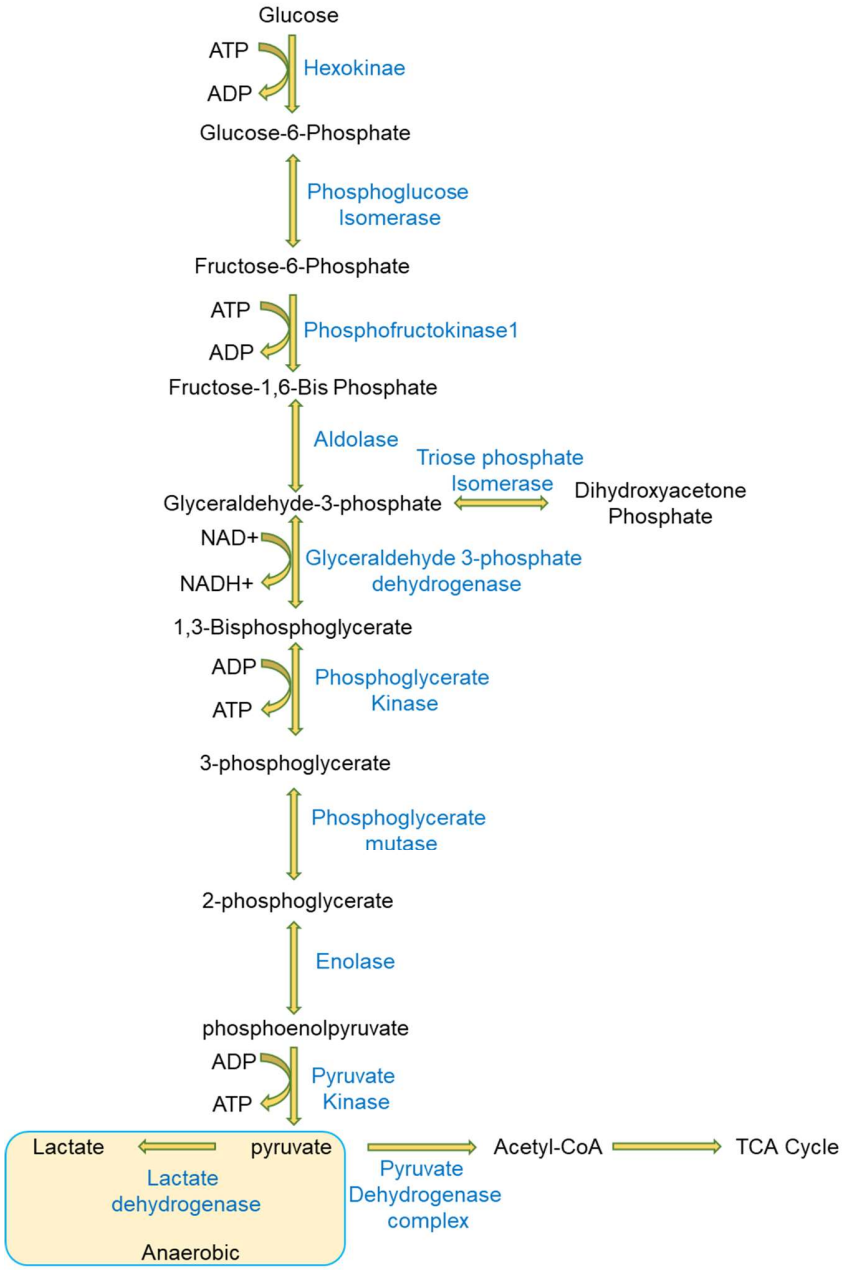


**Figure 5: Glycolysis pathway**

The figure shows the series of reactions involved in the glycolysis pathway under aerobic and anaerobic conditions (Adapted from Molecular Cell Biology, Lodish. 5th Edition)

1.4.1.2. Tricarboxylic acid (TCA) cycle

The pyruvate synthesized in the cytoplasm transferred to mitochondria and converted to acetyl-CoA. The acetyl-CoA is further metabolized through the TCA cycle. TCA cycle, also known as the Krebs cycle, is a series of reactions

from the oxidation of acetyl-CoA to generate energy (Figure 6). A single glucose molecule produces 36 ATP molecules under aerobic conditions through glycolysis, TCA cycle and oxidative phosphorylation. In addition to glucose, other energy sources such as glutamine, fatty acids and amino acids also contribute to the intermediates of the TCA cycle.

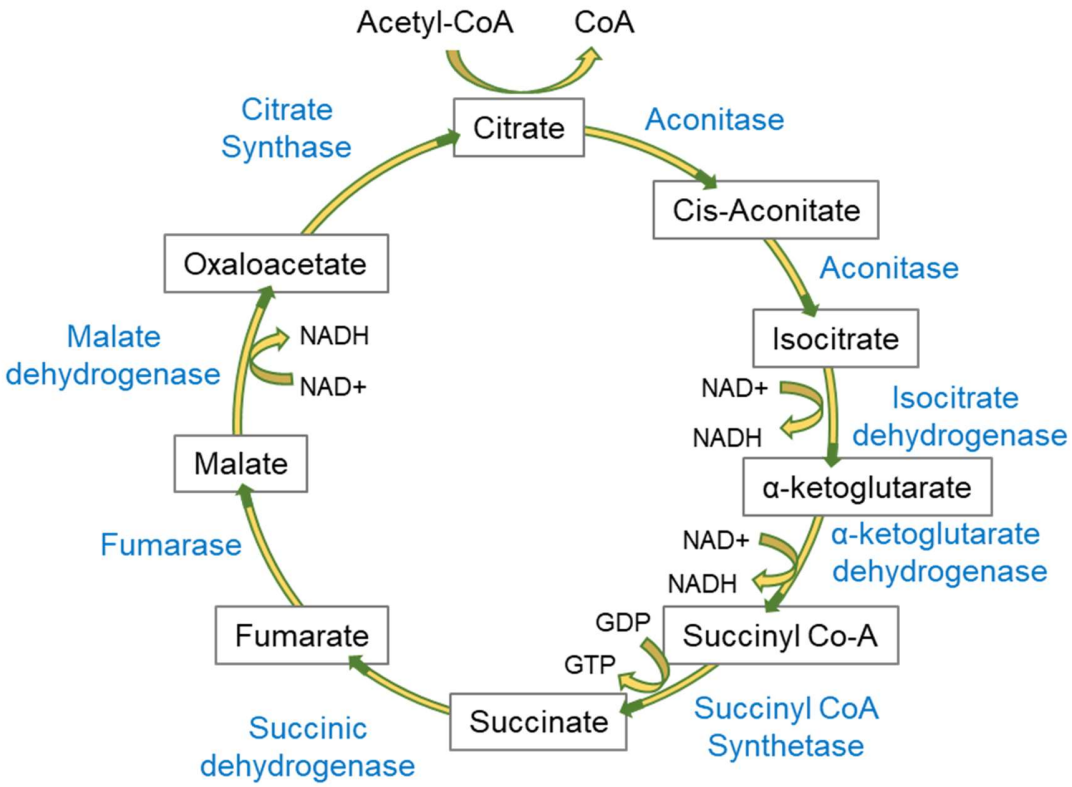


**Figure 6: TCA cycle pathway**

Metabolism of acetyl Co-A through TCA cycle and the series of intermediate reactions involved in the TCA cycle (Adapted from Molecular Cell Biology, Lodish. 5th Edition).

1.4.1.3. Fatty acid metabolism and carnitine transport system

Fatty acids are one of the primary sources of cellular energy. The fatty acid transporter proteins (FATPs), fatty acid-binding proteins (FABPs) and CD36 receptors (fatty acid translocase) promote the transfer of fatty acids across plasma membranes (Anderson & Stahl, 2013; Berlanga, Guiu-Jurado, Porras, & Auguet, 2014). The fatty acids are impermeable through the mitochondrial membrane, and hence they need a unique transporter system to enter mitochondria for β-oxidation. The fatty acids are converted to acyl-CoA

thioesters by FATPs and internalize into mitochondria for β-oxidation through the carnitine transporter system. The Carnitine Palmitoyltransferase I and II (CPT I and II) are the two essential proteins in the outer and inner mitochondrial membranes, facilitating the fatty acyl-CoA into the mitochondrial matrix (Figure 7). Through the series of reactions in β-oxidation, the fatty acyl-CoA is metabolized to acetyl-CoA and enters into the TCA cycle and oxidative phosphorylation to produce ATP. Complete oxidation of palmitic acid produces 129 ATP molecules (Currie, Schulze, Zechner, Walther, & Farese, 2013; Longo, Frigeni, & Pasquali, 2016; Mashek & Coleman, 2006; Melone et al., 2018).

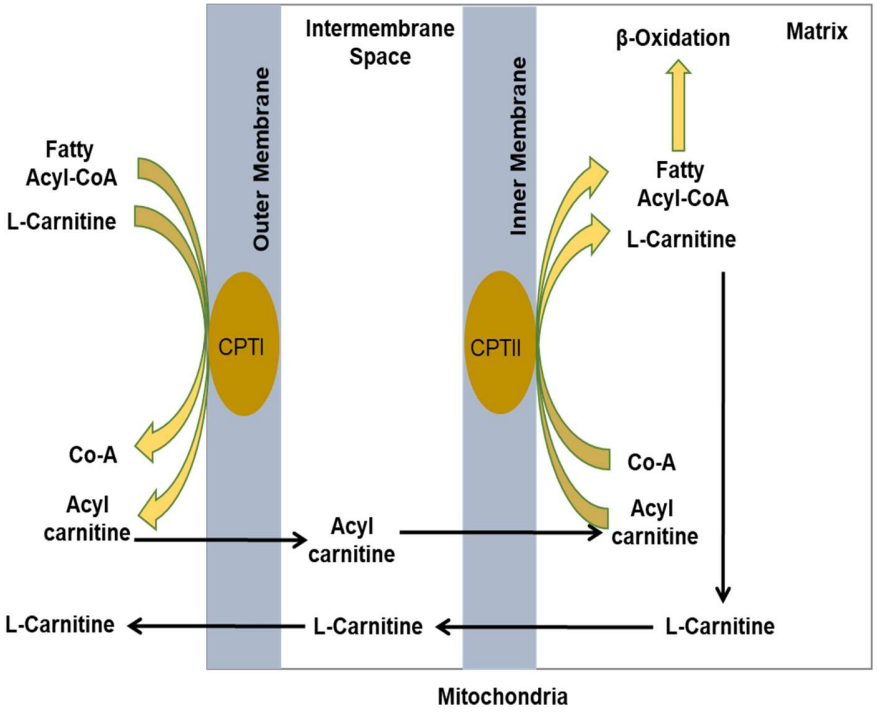


**Figure 7: Carnitine transport system for fatty acid uptake**

Schematic representation of fatty acid transport into the mitochondrial matrix for β-oxidation through the carnitine system (Adapted from (Adeva-Andany, Calvo-Castro, Fernandez-Fernandez, Donapetry-Garcia, & Pedre-Pineiro, 2017; Longo et al., 2016).

#### 1.4.1.4. Glutamine metabolism

Glutamine metabolism is one of the significant anaplerotic reactions contributing to the TCA cycle. L-glutamine enters the cells by passing through the plasma membrane and enters mitochondria. Glutamine converts to

glutamate by glutaminase (GLS) and then enters into the TCA cycle by converting into α-ketoglutarate (AKG) by glutamate dehydrogenase (Figure 8) (Altman, Stine, & Dang, 2016; C. Yang et al., 2014).

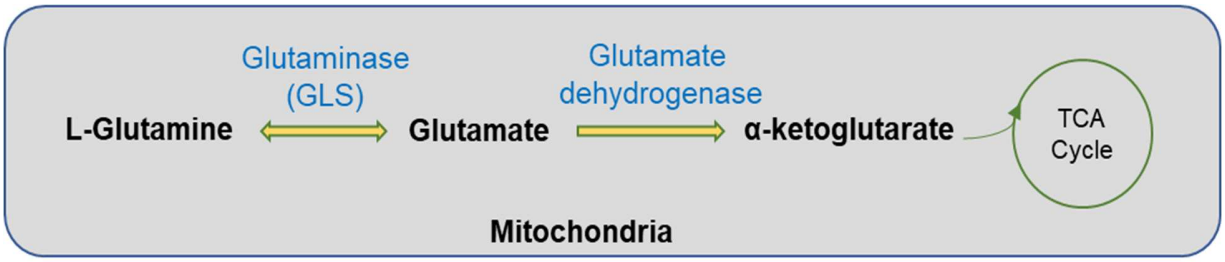


**Figure 8: Glutamine metabolism reactions**

Anaplerotic reactions of glutamine metabolism into α-ketoglutarate and entering of α-ketoglutarate through TCA cycle in mitochondria (Adapted from (Altman et al., 2016)).

#### 1.4.1.5. Electron transport chain and oxidative phosphorylation (OXPHOS)

The electron transport chain (ETC) is a series of five protein complexes (complex I - V) embedded in the inner mitochondrial membrane. These complexes allow the transfer of electrons by transporting protons from NADH and FADH2 into intermembrane space and reducing oxygen to water. The proton transport generates a proton gradient across the inner mitochondrial membrane, and these protons are pumped back into the mitochondrial matrix through the complex V (ATP synthase) of ETC, thereby generating ATP (Figure 9) (Zhao, Jiang, Zhang, & Yu, 2019). As described earlier, a large amount of NADH and FADH2 generates through glycolysis and TCA cycles. Oxidative phosphorylation synthesizes ATP from the proton gradient generated by electron transfer from NADH and FADH2 (Molina et al., 2018). Due to the proton gradient, the inner mitochondrial membrane exhibits potential, known as mitochondrial membrane potential (MMP- $\Delta\Psi m$). MMP represents the mitochondrial activity and ATP synthesis rate (Zorova et al., 2018).

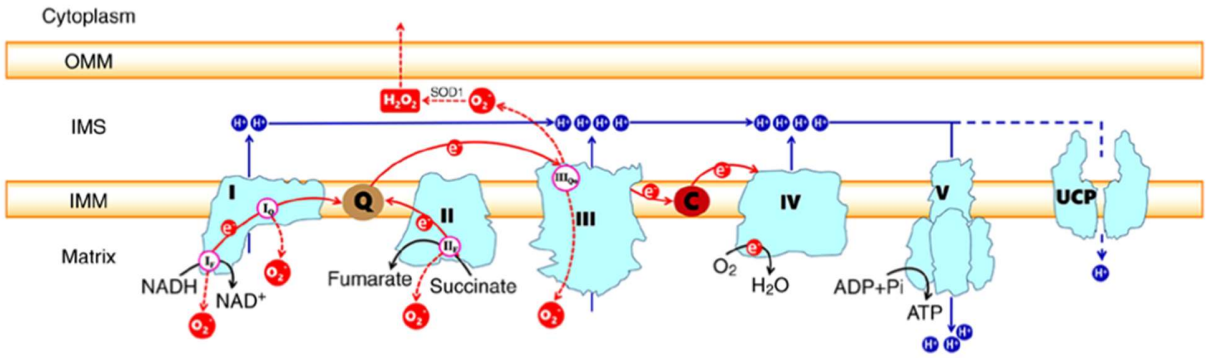


**Figure 9: Electron transport chain system.**

The electron transport chain displays electrons' transport across the complexes (I to V) and ATP synthesis due to proton gradient (Zhao et al., 2019).

#### 1.4.1.6. Reactive oxygen species (ROS)

Aerobic metabolism by OXPHOS generates reactive oxygen species (ROS) as by-products. The electrons leak across the membrane, and hence the mitochondria produce ROS due to the partial reduction of oxygen. ROS is produced mainly at complexes I and III of ETC. ROS include the superoxide anion (O2−), hydrogen peroxide (H2O2), and hydroxyl radicals (OH·) (Sies & Jones, 2020; Suski et al., 2012; Turrens, 2003; Zorov, Juhaszova, & Sollott, 2014). High ROS levels indicate oxidative stress and incur damage to DNA, proteins and lipids. In a state of oxidative stress, the cells depend on ROS scavenger systems such as superoxide dismutase, peroxisomes and glutathione (Schieber & Chandel, 2014). The level of ROS varies according to the cell type in the hematopoietic system. HSCs reside in the oxygen-deprived bonemarrow microenvironment and produce low ROS. The low ROS levels maintain the quiescence of HSCs and are protected from ROS induced stress (Jang & Sharkis, 2007; Prieto-Bermejo, Romo-Gonzalez, Perez-Fernandez, Ijurko, & Hernandez-Hernandez, 2018). ROS levels are upregulated in myeloid leukemia, and hence antioxidants are highly effective as therapeutic options in leukemia (Kaweme, Zhou, Changwe, & Zhou, 2020).

A high MMP induces ROS production, and it can be attenuated by mitochondrial uncoupling. In addition to ATP synthesis, protons are pumped back into the mitochondrial matrix through proton leak and though uncoupling proteins

(UCPs) present in the inner mitochondrial membrane, known as uncoupled respiration (Figure 10). UCPs protect the cells from excess ROS generation and thereby by preventing cellular senescence (Busiello, Savarese, & Lombardi, 2015; Demine, Renard, & Arnould, 2019; Mookerjee, Divakaruni, Jastroch, & Brand, 2010; Zhao et al., 2019).

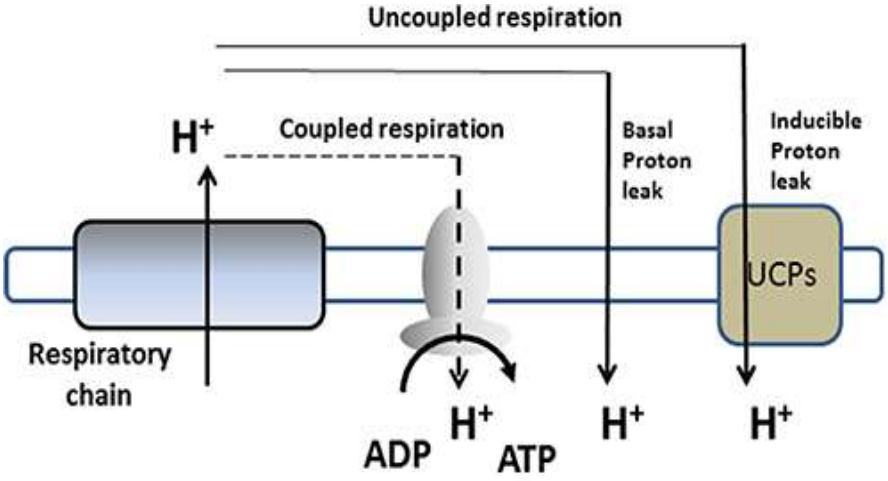


**Figure 10: Mitochondrial uncoupled respiration**

The figure shows ETC induced proton gradient and thereby ATP synthesis (coupled respiration), proton leak and uncoupled respiration (Busiello et al., 2015).

### 1.4.2. Metabolism in cancer cells and Warburg effect

The normal differentiated cells depend mainly on oxidative phosphorylation as an energy source and depend on glycolysis under anaerobic conditions. Cancer cells depend on glycolysis rather than OXPHOS, even in aerobic conditions, a phenomenon known as the ‘ Warburg effect ’. They consume high glucose and secrete high lactate levels. Although the ATP generated by glycolysis is 18 times lower than that by the TCA cycle due to the overall faster kinetics of glycolysis, the final ATP production is similar to the TCA cycle (Shestov et al., 2014). Moreover, the intermediate compounds in the glycolysis provide the building blocks for cell division, such as precursor compounds to synthesize nucleic acids, lipids and amino acids, to promote cell division for highly proliferative cancer cells (Hsu & Sabatini, 2008; Vander Heiden, Cantley, & Thompson, 2009). The AML blast cells exhibit a metabolic reprogramming towards glycolysis under the stromal influence and exhibit

chemoresistance (Mougiakakos, Jitschin, Braun, & Mackensen, 2014). Targetting the Warburg effect by inhibiting glycolysis provides a therapeutic benefit in treating leukemia. Several drugs, including Lonidamine, 2-deoxyglucose (2-DG) and dichloroacetate, have been successfully tested in targeting glycolysis in haematological malignancies (Shanmugam, McBrayer, & Rosen, 2009).

### 1.4.3. Drug targets in metabolism

A wide range of anti-metabolites is successfully used in treating leukemia and various other cancers. Anti-metabolites are compounds that resemble the normal metabolites and act by competitive inhibition and thereby inhibiting enzyme activity and inhibiting DNA replication by incorporating into DNA. Examples include purine and pyrimidine analogues (Luengo, Gui, & Vander Heiden, 2017; M. Tiwari, 2012). Cytarabine, an antimetabolite, is a crucial nucleoside analogue most commonly used in AML treatment is used in this study (section 1.4.3.3). Since most cancers exhibit increased aerobic glycolysis (Warburg effect), several compounds targeting glycolysis have been used. Examples of the glycolysis inhibitors are 2-deoxyglucose, 3-Bromopyruvate, lonidamine, AZD3965, PHAH and TEPP-46 (Ganapathy-Kanniappan & Geschwind, 2013; Luengo et al., 2017; Scatena, Bottoni, Pontoglio, Mastrototaro, & Giardina, 2008). We used Lonidamine targeting glycolysis in the current study (section 1.4.3.2). Tigecycline, a mitochondrial protein synthesis inhibitor, shows therapeutic efficiency with AraC resistant AML cells that present increased OXPHOS (Farge et al., 2017). In addition, we also used metformin, targeting OXPHOS in the current study. Inhibiting glutamine metabolism inhibits tumour progression in some cancers since glutamine metabolism is upregulated in various cancers (Xiang et al., 2015). Various inhibitors targeting serine synthesis, lipid synthesis, nucleotide synthesis were widely established in cancer therapy (Luengo et al., 2017).

#### 1.4.3.1.Metformin

Metformin is a dimethyl biguanide and oral hypoglycaemic compound, widely used in type 2 diabetes. It has both anti-diabetic and antineoplastic effects. The anti-diabetic effect of metformin is by reducing glucose absorption,

decreasing blood glucose levels, and improving insulin sensitivity (Salpeter, Buckley, Kahn, & Salpeter, 2008). It inhibits gluconeogenesis by activating AMP-activated protein kinase (AMPK) and inhibiting mitochondrial glycerophosphate dehydrogenase (mGAPDH) (Madiraju et al., 2014; Pernicova & Korbonits, 2014; Rena, Hardie, & Pearson, 2017). Metformin also inhibits the complex I of the electron transport chain (ETC), decreasing ATP production, increasing ADP: ATP, AMP: ATP ratio, increasing AMP levels, and activating the AMPK pathway (Batandier et al., 2006; Rena et al., 2017). Metformin benefits cancer therapy when treated with standard chemotherapeutic agents and decreases the required dose of chemotherapeutic agents, based on *in-vitro* and *in-vivo* studies (Iliopoulos, Hirsch, & Struhl, 2011; Miranda, Barroso-Sousa, Glasberg, & Riechelmann, 2014). The main anti-cancer effect of metformin targets OXPHOS by inhibiting the complex-I of ETC and AMPK activation. Metformin also shows anti-tumour function by mTOR inhibition through AMPK dependant and independent functions (M. Li, Li, Zhang, & Lu, 2018). In addition, metformin has antiaging, neuroprotective and cardioprotective properties (Y. W. Wang et al., 2017). Various *in-vitro* and *in-vivo* studies show that metformin improves therapeutic efficacy in leukemic treatment (Biondani & Peyron, 2018; Ramos Peñafiel et al., 2013; Scotland et al., 2010). In the current study, we treated leukemic and non-leukemic cells with metformin and measured the therapeutic efficiency in combination with other drugs.

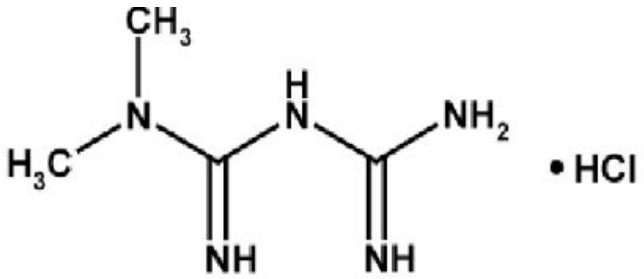


**Figure 11: Structure of metformin hydrochloride (El-Bagary, Elkady, & Ayoub, 2013)**

1.4.3.2. Lonidamine

Many cancer cells exhibit an increased rate of glycolysis (Warburg effect); hence targeting glycolysis is essential. Glucose, the initial substrate for

glycolysis, enters the cells by various glucose uptake transporter proteins (GLUTs) and immediately metabolizes to glucose-6-phosphate by hexokinase to prevent the efflux of glucose. Hexokinase II (HK II), having a high affinity to glucose, is bound to mitochondria by forming a complex with a voltage-dependent anion channel (VDAC). ATP from the mitochondria transfers to HK II -VDAC complex. ATP is the co-substrate and phosphate donor for glucose-6-phosphate synthesis from glucose, catalyzed by HK II (Mathupala, Ko, & Pedersen, 2006). ADP generated by HK II activity controls the mitochondrial membrane potential and ROS levels (da-Silva et al., 2004). Lonidamine [1-(2,4-dichlorobenzyl)-1H-indazole-3-carboxylic acid] is a drug that inhibits HK II activity and aerobic glycolysis. It also inhibits lactic acid export outside the cells by inhibiting monocarboxylate transporter proteins (MCTs) and prevents pyruvate uptake into the mitochondria by inhibiting mitochondrial pyruvate carrier (MPC) (Bhutia, Babu, & Ganapathy, 2016; Nath et al., 2016). In most cancers and leukemia, glycolysis inhibitors show a prominent therapeutic effect combined with other chemotherapeutic agents (Rashkovan & Ferrando, 2019). Although Lonidamine has a low anti-cancer effect when given alone, it showed a synergistic effect when the AML cells were treated with another chemotherapeutic agent, venetoclax (Panina, Pei, Baran, Konopleva, & Kirienko, 2020) and also with a wide range of chemotherapeutic agents in several cancers (Y. Huang et al., 2020). In the current study, we used Lonidamine to improve the therapeutic efficacy of metformin in primary leukemic cells.

#### 1.4.3.3. Cytarabine

Cytarabine, also known as arabinosylcytosine (AraC), is a pyrimidine nucleoside analogue, specifically cytidine analogue. It acts competitively with cytidine and incorporates it into DNA, thereby restricting DNA configuration and preventing DNA replication. Hence, it is effective in highly replicative cells such as cancers (Faruqi & Tadi, 2021). It is the most effective drug against AML, developed a few decades ago, in the early 1960s. It is given as a standard 7+3 induction regimen in treating AML, with seven days of continuous infusion of cytarabine and three days with anthracyclines such as daunorubicin

(Dombret & Gardin, 2016; Faruqi & Tadi, 2021). Over the decades, the treatment strategies of the standard induction regimen have been consistent with few modifications of adding a third drug to the induction, based on the genetic and immunophenotype profile of the patients. In addition, high dose cytarabine was being used as consolidation therapy (Dombret & Gardin, 2016; Faruqi & Tadi, 2021; Magina et al., 2017). Although the conventional high dose AraC provide relapse-free remission in 60-80% of the patients with >60 years of age, several studies based on cohort studies show that a high dose of AraC gives severe side effects, especially with comorbidities and high age (Bishop et al., 1996; Lengfelder et al., 2009; Lowenberg et al., 2011; Reese & Schiller, 2013). A wide range of gene-specific targeted therapy was developed in the past few years, combined with low dose AraC, to enhance its efficacy and reduce toxicity (Daver et al., 2020; Onec et al., 2018). Venetoclax combined with low dose AraC gives a therapeutic benefit in patients above 60 years (Wei et al., 2019). Although AraC treatment gives a high remission rate, many patients exhibit relapse due to chemoresistant leukemic stem cells. These stem cells exhibit resistance to the standard chemotherapeutic regimen due to the high rate of OXPHOS (Farge et al., 2017). Hence, in the current study, we treated the primary leukemic cells from mice with reduced *GFI1* expression with AraC in combination with metformin to see if metformin could improve the efficiency of AraC with low doses.

### 1.5. FOXO proteins

FOXOs are known as forkhead transcriptional factors, and the FOXO proteins include FOXO1, FOXO3, FOXO4 and FOXO6. The expression levels of these proteins vary in various tissues. FOXO proteins can be both the transcriptional activators and repressors, regulating the function of various genes and thereby regulating proliferation, differentiation, oxidative stress, metabolism, inflammation. The FOXO1 and FOXO3 proteins are expressed in most of the tissues. The FOXO proteins share sequence homology and include four common functional domains: forkhead, nuclear export signal, nuclear localization, and transactivation (Figure 12). FOXOs contain nuclear localization and export signals in their protein sequences, which regulate their

transcriptional regulatory activity. Their import into the nuclear promotes the activity while the export to the cytoplasm leads to proteasome degradation. The activity of FOXOs is regulated by phosphorylation, ubiquitination, acetylation and its interaction with other proteins. FOXOs play both the tumour suppressor and tumour promoting functions. FOXO proteins also regulate various metabolic pathways through various other intermediate proteins. The pathways that FOXOs regulate include glycolysis, gluconeogenesis, glutamine, and lipid metabolism pathways (Figure 13) (Y. Wang, Zhou, & Graves, 2014). FOXOs act as tumour suppressors by inhibiting cell proliferation, inhibiting cancer metabolism and promoting apoptosis and senescence (Yadav, Chauhan, Zhuang, & Gan, 2018). FOXOs also act as tumour inducers by maintaining cancer stem cells and inducing chemoresistance in various cancer types. Various signalling pathways regulate them. The PI3K-AKT pathway negatively regulates the activity of FOXOs, while mTORC1 activates FOXOs by inhibiting the PI3K-AKT signalling pathway. FOXOs and c-Myc mutually antagonize each other by various intermediate proteins (Amente et al., 2011; Bouchard, Marquardt, Bras, Medema, & Eilers, 2004; Jensen et al., 2011; Peck, Ferber, & Schulze, 2013; Yadav et al., 2018). FOXOs also form chromosomal translocations, leading to constitutive nuclear localization in cancers such as AML (Fu & Tindall, 2008).

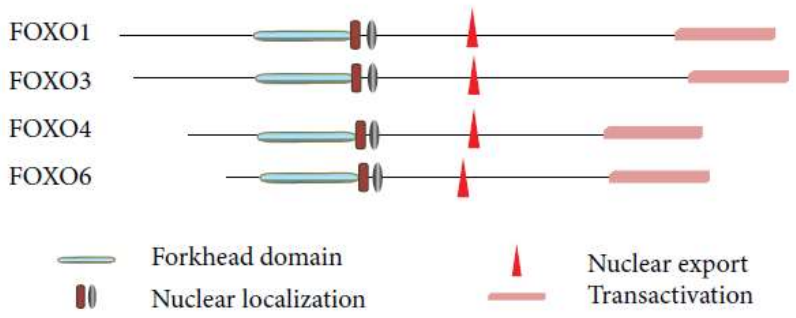


**Figure 12: Structure and functional domains of FOXO proteins.**

The figure shows the homologous domains of FOXO proteins (FOXO1, 3, 4 and 6) (Y. Wang et al., 2014).

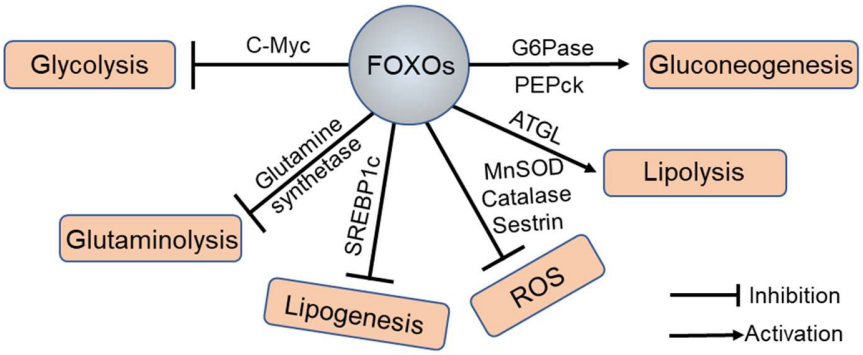


**Figure 13: Metabolism pathways and the intermediate genes regulated by FOXO proteins**

The figure shows the metabolism pathways inhibited and activated by FOXO proteins (Yadav et al., 2018).

### 1.6. C-Myc

*c-Myc* is a master regulator regulating several pathways. It is a helix-loop-helix leucine zipper transcriptional factor, and a proto-oncogene belongs to the *myc* family (Eilers & Eisenman, 2008). A high expression level of *c-Myc* is observed in several cancers (Dang, 2012). C-MYC acts as a transcriptional activator by heterodimerizing with MAX protein (MYC-associated factor X) and binds to the E-box sequence CACGTG of the target gene for activation (Adhikary & Eilers, 2005; Cole & Nikiforov, 2006). While the transcriptional repressor activity of C-MYC is mediated by inhibiting the MIZ-1, a transcriptional activator protein (Kleine-Kohlbrecher, Adhikary, & Eilers, 2006). Several C-MYC target genes were reported previously with diverse cellular functions such as proliferation, metabolism, differentiation and apoptosis (Adhikary & Eilers, 2005; Hartl, 2016; Zeller, Jegga, Aronow, O'Donnell, & Dang, 2003). C-MYC regulates metabolism in distinct ways (Miller, Thomas, Islam, Muench, & Sedoris, 2012). C-MYC stimulates glycolysis and promotes the Warburg effect by directly inducing the expression of several genes such as GLUT1, hexokinase 2 (HK2), phosphofructokinase (PFKM), enolase 1 (ENO1) and lactate dehydrogenase A (LDHA) (Miller et al., 2012), C-MYC is also described to enhance mitochondrial synthesis and also glutamine metabolism (Gao et al., 2009). Increased expression of C-MYC promotes glutamine metabolism and enhances its cellular addiction (Wise et al., 2008). While it also enhances fatty acid biosynthesis by

promoting the synthesis of mitochondrial acetyl Co-A and exporting from the mitochondria to the cytoplasm to synthesise fatty acids (Morrish et al., 2010). A wide range of proteins has been described to regulate C-MYC function. This section explains protein interactions, which play an essential role in the current study.

### 1.6.1. MYC and MXD protein interactions

The MXD family protein (MAX dimerization proteins) such as MXI1 negatively regulates C-MYC function. MXD proteins form complexes with MAX, and the MXD-MAX complexes bind to the C-MYC target genes competitively and inhibit C-MYC function (Grinberg, Hu, & Kerppola, 2004; Hooker & Hurlin, 2006).

### 1.6.2. MYC and FOXO1 interactions

FOXO proteins negatively regulated C-MYC and C-MYC target genes (Bouchard et al., 2004; Peck et al., 2013). Activating the PI3-AKT signalling cascade promotes AKT to phosphorylate FOXO proteins, thereby inactivating the FOXO proteins by cytoplasmic localisation (section 1.5). While the non-phosphorylated, active FOXO proteins negatively regulate the C-MYC activity through various intermediate factors. FOXO proteins activate MXI1 protein by binding to its promoter, thereby inhibiting C-MYC function (Delpuech et al., 2007). FOXO proteins also promote the phosphorylation of C-MYC at the phosphodegron motif and enhance its degradation (Ferber et al., 2012). FOXOs promote the degradation of *C-MYC* mRNA and inhibit protein translation by intermediate miRNAs. Under stress conditions, FOXO downregulates C-MYC proteins through *FILNC1* (FoxO-induced long non-coding RNA 1) (Xiao et al., 2017).

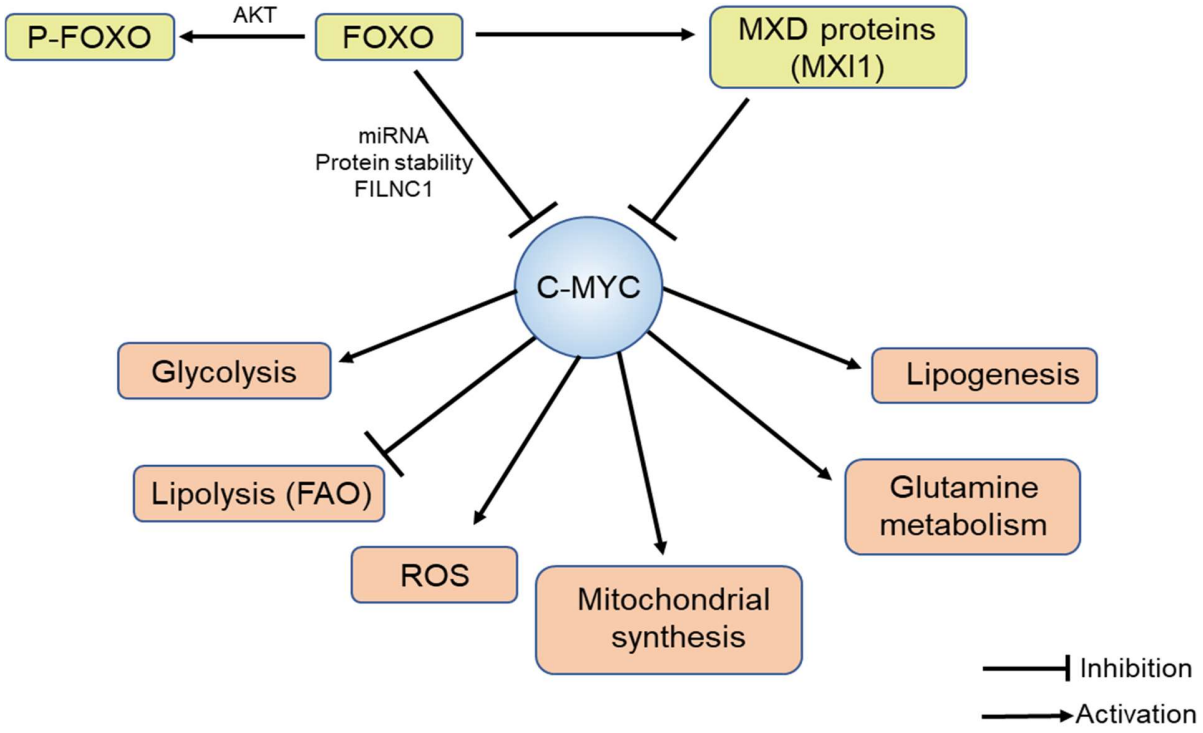


**Figure 14: Proteins regulating C-MYC function and metabolic pathways regulated by C-MYC.**

The figure depicts how FOXO proteins inhibit C-MYC activity and how C-MYC regulates metabolic pathways.

## 2. Objectives

Acute Myeloid Leukemia (AML) is one of the most prevalent leukemias, accounts for 25% of all leukemias in adults and has an increasing incidence rate (Thomas, 2009). A wide range of treatment possibilities was available to treat AML, and several mutational specific targeting drugs have been developed in the past two decades (Medinger, Lengerke, & Passweg, 2016). However, the standard first-line therapy regimen, on the other hand, remains unchanged (Dombret & Gardin, 2016; Kantarjian et al., 2021), and the overall treatment outcome remains poor (Bhatnagar et al., 2020; Thomas, 2009; Van Weelderen, Klein, Natawidjaja, De Vries, & Kaspers, 2021; Y. L. Yang et al., 2021). The high relapse rate despite a high rate of remission (Yilmaz et al., 2019) and chemoresistance is the primary concern with the current treatment strategies (Yilmaz et al., 2019; J. Zhang, Gu, & Chen, 2019). The accumulation of chemoresistant clones after chemotherapy significantly contributes to the high relapse rate (Vosberg & Greif, 2019). An essential factor for the chemoresistance development in AML is the altered metabolism pathways (Farge et al., 2017; Song et al., 2016). Several drugs targeting metabolic pathways have been established to provide additional therapeutic options in addition to the standard regimens (Castro, Sampaio-Marques, & Ludovico, 2019; Stuani, Sabatier, & Sarry, 2019).

Along with the metabolic factors, transcriptional regulators play a crucial role in AML development (Assi et al., 2019; Takei & Kobayashi, 2019). Growth Factor Independence 1 (GFI1) is one such transcriptional factor whose low expression levels are associated with a poor prognosis and poor therapeutic outcome in AML (Fraszczak et al., 2019). A recent report also shows that *GFI1* expression levels have metabolic significance (Fraszczak et al., 2019). However, the elaborate metabolic changes associated with expression levels of *GFI1* are still unexplored. Inquisition of the metabolic changes could open up new therapeutic options to treat patients with a low level of *GFI1* expression.

Hence, we aim to explore the following aspects in the current study:

- To investigate how the expression levels of *GFI1* regulate the metabolic changes in non-leukemic and leukemic aspects.
- To inspect the dependency of metabolic pathways such as glycolysis, fatty acid oxidation and glutamine metabolism with enhanced and reduced *GFI1* expression.
- To explore if any of the existing drugs targeting the metabolic pathways could be a therapeutic advantage to treat AML cells expressing a low level of *GFI1*.
- To investigate if any drugs targeting the metabolic pathways could increase the therapeutic efficiency when combined with the existing therapeutic regimen to treat AML cells with a low level of *GFI1* expression.

# 3. Materials

## 3.1. Consumables

**Table 3:List of consumables used**

| Consumable | Catalog No | Company |
|---|---|---|
| 10 µl TipOne® Filter tips | S1121-3810 | STARLAB GmbH |
| 10 µl TipOne® tips | S1111-3800 | STARLAB GmbH |
| 100 µl TipOne® Filtertips | S1183-1840 | STARLAB GmbH |
| 100 µl TipOne® UltraPoint Filtertips | S1123-1840 | STARLAB GmbH |
| 1000 µl TipOne® Filtertips | S1126-7810 | STARLAB GmbH |
| 1000 µl TipOne® Filtertips | S1111-6800 | STARLAB GmbH |
| 15 mL PP Centrifuge Tubes | 430791 | Corning |
| 200 µl TipOne® Filtertips | S1120-8810 | STARLAB GmbH |
| 200 µl TipOne® UltraPoint tips | S1113-1800 | STARLAB GmbH |
| 24-well Flat Bottom Not Treated Cell Culture Plate | 351147 | Corning |
| 48-well Flat Bottom Not Treated Cell Culture Plate | 351178 | Corning |
| 50 mL PP Centrifuge Tubes | 430291 | Corning |
| Adhesion -microscope slide SuperFrost® plus | 03-0060 | R. Langenbrinck |
| BD Discardit™ II Syringes 20 ml | 300296 | Becton Dickinson |
| BD Discardit™ II Syringes 5 ml | 309050 | Becton Dickinson |
| BD Discardit™ II Syringes10 ml | 309110 | Becton Dickinson |
| BD MicroFine™+ Insulin Syringes | 324824 | Becton Dickinson |
| BD Microlance 3 cannula 20G | 301300 | Becton Dickinson |
| BD Microlance 3 cannula 25G | 300400 | Becton Dickinson |
| BD Microlance 3 cannula 27G | 302200 | Becton Dickinson |
| BD Plastipak Insulin syringes without cannula 1 ml | 303173 | Becton Dickinson |
| BD Plastipak™ syringe with mit Luer-system, 1ml | 300013 | Becton Dickinson |
| Blunt-End Needles, 16 Gauge | 28110 | STEMCELL Technologies |
| Cell culture dishes, PS, 100/20 MM | 664160 | Greiner Bio-One |
| Cell culture dishes, PS, 145/20 MM | 639160 | Greiner Bio-One |
| Cell culture flasks, 175 cm² sterile | 660175 | Greiner Bio-One |
| Cell culture flasks, 25 cm² sterile | 690175 | Greiner Bio-One |
| Cell culture flasks, 75 cm² sterile | 658175 | Greiner Bio-One |
| Cell culture Microplate, 96 Well, TC | 655180 | Greiner Bio-One |
| Cell culture Multiwell Plate, 12 Well PS sterile TC | 665180 | Greiner Bio-One |
| Cell culture Multiwell Plate, 24 Well TC | 662160 | Greiner Bio-One |
| Cell culture Multiwell Plate, 48 Well, TC | 677180 | Greiner Bio-One |
| Cell culture Multiwell Plate, 6 Well, TC | 657160 | Greiner Bio-One |
| Cell strainers 40 µm Filter | 542040 | Becton Dickinson |

| | | |
|---|---|---|
| Cell strainers, 100 µm Filter | 542000 | Greiner Bio-One |
| CellTrics disposable filters 100 µm | 04-00422318 | Sysmex |
| Coverglass | Z692263-100EA | Sigma-Aldrich |
| Coverglass, strength 1 | BB02200500A 113MNT0 | Thermo Fisher Scientific |
| CryoPure Tube 1.6ml white | 72.380 | Sarstedt |
| Cytospin slide | 27157 | Thermo Fisher Scientific |
| DNA LoBind Tubes, 1,5ml | 30108051 | Eppendorf |
| FACS-reaction tubes 5-ml | 352052 | Falcon |
| Falcon® 100 µm Cell Strainer | 352360 | Corning |
| Immobilon-E PVDF Membrane | IEVH00005 | Merck Millipore |
| ImmunoSelect Adhesion Slides | SQ-IS-10050 | Squarix biotechnology |
| LS Columns | 130-042-401 | Miltenyi Biotec |
| Microamp™ fast, optical 96-Well-reaction microtiter plate | 4346907 | Applied Biosystems |
| MicroAmp™ Optical Adhesive Film | 4311971 | Thermo Fisher Scientific |
| MiniCollect® RÖHRCHEN 0,25/0,5 ml K3E K3EDTA | 450530 | Greiner Bio-One |
| Mini-Collect-blood collection tubes, K3EDTA | 450476 | Greiner Bio-One |
| Pre-Separation Filters (30 µm) | 130-041-407 | Miltenyi Biotec |
| Reaction tube PCR 0,2ml PP | 683201 | Greiner Bio-One |
| Röhre 15ml V-Boden PP | 62554502 | Sarstedt |
| Röhre 50ml V-Boden PP | 62547254 | Sarstedt |
| SafeSeal reaction vessel 1,5 ml | 72706 | Sarstedt |
| Sample tube 75 x 12 mm | 551.579 | Sarstedt |
| STEMgrid™-6 | 27000 | STEMCELL Technologies |
| Stripette™ Serological Pipets 10 ml | 4488 | Corning |
| Stripette™ Serological Pipets 25 ml | 4489 | Corning |
| Stripette™ Serological Pipets 50 ml | 4490 | Corning |
| Stripette™ Serological Pipets. 5 ml | 4487 | Corning |
| SuperFrost Ultra Plus™ GOLD adhesion slides | 11976299 | Thermo Fisher Scientific |
| Syringe filter 0.2 µm | 831.826.001 | Sarstedt |
| Syringe filter 0.45µm | 831.826 | Sarstedt |
| Western Blotting Filter Paper, 7 cm x 8.4 cm | 84783 | Thermo Fisher Scientific |

## 3.2. Chemicals and reagents

**Table 4: List of chemicals used**

| Chemical / Reagent | Catalog No | Company |
|---|---|---|
| (+)-Etomoxir sodium salt hydrate | E1905 | Sigma-Aldrich |
| (±)-Verapamil -hydrochloride | V4629-1G | Sigma Aldrich |
| 100 bp DNA Ladder | N3231L | New England Biolabs |
| 1M HEPES | 15630080 | Thermo Fisher Scientific |
| 25mM MgCl2 | A3511 | Promega |
| 2-Deoxy-D-glucose | D8375 | Sigma-Aldrich |
| 5X Green GoTaq® Reaction Flexi Buffer | M891A | Promega |
| Acetic Acid | A0820 | AppliChem |
| Agarose | 16500-500 | Invitrogen |
| Agarose | 1138899101 | Roche |
| Albumin Fraction V | 8076.2 | Carl Roth |
| Ampicillin Sodium Salt | A9518 | Sigma-Aldrich |
| Annexin V Binding Buffer | 556454 | BD Biosciences |
| Antimycin A | A8674 | Sigma-Aldrich |
| Aqua ad iniectabilia 10 ml miniplasco | 1001346 | B Braun |
| Aqua B. Braun | 0082423E | B Braun |
| Baytril 10% | PZN-05978897 | Bayer |
| BglII | R0144S | New England Biolabs |
| BPTES | SML0601 | Sigma-Aldrich |
| BSA Fraction V | K41-001 | PAA Laboratories |
| CD117 MicroBeads, mouse | 130-091-224 | Miltenyi Biotec |
| CellROX™ Deep Red Reagent | C10422 | Thermo Fischer |
| Corning™ Cell-Tak Cell and Tissue Adhesive | 10317081 | Fischer Scientific |
| COULTER CLENZ® Cleaning Agent | 8448222 | Beckman Coulter |
| COULTER® Z1 & Z2 Balanced electrolyte solution | 8320312 | Beckman Coulter |
| Cytarabine | S1648 | Selleckchem |
| D-(+)-Glucose solution | G8769 | Sigma Aldrich |
| DAPI | 32670 | Sigma-Aldrich |
| Dimethyl sulfoxide anhydrous | 276855 | Sigma Aldrich |
| Dimethylsulfoxide (DMSO) for cell culture | P60-36720100 | PAN Biotech |
| dNTP Mix | U1511 | Promega |
| Doxycycline Hyclate | D9891 | Sigma-Aldrich |
| DPBS | 14190 | Gibco |
| EDTA | E9884 | Sigma-Aldrich |
| Ethanol | 32205 | Sigma-Aldrich |

| | | |
|---|---|---|
| Ethanol, 96%, 2,5l, Plastic | P075.4 | Carl Roth |
| Ethylenediaminetetraacetic acid disodium salt dihydrate | E5134 | Sigma-Aldrich |
| FACS Clean | 340345 | BD Biosciences |
| FACS Flow | 10638814 | BD Biosciences |
| FACS Rinse | 340346 | BD Biosciences |
| FCCP | C2920 | Sigma-Aldrich |
| FCS | P30-3702 | PAN Biotech |
| Formaldehyde | F8775 | Sigma-Aldrich |
| GeneRuler 1 kb Plus DNA Ladder | SM1331 | Thermo Fisher Scientific |
| Glycerol | G5516 | Sigma-Aldrich |
| Glycine | 3790.2 | Carl Roth |
| GoTaq® Hot Start Polymerase | M5005 | Promega |
| Halt™ Protease Inhibitor Cocktail, EDTA-Free (100X) | 78437 | Thermo Fisher Scientific |
| HCl | Z00206816 | Merck Millipore |
| HindIII-HF | R3104S | New England Biolabs |
| Hoechst 33342 Solution (20mM) | 62249 | Thermo Fischer |
| Hydrochloric Acid 32 % | X896.1 | Carl Roth |
| KCl | P9541 | Sigma-Aldrich |
| LB Broth | L3022 | Sigma-Aldrich |
| LB Broth Agar | L2897 | Sigma-Aldrich |
| LB-Medium | X968.2 | Carl Roth |
| Leupeptin | L2884-.5MG | Sigma-Aldrich |
| L-Glutamine Solution 200 mM | 59202C-100ML | Sigma Aldrich |
| Lonidamine | L4900 | Sigma Aldrich |
| Lumi-Light Western Blotting Substrate | 12015200001 | Roche |
| Luna® Universal qPCR Master Mix | M3003S | New England Biolabs |
| Magnesium chloride solution | 68475-100ML-F | Sigma-Aldrich |
| Metformin Hydrochloride | PHR1084 | Sigma Aldrich |
| Methanol | 322415 | Sigma-Aldrich |
| $MgCl_2$ | M8266 | Sigma-Aldrich |
| Milk Powder | T145.2 | Carl Roth |
| MitoTracker™ Deep Red FM | M22426 | Thermo Fischer |
| Mouse IL-3 | 130-096-687 | Miltenyi Biotec |
| Mouse IL-6 | 130-094-065 | Miltenyi Biotec |
| Mouse SCF | 130-101-741 | Miltenyi Biotec |
| $Na_2EDTA$ | E5134 | Sigma-Aldrich |
| NaCl | 1064040500 | Merck Millipore |
| NaOH Powder | S3014 | Sigma-Aldrich |
| NEBuffer Pack for T4 DNA Ligase | B0202S | New England Biolabs |
| N-Lauryl Sarcosine Sodium Salt | L5125 | Sigma-Aldrich |
| Nuclease-Free Water (not DEPC-Treated) | AM9938 | Thermo Fisher Scientific |

| | | |
|---|---|---|
| NuPAGE Antioxidant | NP0005 | Invitrogen |
| NuPAGE SDS Sample Buffer 4x | NP0007 | Invitrogen |
| NuPAGE™ Sample Reducing Agent (10X) | NP0009 | Invitrogen |
| Oligomycin | O4876 | Sigma-Aldrich |
| One Shot™ ccdB Survival™ 2 T1R Competent Cells | A10460 | Thermo Fischer |
| One Shot™ TOP10 chemically competent E. coli | C404010 | Invitrogen |
| PageRuler Prestained Protein Ladder | 26616 | Thermo Fisher Scientific |
| Penicillin-Streptomycin | P4333 | Sigma-Aldrich |
| Pharm Lyse | 555899 | BD Biosciences |
| PhosphoSafe™ Extraction Reagent | 71296-3 | Merck Millipore |
| PhosSTOP™ | 4906845001 | Sigma-Aldrich |
| PMSF Protease Inhibitor | 36978 | Thermo Fisher Scientific |
| Polybrene Infection/Transfection Reagent | TR-1003-G | Merck Millipore |
| Poly-D-lysine hydrobromide (PDL) | P6407 | Sigma-Aldrich |
| Polyethylenimine, Linear, MW 25,000 (PEI 25000) | 23966-2 | Polysciences |
| Polyinosinic–polycytidylic acid sodium salt | P0913-50MG | Sigma Aldrich |
| Power SYBR™ Green PCR-Master-Mix | 4367659 | Thermo Fischer |
| Primers and shRNA (Table 11, Table 12 and Table 14) | - | Eurofins |
| Propidium Iodide | P-4170 | Sigma-Aldrich |
| Propidium Iodide Staining Solution | 51-66211E | BD Biosciences |
| Proteinase K | 1008236 | Carl Roth |
| Proteinase K | 17916 | Thermo Fisher Scientific |
| Puromycin | P9620 | Sigma-Aldrich |
| Quick-Load Purple 100 bp DNA Ladder | N0551L | New England Biolabs |
| Radiance Plus | 512103 | Azure Biosystems |
| Retronectin | T100A | Takara Bio |
| RetroNectin | T100B | Takara Bio |
| RNase-Free DNase Set | 79254 | Qiagen |
| Rotenone | R8875 | Sigma-Aldrich |
| ROTI®GelStain | 3865.1 | Carl Roth |
| Rotiphorese Gel (Acrylamide/Bis-acrylamide) | T802.1 | Carl Roth |
| SDS Pellets, 250 g | CN30.1 | Carl Roth |
| Seahorse XF Calibrant | 100840-000 | Agilent Technologies |

| | | |
|---|---|---|
| SeeBlue® Plus2 Pre-stained Protein Standard | LC-5925 | Thermo Fisher Scientific |
| Sodium bicarbonate | S6014 | Sigma-Aldrich |
| Sodium Butyrate | 303410 | Sigma-Aldrich |
| Sodium Chloride | 9265.1 | Carl Roth |
| Sodium pyruvate solution 100 mM | S8636 | Sigma Aldrich |
| ST1326 | 870853P | Sigma-Aldrich |
| Sterile destilled water | 123 | B Braun |
| T4 DNA Ligase | 15224-025 | Thermo Fischer |
| TaqMan Gene Expression Master Mix | 4369016 | Applied Biosystem |
| Tris | 5429.5 | Carl Roth |
| TrisCl | T1503 | Sigma-Aldrich |
| Triton X-100 | X100 | Sigma-Aldrich |
| Trypan Blue | T8154 | Sigma-Aldrich |
| Trypsin-EDTA (0.25 %), Phenol Red | 25200072 | Gibco |
| Tween-20 | P9416 | Sigma-Aldrich |
| UK5099 | PZ0160 | Sigma-Aldrich |
| β-Mecaptoethanol | M3148 | Sigma-Aldrich |

### 3.3. Kits

**Table 5: List of Kits used**

| Name of the Kit | Catalog No | Company |
|---|---|---|
| Clariom™ S Assay, human | 902926 | Thermo Fisher Scientific |
| High-Capacity cDNA Reverse Transcription Kit with RNase Inhibitor, Applied Biosystems™ | 4374966 | Thermo Fisher Scientific |
| Lineage Cell Depletion Kit, mouse | 1012358 | Miltenyi Biotec |
| MTT Assay Kit (Cell Proliferation) | ab211091 | Abcam |
| NE-PER Nuclear and Cytoplasmic Extraction Reagents | 78833 | Thermo Fisher Scientific |
| Nucleobond Xtra midi plus Kit | 740412.50 | Macherey-Nagel |
| NucleoSpin RNA, Mini Kit for RNA purification | 740955250 | Macherey-Nagel |
| Pierce BCA Protein Assay Kit | 23225 | Thermo Fisher Scientific |
| QIAquick Gel Extraction Kit | 28704 | Qiagen |
| Rneasy Micro Kit | 74004 | Qiagen |
| Rneasy Mini Kit | 74104 | Qiagen |
| Seahorse XFe96 FluxPak | 102416-100 | Agilent Technologies |
| Seahorse XFp FluxPak | 103022-100 | Agilent Technologies |
| TMRE-Mitochondrial Membrane Potential Assay Kit | ab113852 | Abcam |

### 3.4. Buffers

**Table 6: List of buffers used with their composition and methods**

| Name | Composition | Method |
|---|---|---|
| 10x TBS-Buffer | 1 l H2O + 24,23 g Tris (200 mM) + 87,66 g NaCl (1,5 M) pH: 7,4 | Western Blot |
| 10x TG- Buffer | 1 l $H_2O$ + 30 g Tris + 144 g Glycine + 10 g SDS | Western Blot |
| 1x Annexin-Binding Buffer | Annexin V Binding Buffer (10x) diluted at 1:10 in PBS | FACS staining |
| 1x SDS-Running Buffer | 200 ml 5x SDS-Running Buffer + 800 ml dest. H2O | Western Blot |
| 1x TBS-T- Buffer | 100 ml 10x TBS-Buffer + 900 ml dest. $H_2O$ + 1 ml Tween- 20 | Western Blot |
| 1x TG- Buffer | 200 ml abs. Ethanol + 100 ml 10x TG-Buffer + 700 ml dest. $H_2O$ | Western Blot |
| 5% Milk | 5 g Milk Powder in 100ml 1x TBS-T Buffer | Western Blot |
| 50x TAE Buffer | 2,0 M Tris + 0,05 M $Na_2EDTA$ + 1,0 M acetic acid pH: 8,3 | Gel Electrophoresis |
| 5x SDS-Running Buffer | 1 l dest. $H_2O$ + 15,1 g Tris (125 mM) + 72 g Glycin + 25 ml 20%iges SDS | Western Blot |
| Erylyse-Buffer | BD Pharm Lyse (10x) diluted at 1:10 in sterile $H_2O$ | Erythrocytes lysis of mice BM cells |
| FACS- Buffer | PBS + 2,5 % FBS +1% P/S | FACS washing and staining |
| Freezing Medium for cell lines | RPMI + 20% FBS + 10% DMSO | Freezing cells |
| Freezing Medium for primary cells | IMDM + 20% FBS + 10% DMSO | Freezing cells |
| HBS-Buffer | 1,4 mM $Na_2HPO_4$ + 42 mM HEPES + 10mM KCl + 274 mM NaCl + 11 mM Glucose in $H_2O$ pH: 7,05 | Retrovirus Production |
| Lysis Buffer | Lysis Buffer (Stock Solution) diluted 1:10 with nuclease free $H_2O$ | Mouse genotyping |
| Lysis Buffer | 10mM Tris-HCL PH 7,5 + 50mM NaCl + 6,25mM MgCl2 + 0,045% NP40 + 0,45% Tween 1mg/ml proteinase K was added freshly on the day of lysis | To lyse the cells for mitochondrial DNA quantification (de Almeida, Luchsinger, Corrigan, Williams, & Snoeck, 2017) |
| Lysis Buffer (Stock Solution) | 100 ml DNA-freies $H_2O$+ 100 mM Tris-HCl + 500 mM KCl + 20 mM $MgCl_2$ + 0,01% Gelantine + 0,45% Tween-20 + | Mouse genotyping |

| | | |
|---|---|---|
| | 0.45 NP-40 + 500 µg/ml Proteinase K pH:8,2 - 8,3 | |
| MACS Buffer | PBS + 0,5% BSA + 2 mM EDTA | Isolation of lineage depleted cells from mice |
| RIPA Buffer | 50 mM Tris (pH:8) + 150 mM NaCl + 1% NP-40 + 0,5 % Sodium deoxycholate + 0,1% SDS in $H_20$ | Protein-Isolation |
| RLT Buffer | 1 ml RLT-Buffer (Qiagen) + 10 µl β-Mecaptoethanol | RNA-Isolation |
| S.O.C. Medium | 500 ml H2O + 2,5 g Yeast Extract + 0,25 g NaCl -> autoclave and then add 1,25 ml 1 M KCl + 5 ml 1 M $MgCl_2.6H_20$ + 3,6 ml 50 % Glucose solution | Transformation |
| SCM (Stem cell medium) | IMDM + 20% FBS + 1% P/S + 10 ng/ml IL-3 + 10 ng/ml Il-6 + 20 ng/ml mSCF | Culturing of primary cells |
| Separation buffer | 500 ml dest. $H_20$ + 90,9 g Tris (375 mM)+ 10 ml 20%iges SDS pH: 8,8 | SDS-Gel (western blot) |
| Stacking buffer | 250 ml dest. $H_20$ + 15,15 g Tris (32 mM) + 5 ml 20%iges SDS pH: 6,8 | SDS-Gel (western blot) |

### 3.5. Media

**Table 7: List of media used**

| Medium | Catalog No | Company |
|---|---|---|
| DMEM Media high glucose | 41965-039 | Gibco |
| IMDM | 1023936 | Gibco |
| MethoCult™ H4434 Classic | 4434 | StemCell Technologies |
| MethoCult™ GF M3434 | 3434 | StemCell Technologies |
| RPMI 1640 | 21875-034 | Thermo Fisher Scientific |
| Seahorse XF base medium | 103334-100 | Agilent Technologies |

### 3.6. Antibodies for FACS analysis

**Table 8: List of antibodies used for FACS analysis**

| Antibody | Fluoro-chrome | Catalog No | Company |
|---|---|---|---|
| Annexin V | APC | 640920 | BioLegend |
| Annexin V | PerCP Cy5.5 | 640936 | BioLegend |
| anti-mouse CD117 (c-Kit) Antibody | PE | 135106 | BioLegend |
| anti-mouse CD117 (c-Kit) Antibody | APC | 105811 | BioLegend |
| anti-mouse CD4 Antibody | PerCP Cy5.5 | 100433 | BioLegend |
| anti-mouse CD8a Antibody | PE | 100708 | BioLegend |
| anti-mouse CD8a Antibody | APC | 100711 | BioLegend |
| anti-mouse Ly-6G/Ly-6C (Gr-1) Antibody | PerCP Cy5.5 | 108427 | BioLegend |
| anti-mouse Ly-6G/Ly-6C (Gr-1) Antibody | PE | 108408 | BioLegend |
| anti-mouse Ly-6G/Ly-6C (Gr-1) Antibody | APC | 108411 | BioLegend |
| anti-mouse TER-119/Erythroid Cells Antibody | PE | 116208 | BioLegend |
| anti-mouse TER-119/Erythroid Cells Antibody | APC | 116211 | BioLegend |
| anti-mouse/human CD11b Antibody | PerCP Cy5.5 | 101228 | BioLegend |
| anti-mouse/human CD11b Antibody | APC | 101211 | BioLegend |
| anti-mouse/human CD45R/B220 Antibody | PerCP Cy5.5 | 103234 | BioLegend |
| Purified Rat Anti-Mouse CD16/CD32 (Mouse BD Fc Block™) | - | 553141 | BD Pharmingen™ |

**Table 9: List of antibodies used for western blot**

| Antibody | Catalogue no | Dilution | Milk or BSA | Primary or secondary | Company |
|---|---|---|---|---|---|
| Anti-mouse (goat) IgG HRP | sc-2005 | 1:2000 | 5% Milk | Secondary | Santa Cruz |
| C-MYC | Ab32072 | 1:1000 | 5% Milk | Primary | Abcam |
| donkey anti-goat IgG-HRP | sc-2020 | 1:5000 | 5% Milk | Secondary | Santa Cruz |
| FOXO1 | 14952T | 1:1000 | 5% Milk | Primary | Cell Signalling technology |
| GFI-1 Antibody | AF3540 | 1:2000 | 5% Milk | Primary | R&D Systems |
| mouse anti-goat IgG-HRP | sc-2354 | 1:5000 | 5% Milk | Secondary | Santa Cruz |
| mouse anti-rabbit IgG-HRP | sc-2357 | 1:2000 | 5% Milk | Secondary | Santa Cruz |
| VCP antibody | ab11433 | 1:2000 | 5% Milk | Primary | Abcam |

### 3.7. Primers and Taqman probes

**Table 10: List of Taqman probes used for RT-PCR**

| Gene | Primer ID | Company |
|---|---|---|
| C-MYC (Human) | Hs00153408_m1 | Thermo Fischer Scientific |
| c-Myc (Mouse) | Mm00487804_m1 | |
| GAPDH (Human) | Hs04420697_g1 | |
| Gapdh (Mouse) | Mm99999915_g1 | |
| GFI1 (Human) | Hs00382207_m1 | |
| Gfi1 (Mouse) | Mm00515853_m1 | |
| HPRT (Human) | Hs00172187_m1 | |
| Hprt (Mouse) | Mm03024075_m1 | |

**Table 11: List of PCR primers used**

| Name | Sequence (5'-3') | Function | Host | Reference |
|---|---|---|---|---|
| ActinB_F | CGGCTTGCGGGTGTTAAAAG | Nucleus specific genes for mitochondrial DNA quantification | Mouse | (de Almeida et al., 2017) |
| ActinB_R | CGTGATCGTAGCGTCTGGTT | | Mouse | |
| Beta-2-Microglobulin F | TGCTGTCTCCATGTTTATGTATCT | | Human | |
| Beta-2-Microglobulin R | TCTCTGCTCCCCACCTCTAAGT | | Human | |
| Cytochrome-b F | CTTCATGTCGGACGAGGCTTA | Mitochondrial specific genes for mitochondrial DNA quantification | Mouse | (de Almeida et al., 2017) |
| Cytochrome-b R | TGTGGCTATGACTGCGAACA | | Mouse | |
| tRNA Leucine F | CACCCAAGAACAGGGTTTGT | | Human | |
| tRNA Leucine R | TGGCCATGGGTATGTTGTTA | | Human | |
| GFI1 F | AACAGCTAGCGCCACCAT GCCGCGCTCATTTCTC | Cloning and Sequencing | Human | (Hones et al., 2017) |
| GFI1 R | CTATTGGATCCTCATTTGA GCCCATGCTGC | Cloning and Sequencing | Human | |
| Additional Bases | Restriction Site | | Kozak Sequence | |
| FOXO1 F | TTCAATTCGCCACAATCTGTCC | RT-PCR | Mouse | (X. Zhang et al., 2011) |
| FOXO1 F | CTACGAGTGGATGGTCAAGAGC | RT-PCR | Human | (Sequence retreived from Origene CAT#: HP205770) |
| FOXO1 R | GGGTGATTTTCCGCTCTTGC | RT-PCR | Mouse | (X. Zhang et al., 2011) |
| FOXO1 R | CCAGTTCCTTCATTCTGCACACG | RT-PCR | Human | (Sequence retreived from Origene CAT#: HP205770) |
| GAPDH F | CCTGCACCACCAACTGCTTA | RT-PCR | Mouse | Designed using NCBI primer blast tool |
| GAPDH F | GAAGGTGAAGGTCGGAGTC | RT-PCR | Human | |
| GAPDH R | TCATGAGCCCTTCCACAATG | RT-PCR | Mouse | |
| GAPDH R | GAAGATGGTGATGGGATTTC | RT-PCR | Human | |
| pMSCV F | CCCTTGAACCTCCTCGTTCGACC | shRNA Sequencing | Human | Sequence received |

| | | | | |
|---|---|---|---|---|
| pMSCV R | GAGACGTGCTACTTCC ATTTGTC | shRNA Sequencing | Human | from Prof. Dr. Med. Georg Lenz (Davis et al., 2010; Erdmann et al., 2017; Ngo et al., 2006) |
| mGfi21 | CTTGTGGCAGAGTTCT GGAG | Genotyping | Mouse | (Khandanpou r et al., 2012) |
| mGfi28 | CTTGTTTGAAGTATTC AGGTCTG | Genotyping | Mouse | |
| mGfi32 | GCACACATTCCCAACT AATCC | Genotyping | Mouse | |
| neo1500 | ATCGCCTTCTATCGCCT TCTTGACGAG | Genotyping | Mouse | |

**Table 12: List of PCR primers used for mycoplasma testing**

| | Name | Sequence (5'-3') | Reference |
|---|---|---|---|
| Forward Primers | Myco-F-1 | CGCCTGAGTAGTACGTTCGC | (Uphoff & Drexler, 2002, 2004) |
| | Myco-F-2 | CGCCTGAGTAGTACGTACGC | |
| | Myco-F-3 | TGCCTGAGTAGTACATTCGC | |
| | Myco-F-4 | TGCCTGGGTAGTACATTCGC | |
| | Myco-F-5 | CGCCTGGGTAGTACATTCGC | |
| | Myco-F-6 | CGCCTGAGTAGTATGCTCG | |
| Reverse Primers | Myco-R-1 | GCGGTGTGTACAAGACCCGA | |
| | Myco-R-2 | GCGGTGTGTACAAAACCCGA | |
| | Myco-R-3 | GCGGTGTGTACAAACCCCGA | |

### 3.8. Plasmids

**Table 13: List of plasmids used and their function**

| Plasmid | Function | Virus Type | Reference |
|---|---|---|---|
| pRSMX-PG | Expression plasmid backbone | Retrovirus | Plasmids received from Prof. Dr. Med. Georg Lenz (Davis et al., 2010; Erdmann et al., 2017; Ngo et al., 2006) |
| pHIT60 | Helper plasmid | Retrovirus | |
| pHit EAG | Envelope plasmid | Retrovirus | |
| pCL6IEGwo | Expression plasmid backbone | Lentivirus | (Hones et al., 2017) |
| pCL6IEGwo_*GFI136S* | Expression plasmid cloned with the human *GFI1* coding sequence | Lentivirus | |
| pCD NL-BH | Helper plasmid | Lentivirus | |
| pCO-PE | Envelope plasmid | Lentivirus | |
| *MCSV-MLL-AF9-IRES-GFP* | Expression plasmid cloned with the human *MLL-AF9* fusion gene | Retrovirus | (Hönes et al., 2013; Hones et al., 2016) |
| *MCSV- AML1-ETO9a -IRES-GFP* | Expression plasmid cloned with the human *AML1-ETO9a* fusion gene | Retrovirus | |
| pCL-Eco | Helper and Envelope plasmid | Retrovirus | |

### 3.9. shRNA

**Table 14: List of shRNAs used in this study**

| Name | RNAi sequence (5'-3') (Sense Strand) | Function | Target |
|---|---|---|---|
| SCR(Pongas, Annunziata, & Staudt, 2017) | CTCTCAACCCTTTAAATCTGA | Scrambled Sequence | None |
| GFI1 *KD*1 | GCTGAACAGTTACTTCAAAGA | *KD* of GFI1 | 3'UTR of GFI1 |
| GFI1 *KD*2 | GAGCTTTGACTGTAAGATCTG | *KD* of GFI1 | CDS of GFI1 |
| GFI1 *KD*3 | CGAGCAGACAGCACTTCAAAT | *KD* of GFI1 | CDS of GFI1 |
| **shRNA structure sequence** | | | |
| shRNA loop sequence | | TTCAAGAGA | |
| 5' overhang sequence for the sense strand | | GATCCC | |
| 5' overhang sequence for anti-sense strand | | AGCTAAAAA | |
| 3' overhang sequence for the sense strand | | TTTTT | |
| 3' overhang sequence for anti-sense strand | | GG | |

### 3.10. Instruments

**Table 15: List of instruments used**

| Instrument | Company |
|---|---|
| Amersham Imager 600 | GE Healthcare LifeSciences |
| Animal Blood Counter | scil Vet abc |
| Attune NxT | Invitrogen |
| Cat-ST5 | Cat |
| Centriuge 4K15 | Sigma Laboratory Centrifuges |
| Centriuge 5415D | Eppendorf |
| Centriuge 5417R | Eppendorf |
| Centriuge Allegra 6KR | Beckman Coulter |
| Centriuge Allegra RX-15R | Beckman Coulter |
| Centriuge Allegra X-15R | Beckman Coulter |
| Centriuge Mikro 200R | Hettich Centrifuges |
| Centriuge Rotanta 460R | Hettich Centrifuges |
| CHEMOSTAR Touch ECL & Fluorescence Imager | Intas Science Imaging |
| CoolCell | BioCision |
| Cytospin 2 | Shandon |
| Dry Bath System | StarLab |
| EG 2200-2NM | Kern & Sohn Gmbh |
| Electrophoresis Sub-Cell GT | Bio-RAD |
| FACSAria II | BD Biosciences |
| FACSAria III Cell Sorter | BD Biosciences |
| FACScan | BD Becton Dickinson |
| FACSDiva | BD Biosciences |
| Faxitron CP-160 | Faxitron |
| Foam Pads for Mini Trans-Blot® Cell | Bio-Rad |
| Gel iX20 Imager | INTAS Science Imaging |
| Hemocytometer (Neubauer) | Assistent |
| Heracell 150i $CO_2$ Incubator | Thermo Fisher Scientific |
| HERASafe | Kendro Laboratory |
| IKA KS 4000 I control | IKA |
| iMark Microplate reader | Bio-Rad |
| Infinite® 200 PRO | TECAN |
| KNF Laboport® mini-pump | Sigma-Aldrich |
| LSR II | BD Becton Dickinson |
| Mastercycler Nexus eco | Eppendorf |
| Mettler Toledo FiveEasy™ Plus pH / mV bench meter | Sigma-Aldrich |
| Microscope Leica Typ 11090137002 | Leica |
| Mini Gel Holder Cassette | Bio-Rad |
| Mini Trans-Blot Central Core | Bio-Rad |

| | |
|---|---|
| Mini Trans-Blot® Cell | Bio-Rad |
| Mini-PROTEAN Tetra Cell Casting Stand & Clamps | Bio-Rad |
| Mr. Frosty™ Freezing Box | Thermo Scientific™ |
| Multifuge X3R centrifuge | Thermo Fisher Scientific |
| MultiRad 225 | Precision X-Ray |
| Pipetten 1000 µl, 200 µl , 100 µl , 20 µl and 10 µl | Eppendorf |
| Pipetten 1000 µl, 200 µl , 100 µl , 20 µl and 10 µl | StarLab |
| Pipetus | Hirschmann Laborgeräte |
| PowerPac™ HC High-Current Power Supply | Bio-Rad |
| RH basic 2 | IKA |
| ROCKY 3D | Fröbel Labortechnik |
| Rollenmischer RM 5 (348) | Hecht Assistent |
| Rotana 460R | Hettich Zentrifugen |
| Rotator SB3 | Stuart |
| Seahorse XFe96 Analyzer | Agilent Technologies |
| Seahorse XFp Analyzer | Agilent Technologies |
| Sigma Laborzentrifuge 2K15 | Sigma |
| Spectrophotometer ND-100 | NanoDrop Technologies |
| Sprout® Mini Centrifuge | Heathrow Scientific |
| StepOne Plus Real-Time PCR System | Applied Biosystems |
| Thermomixer compact | Eppendorf |
| Unimax 1010 Inkubtor 1000 | Heidolph |
| Victor X3 Multimode Plate Reader | Perkin Elmer |
| Vortex-Genie 2 | Scientific Industries |
| Waage ALJ 220-4NM | Kern & Sohn Gmbh |
| Waage EW 4200-2NM | Kern & Sohn Gmbh |
| Wasserbad GFL 1083 | GFL |
| X-Ray System X-RAD320 | Precision X-Ray |
| Z2 Coulter Particle and size analyzer | Beckman Coulter |
| Zeiss AxioObserver.Z1 and Apotome | Zeiss |

### 3.11. Software and databases

| Softwares and databases | Company or Source |
|---|---|
| ACAS II | Ahrens Electronics, Bargteheide |
| Attune Nxt Software v.3.1.2 | Thermo Fisher Scientific |
| BD Diva | BD Biosciences |
| ClueGO & CluePedia Plug-in von Cytoscape | (Bindea, Galon, & Mlecnik, 2013; Bindea et al., 2009) |
| CODEX | (Sanchez-Castillo et al., 2015) |
| Cytoscape | (Shannon et al., 2003) |
| DEGseq2 | (Love, Huber, & Anders, 2014) |
| FACSDiva Software Version 6.1.3 | BD Biosciences |
| FlowJo-Software | BD Lifesciences |
| GraphPad Prism 6 | GraphPad Software |
| GSEA/MSigDB Version: 7.1 | Broad Institute, Inc |
| Image J/ Fiji | (Schindelin et al., 2012) |
| Microsoft Office | Microsoft |
| NanoDrop-1000 v3.8.1 | ThermoFisher Scientific |
| Perkin Elmer 2030 Manager | Perkin Elmer |
| StepOnePlus Software v2.3 | Applied Biosystems |
| UCSC Genome Browser | (Kent et al., 2002) |
| Seahorse Wave Desktop Software | Agilent Technologies |
| IGV | Integrative Genomics Viewer (Robinson, Thorvaldsdottir, Wenger, Zehir, & Mesirov, 2017; Robinson et al., 2011) |
| Primer-Blast | NCBI |

# 4. Methods

## 4.1. Cell Culture

The cell lines K-562, THP-1, KG-1, HEK293T, Phoenix Eco and NIH3T3 cells were ordered from DSMZ, Braunschweig, Germany. The modified leukemic cell lines K-562 TRBSR and THP-1 TRBSR and CEB cells were kindly provided by Prof. Dr. Med. Georg Lenz. The cell line that needed to be cultured was collected from the liquid nitrogen and thawed very quickly at 37°C in a water bath. The thawed cells were immediately resuspended in 10ml of their respective media in a sterile falcon tube and centrifuged at 350G for 5 minutes at 4°C. The pellet was resuspended in the respective media (Table 16). All the cell lines were cultured at 37°C, in an incubator at 5% $CO_2$. The cells were split every alternative day to maintain the desired culture range (Table 16). The cultured cells were regularly collected for freezing during the initial 5-10 passages to maintain the cell line stocks. For freezing, 5 -10*10^6 cells were harvested, centrifuged (350G, 5 mins, 4°C), and resuspended in 1ml of freezing media (Table 16). The cells were transferred to a pre-cooled cryovial (CryoPure), and the vials were transferred to a pre-cooled freezing box (Mr. Frosty). The frosty box with the vials was kept at -80°C for 24 hours, and the vials were then transferred to liquid nitrogen for long-term storage in cryogenic freezer boxes.

**Table 16: List of cell lines used and their cultured media conditions.**

| Cell Lines | Culture Range | Culture Media | Freezing Media |
|---|---|---|---|
| K-562 | 0.1 – 1 *10^6 Cells/ml | RPMI + 10% FCS + 1% P/S | RPMI + 20% FCS + 10% DMSO + 1% P/S |
| THP-1 | 0.2 – 1 *10^6 Cells/ml | RPMI + 10% FCS + 1% P/S | RPMI + 20% FCS + 10% DMSO + 1% P/S |
| KG-1 | 0.1 – 1 *10^6 Cells/ml | RPMI + 10% FCS + 1% P/S | RPMI + 20% FCS + 10% DMSO + 1% P/S |
| K-562 TRBSR | 0.2 – 1 *10^6 Cells/ml | RPMI + 20% FCS + 1% P/S | RPMI + 20% FCS + 10% DMSO + 1% P/S |
| THP-1 TRBSR | 0.2 – 1 *10^6 Cells/ml | RPMI + 20% FCS + 1% P/S | RPMI + 20% FCS + 10% DMSO + 1% P/S |
| HEK293T | 20-90% confluency | DMEM + 10% FCS + 1% P/S | DMEM + 20% FCS + 10% DMSO + 1% P/S |
| CEB | 20-90% confluency | DMEM + 10% FCS + 1% P/S | DMEM + 20% FCS + 10% DMSO + 1% P/S |
| Phoenix ECO | 20-90% confluency | DMEM + 10% FCS + 1% P/S | DMEM + 20% FCS + 10% DMSO + 1% P/S |
| NIH3T3 | 20-90% confluency | DMEM + 10% FCS + 1% P/S | DMEM + 20% FCS + 10% DMSO + 1% P/S |

### 4.2. Mycoplasma testing

All the cell lines were maintained free of contamination by frequently testing for mycoplasma. A PCR-based test was used, and the primers are listed in Table 12. The forward and reverse primer mixes were prepared to reach the final concentration of 10µM each by adjusting the volume with nuclease-free water. Briefly, 100µl of cell culture supernatant media was collected from a cell culture flask from an 80-100% confluent culture without dilution into an Eppendorf tube. For the adherent cells, the sample was collected directly from the flask. While for the suspension cells, the supernatant was collected by centrifugation (350G, 5 minutes, RT). The sample was heated at 95°C for 5 minutes. The samples were spun at 16000G for 2 minutes, and the supernatant collected was used as a template for the PCR. The PCR reaction was prepared as described in Table 17, and the PCR was run with the cycling conditions mentioned in

Table 18. A negative control was included by adding nuclease-free water as a template. After the PCR, 10µl of each sample was run on an agarose gel. The remaining sample was stored at -20°C as a backup to re-run the reaction again if there was a problem with the previous run. The presence of a band at 500bp indicates the contamination with mycoplasma.

**Table 17: PCR mix composition for mycoplasma testing**

| Reagent | Volume (µl) |
|---|---|
| 5x GoTaq PCR Buffer | 5 |
| 25 mM MgCl2 | 1.4 |
| 10mM dNTPs | 0.5 |
| Forward primers | 1.0 |
| Reverse primers | 1.0 |
| Cell culture supernatant | 2.0 |
| Taq polymerase | 0.1 |
| Water | 14 |
| Total | 25 |

**Table 18: PCR cycling conditions for mycoplasma testing**

| Step | Temperature (°C) | Time (minutes) |
|---|---|---|
| Initial Denaturation | 95 | 2:00 |
| 5 Cycles | 94 | 0:30 |
| | 50 | 0:30 |
| | 72 | 0:35 |
| 30 Cycles | 94 | 0:15 |
| | 56 | 0:15 |
| | 72 | 0:30 |
| Hold | 4 | Infinity |

### 4.3. RNA Isolation and cDNA synthesis

We used the nucleo spin RNA mini kit (Macherey-Nagel) to extract RNA from the desired human and mouse cells. The RNA was extracted as per the manufacturer instructions. Always fresh cells were lysed to extract the RNA.

Briefly, 1 to 5*$10^6$ cells were lysed in 350µl of RA1 buffer supplemented with 3.5µl of β-mercaptoethanol (Sigma Aldrich) and passed through a nucleo spin filter with the violet ring to remove cell debris. The RNA from the cell extract was precipitated by adding 350µl of 70% ethanol and passed through the RNA column (column with the blue ring) by centrifugation. The RNA bound to the column was washed with 350µl of membrane desalting buffer (MDB), and the DNA on the column was digested by incubation with 95µl of rDNAse mixture for 15 minutes. The membrane was washed one time with 200µl of RAW2 and two times with 600 and 250µl of RA3 buffers. The RNA that bound to the membrane was eluted into 30-50µl of nuclease-free water. All the centrifugations steps during the RNA extraction were performed at 11000G, room temperature. The RNA concentration was measured by nanodrop (Thermo Fischer) and further stored at -80°C until cDNA was synthesised.

cDNA was synthesised from the extracted RNA using a high-capacity cDNA reverse transcription kit (Thermo Fischer). The reaction composition for cDNA synthesis is shown in Table 19. The incubation conditions are as follows: 10 minutes at 25°C, 120 minutes at 37°C and 5 minutes at 85°C. The cDNA synthesised from 2000 ngRNA was diluted with 80µl of nuclease-free water to make a total volume of 100µl. The diluted cDNA was stored at -80°C and proceeded to real-time PCR to quantify the gene expression.

**Table 19: A single reaction composition for cDNA synthesis**

| Constituents | Volume |
|---|---|
| 10× RT buffer | 2µl |
| 25× dNTP Mix (100 mM) | 0.8µl |
| 10× RT Random Primers | 2µl |
| Reverse Transcriptase | 1µl |
| RNase Inhibitor | 1µl |
| RNA (Upto 2ug) | Upto 2000ng |
| Nuclease-free H2O | Upto 20µl |

### 4.4. Real-Time PCR

Real-time PCR was used to quantify the mRNA expression levels of the genes. It was performed using either SYBR green detection (Thermo Fischer) or TaqMan reagents (Thermo Fischer). The PCR reaction composition for the

TaqMan and SYBR methodology is shown in Table 20 and Table 21. The samples were prepared and loaded into each well of a microamp optical 96-Well-reaction microtiter plate (Applied Biosystems), and the plate was sealed with microamp optical Adhesive Film (Thermo Fischer) to prevent the evaporation of the sample. Each sample was analyzed at least with triplicates. The plate was then run using StepOnePlus™ Real-Time PCR System (Thermo Fischer) with the cycling conditions from the Real-Time PCR System, as mentioned in Table 20 and Table 21. The analysis was performed by using the ddCt method in Excel (Livak & Schmittgen, 2001). I used *GAPDH* as a housekeeping gene for endogenous control.

**Table 20: PCR composition and cycling conditions for real-time quantification with Taqman reagents.**

| | Volume (µl) |
|---|---|
| Master Mix 2X | 7.5 |
| Taqman Assay | 0.75 |
| Nuclease free water | 3.75 |
| Template | 3 |

| Step | Temperature | Duration | |
|---|---|---|---|
| AMPerase Activation | 50°C | 2 Minutes | |
| Taq Activation | 95°C | 10 Minutes | |
| Denaturation | 95°C | 15 Seconds | 40 Cycles |
| Annealing | 60°C | 1 Minute | |

**Table 21: PCR composition and cycling conditions for real-time quantification with SYBR green reagents.**

| | Volume (µl) |
|---|---|
| SYBR Green master mix | 7.5 |
| Forward Primer (5µM) | 0.9 |
| Reverse Primer (5µM) | 0.9 |
| Nuclease free water | 4.7 |
| Template | 1 |

| Step | Temperature | Duration | |
|---|---|---|---|
| DNA Polymerase Activation | 95°C | 10 Minutes | |
| Melting | 95°C | 15 Seconds | 40 Cycles |
| Annealing and Extension | 60°C | 1 Minute | |

### 4.5. Western Blot

The cells from the cell culture were washed with PBS to remove residual media and were lysed with a phosphosafe extraction reagent (Merck Millipore) to extract the protein. The extraction reagent was added with complete EDTA free protease inhibitors (Sigma Aldrich) and phosphostop (Sigma Aldrich) to prevent protein degradation and dephosphorylation. 2 to 5*106 cells were washed with PBS and resuspended in 50-100µl of extraction reagent to lyse the cells. The cell suspension was incubated on ice for 30 minutes while vortexing at high speed for 30 seconds every 5 minutes. The lysate supernatant was collected by centrifugation at 16000G for 30 minutes at 4°C. The extracted proteins were quantified by the Pierce BCA protein assay kit (Thermo Fischer). The kit contains 2000µg of standard BSA protein. The standard protein was serially diluted with the protein lysis buffer to get the final concentrations in the range of 2000-25µg/ml. The extracted protein sample was diluted five times with the lysis buffer for accurate protein estimations. The solution A and B from the kit were mixed in the ratio of 50:1, and 200µl of the mixture was added to each well of a flat bottomed 96 well plate (Greiner Bio-One). 10µl of the standard diluted BSA stocks and 10µl of the diluted protein sample was added to each well of the 96 well plates. Two replicates were prepared for each standard dilution and test sample. The plate was incubated at 37°C for 30 minutes and then measured for absorbance at 595nm using a Victor X3 Multimode Plate Reader. The concentration of the protein samples was calculated in Excel according to the absorbance value of the test and standard samples. The protein samples after the extraction were stored at -80°C for long-term storage.

To load the protein sample for electrophoresis, the sample was prepared by mixing 20-30µg of protein with 4X SDS NUPAGE sample buffer (Thermo Fischer) and 10X NUPAGE reducing agent (Thermo Fischer) to get a final volume of 25-35µl per sample. The sample mixture was heated to 95°C for 5 minutes for protein denaturation. The 10% polyacrylamide gels were prepared using the stacking and separating buffers (Table 6). The gel composition is shown in Table 22. The samples were loaded onto the gel and run for 90 minutes at 100V in the SDS running buffer (Table 6). The page ruler prestained

protein ladder (Thermo Fischer) was used to estimate the protein size. 5µl of the page ruler protein ladder was loaded for each well. After the gel run, the proteins from the gel were then transferred to the PVDF membrane (Merck Millipore) in the transfer buffer (Table 6) for 2 hours at 100V at 4°C. After the transfer, the PVDF membrane was blocked with 5% milk prepared in TBST buffer (Table 6) for one hour. The membrane was incubated overnight in the cold room with tethering in the primary antibody diluted with 5% milk or 5% BSA (Bovine Serum Albumin) prepared in TBST (Table 9). The membrane was then washed three times with TBST for 5 minutes and incubated with the secondary antibody (Table 9) for one hour, tethering at room temperature. The protein bands were detected using Radiance Plus Chemiluminescent substrate kit. The two components in the kit were mixed at a 1:1 ratio and loaded on the membrane. The chemiluminescent bands were detected using an INTAS ECL Chemostar machine. To detect another protein using the same membrane, the membrane was stripped with 5-10ml of restore™ plus western blot stripping buffer, incubating for 10 minutes at room temperature with tethering. The membrane was then washed three times with TBST buffer and blocked with 5% milk (in TBST) for 1 hour at room temperature. The blocked membrane was then incubated with primary and secondary antibodies, as explained earlier.

**Table 22: Compositions for stacking and separating gels.**

| Component | 10% Stacking gel | Separating gel |
|---|---|---|
| Water | 2.94 ml | 1.46ml |
| Buffer (Stacking/separating) | 1.5ml | 273µl |
| Rotiphorese Gel 40 | 1.5ml | 250µl |
| 10% APS | 60µl | 20µl |
| TEMED | 2µl | 2µl |

### 4.6. Plasmid Isolation

The bacterial glycerol stock was primary inoculated into 5ml LB broth with ampicillin antibiotic (100µg/ml) and incubated for 8 hours at 37°C in the bacterial shaker incubator (IKA) at 350rpm. The 5ml of the primary culture was secondary inoculated into 250ml of LB broth with ampicillin antibiotic (100µg/ml) and incubated overnight at 37°C in the bacterial shaker incubator

at 350rpm. A nucleobond Xtra midi plus kit (Macherey Nagel) was used to extract the plasmid from the bacterial culture and performed as per manufacturer's instructions. Briefly, 250ml of the bacterial culture was pelleted by centrifugation (4,500G), and the pellet was resuspended in 8ml resuspension (RES) buffer. The bacteria were lysed in 8ml lysis (LYS) buffer and neutralised with 8ml neutralisation (NES) buffer. The nucleobond xtra column with the filter paper was equilibrated with 12ml equilibration Buffer (EQU), and the lysate was passed through the column as per the instructions from the kit. The column was washed with 5ml EQU buffer, and the plasmid was eluted into 5ml elution buffer (ELU). The extracted plasmid was then precipitated with 3.5ml isopropanol and then washed with 2ml 70% ethanol. The plasmid pellet was air-dried and resuspended in 50µl nuclease-free water, and the concentration of the plasmid was measured by nanodrop.

## 4.7. Enforced GFI1 expression in human leukemic cell lines

### 4.7.1. Lentivirus Production

The plasmids used for lentivirus production is detailed in Table 13. To increase the expression of *GFI1*, the coding sequence encoding human wildtype *GFI1* (*GFI1-36S*) was cloned into the lentiviral vector pCL6IEGwo, hence named as *pCL6IEGwo_GFI136S*. The primers and restriction enzymes used for cloning are listed in Table 11. In addition to the transfer plasmid pCL6IEGwo, the helper plasmid pCD NL-BH and the envelope plasmid pCO-PE were used to synthesize the lentivirus. These plasmids were received by the kind contribution of Prof. Dr. med. H. Hanenberg, Center for Pediatric and Adolescent Medicine / Clinic for Pediatrics III, University Hospital Essen.

The empty vector pCL6IEGwo was used as a control. The lentivirus for increased *GFI1* expression was produced from human fibroblastic cell lines HEK293T by polyethyleneimine (PEI) based transfection. HEK293T cells were cultured in 175 $cm^2$ dishes (Greiner Bio-One) to reach the confluency of 40-60% (Table 7). On the day of transfection, the plasmids (45µg *pCL6IEGwo_GFI136S* or 45µg pCL6IEGwo, 7µg pCO-PE and 45µg pCD NL-BH) were mixed in a falcon tube with 6ml DMEM, and 270 µL of 1 mg/mL PEI solution (PEI 25000, polysciences) was added to another tube with 6ml DMEM.

The tubes were vortexed briefly, and the PEI solution with DMEM was added to the tube with the plasmid solution with DMEM, followed by incubation for 30 minutes in the dark. After the incubation, the media from the HEK293T flasks was replaced with fresh 12 ml of DMEM + 15% FCS + 1.5% P/S. Then, 6ml of the plasmid and PEI mixture was added to the cells (makes up the total volume of 18ml) and incubated overnight. The next day, the cells were stimulated with 10mM sodium butyrate (Sigma Aldrich) dissolved in 20 ml fresh media (DMEM + 10% FCS + 1.5% P/S) for 6-8 hours to stimulate the virus production. The viral supernatant was collected on day three, and fresh medium was added for the day four virus. The collected virus was filtered through a 0.45µm syringe filter to eliminate the possible cell contamination in the viral supernatant. The collected virus was used for viral transduction.

#### 4.7.2. Lentiviral transduction

The human leukemic cell lines THP-1, K-562 and KG-1 were transduced with the collected lentivirus to increase the *GFI1* expression. The cells were maintained in the confluency range and cell culture media as described in section 4.1. The transduction was performed by spinoculation using polybrene (Merck Millipore) to enhance the efficiency of transduction. Polybrene acts by neutralizing the charge repulsion between viral particles and the cell surface. Spinoculation was performed in a 12 well tissue culture plate (Greiner Bio-One). Each well was loaded with 1ml of virus supernatant and 0.5ml of the cell suspension to reach the final cell concentration of 0.2-0.3*10^6 cells /ml. Polybrene was added to each well of the virus and cell suspension at 8µg/ml concentration, and the plate was centrifuged at 800G at 32°C for 90 minutes. After the spin infection, 1ml of supernatant was removed from each well, and 1ml new media (RPMI + 10% FCS + 1.5% P/S) with polybrene (8µg/ml) was added to each well and incubated for 48 hours. After the incubation, the cells were FACS sorted to collect pure GFP+ cells.

#### 4.7.3. FACS sorting of GFP+ cells

After the spin infection and incubation, the cells were collected and pelleted (350G, 5 minutes, 4°C) to remove the culture media. The cells were resuspended in FACS buffer (section 3.4) and centrifuged (350G, 5 minutes,

4°C) to wash the cells. The cells were washed at least three times with FACS buffer and resuspended in 500-1000µl FACS buffer, and the cells were then collected into FACS tubes by pipetting through 100 µm sterile filters (CellTrics, Sysmex) to get a single cell suspension. The GFP+ cells were sorted using a FACSAria III Cell Sorter. The sorted GFP+ cells were used for metabolic analysis. The metabolic experiments were detailed in section 4.11.

### 4.8. Microarray analysis with enhanced *GFI1* expression in K562 cells

A transcriptomic expression profiling with enhanced *GFI1* expression was performed with K-562 cells. The Human Clariom$^{TM}$ S Assay was utilized to profile expression. K-562 cells were lentivirally transduced (section 4.7.2) with empty vector (*eGFP*) and overexpression plasmid (*GFI1*). 2-3*$10^6$ GFP+ cells were FACS sorted (section 4.7.3), and RNA was extracted (section 4.3) as soon as the cells were sorted. The RNA was quantified by nanodrop analysis (Thermo Fischer) and was frozen at -80°C till the analysis. The RNA samples were prepared from three biological replicates. The samples were sent to the Priv.-Doz. Dr. rer. nat. Ludger Klein-Hitpass, former leader of BioChip-Labor, Universitätsklinikum Essen for the analysis. Dr Lothar Vassen analysed the transcriptomic data. One way ANOVA was used to calculate the significance among the groups.

### 4.9. Generation of knock-down clones

#### 4.9.1. Design of shRNA oligos

The shRNAs against the human *GFI1* gene to knock down its expression was designed by Prof. Dr. med. Georg Lenz. Out of the designed shRNAs, at least ten shRNAs targeting the various coding sequence regions were initially screened to measure the knock-down efficiency. The three best shRNAs that exhibited maximum efficiency were selected for further experiments. A non-specific scrambled (SCR) shRNA sequence was used as a control.

#### 4.9.2. shRNA cloning

##### 4.9.2.1.Annealing

The shRNA oligos were reconstituted with nuclease-free water to get the concentration of 100µM. 5µl each of both the forward and reverse oligos of

each shRNA was mixed with 10µl of PCR buffer and annealed in a thermocycler with a gradual decrease in temperature from 95°C to 4°C. The annealing conditions were as follows: 95°C for 2min- 85° for 9mins- 75° for 9 mins- 65° for 9 mins- 55° for 9 mins- 45° for 9 mins- 35° for 9 mins- 25° for 10 mins- 4°. The annealed oligos were diluted to 1:200 in nuclease-free water.

4.9.2.2. Restriction digestion

The shRNAs were cloned using the plasmid pRSMX-PG. The plasmid was kindly received from Prof. Dr. med. Georg Lenz. The shRNAs were cloned into the cloning sites of the restriction enzymes HindIII and BglII (New England Biolabs). Hence the shRNAs were designed with these restriction enzymes, as mentioned in section 4.9.1. The plasmids were restriction digested serially since the enzymes lack the compatibility buffer for digestion. The plasmid was initially digested with HindIII, followed by gel elution (section 4.9.2.3), digestion with BglII and gel elution. The plasmid was isolated, as shown in section 4.6. For the restriction digestion, 1500µg of the plasmid was used for a single reaction with 1µl of the enzyme, 6µl of buffer and adjust the volume up to 30µl with nuclease-free water. The plasmid was digested for one hour at 37°C. Ten reactions were performed to get enough plasmid after digestion. After the digestion, the reaction replicates were pooled and run on 1% agarose gel for 30 minutes at 100-120V. After single digestion, the linear plasmid band at 8400 bp was gel eluted (section 4.9.2.3), and the concentration was measured by nanodrop analysis. The eluted plasmid was then digested with BglII as described previously. The digestion product was run on the agarose gel, and the band at 6900 bp was gel eluted (section 4.9.2.3). The concentration of the final double digested product was measured by nanodrop.

4.9.2.3.Elution of DNA from gels

We used a QIAquick gel extraction kit (Qiagen) to extract the DNA from the gel. The gel slice containing the desired DNA fragment was cut out and dissolved in 600µl of QG buffer at 50°C by shaking at 500rpm until the gel dissolved. The DNA was precipitated by adding 200µl isopropanol and passed through the spin column. The DNA binds to the column, was washed with750µl

of PE buffer and eluted with 30µl nuclease-free water. The concentration of the gel elutes was measured by nanodrop analysis.

4.9.2.4. Ligation of DNA fragments and transformation of bacteria

The digested plasmid was ligated to the annealed oligos with T4 DNA ligase. The composition of the ligation mixture is shown in Table 23. The ligation mixture was incubated overnight at 16°C in a thermocycler and used to transform competent bacteria the next day. ccdB survival competent cells (Thermo Fischer) were used to transform the ligated product since the plasmid pRSMX-PG encodes the ccdB gene. 50µl of ccdB cells were thawed on ice, and 5µl of the ligation mixture was added to the cells and incubated for 15 minutes on ice. The cells with the added ligation product were heat-shocked at 42°C for one minute in a water bath. The cells were then incubated for two minutes on ice, and 250µl of S.O.C media (Table 6) was added. The cells were then incubated at 37°C for one hour at 400 rpm in a thermal shaker. Meanwhile, the LB broth agar plates were prepared with 100µg/ml ampicillin. After the incubation, 120µl of the cells suspension was plated on each agar plate and incubated overnight at 37°C to get distinct bacterial colonies.

**Table 23: Mastermix composition for the ligation of shRNA cloning**

| Component | Volume |
|---|---|
| pRSMX-PG vector (Double digested with HindIII and BglII) | 0.5µl (5ng) |
| T4 DNA Ligase | 1µl |
| 5X Ligation buffer | 1µl |
| Nuclease Free Water | 1.5µl |
| Insert (annealed oligos diluted with water) (section 4.9.2.1) | 1µl |
| Total volume | 5µl |

4.9.2.5. Screening of colonies

The colonies were screened to identify the colony that contains the plasmid with the shRNA insert. The next day after the incubation, some bacterial colonies were patched onto a fresh agar plate with the added ampicillin and incubated overnight at 37°C for the patches to grow. At least five colonies were picked for each shRNA and resuspended in a PCR tube with the added reaction master mix (Table 17). The primers used for the PCR were designed from the

plasmid sequences with the flanking sites of shRNA cloning. The primers sequences are listed in Table 11. The PCR cycling conditions were as follows:

Initial denaturation: 95°C for 10 Mins

35 Cycles: 95°C for 30 mins

58°C for 30sec

72°C for 60 secs

Final Extension: 72°C for 10 mins

The samples were run on agarose gel, and a band at around 2000 bp indicates a positive clone. In case of the absence of any positive clone, other colonies were selected, and the PCR has performed again. The positive clone was gel eluted (section 4.9.2.3 ) and sent for sequencing to LGC genomics to further confirm the presence of the intact shRNA insert. The positive clones from the sequencing results were inoculated for plasmid isolation in LB broth, and a glycerol stock was prepared, as explained in section 4.6.

4.9.3. Retroviral production and transduction to generate knock-down clones

4.9.3.1.Virus Production

CEB cells were used for transfection and to produce the virus. The culture conditions are listed in Table 16. The day before the transfection, $1*10^6$ CEB cells in 2ml media were seeded in a six-well plate, with one well per shRNA. The plate was incubated overnight at 37°C, with 5% $CO_2$. The helper plasmids pHIT EAG and pHIT 60 were used along with the plasmids pRSMX-PG, which contained the shRNA. The plasmids were isolated as described in section 4.6. The transfection was performed using Xfect transfection reagent. The next day, the transfection mixture was prepared by adding 1.5µg pHIT EAG, 1.5µg pHIT 60, 4.5µg target plasmid to 100µl of xfect buffer, followed by vortexing for 5 seconds. The Xfect polymer was vortexed thoroughly, and 2.25µl of the polymer was added to each tube with the transfection mixture, followed by vortexing for 10 seconds. The mixture was incubated for 10 minutes at room temperature. The transfection mixture was added to each well with CEB cells dropwise and incubated for 4 to 8 hours at 37°C, 5% $CO_2$. After the incubation,

the media with the transfection nanoparticle was removed, and 6ml of fresh media was added to each well. The plate was incubated, and the viral supernatant was collected for 48 hours. A fresh prewarmed media was added again, and the virus was collected again for 72 hours. The collected virus was syringe filtered through a 0.45 filter (Sarstedt) and proceeded directly for transduction.

4.9.3.2. Transduction and puromycin selection

The modified human leukemic cell lines THP-1 TRBSR and K-562 TRBSR were used to generate the knoc*KD*own clones. Polybrene was added to the filtered viral supernatant to get the final concentration of 8µg/ml. The initial transduction was performed with the virus collected after 48 hours. Each well of 12-well plates was loaded with 1 to 2 ml of the viral supernatant and 500µl of cell suspension with the cell density of 0.2- 0.3 $*10^6$ cells per well. The plates were centrifuged at 450G for 90 minutes at room temperature without a brake. After the spin infection, 1ml of fresh medium (Table 16) was added and incubated overnight at 37°C at 5% $CO_2$. The spin infection was repeated with the virus collected after 72 hours. The infection rate was measured by calculating the percentage of GFP positive cells after 48 hours of spin infection. In order to achieve >99% GFP positivity, the cells were treated with puromycin with the concentration of 5µ/ml and 10 µg/ml for THP-1 TRBSR and K-562 TRBSR, respectively. After the puromycin selection, the GFP+% was measured by FACS, and the cells were centrifuged at low speed (200G, 5 minutes, RT) to remove the dead cells. The puromycin selection was performed repeatedly to achieve the percentage of GFP+ to greater than 99%.

4.9.3.3. Doxycycline treatment

Since the knock-down system is an inducible one, the knock-down was induced by adding doxycycline. After the puromycin selection, the cells were centrifuged (350G, 5 minutes, RT) and resuspended in media with the added doxycycline (0.5µg/ml). Every 48 hours, the media was replaced with new media containing doxycycline. The cells were induced for at least four days. The knock-down was confirmed by real-time PCR (section 4.3) and western blot (section 4.5).

## 4.10. Mouse experiments

### 4.10.1. Mouse strains

All the mouse experiments in this study were carried out with the consent of the ethical committees from the local authorities at University Hospital Essen and Münster. The animal grant project numbers used in the study include Az: 84-02.04.2015.A022 and 81-02.04.2020.A443. The mouse strains employed were originated from the Jackson Laboratory's C57BL/6 mouse strain (Bar Harbor, Maine, USA). All mouse strains were backcrossed with C57BL / 6 (WT) mice regularly for every 5-10 generations. The ZTL of the Essen University Hospital and the ZTE of the Münster University Hospital provided some of the C57BL / 6 mice, while the others were acquired directly from Charles River (Sulzfeld, Bavaria, Germany).

In the current study, we used mouse models to study the metabolic phenotype with reduced expression of *GFI1*. In the *GFI1 KI* mouse model, the murine *Gfi1* gene was replaced with human *GFI1*. At the same time, the *GFI1 KD* mice express 10-20% of human *GFI1*, generated by inserting human *GFI1* cDNA along with the neo cassette into the mouse *Gfi1* locus. The *GFI1 KI* and *KD* mouse models were developed and described previously (Fiolka et al., 2006; Hones et al., 2016; Khandanpour et al., 2012).

### 4.10.2. Mouse Genotyping

To perform the genotype of the newborn mice, ear samples (2-3mm in diameter) were collected while numbering the mice. 100µl of ear lysis buffer (Table 6) was added to each earmark and shaken overnight at 57°C and 400rpm to extract the DNA. The next day, the samples were heated to 95°C for 10 minutes to inactivate the proteinase-K in the buffer. Up to 2-5µl of the extract was used as a template for PCR with the following composition and PCR cycling conditions (Table 24). The primers used for the PCR are shown in Table 11.

**Table 24: PCR master mix composition and buffers concentration.**

| | Stock Concentration | Final Concentration | Volume for the final concentration |
|---|---|---|---|
| 5x Green GoTaq® Reaction Flexi Buffer | 5X | 1X | 5µl |
| MgCl2 | 25mM | 1.4mM | 1.4µl |
| dNTP | 10mM | 0.2mM | 0.5µl |
| Primers (mGfi21, mGfi28, mGfi32, neo1500) | 10 pmol/µl each | 0.4 pmol/µl each | 1µl each |
| Taq Pol | | | 0.1µl |
| Sample | | | 2-5µl |
| H20 | | | Up to 25µl |

PCR Cycling conditions:

Initial denaturation: 95°C for 4 Mins

35 Cycles: 94°C for 15 mins

58°C for 30sec

72°C for 60 secs

Final Extension: 72°C for 10 mins

2% agarose gel was prepared in 1X TAE buffer (Table 6). 5µl of ROTI®GelStain was added to 100ml of agarose during the gel preparation to detect the DNA. The PCR products were loaded and allowed to run for 40 minutes at 100-120V, depending on the size of the chamber. Along with the samples, 10µl of the 100bp DNA ladder from NEB (mixture prepared with 3X loading dye and nuclease-free H2O). The size of the bands was observed under UV light (312nm), and the genotype of the mice was determined according to the size of the bands. A band size of 352 bp was represented as wildtype (WT- murine *Gfi1*), 400bp as *GFI1* knock-down (*GFI1 KD*) and 500bp as *GFI136S KI* (*GFI1 KI*- presence of human *GFI1* instead of mouse *Gfi1*). The presence of two bands indicated heterozygous to that genotype according to the band size (Khandanpour et al., 2012).

4.10.3. Isolation of lineage depleted cells

Lineage depleted cells were isolated using the Lineage Cell Depletion kit, mouse (Miltenyl Biotec) to get the progenitor cells from the mice. MACS buffer

was prepared on the day before the isolation of lineage depleted cells, and the buffer was kept at 4°C overnight to eliminate any possible air bubbles due to bovine serum albumin (BSA). Mice within the age range of 8-16 weeks were used. The mice were euthanized in a $CO_2$ chamber, and the bone marrow from the forelimb bones, humerus and radius-ulna, the hindlimb bones, femur and tibia-fibula was flushed into FACS buffer as described in section 4.10.9.1. The cells were centrifuged and lysed for erythrocytes, as explained in section 4.10.9.1. The total number of cells were then counted and centrifuged (350G, 5 minutes, 4°C), and the supernatant was discarded. The cell pellet was resuspended in FACS buffer (40µl per $10^7$ cells), and a biotin-antibody cocktail (10µl per $10^7$ cells) was added and incubated for 11 minutes at 4°C. Then the FACS buffer (30µl per $10^7$ cells) and anti-Biotin microbeads (20µl per $10^7$ cells) were added and incubated for 15 minutes at 4°C. 25ml of FACS buffer was added to wash the cells and centrifuged (350G, 4°C) for 10 minutes. The pellet was resuspended in 500µl of MACS buffer. Meanwhile, the LS or MS columns (Miltenyl Biotec) were used to isolate the cells with the total cell number of $2*10^9$ and $2*10^8$ cells, respectively. The columns were placed in the magnetic field of the magnetic separator (Miltenyl Biotec), and a pre-separation filter (30µm, Miltenyl Biotec) was placed on the top of the column. The cells resuspended in the MACS buffer were passed through the column, and the lineage positive cells were attached to the column through the magnetic beads while the lineage depleted cells were collected as flow through. The column was washed thrice with the MACS buffer 500µl each time to get a final elution volume of 2ml. The cells were counted, centrifuged (350G, 5 minutes, 4°C), resuspended in SCM media, and cultured with a seeding density of 0.2 - $0.3*10^6$ cells/ml.

#### 4.10.4. Retrovirus production and titration

To induce AML development in the mice, the lineage depleted cells were transduced with retroviruses expressing the *MLL-AF9* or *AML1-ETO9a* fusion oncogenes, respectively. The retroviruses were produced from the human embryonic kidney cell lines HEK293T. Before the transfection, $10*10^6$ cells were seeded in 145 $cm^2$ dishes in 25ml media (Table 16) and equally

distributed on the surface of the dishes and cultured overnight at 37°C, 5% $CO_2$. The next day, the cells reached the confluency of 60-70%, and the media was changed with prewarmed media (DMEM + 10% FCS + 1% FCS) to 37°C, at least two hours before the transfection. A transfection mixture was created by slowly adding a mixture of 100µl 2.5M CaCl2, plasmids (20µg of transfer plasmid- *MCSV-MLL-AF9-IRES-GFP* or *MCSV-AML1-ETO9a-IRES-GFP* and 2.25µg of envelope plasmid- pCL-Eco) and sterile water (up to 2ml) to 1000µl of HEBS buffer at the rate of one drop per second and vortexing at a medium speed. The mixture was incubated at room temperature for 10 minutes. Meanwhile, the media from the dishes with HEK293T cells were again changed by adding 15ml of media (DMEM + 10% FCS + 1% P/S + 20mM HEPES) prewarmed to 37°C. The transfection mixture was added drop by drop, and the plate was swirled gently to get a uniform distribution. The plate was then incubated overnight at 37°C at 5% $CO_2$. After 24 and 48 hours of transfection, the media was changed by adding 15ml of DMEM + 10% FCS + 1% P/S + 10mM HEPES prewarmed to 37°C. The viral supernatant was collected after 48 and 72 hours post-transfection and filtered through a 0.45µm filter (Sarstedt). The collected virus was aliquoted for titration, and the rest of the virus was stored at -80°C for long-term use.

Titration of the virus was performed to measure the efficiency of the collected virus. $2*10^4$ NIH3T3 cells were seeded in each well of 12 well plates with 1ml of media (Table 16), and two extra wells were seeded for counting the cells at the later steps. The cells were incubated overnight at 37°C at 5% $CO_2$. On day 2, the cells from the extra wells were counted. The virus was serially diluted at 1:10, 1:100 and 1:1000 with the media added with 8µg/ml polybrene (Merck Millipore). 70µl of the diluted virus was added to each well and infected for 1 hour at 37°C, 5% $CO_2$. During the incubation, the plate was agitated twice by gently shaking orbitally with hands after 20 minutes and 40 minutes of incubation and 300µl of the media with polybrene (8µg/ml) was added after the incubation. The next day, media was changed with 1 ml of fresh media per well (Table 16). 48 hours after the infection of cells, the media was removed, and the wells were washed with PBS. The cells were extracted by adding 500µl

trypsin and incubation for 5 minutes at 37°C. The cells were then washed with FACS buffer and resuspended in 250µl of FACS buffer. The cells infected with different dilutions of the virus were then analyzed for GFP expression by FACS analysis. At least two replicates for each dilution was analyzed, and negative control was also included. The viral titer was calculated according to the percentage of GFP positive cells.

4.10.5. Retroviral transduction of lineage depleted cells and FACS sorting

The lineage depleted cells were isolated as described in section 4.10.3, and the cells were cultured in SCM media for 48 to 72 hours to proceed for transduction to induce the expression of *MLL-AF9* or *AML1-ETO9a* fusion protein. The cells were then collected and counted. The cells were resuspended, centrifuged, and resuspended in SCM media with the added polybrene (8µg/ml) at the cell density of $1*10^6$ cells/ml. The frozen retrovirus was thawed on ice, and polybrene was added to the thawed virus at the concentration of 8µg/ml. 1ml of the virus was aliquoted into each well of 12 well plates, and 500µl of the prepared cells was aliquoted into each well. The plate was then centrifuged at 800G for 90 minutes at 32°C. After the centrifugation, 500-750µl of the supernatant was discarded from each well and 1ml of fresh SCM with added polybrene (8µg/ml) was added and incubated overnight at 37°C with 5% $CO_2$. The process was repeated on day two by collecting the cells from the first-day transduction. The cells were collected from the plate on day four and washed with FACS buffer. To get a single cell suspension, the cells were resuspended in FACS buffer and passed through 100 µm sterile filters (CellTrics, Sysmex). Using the FACSAria III Cell Sorter, the GFP+ cells were sorted. The cell sorting was performed at the sorting facility of Prof. Dr. Frank Rosenbauer, Institute of Molecular Tumor Biology, University Hospital, Münster and by Ms. Annegret Rosemann, University hospital, Münster. The sorted GFP+ cells were further cultured in SCM media and proceeded for metabolic analysis.

4.10.6. Mouse Irradiation

To perform the transplantation, the mice were lethally and sublethally irradiated for primary and subsequent transplantations, respectively. For the lethal

irradiation, mice were irradiated with 7Gy in the morning and 3Gy in the evening. For the sublethal irradiation, the mice were irradiated one time with 3Gy. A X-Ray System X-RAD320 was used at Universitätsklinikum Essen and Faxitron CP-160 or MultiRad 225 (precision) device was used at Universitätsklinikum Münster (ZTE facility).

#### 4.10.7. Primary Transplantation

The transplantation of *in-vitro* transduced lineage depleted cells with an oncogene into lethally irradiated mice was used to develop leukemia in the mice. The lineage depleted cells were first isolated from the *GFI1 KI* and *GFI1 KD* mice (section 4.10.3) and transduced with retrovirus encoding the *MLL-AF9* fusion protein (Section 4.10.5). The plasmid (*MCSV-MLL-AF9-IRES-GFP*) encodes the MLL-AF9 protein coexpressing a GFP marker protein to select for successfully transduced cells. GFP is the selection marker for MLL-AF9 fusion. After the transduction, the GFP+ cells were FACS sorted for transplantation. One day before the transplantation, the wild type mice (C57Bl/6) were lethally irradiated with 7 + 3 Gy. To prevent any secondary infections due to immunosuppression expedited by irradiation, the irradiated mice were provided with 0.1% Baytril in the drinking water beginning from the day of irradiation. Baytril was provided for three weeks by changing freshwater with Baytril every week. To transplant the irradiated mice, 100000 GFP+ cells were mixed with 200000 healthy bone marrow cells in 200µl of sterile PBS and injected intravenously through the tail vein using a 27 G cannula (Figure 15). The mice were observed for symptoms such as anaemic paw, swollen abdomen indicative of enlarged spleen, weight loss, apathy etc., every day until the mice developed these symptoms. The presence of these symptoms is indicative of AML development. The mice were then euthanized in a $CO_2$ chamber. The mice were initially examined for the presence of enlarged spleen, liver and pale bones. The development of AML was further confirmed by FACS analysis of bone marrow and spleen cells for granulocytes, monocytes, c-Kit + and GFP+ cells (section 5.4.1). The bone marrow cells were further processed for metabolic experiments, presented in individual experimental sessions. Some of the total bone marrow cells were frozen in IMDM with 20% FCS and 1%

penicillin / Streptomycin (P/S) (section 4.1) in liquid nitrogen for secondary transplantations.

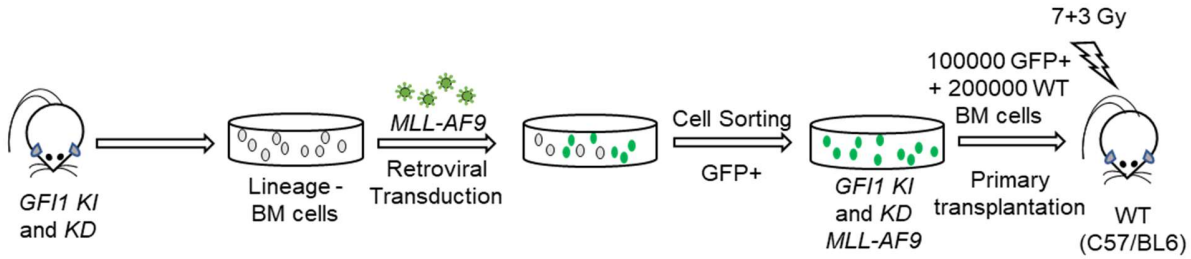


**Figure 15: Schematic representation of retroviral transduction, followed by primary transplantation.**

4.10.8. Secondary and subsequent transplantations:

The WT (C57Bl/6) mice were sublethally irradiated with 3Gy on the day before the secondary transplantation. The antibiotic Baytril was added to drinking water, as discussed previously (4.10.7). To prepare the leukemic cells for secondary transplantation, the frozen vials of total bone marrow from the primary leukemic mice were partially thawed at 37°C in a water bath and resuspended in IMDM with 20% FCS and 1% P/S. The cells were spun at 350G for 5 minutes at 4°C, washed with sterile PBS and resuspended in 1ml sterile PBS. The live cells were counted by trypan blue staining using Neubauer counting slide, and FACS analysis measured the percentage of GFP+ cells. The volume for the number of GFP+ live cells was calculated as (live cell count /100) * % GFP+ cells. 50000-100000 GFP+ cells resuspended in 150µl sterile PBS was used for secondary transplantation. The mice were observed every day for the symptoms of AML development and euthanized and analyzed as described previously (4.10.7). The leukemic total bone marrow cells from secondary and tertiary transplanted mice were used for tertiary and quaternary transplantations, respectively (Figure 16)

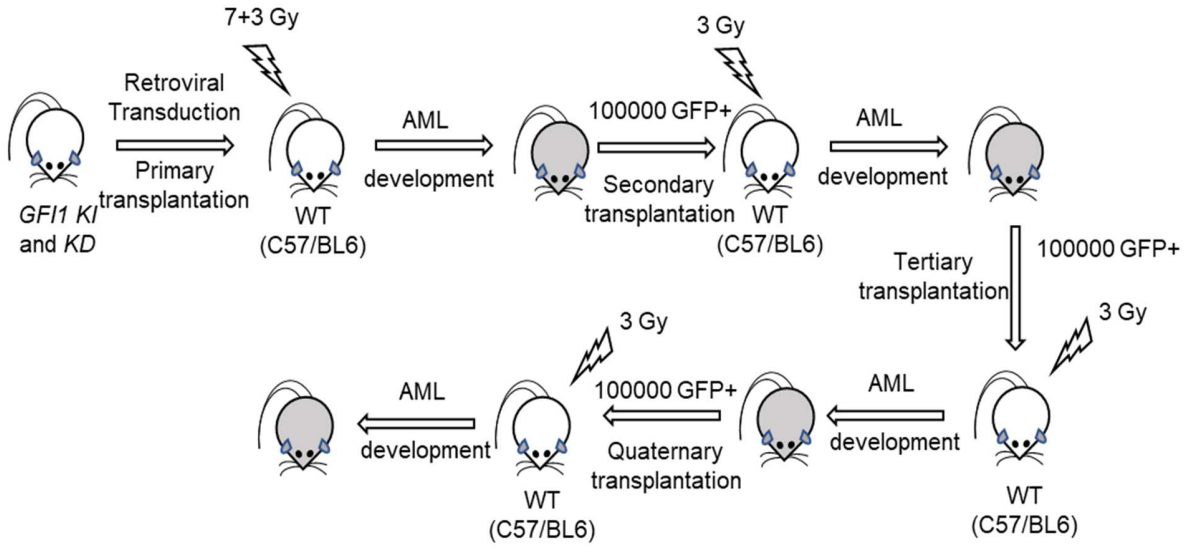


**Figure 16: Experimental overview of serial transplantation (from primary to quaternary)**

The figure shows the series of transplantations from primary to quaternary with the leukemic cells expressing *MLL-AF9* oncofusion from *GFI1 KI* and *KD* mice.

### 4.10.9. Analysis of leukemic mice

#### 4.10.9.1. Isolation of peripheral blood and bone marrow

Once the mice were observed with the symptoms of AML, they were euthanized. The blood from the heart was collected immediately into K3EDTA (Greiner Bio-One) vials using a 25G cannula (Becton Dickinson). The cell counts of WBC, platelets, haemoglobin were measured using an animal blood counter (scil vet). The organs such as the spleen and liver were collected into FACS buffer and measured for increased size and weight. The forelimb bones humerus and radius-ulna, the hindlimb bones femur and tibia-fibula were collected into FACS buffer by removing the adjacent tissues. The bone marrow (BM) from the bones was flushed with a syringe using a 25G cannula using FACS buffer, and the bonemarrow was homogeneously resuspended using a 20G cannula. The cells were then filtered through a 100µm cell strainer to get a single cell suspension and remove any tissue debris. The spleen (SPL) was collected into FACS buffer and crushed through slides to get cells extracted from the spleen. The spleen cells were then resuspended using a 20G cannula and passed through a 100µm cell strainer to get a single cell suspension. The

BM and SPL cells were spun down at 350G for 5 minutes at 4°C, and the supernatant was discarded. The pellet was resuspended in 1ml 1X erylysis buffer (BD Pharm Lyse) for 7 minutes at room temperature to lyse the erythrocytes. The erylysis buffer was then inactivated by adding 10-15ml of FACS buffer and spun down at 350G for 5 minutes at 4°C. The pellet was then resuspended in a 5ml FACS buffer. The live cells from the BM and SPL were counted manually by staining with trypan blue and using a Neubauer chamber and processed for FACS staining. Similarly, the collected blood was erylysed twice with 1ml 1X erylyse buffer each time. $1*10^6$ cells were washed (350G, 5 mins, 4°C), resuspended in 80µl of FACS buffer, and processed for FACS staining.

4.10.9.2. Cellular characterization of bone marrow cells and peripheral blood by surface marker FACS analysis

Every cell expresses specific surface markers known as Cluster of Differentiation (CD) markers. All the cell types in the hematopoietic system express diverse CD markers. The distribution of various cell types in the total bone marrow, and peripheral blood is measured based on CD markers expression. The antibodies used against the CD markers were conjugated with fluorochromes. The CD markers used and their fluorochrome-conjugated antibodies used are listed in Error! Reference source not found..

**Table 25: List of cell surface marker antibodies used for the leukemic mice analysis**

| Cell Type | CD Marker | Antibody Clone | Fluorochrome |
|---|---|---|---|
| Granulocytes | Gr1 | RB6-8C5 | APC / PE |
| Macrophages | CD11b | M1/70 | PerCP Cy5.5 |
| Helper T Cells | CD4 | GK1.5 | PerCP Cy5.5 |
| Cytotoxic T Cells | CD8a | 53-6.7 | APC / PE |
| Erythroid Lineage | Ter119 | TER-119 | APC / PE |
| B Lymphocytes | B220 | RA3-6B2 | PerCP Cy5.5 |
| Leukemic Stem Cells | c-Kit (CD117) | 2B8 | APC / PE |

.

For the FACS staining, $0.5\text{-}1*10^6$ BM, SPL and PB cells were collected in the FACS tubes and centrifuged at 350G for 5 minutes at 4°C. The supernatant was discarded, and 10µl of Fc block (CD16/32, Mouse BD Fc Block) is added to block the Fc receptors for preventing the non-specific binding of antibodies

to Fc receptors and incubated for 10 minutes at 4°C. After incubation, the cells were washed with 1ml FACS buffer (350G, 5 mins, 4°C) and added 80 µl of the antibody mixture (0.2µg/ml) prepared in FACS buffer and incubated for 10 minutes at 4°C. The list of antibody combinations used is mentioned in Table 26 below. After the incubation, the cells were washed with 1ml FACS buffer (350G, 5 mins, 4°C), and 300µl of FACS buffer was added and proceeded for FACS measurement.

**Table 26: List of antibody combinations used for FACS staining**

| Antibody combination | Samples stained |
|---|---|
| Gr1 + CD11b | BM, SPL |
| Ter119 + B220 | BM, SPL |
| CD8 + CD4 | BM, SPL |
| c-Kit | BM, SPL, PB |

4.10.9.3. Isolation of c-Kit and GFP positive cells

Once the mice develop leukemia, the bones are flushed and erylysed, as explained in section 4.10.9.1. The c-Kit (CD117) positive cells were isolated using CD117 microbeads (Miltenyl Biotec) from the total bone marrow cells. In short, the cells were counted, centrifuged (300G, 10 minutes), and the cell pellet was resuspended in 80µl of FACS buffer and 20µl of beads per $10^7$ cells and incubated for 15 minutes at 4°C. The cells were washed with FACS buffer and resuspended in 500µl of MACS buffer (Table 6). The MACS column (Miltenyl Biotec) was then placed in the magnetic field, and the LS column was rinsed with 3ml of MACS buffer. The cell suspension was passed through the LS column by passing through a pre-separation filter. The c-Kit positive cells labelled with beads bind to the column through the magnetic field. The column was washed two times, each time with 1ml MACS buffer. The c-Kit positive cells were plunged out of the column with 2ml of MACS buffer. To sort the double positive cells (c-Kit+ GFP+ cells), the isolated c-Kit+ cells were counted and stained with c-Kit (CD117) APC antibody (BD Biosciences) (Table 8). We used 1µl of antibody per $10^6$ cells. The cells were stained by centrifuging (300G, 5 minutes) and resuspended in 100µl of FACS buffer with the added antibody. The cells were incubated for 10 minutes at 4°C and washed with

FACS buffer. The stained cells were FACS sorted for the double-positive cells. After the sorting, the cells were cultured with the media (Table 7) for metabolic experiments.

### 4.11. Metabolic experiments

#### 4.11.1. Measurement of glucose consumption, lactate secretion and LDH activity

The cell culture supernatant was collected by centrifugation (1000G, 5 minutes) to measure the glucose and lactate levels. To measure the intracellular lactate dehydrogenase (LDH) activity, $1*10^6$ cells were collected and washed with PBS to remove residual media and lysed in RIPA lysis buffer (Table 6) with the added protease inhibitor (Merck). The cell lysate supernatant was collected by centrifugation (16000G, 15 minutes). The culture supernatant and lysate samples were frozen at -20°C until the measurement. The samples were sent to the diagnostics laboratory of Prof. Dr. med. Jerzy-Roch Nofer, University Hospital Münster for glucose, lactate and LDH levels measurement by biochemical analysis.

#### 4.11.2. Seahorse Mitostress and Glycostress tests

Seahorse Mitostress and Glycostress tests were performed to measure the rate of oxidative phosphorylation (OXPHOS) and glycolysis, respectively. Seahorse XFe96 FluxPak (Agilent Technologies) was used to perform the seahorse experiments. Before starting the experiment, the sensor cartridge from the FluxPak was hydrated with 200µl distilled water to each well and incubated overnight at 37°C in a non-$CO_2$ incubator. 20ml of XF calibrant solution was collected in a falcon tube and incubated overnight at 37°C in the non-$CO_2$ incubator. On the experiment day, the cell culture plate from the fluxpak was coated by adding 25µl of Poly-D-lysine hydrobromide (PDL- Sigma) (50µg/ml) to each well, incubated for 20 minutes at room temperature. The plate was then washed two times with 200µl of sterile PBS, and the PDL coated plate was kept at 4°C until the cells were loaded. A non-buffered media was prepared, and the media composition varies between cells, as shown in Table 27. To prepare the media, the XF base media was prewarmed to 37°C in a water bath, and the components D-Glucose (Sigma Aldrich), L-Glutamine (Sigma Aldrich) and

Sodium Pyruvate (Sigma Aldrich) were added according to the cell types (Table 27). The pH of the media was adjusted to 7.3 - 7.4 with 0.1M NaOH, and the media was syringe filtered through a 0.45 µm filter (Sarstedt).

**Table 27: Seahorse media composition used for experiments with human cell lines and the primary cells from mice.**

| Compound | Human cell lines | | Primary cells from mice | |
|---|---|---|---|---|
| | Final Concentration | Volume | Final Concentration | Volume |
| XF Base medium (DMEM) | | 49,278ml | | 48ml |
| D-Glucose (2.5mM) | 11.1mM | 222µl | 25mM | 500 |
| L-Glutamine (200mM) | 2mM | 500µl | 4mM | 1000µl |
| Sodium Pyruvate (100mM) | - | - | 1mM | 500µl |
| Total volume | | 50ml | | 50ml |

The cells that needed to be analyzed were counted and centrifuged (350G, 5 mins, 4°C), and culture media was removed. The cells pellet was resuspended in the prepared seahorse media, and 180µl of cell suspension was loaded to each well of PDL coated cell culture plate. The four wells in the corners of the plate were loaded with empty media. The requisite cell number depends on the cell types and is optimized as explained in section 4.11.3 and listed in Table 28. The cell plate was centrifuged (300G, 5 mins, RT, 5 acceleration, 5 deceleration) for the cells to adhere uniformly to the plate. The plate was allowed to equilibrate in a non-$CO_2$ incubator until the seahorse measurement. The water from the hydrated cartridge was replaced with the prewarmed calibrant and incubated in the non-$CO_2$ incubator for at least one hour before the seahorse run. The first three ports (A, B and C) of the cartridge were then loaded with Oligomycin, FCCP and Rotenone + Antimycin for mitostress tests (Sigma Aldrich), while the first two ports (A and B) were loaded with oligomycin and 2-Deoxy glucose (2-DG) for Glycostress tests. The concentrations of these inhibitors were optimized according to the cell types described in section 4.11.3 and listed in Table 28. Seahorse XFe96 analyzer (agilent technologies) was used to run the seahorse experiment. The cartridge loaded with the inhibitors was then calibrated in the instrument, and then the cell plate was loaded. Three

basal measurements were recorded, and then the compounds were injected sequentially at regular time intervals into ports A, B, and C, ensuring that at least three measurements were taken before each port injection. After the seahorse run, the cells were stained with Hoechst 33342 (Thermo Fischer) to normalize the data. The plate was centrifuged (1000G, 5 minutes, room temperature), and the media was carefully pipetted out. Each well was loaded with 200µl of 5µg/ml of Hoechst 33342 solution prepared in PBS, mixed with pipetting and incubated in the dark for 20 minutes at room temperature. The plate was then centrifuged (300G, 5 mins) to have a uniform distribution of the cells. The fluorescence was detected using a plate reader (TECAN) with the excitation of 350nm and emission of 460nm.

#### 4.11.3. Optimization of seahorse experiments

The seahorse XFp analyzer (agilent technologies) was employed with the XFe96 analyzer to optimize the seahorse studies. The titration of cells was done to calculate the desired number of cells to be loaded per well. The optimization was carried out to achieve the appropriate seeding density, with the basal oxygen consumption rate (OCR) values falling between 20 and 160 and the basal extracellular acidification rate (ECAR) lying between 10 and 90. The seahorse runs were then performed with gradient doses of oligomycin and FCCP to achieve maximum inhibition and OCR induction. The concentration of rotenone and antimycin were based on previous publications (Hao et al., 2019; Hou et al., 2020). The optimized cell number and inhibitor concentrations are indicated in Table 28 below.

**Table 28: List of cell types used in seahorse mitostress and glycostress tests, along with their optimized seeding density and inhibitor concentrations.**

| Cell Type | Cell Number / well | Oligom-ycin | FCCP | Rotenone | Antimy-cin | 2-Deoxy Glucose |
|---|---|---|---|---|---|---|
| K-562 | 50,000 | 1µM | 0.25µM | 0.5µM | 0.5µM | 50mM |
| THP-1 | 50,000 | 1µM | 0.25µM | 0.5µM | 0.5µM | 50mM |
| KG-1 | 50,000 | 1µM | 0.125µM | 0.5µM | 0.5µM | 50mM |
| K562 TRBSR | 50,000 | 1µM | 0.25µM | 0.5µM | 0.5µM | 50mM |
| THP-1 TRBSR | 50,000 | 1µM | 0.25µM | 0.5µM | 0.5µM | 50mM |
| Lineage depleted cells (Lin-) | 150,000 | 2µM | 2µM | 0.5µM | 0.5µM | 100mM |
| Lin- transduced with *MLL-AF9* or *AML1-ETO9a* | 150,000 | 2µM | 2µM | 0.5µM | 0.5µM | 100mM |
| c-Kit+ GFP+ cells | 150,000 | 2µM | 2µM | 0.5µM | 0.5µM | 100mM |

### 4.11.4. Seahorse XF Substrate Oxidation Stress Test

Multiple inhibitors, including UK5099 (Sigma Aldrich), BPTES (Sigma Aldrich), Etomoxir (Sigma Aldrich) and ST1326 (Sigma Aldrich), were used to measure the significant energy source by inhibiting the glucose, glutamine, and fatty acid metabolism pathways. UK5099 (2-cyano-3-(1-phenyl-1H-indol-3-yl)-2-propenoic acid) is a mitochondrial pyruvate carrier (MPC) blocker, preventing the transfer of pyruvate to mitochondria, thereby inhibiting glucose-derived OXPHOS (Vacanti et al., 2014; Zhong et al., 2015). BPTES (Bis-2-(5-phenylacetamido-1,3,4-thiadiazol-2-yl)ethyl sulfide) is a Glutaminase1 (GLS1) inhibitor and prevents glutamine mediated OXPHOS (Matre et al., 2016). Etomoxir inhibits the fatty acid metabolism through the irreversible inhibition of CPT-1 (carnitine palmitoyltransferase-1) (Samudio et al., 2010), while ST1326 ((R)-3-(3-tetradecylureido)-4-(trimethylammonio)butanoate) is a reversible inhibitor (Ricciardi et al., 2015).

Initial steps of the substrate oxidation stress tests were performed as described in section 4.11.1. Either of these inhibitors was added into port A, and then

oligomycin, FCCP and Rotenone + Antimycin into ports B, C and D. A media control was always included. The rate of inhibition to these inhibitors was measured by the decrease in OCR concerning empty media. The concentrations of UK5099, BPTES and Etomoxir, were used as described previously (Fuhrmann et al., 2019) and stated in Table 29.

**Table 29: Inhibitor concentrations used for substrate oxidation stress tests**

| Cell Type | UK5099 | BPTES | Etomoxir |
|---|---|---|---|
| K-562 | 2µM | 3µM | 4µM |
| THP-1 | 2µM | 3µM | 4µM |
| KG-1 | 2µM | 3µM | 4µM |
| K-562 TRBSR | 2µM | 3µM | 4µM |
| THP-1 TRBSR | 2µM | 3µM | 4µM |
| Lineage depleted cells (Lin-) | 4µM | 6µM | 8µM |
| Lin- transduced with *MLL-AF9* or *AML1-ETO9a* | 4µM | 6µM | 8µM |
| c-Kit+ GFP+ cells | 4µM | 6µM | 8µM |

### 4.11.5. Substrate oxidation measurement through cell counts

In addition to the mitostress tests, to measure the substrate dependency, the cells were treated with the substrate inhibitors UK5099, BPTES, Etomoxir and ST1326. The leukemic and non-leukemic cells were treated with these inhibitors, and the live cell counts were measured using a Neubauer chamber after 72 hours of treatment. The rate of decrease in the cell counts with the treatment indicates the rate of substrate dependency of that substrate. The concentrations of the inhibitors used are listed in Table 30.

**Table 30: Concentrations of substrate inhibitors used for cell counting assay**

| Inhibitor | Concentration |
|---|---|
| Etomoxir | 80µM |
| ST1326 | 50µM |
| UK5099 | 100µM |
| BPTES | 20µM |

4.11.6.Mitochondrial Membrane Potential (MMP)

0.25*10^6 cells were collected for each tube in 500µl of prewarmed media (cell culture media, depending on cell type as listed in Table 16). To the control tube, 0.4µl of FCCP (20µM working concentration- Abcam) was added and incubated for 10 minutes at 37°C in a $CO_2$ incubator. To both the control and test tubes, 0.5µl of verapamil (Sigma Aldrich - 50µM working concentration) is added and incubated for 10 minutes at 37°C in a $CO_2$ incubator. To both the tubes, 2.5µl of TMRE (50nM working concentration - Abcam) was added and incubated for 20 minutes at 37°C in a $CO_2$ incubator. The cells were then measured by FACS analysis using the YL3 (Yellow Laser) channel (488/575nm).

4.11.7.Mitotracker deep red staining

0.25*10^6 cells were collected in 500µl of prewarmed media (only RPMI or IMDM without FCS), and 0.5µl of verapamil (50µM working concentration) was added and incubated for 10 minutes at 37°C in a $CO_2$ incubator. 2.5µl of mitotracker deep red reagent is added (50nM final concentration) and incubated for 20 minutes at 37°C in a $CO_2$ incubator. The cells were then measured directly by FACS using the RL3 (Red Laser) channel (644/665 nm).

4.11.8.ROS measurement

0.25*10^6 cells were collected and resuspended in 500µl of prewarmed media (cell culture media, depending on cell type as listed in Table 16). 1µl of cell rox deep red reagent is added (Thermo Fischer- 5µM final concentration) and incubated for 20 minutes at 37°C in a $CO_2$ incubator. FACS measured the cells using the RL1 (Red Laser) channel (644/665 nm).

4.11.9.Mitochondrial DNA copy number

0.25*10^6 cells were collected and washed with PBS (350G, 5 mins, 4°C) to remove the media. The cells were resuspended in 50µl of lysis buffer with the added proteinase K (Table 6), and the cells were lysed by incubating for 2 hours at 56°C followed by 15 minutes at 95°C in a thermocycler (Eppendorf). Following the lysis, the lysate was centrifuged at 1000G for 5 minutes at 4°C, and the supernatant was collected and used as a template for PCR. The mitochondrial DNA was quantified to nuclear DNA by real-time PCR, and the

primers used were listed in Table 11. The primers were dissolved in nuclease-free water to give 100µM (the volume according to the datasheet from the Eurofins) and incubated at 50°C at 500 rpm for 15 minutes. The primers were further diluted to 5µM with nuclease-free water. The PCR master mix was prepared as described in Table 31, and the PCR was run as explained in session 4.3. The mitochondrial DNA copy number relative to nuclear DNA was calculated according to the formula (de Almeida et al., 2017):

$$\Delta C_T = (\text{nucDNA } C_T - \text{mtDNA } C_T)$$

$$\text{Relative mitochondrial DNA content} = 2 \times 2^{\Delta CT}$$

**Table 31: PCR composition to quantify mitochondrial DNA**

| | Stock Concentration | Final Concentration | Volume (for 15µl) |
|---|---|---|---|
| SYBR green master mix | 2X | 1X | 7.5 µl |
| Forward Primer | 5µM | 300nM | 0.9 µl |
| Reverse Primer | 5µM | 300nM | 0.9 µl |
| Template (cell Lysate) | - | - | 3µl |
| H2O | | | 2.7µl |

### 4.12. CFU Assay

We used mouse methylcellulose media (MethoCult™ GF M3434- stem cell technologies) to perform the colony-forming assay. The methocult media was vortexed and allowed to settle to remove the air bubble. The leukemic cells were counted and calculated as 500 cells per 1000µl media per well of a 12-well plate. The cells were mixed with the media by vortexing and added to each well of a 12-well plate. The plate was incubated for two weeks, and the number of colonies was counted after two weeks. To stain the colonies, each well was added with 100µl of p-Iodonitrotetrazolium Violet (INT) (1mg/ml) and incubated overnight at 37°C in an incubator with 5% $CO_2$, as explained previously (Dong, Guo, Zhou, Li, & Zhang, 2021). Pictures were taken from the stained colonies for representation.

### 4.13. Drugs Treatment

The primary leukemic and non-leukemic cells from mice were treated with metformin hydrochloride (sigma), Cytarabine (AraC) (Selleckchem) and Ionidamine (sigma). The concentration of the drugs used is shown in the results sections 5.7.3, 5.7.4 and 5.7.5. The cells were seeded at a seeding density of $0.3*10^6$ cells/ml in the IMDM media supplemented with cytokines (Table 7). The cells were seeded in a 24-well plate, with 500µl of cells per well. Drugs were added to each well, and the live cell counts were measured by trypan blue staining after 72 hours of treatment.

### 4.14. Bioinformatics and Statistical Analysis

The statistical analyses were performed using graph pad prism software (version 6.01, La Jolla, California, USA). A two-tailed, unpaired T-test was used to calculate the p-value. A p-value < 0.05 was considered significant. The p-values of the individual data are represented in the respective figures.

For the analysis of potential Gfi1 target genes, available chromatin immunoprecipitation (ChIP) sequencing data sets of Gfi1 from CODEX were used. The data sets include GSE69101 (Goode et al., 2016; Lie et al., 2018), GSE50806 (Spooner et al., 2013), GSE42518 (Moignard et al., 2013). With the help of the UCSC Genome Browser, the results of the ChIP-sequencing data sets were analysed (Kent et al., 2002).

The RNAseq analysis was performed by my colleague Dr. Daria Frank. The ATACseq analysis was performed by my colleague Xiaoqing Xie. The bioinformatic analysis of RNAseq and ATACseq was performed by our collaboration partner Lanying Wei (Medical Clinic A of the Münster University Hospital and the Institute for Medical Informatics of the University of Münster). For the analysis of differentially expressed genes (DEG) from the RNAseq data, Salmon (Patro, Duggal, Love, Irizarry, & Kingsford, 2017) and DESeq2 (Love et al., 2014) were used. GSEA 7.1 (Subramanian et al., 2005) was used to analyze the RNA sequencing data. At the GSEA, the “hallmark gene sets” were analyzed from the Molecular Signatures Database v7.1 (MSigDB) (Liberzon et al., 2015). Salmon (Patro et al., 2017) and DEGseq2 (Love et al., 2014) were

used to analyze the differentially expressed genes (DEG) from the RNA sequencing results

For the ATACseq analysis, a q-value of <0.05 was considered significant. Integrated Genomics Viewer (IGV) tool (Robinson et al., 2017; Robinson et al., 2011) was used to analyse the ATACseq peaks, and mouse genome assembly (mm10) was used.

# 5. Results

## 5.1. An increased expression of *GFI1* reduced cell growth and induced differentiation.

### 5.1.1. Real-time PCR and Western blot analysis showed an increase in *GFI1* expression.

Low levels of GFI1 have previously been linked to a poor outcome in AML patients (Hones et al., 2016). Knock-down of *GFI1* expression in mice also causes myeloproliferative disease (MPN), which could progress to AML (Fraszczak et al., 2019). We were interested in the dose-dependent role of GFI1 in leukemic cells and its influence on proliferation, differentiation and metabolism. We first investigated the effect of increased expression of *GFI1* on the function of leukemic cells. In order to investigate the resulting phenotype with higher levels of GFI1, we increased *GFI1* expression levels lentivirally in human leukemic cell lines K-562, THP-1 and KG-1. After the transduction, the cells were FACS sorted for GFP+ cells (Figure 17A). Real-time PCR and western blot confirmed the enhanced expression of *GFI1*/ GFI1 at the mRNA and protein levels.

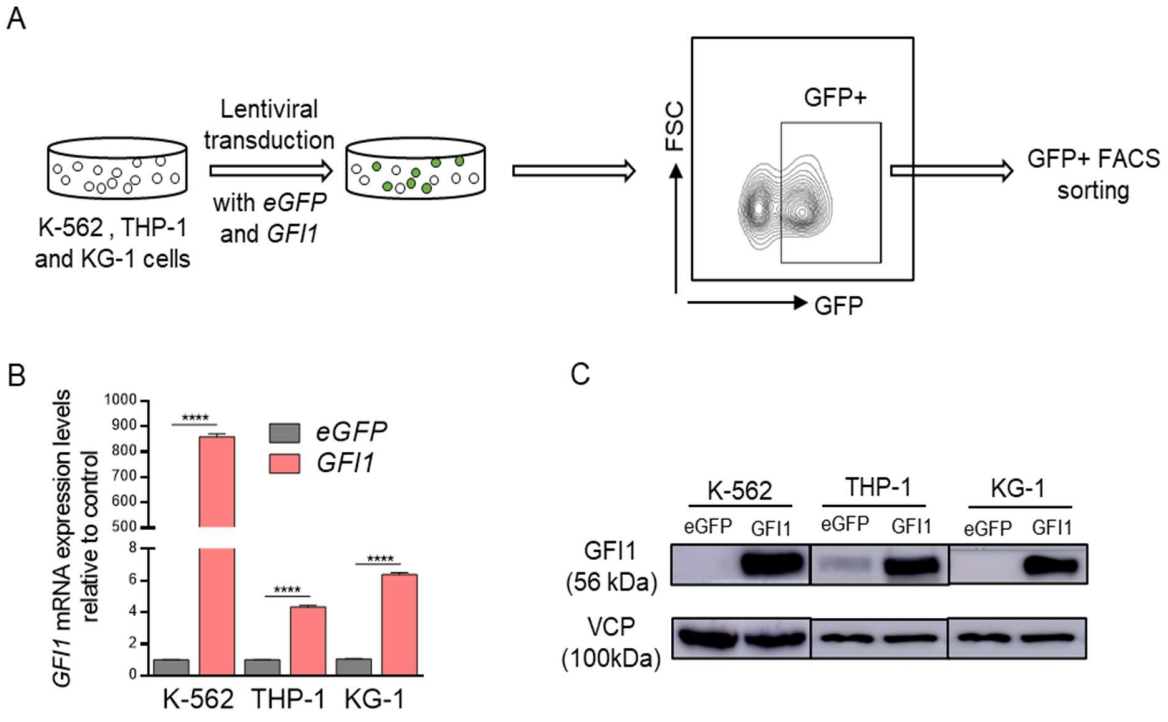

**Figure 17: Lentiviral transduction and expression levels of GFI1.**

**(A)** Lentiviral transduction is depicted schematically, followed by a FACS XY plot showing the sorting of GFP+ cells. (**B)** mRNA expression levels show upregulation of *GFI1* mRNA with increased *GFI1* expression in K-562, THP-1, KG-1 cell lines. The data are normalised to *GAPDH* expression as endogenous control. Average ± SD. ****P≤ 0.0001 (**C)** Western blot results show increased GFI1 protein levels with increased *GFI1* expression in K-562, THP-1, KG-1 cell lines. GFI1 and VCP protein bands appear at 56, and 100 kDa, respectively and VCP was used as a control. The data represent a single representative experiment. At least three independent experiments with similar results were performed.

### 5.1.2. Increased expression of *GFI1* reduced cell growth and induced differentiation

A liquid culture assay was used to determine the effect of increased *GFI1* expression on cell proliferation. After sorting GFP+ cells, cell counts were measured in liquid culture at 24, 48, and 72 hours after seeding. Increased *GFI1* expression correlated with a reduced rate of cell proliferation. We also determined the effect of increased *GFI1*-expression on the ability of cells to generate colonies. Transduced cells were sed in methylcellulose, and the number of colonies were examined after three weeks in culture. Increased *GFI1* expression resulted in a decrease in the number of colonies as well as a reduction in the size of colonies as measured by the number of cells per colony.

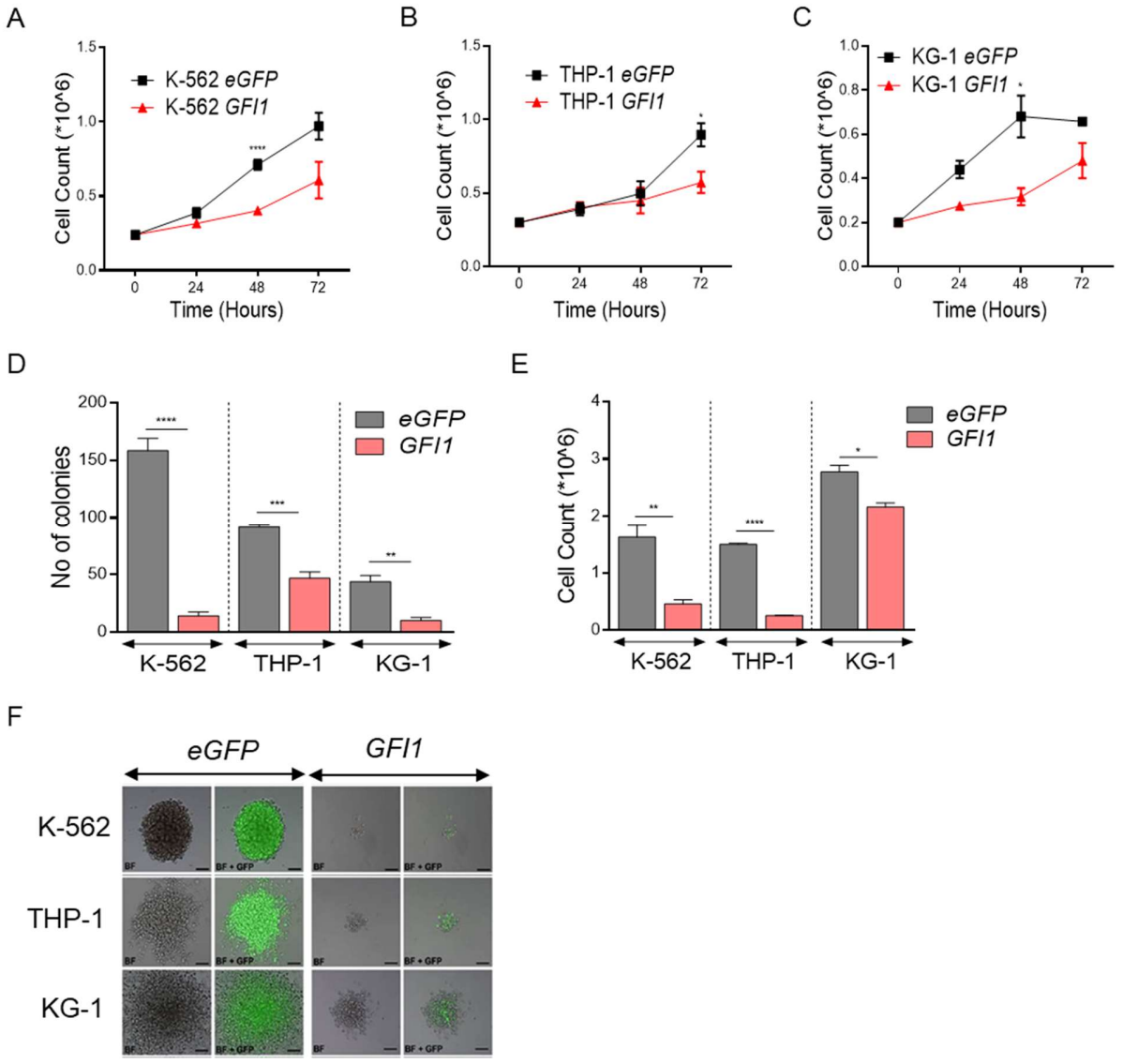


**Figure 18: Growth rate of human leukemic cell lines with induced *GFI1* expression.**

Increased expression of *GFI1* reduced the proliferation and promoted differentiation of human leukemic cell lines. Cell counts measurements in the liquid culture assay shows a reduction in cell growth with increased *GFI1* expression in K-562 (**A**), THP-1 (**B**) and KG-1 (**C**) cell lines. CFU assay showed a reduction in the colonies' number (**D**) and size (**F**) and a reduction in the total number of cells (**E**). (**F**) The right lane represents increased *GFI1* expression, and the left lane represents empty vector control. *GFP* represents cells transduced with the empty vector, and *GFI1* represents cells with an increased expression of *GFI1*. Average ± SEM, n=2, ****P≤ 0.0001, ***P=0.0003, **P≤ 0.0065, *P≤ 0.0236.

## 5.2. Increased expression of *GFI1* promoted the cells depending on OXPHOS

### 5.2.1. Increased *GFI1* expression upregulates OXPHOS, as assessed by microarray analysis.

We employed K-562 cells to explore the effect of enhanced *GFI1* expression on a whole transcriptomic level. We used K-562 cells since the baseline expression levels of *GFI1* are low. A next-generation transcriptomic expression profiling (Clariom™ S Assay, human) was carried out with enhanced *GFI1* expression in K-562 cells. The substantially altered hallmark pathways were estimated using gene set enrichment analysis, and their results are shown in Figure 19. The expression profile of the genes involved in the metabolic pathways of glycolysis, TCA cycle and fatty acid metabolism with increased expression of *GFI1* were represented as a heatmap (Figure 20).

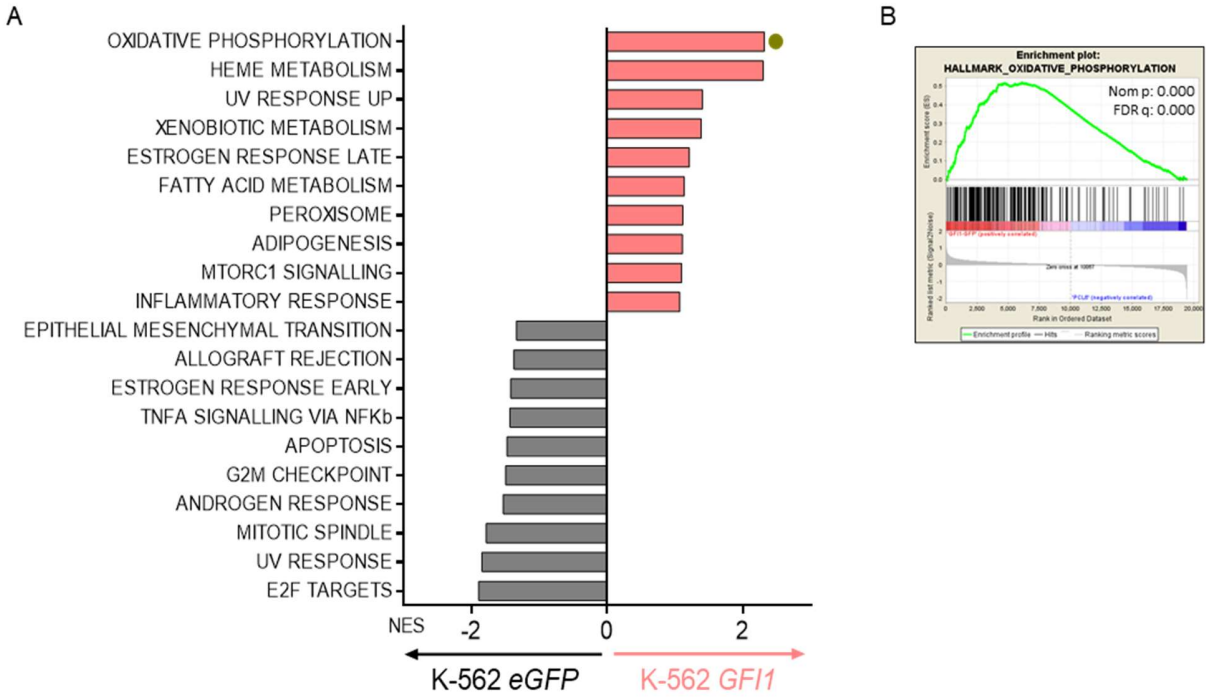


**Figure 19: Gene set enrichment analysis of microarray data with induced *GFI1* expression in K-562 cells.**

Transcriptomic expression profile of human K-562 cells with induced *GFI1* expression (K-562 *GFI1*) showed deregulation of metabolic gene signatures compared to the empty vector control (K-562 *eGFP*). **(A)** Hallmark gene set enrichment analysis indicates upregulation and downregulation of several pathways. **(B)** Enrichment plot showing significant upregulation of the genes in

oxidative phosphorylation (OXPHOS) pathway with induced expression of *GFI1*. NES: Nominal Enrichment Score.

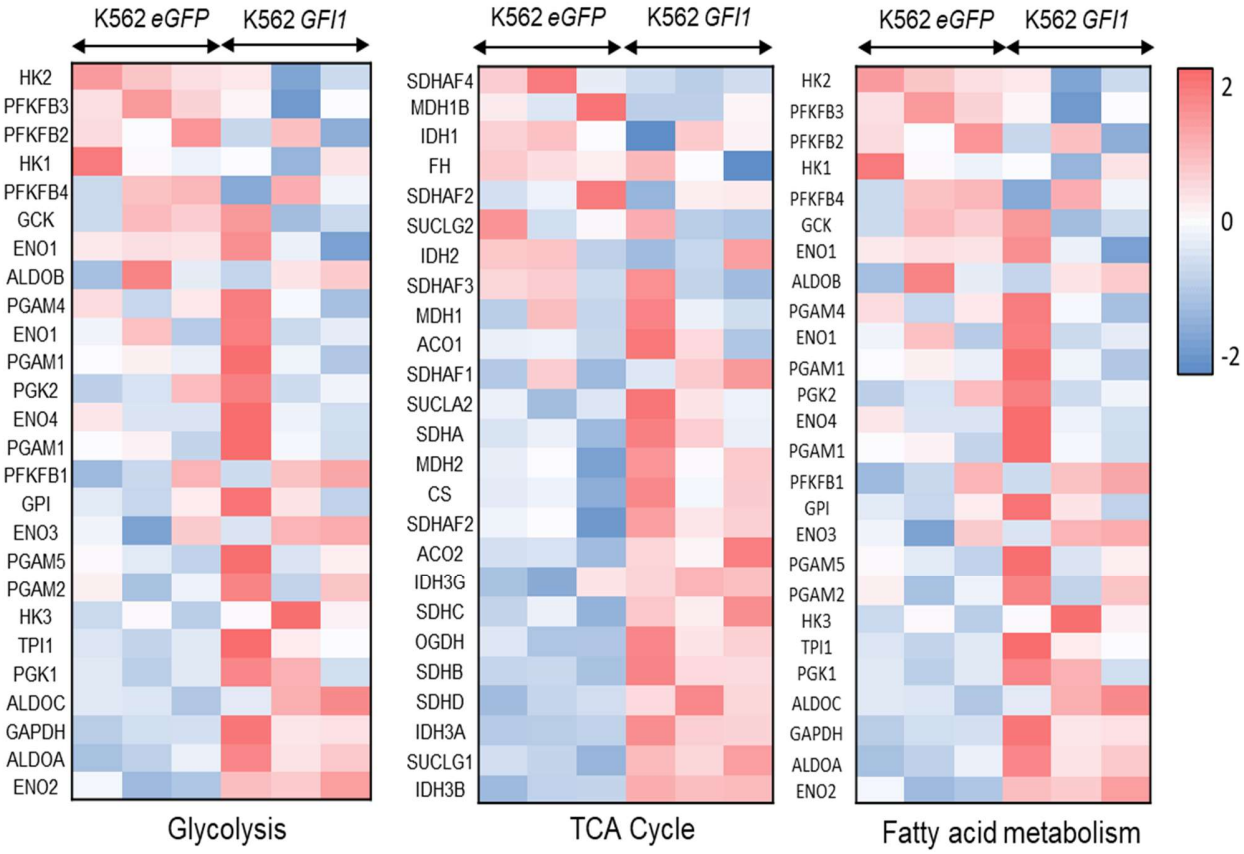


**Figure 20: Heatmap of metabolism genes with altered expression in cells with induced *GFI1* expression.**

Heatmap representation of expression profile of assorted metabolic genes involved in glycolysis, TCA cycle, and fatty acid metabolism as measured by microarray in K562 overexpression (K562 *GFI1*) compared to the empty vector control (K562 *eGFP*). Upregulation of the genes is represented by values closer to 2; downregulation is represented by values closer to -2.

### 5.2.2. Increased expression of *GFI1* reduced the glycolytic function in human leukemic cell lines

The rate of glucose consumption, lactate secretion, and intracellular lactate dehydrogenase (LDH) activity was assessed to measure how enhanced *GFI1* expression affected the rate of glycolysis. The human leukemic cell lines (K-562, THP-1 and KG-1) were lentivirally transduced with *GFI1* overexpressing (*GFI1*) and empty vector (*eGFP*) constructs, and GFP+ cells were FACS sorted as shown in Figure 17A. The sorted GFP+ cells were

cultured and the amount of glucose consumed and lactate secreted by the cells was measured from the cell culture supernatant collected after 24 and 48 hours in the culture, and the resulting values were normalized to cell count. The LDH activity was measured from the cell lysate of $1*10^6$ cells.

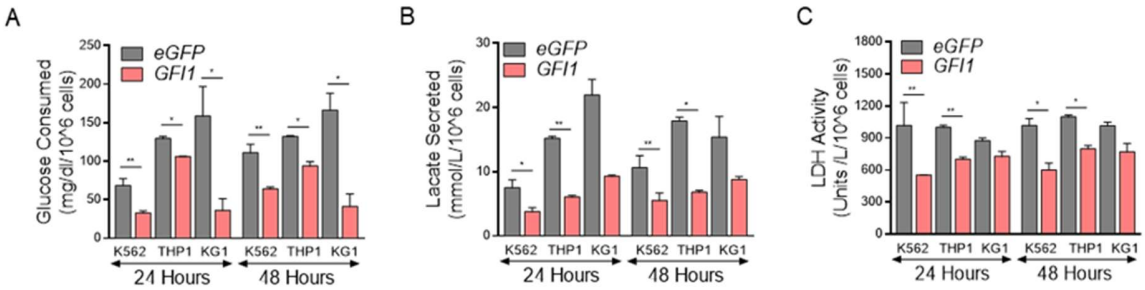


**Figure 21: Glucose consumed, lactate secreted and LDH levels with enhanced *GFI1* expression in human leukemic cell lines**

(**A**) Increased expression of *GFI1* showed a reduction in glucose consumption in K-562, THP-1 and KG-1 cells after 24 and 48 hours in culture. (**B**) Increased expression of *GFI1* showed a reduction in lactate secretion in K-562, THP-1 and KG-1 cell lines after 24 and 48 hours in culture. (**C**) Increased expression of *GFI1* showed a reduction in intracellular lactate dehydrogenase (LDH) activity in K-562, THP-1 and KG-1 cell lines after 24 and 48 hours in culture. All the values were normalized to cell count. *eGFP* represents the cells transduced with empty vector, and *GFI1* represents cells transduced with the increased expression of *GFI1* in respective cell lines. Average ± SEM, n=3, **P≤ 0.0065, *P≤ 0.0236.

5.2.3. Increased expression of *GFI1* reduced the rate of glycolysis in comparison with oxidative phosphorylation (OXPHOS)

Since increased expression of *GFI1* was associated with a reduction in glycolytic parameters, seahorse extracellular flux assays were performed to measure how the rate of oxidative phosphorylation and glycolysis were affected with increased *GFI1* expression in human leukemic cell lines. The GFP+ cells were sorted and seeded into 96-well plates to perform the seahorse experiments, as outlined in section 4.11.1. Seahorse mitostress and glycostress tests were performed to measure the rate of OXPHOS and glycolysis, respectively. Oxygen Consumption Rate (OCR) was measured to calculate the oxygen consumed by the cells, which is proportional to the OXPHOS as most of the oxygen consumed by the cells is through OXPHOS. Extracellular Acidification Rate (ECAR) was measured to calculate the rate of

glycolysis, proportional to the lactate secreted by the cells. The basal and maximum OCR and ECAR values were calculated before oligomycin and after FCCP treatment, respectively. The ratio of OCR to ECAR was calculated to estimate metabolic dependency. High OCR to ECAR was observed with increased *GFI1* expression, indicating that the cells were more dependent on OXPHOS due to a reduction in glycolysis.

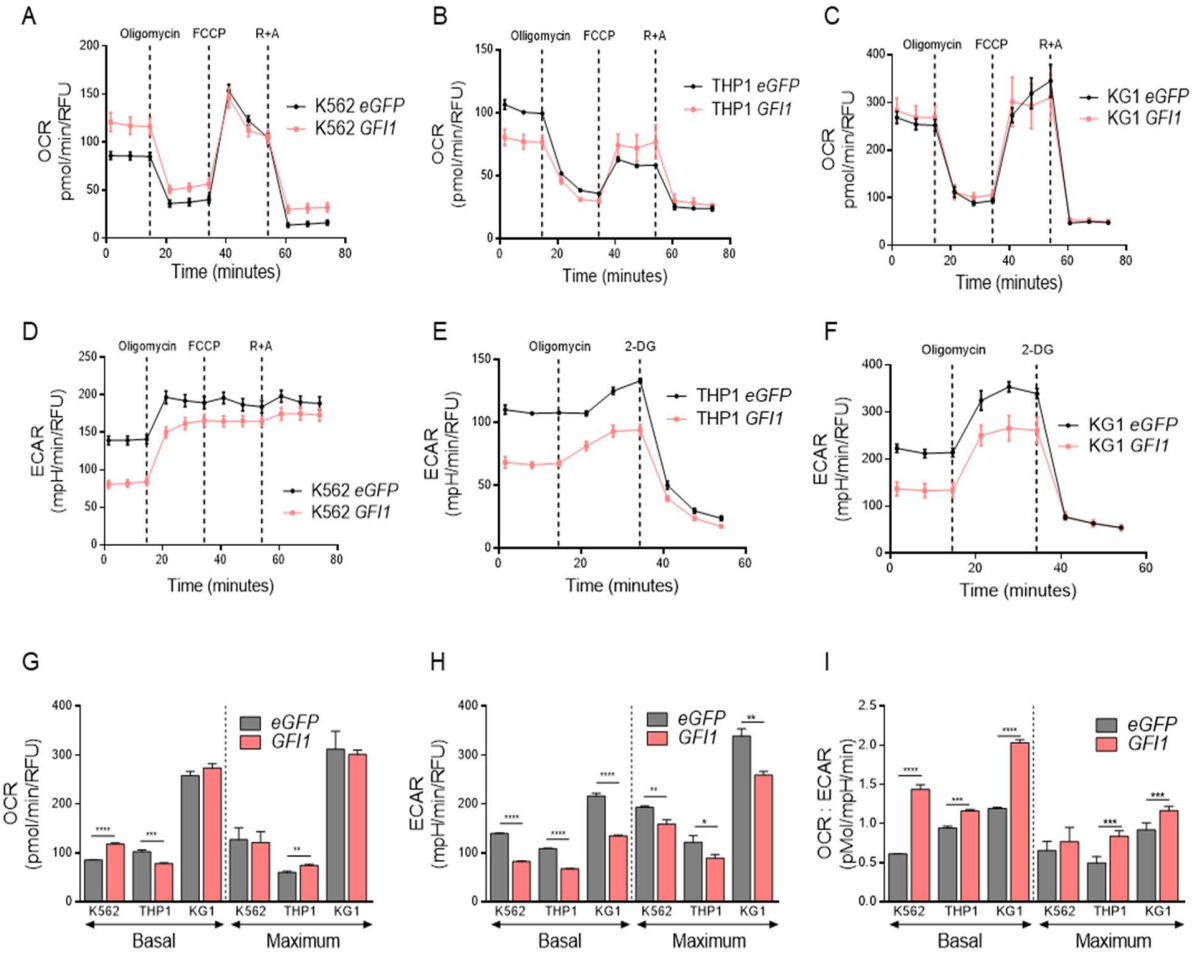


**Figure 22: Seahorse mitostress and glycostress tests with induced *GFI1* expression in human leukemic cell lines.**

(**A, B, C**) Seahorse Mitostress tests revealed no consistent change in the rate of OCR with increased expression of *GFI1* in human leukemic cell lines K-562, THP-1 and KG-1. (**D, E, F**) Seahorse glycostress tests showed a significant reduction in the rate of ECAR with increased expression of *GFI1* in human leukemic cell lines K-562, THP-1 and KG-1. (**G**) Basal and maximum OCR values calculated with increased *GFI1* expression showed no persistent change. (**H**) Basal and maximum ECAR values showed a reduction in ECAR rates with increased *GFI1* expression. (**I**) A high OCR to ECAR ratio was observed with increased *GFI1* expression. *GFI1* - Increased expression; *eGFP*-

empty vector control; OCR- Oxygen Consumption Rate; ECAR- Extracellular Acidification Rate; Average ± SD. The data represent a single individual experiment; n=3; ***P≤ 0.0065, ***P≤ 0.0065, **P≤ 0.0065, *P≤ 0.0236. Three individual experiments were performed with a similar outcome.

### 5.2.4. Increased expression of *GFI1* promoted the cells' dependence on fatty acid oxidation

Enforced expression of *GFI1* was associated with a decrease in the rate of glycolysis and a subsequent higher dependency on OXPHOS due to a high rate of OCR to ECAR (5.2.3). A seahorse mitostress test in combination with the substrate oxidation stress test was performed to identify the predominant active pathway and, as a result, the primary energy source for OXPHOS. The inhibitors Etomoxir, UK5099 and BPTES, were used to measure fatty acid, glucose and glutamine metabolism, respectively. The maximum response of the cells to these inhibitors was measured by calculating the decrease in OCR compared with empty media control after FCCP injection. The degree of reduction in OCR values after adding the inhibitor compared to empty media was used to calculate the response rate of specific inhibitors. The amount of decline in OXPHOS was represented by the rate of reduction in OCR values. The overall response to the three inhibitors was set to 100%, and the response rate to each inhibitor was computed correspondingly. K-562 and THP-1 cells with increased *GFI1* expression showed a high reduction in OCR values with Etomoxir treatment compared to their empty vector controls. This demonstrated that K-562 and THP-1 cells with enhanced *GFI1* expression were more reliant on fatty acid oxidation.

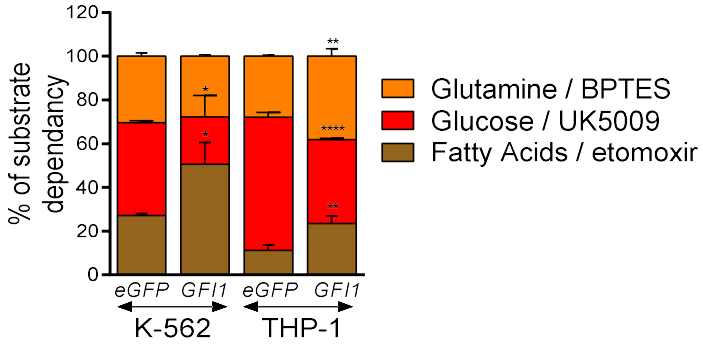


**Figure 23: Seahorse substrate oxidation tests with induced *GFI1* expression in human leukemic cell lines.**

Substrate oxidation test revealed increased fatty acid oxidation with enhanced *GFI1* expression in K-562 and THP-1 cell lines. The percentage of substrate dependency was calculated by decreasing OCR values with the addition of inhibitor compared to empty media control. The maximum response to the inhibitors was calculated after FCCP treatment. *GFI1* - Increased expression; *eGFP* - empty vector control; Average ± SEM, the data represents from three independent experiments; ****P≤ 0.0001, **P≤ 0.0076, *P≤ 0.0225.

### 5.3. Primary lineage depleted cells with reduced expression of *GFI1* promotes OXPHOS

As shown in section 5.2, when GFI1 protein levels were high, the rate of glycolysis was reduced, increasing the cells' reliance on OXPHOS. To further assess the dose-dependent role of GFI1, we examined how reduced expression of *GFI1* altered the function of non-malignant and malignant haematopoietic cells. We employed *GFI1* knock-in (*KI*) and knock-down (*KD*) mouse models to evaluate metabolic alterations in an *in-vivo* and *ex-vivo* setting. The *GFI1 KD* mice express 10-20% of human GFI1 protein. The mouse models are described in section 4.10.1.

5.3.1. Reduced levels of GFI1 in the murine models was confirmed by real-time PCR, Western blot and FACS analysis.

The *GFI1 KI* and *KD* mice were genotyped as described in section 4.10.2. The mice were sacrificed at a minimum age of 6 weeks, and the lineage depleted cells (lin-) were extracted from the total bone marrow (section 4.10.3). The expression levels of *GFI1* in the *GFI1 KI* and *KD* mice was further confirmed

by real-time PCR for mRNA levels and Western blot for protein levels (Figure 24).

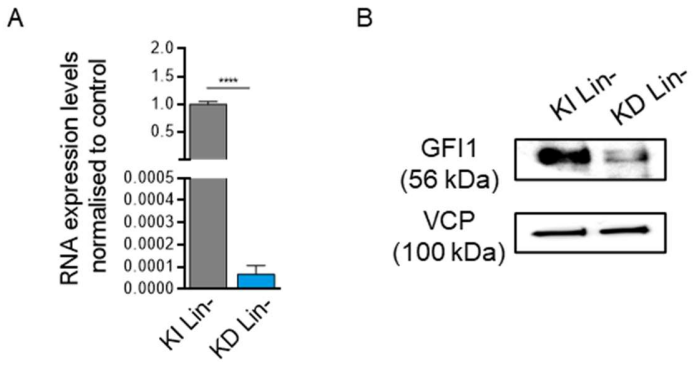


**Figure 24: *GFI1* expression levels in *GFI1 KI* and *KD* lineage depleted cells.**

(**A**) Relative fold change in the *GFI1* mRNA expression levels showed a reduction in *GFI1 KD* lineage depleted cells compared to *GFI1 KI* cells. The *Gapdh* endogenous control was used to normalize the expression levels. (**B**) Western blot data showed a reduction in GFI1 protein levels in the *GFI1 KD* lineage depleted cells compared to the *GFI1 KI* cells. The VCP bands represent the endogenous control for protein measurement. Average ± SD. The data represents a single experiment. Three individual experiments were performed with similar results, n=3; ****P≤ 0.0001.

In addition to genotyping, real-time and western blot, the *GFI1 KI* and *KD* mice were also characterized by FACS staining of the granulocytes and monocytes. A typical example of the difference in the granulocytes and monocytes between *GFI1 KI* and *KD* is shown in the following Figure 25. The *GFI1 KD* BM cells showed low granulocytes and high monocytes compared to the *GFI1 KI* cells.

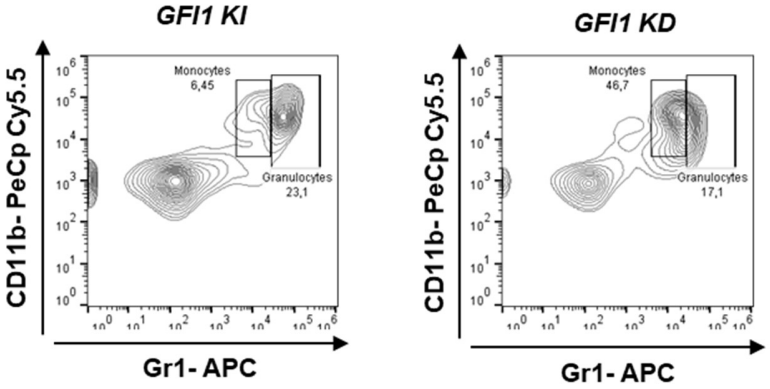


**Figure 25: Flow cytometric staining of granulocytes and monocytes from the total bone marrow cells of *GFI1 KI* and *KD* mice.**

A FACS XY plot shows the distinction of *GFI1 KI* and *KD* mice through flow cytometric staining of bone marrow cells with Gr1 APC and CD11b PerCPCy5.5 antibodies for granulocytes and monocytes, respectively.

*5.3.2.* Reduced levels of *GFI1* expression promoted the cell growth *in-vitro*

Purified lineage depleted cells from the *GFI1 KI* and *KD* mice were cultured *in-vitro,* and the cell growth was measured for three days at 24-hour intervals. The cells were seeded at the initial density of $0.2*10^6$ cells/ml in SCM media. *GFI1 KD* cells proliferated faster compared to the *KI* cells (Figure 26).

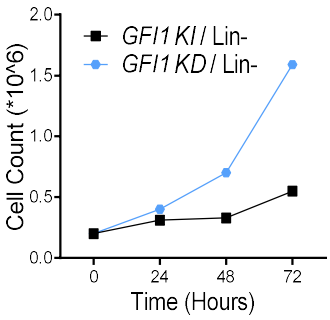


**Figure 26: Growth curve of lineage depleted cells of *GFI1 KI* and *KD* mice.**

The lineage depleted cells from the *GFI1 KD* mice showed a high proliferation rate compared to the *KI* mice. The data represents a single experiment; n=3.

5.3.3. Reduced levels of *GFI1* expression showed no change in the rate of glycolysis

It has been shown earlier that the increased expression of *GFI1* reduced the rate of glucose consumed and lactate secreted by the cells (section 5.2.2). To investigate the metabolic changes with a low level of *GFI1* expression, the glucose consumption and lactate secretion were measured biochemically (see section 4.11.1) from the lineage depleted cells cultured *in-vitro*. Reduced expression of *GFI1* showed no change in glucose consumption and lactate secretion levels (Figure 27).

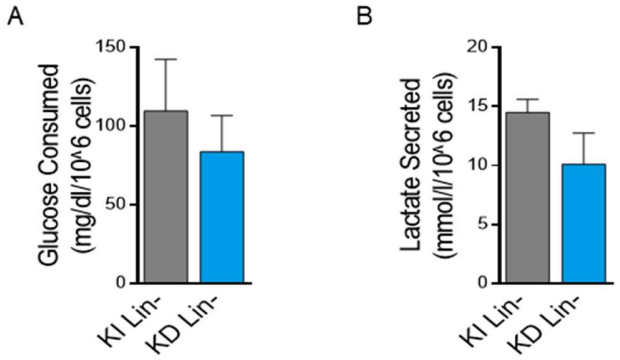


**Figure 27: Glucose consumption and lactate secretion measurements from *GFI1 KI* and *GFI1 KD* lineage negative cells.**

Glucose consumption (**A**) and lactate secretion (**B**) values from the supernatant of *GFI1 KI* and *GFI1 KD* lineage depleted cells. The values were normalised to the cell count. Average ± SEM; n=3.

### 5.3.4. Reduced expression of *GFI1* in lineage depleted cells upregulated OXPHOS

The metabolic regulation of *GFI1* in a non-leukemic setting was measured using seahorse mitostress and glycostress tests with lineage depleted cells from *GFI1 KI* and *KD* mice. The lineage depleted cells were isolated and cultured *in-vitro.* The seahorse mitostress and glycostress experiments were performed from the cultured cells, as described in section 4.11.2. *GFI1 KD* cells showed an increase in the OCR at the basal levels before oligomycin injection and maximum levels of OCR after FCCP treatment (Figure 28A). At the same time, the glycostress test showed no significant change in the rate of ECAR both at the basal and maximum levels (Figure 28B). The ratio of OCR to ECAR was calculated to define the dominant pathway. Reduced expression of *GFI1* showed a high rate of OCR to ECAR at the basal and maximum levels (Figure 28C), indicating the *GFI1 KD* cells depended on OXPHOS rather than glycolysis in a non-leukemic background. In addition, *GFI1 KD* cells also showed a high rate of ATP production and spare respiratory capacity (Figure 28D), indicating a higher mitochondrial activity in *GFI1 KD* cells. To quantify the mitochondria, the mtDNA copy number was evaluated by real-time PCR. The *GFI1 KD* cells showed a higher mtDNA copy number compared to *GFI1 KI* cells (Figure 28E).

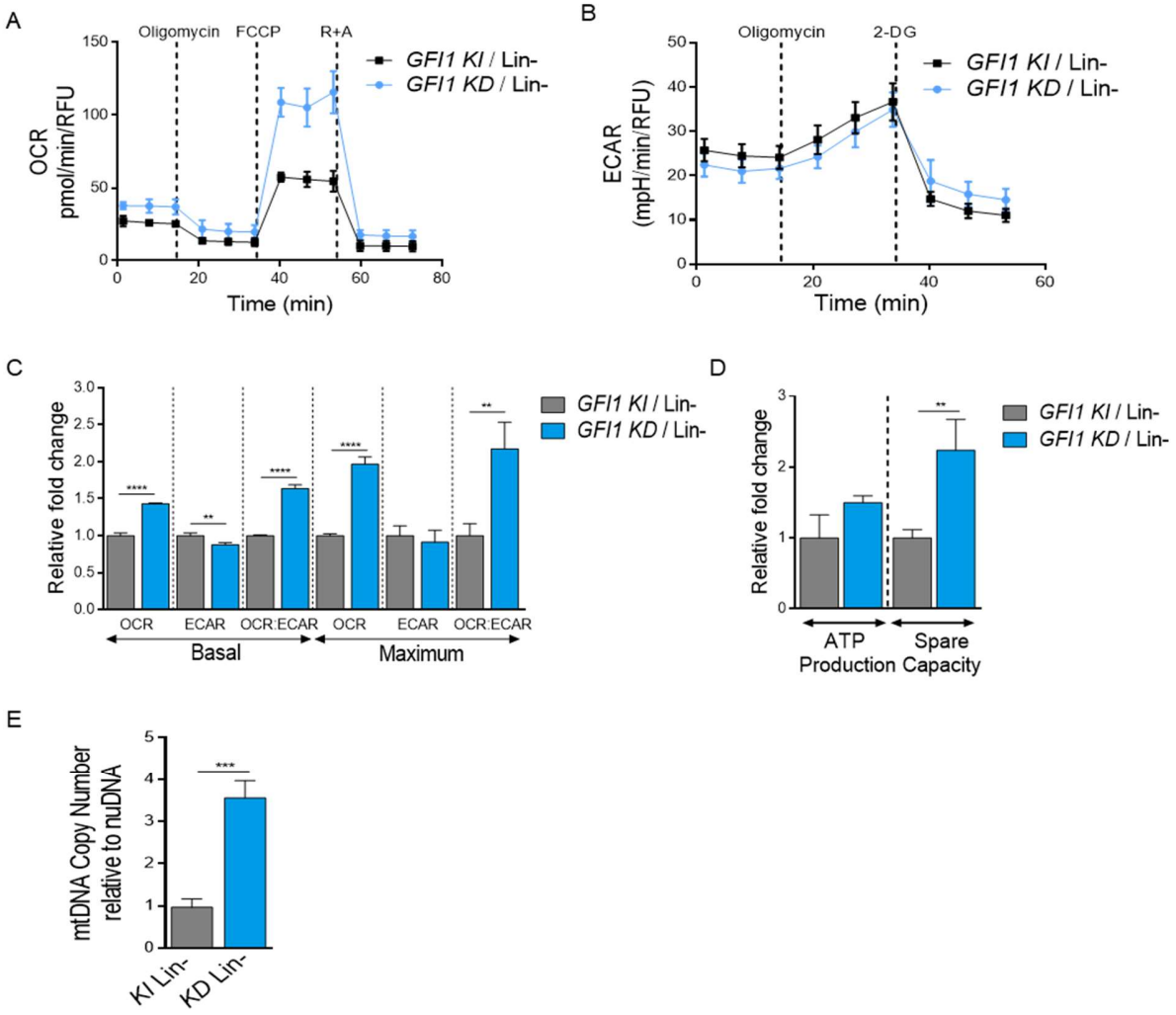


**Figure 28: Seahorse experiments and mtDNA copy number measurement with *GFI1 KI* and *GFI1 KD* lineage depleted cells.**

(**A** and **B**) Seahorse mitostress and glycostress tests show OCR and ECAR measurements, analysed with *GFI1 KI* and *GFI1 KD* lineage depleted cells. Average ± SD; n=3. (**C**) The ratio of OCR to ECAR at the basal and maximum levels. Average ± SD; n=3. (**D**) ATP production and spare respiratory activity were calculated from the mitostress values. Average ± SD; n=3 (**E**) Mitochondrial DNA (mtDNA) copy number relative to nuclear DNA in *GFI1 KI* and *KD* lineage depleted cells. Average ± SD; n=3. Each data set represents a single representative experiment. Three individual experiments were performed with similar results. ****P≤ 0.0001; ***P=0.0006; **P≤ 0.0092.

5.3.5. *GFI1 KD* lineage depleted cells downregulated the fatty acid metabolism and promoted glutamine metabolism.

A seahorse substrate oxidation stress test was performed with the lineage depleted cells from the *GFI1 KI* and *GFI1 KD* mice, as outlined in section

4.11.4. The *GFI1 KD* lineage depleted cells showed a low reduction in OCR values after Etomoxir treatment compared to *GFI1 KI* lineage depleted cells. This indicated a lower response to Etomoxir, therefore a lower fatty acid oxidation in *GFI1 KD* lineage depleted cells. On the other hand, the *GFI1 KD* lineage depleted cells showed a higher decrease in OCR values with BPTES treatment, denoting a high glutamine metabolism compared to *GFI1 KI* cells (Figure 29).

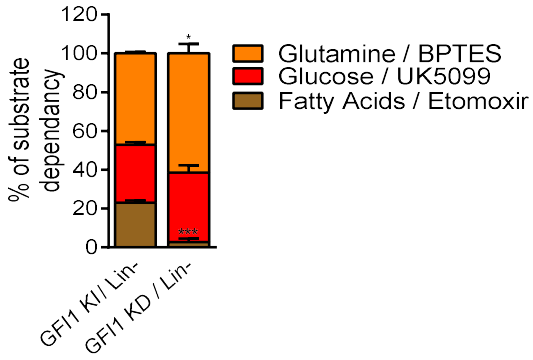


**Figure 29: Substrate oxidation stress test with lineage depleted cells from *GFI1 KI* and *KD* mice.**

The percentage of substrate dependency was calculated from *GFI1 KI* and *GFI1 KD* lineage depleted cells by seahorse OCR measurements after inhibitor treatment. It was calculated at the maximum response after FCCP treatment. Average ± SD; n=3. The data represents a single representative experiment, out of three individual experiments with similar outcome *P=0.0421, ***p=0.0007.

### 5.4. Reduced expression of *GFI1* in *MLL-AF9* expressing AML cells leads to upregulation of OXPHOS.

Since the lineage depleted cells with the low expression level of *GFI1* displayed a high rate of OXPHOS, we investigated whether the same applied to a leukemic background. To explore this, we used the *MLL-AF9* induced AML model. The retroviral expression of the *MLL-AF9* fusion oncogene transform hematopoietic cells, and after transplantation into irradiated mice, the mice will develop AML (Botezatu, Michel, Helness, et al., 2016; Chen et al., 2019; Milne, 2017). The lineage depleted cells were isolated from the *GFI1 KI* and *GFI1 KD* mice (section 4.10.3). The cells were transduced with retrovirus carrying *MLL-*

*AF9* oncofusion, and the GFP+ cells were FACS sorted to enrich the cells encoding MLL-AF9 fusion protein (section 4.10.5). The sorted lineage depleted cells were primarily transplanted into lethally irradiated mice, and upon the development of leukemia, the leukemic cells from the primary transplanted mice were further transplanted for secondary and tertiary transfers (section 4.10.8, Figure 16). The *in-vitro* metabolic experiments in this study were performed with the sorted GFP+ cells after the transduction of lineage depleted cells with a retrovirus expressing MLL-AF9 fusion protein tagged with GFP marker. To perform the metabolic analysis from the leukemic mice *ex-vivo*, GFP+ c-Kit+ cells (considered leukemic blasts) were isolated by isolating c-Kit+ cells first by MACS columns followed by FACS sorting GFP+ cells (section 4.10.9.3). The experiments from the leukemic mice were considered *ex-vivo*.

### 5.4.1. FACS analysis of bone marrow cells from leukemic mice to score for AML development

Once the mice show signs of overt AML (as described in section 4.10.9), the expression of respective cell surface marker proteins was determined using FACS analysis, as shown in section 4.10.9. In addition, a non-leukemic mouse was analysed as a control. The cellular characteristics and the percentages of various blood cell populations from the leukemic mice were analysed by flow cytometry. The surface marker c-Kit is widely expressed in leukemic blast cells (Heo et al., 2017; Ikeda et al., 1991; Valverde et al., 1996; C. Wang, Curtis, Geissler, McCulloch, & Minden, 1989). Hence, GFP+ cells expressing c-Kit receptors were considered enriched for leukemic blast cells (Valverde et al., 1996). The leukemic mice featured increased frequency of the c-Kit+ cells, while the frequency of CD4 and B cells was decreased compared to the non-leukemic control mice (Figure 30).

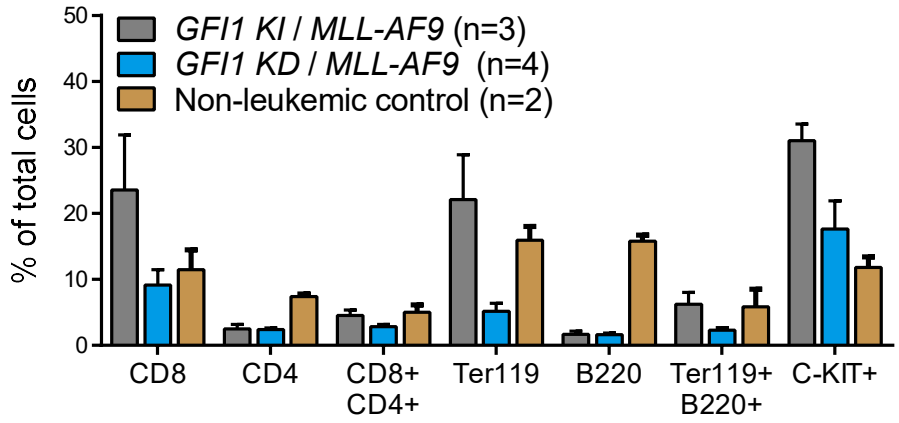


**Figure 30: Flow cytometric analysis of BM subpopulations in leukemic mice.**

The flow cytometric analysis showed the percentage of various blood cell populations in the bone marrow of leukemic mice transplanted with *GFI1 KI* and *GFI1 KD MLL-AF9* cells. The data represent a representative experiment with more than three mice in each group. Three individual transplantation experiments were performed with similar results, and each transplantation was performed with three mice in each group. Average ± SEM; n≥3.

### 5.4.2. Blood cell measurement of peripheral blood from the leukemic mice

To further characterize the leukemic mice, peripheral blood was collected and was measured for the number of white blood cells (WBC) and platelets using a blood counter (scil Vet abc) (section 4.10.9). The AML development was associated with an increased WBC and reduced platelet count in the peripheral blood, compared to a control non-leukemic mice (Figure 31).

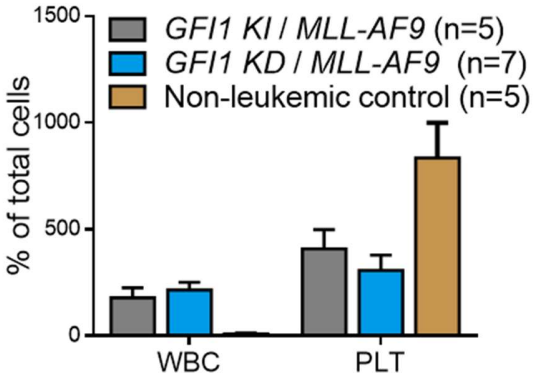

**Figure 31: Peripheral blood measurement of leukemic and non-leukemic mice**

The white blood cells (WBC) and platelets (PLT) numbers were measured using a blood counter from peripheral blood of the leukemic and non-leukemic control mice. The data represents the cumulative of multiple experiments. Average ± SEM; n≥5.

### 5.4.3. The growth rate of leukemic cells

*GFI1 KD* leukemic cells expressing *MLL-AF9* showed a significantly increased growth rate compared to *GFI1 KI* leukemic cells (Figure 32).

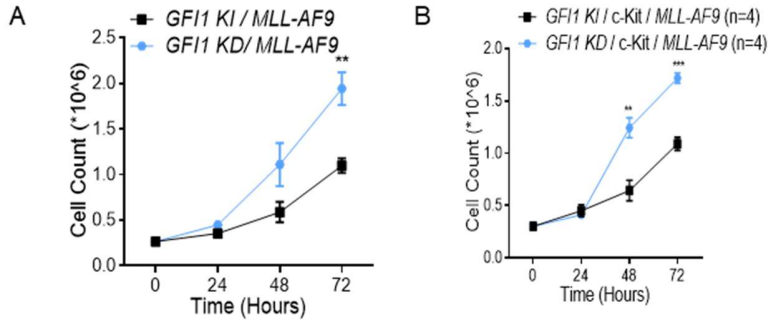


**Figure 32: Growth rate of *GFI1 KI* and *KD* leukemic cells from *in-vitro* and *ex-vivo* cultures.**

Growth curves of *MLL-AF9* induced leukemic cells derived from *in-vitro* culture (**A**) (n≥3) and *ex-vivo* culture (**B**) (n=4). The data set is representative of at least three independent experiments. Average ± SEM. ***P=0.0002; **P≤0.0033.

### 5.4.4. Glucose uptake and lactate secretion assay

Glucose consumed, and lactate secreted by the cells represent glycolysis rate (TeSlaa & Teitell, 2014). The *MLL-AF9* expressed leukemic cells from the *in-vitro* experiments were cultured, and the supernatant was collected after 48 hours to measure the amount of glucose consumed and lactate secreted by the cells (explained in section 4.11.1). The *GFI1 KD* leukemic cells expressing the *MLL-AF9* oncofusion gene consumed more glucose than *GFI1 KI* cells (Figure 33A). However, there was no change in the amount of lactate secreted by the cells (Figure 33B).

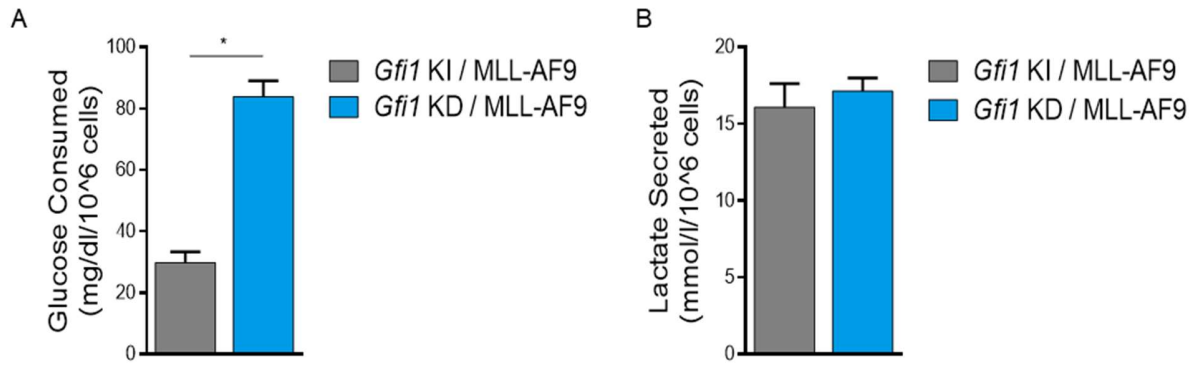


**Figure 33: Glucose consumed and lactate secreted from *in-vitro* cultured leukemia cells.**

The rate of glucose consumed (**A**) and lactate secreted (**B**) by the leukemic cells *in-vitro*, measured from the media supernatant. The data were normalized to cell counts. The data represents the cumulative of two individual experiments. Average ± SEM. *P=0.0135.

### 5.4.5. A low level of *GFI1* in MLL-AF9 induced leukemic cells upregulated OXPHOS

Seahorse mitostress and glycostress tests were performed to measure the rate of OXPHOS and glycolysis with *MLL-AF9* induced leukemic cells. The experiment was performed with *GFI1 KI* and *GFI1 KD* leukemic cells from *in-vitro* and *ex-vivo* cultures (section 4.11.2). Seahorse mitostress assay revealed increased OCR values with reduced *GFI1* expression in leukemic cells cultured *in-vítro* and *ex-vivo* (from secondary and tertiary transplantations) (Figure 34A). *GFI1 KD* leukemic cells with the glycostress experiment showed an increase in the ECAR values in *in-vitro* studies and no consistent change in ECAR values in *ex-vivo* studies compared to *GFI1 KI* leukemic cells (Figure 34B). To measure the contribution of OXPHOS towards overall metabolism and how this compared to glycolysis, the ratio of OCR to ECAR was calculated at the basal and maximum levels. The *GFI1 KD* leukemic cells displayed a significant upregulation of OCR to ECAR at the basal and maximum levels from the *in-vitro* and *ex-vivo* analyses, which indicates the *GFI1 KD* leukemic cells were more dependent on OXPHOS compared to *GFI1 KI* cells (Figure 35A and B). The ATP production capacity calculated from mitostress tests showed a

high rate of ATP production with a low level of *GFI1* expression from the *in-vitro* and tertiary transplantation analysis (Figure 35c).

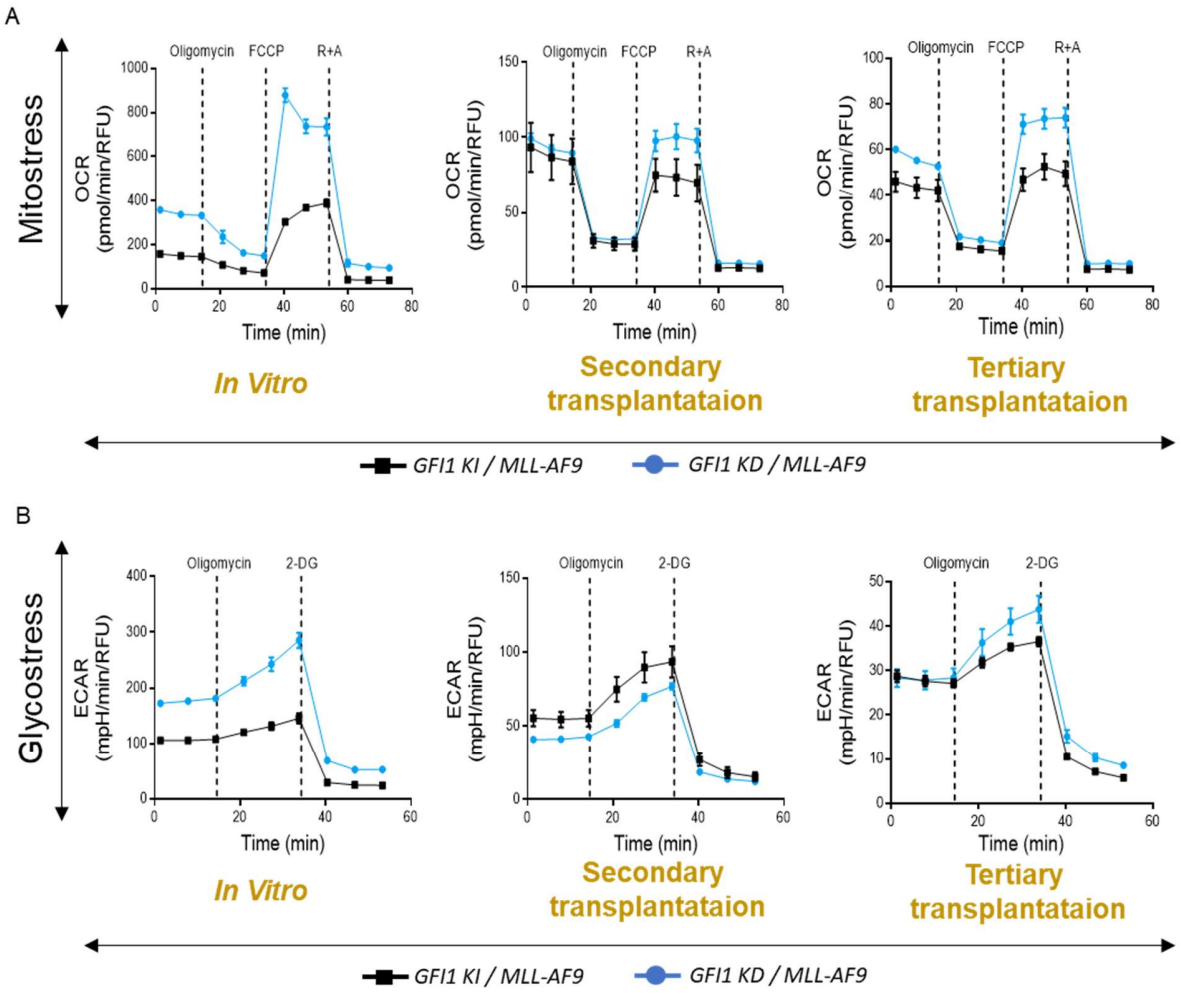


**Figure 34: Seahorse experiments with *GFI1 KI* and *KD* leukemic cells.**

Seahorse mitostress (**A**) and glycostress (**B**) tests displayed OCR and ECAR values, respectively. The data set represents a single representative experiment, and each experiment was performed with at least three replicates. Three independent experiments were performed, and every experiment was performed with the leukemic cells from individual mice: Average ± SD, n≥3.

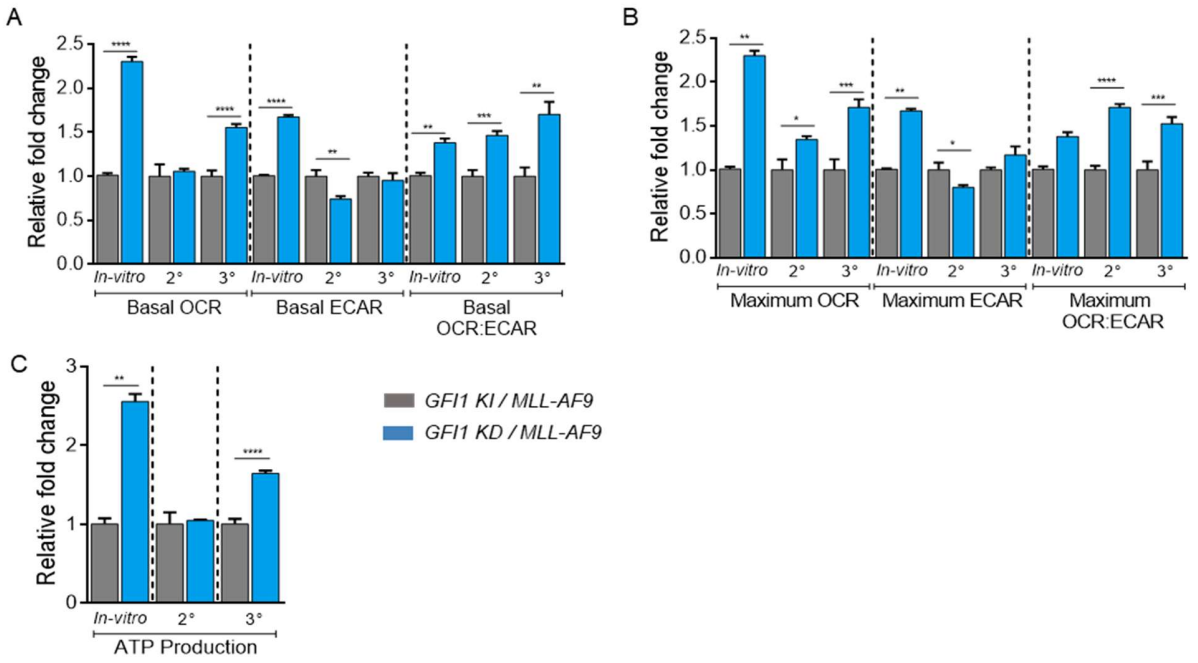


**Figure 35: Relative fold change of OCR and ECAR in *GFI1 KI* and *GFI1 KD* leukemic cells.**

(**A** and **B**) Calculation of OCR, ECAR and OCR to ECAR ratio at the basal and maximum levels from the sea-horse mitostress and glycostress tests. (**C**) The rate of ATP production rate was calculated from the mitostress tests. The relative fold change was calculated by comparing it to the *GFI1 KI* cells. The data set represents a single representative experiment. Three individual experiments were performed with similar results: Average ± SD, n=3.

### 5.4.6. *GFI1 KD* leukemic cells showed increased mitochondrial DNA copy number

As outlined in the previous section 5.4.5, the *GFI1 KD* leukemic cells exhibited a higher rate of OXPHOS. We measured mitochondrial DNA (mtDNA) copy numbers to see if an increase in mitochondria numbers caused the increased OXPHOS. It was calculated as explained in section 4.11.9. The *GFI1 KD* leukemic cells featured a higher mtDNA copy number compared to *GFI1 KI* leukemic cells (Figure 36). This indicates that the increase in OXPHOS might be through the increase in mitochondrial number.

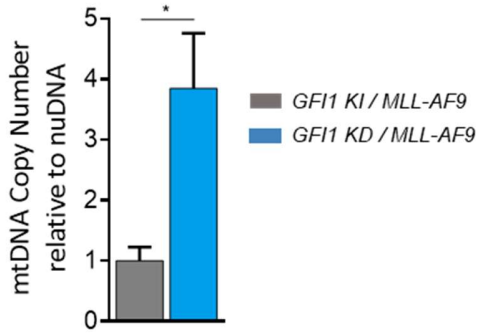


**Figure 36: Mitochondrial DNA copy number of *in-vitro* cultured leukemic cells.**

Mitochondrial DNA copy number relative to nuclear DNA was calculated from the *GFI1 KI* and *KD* leukemic cells. Average ± SD, n≥3; *P=0.0383.

5.4.7. *GFI1 KD* leukemic cells downregulated fatty acid metabolism and upregulated glutamine metabolism.

Since the *GFI1 KD* leukemic exhibited a high rate of OXPHOS, we performed a seahorse substrate oxidation stress test as explained in section 4.11.4 to determine the source of metabolites for OXPHOS. The *in-vitro* cultured *GFI1 KD* leukemic cells were less sensitive to Etomoxir while showing increased sensitivity to UK5099 and BPTES than *GFI1 KI* cells (Figure 37). This indicates that the *GFI1 KD* leukemic cells showed reduced fatty acid oxidation, while the increased OXPHOS in the *GFI1 KD* cells was due to increased glutamine metabolism.


**Figure 37: Substrate oxidation stress test with *in-vitro* cultured leukemic cells from *GFI1 KI* and *GFI1 KD* mice.**

The percentage of substrate dependency was calculated from *GFI1 KI* and *GFI1 KD* leukemic cells by seahorse OCR measurements after inhibitors treatment. It was calculated at the maximum response after FCCP treatment. Average ± SD; n=3. The data represents a single representative experiment. Three independent experiments were performed, and a similar outcome was obtained **P=0.0010,****P≤0.0001.

We also measured the cell counts after treatment with substrate inhibitors. The *in-vitro* cultured leukemic cells were treated with glucose, fatty acid and glutamine metabolism inhibitors, UK5099, Etomoxir, ST1326 and BPTES (section 4.11.5), and the response to these inhibitors was calculated by counting the live cells after 72 hours of treatment. The *GFI1 KD* leukemic cells showed a significant response only to UK5099 and BPTES and no decrease in cell counts after ST1326 treatment. In contrast, the *GFI1 KI* leukemic cells showed a reduction in cell count with the three inhibitors ST1326, UK5099 and BPTES (Figure 38). This result indicated a low rate of fatty acid oxidation in *GFI1 KD* leukemic cells, and the increased OXPHOS might be fueled by increased glutamine metabolism, as the cells showed a significant response to BPTES. On the other hand, the *GFI1 KI* cells showed a high fatty acid, glucose and glutamine metabolism rate.

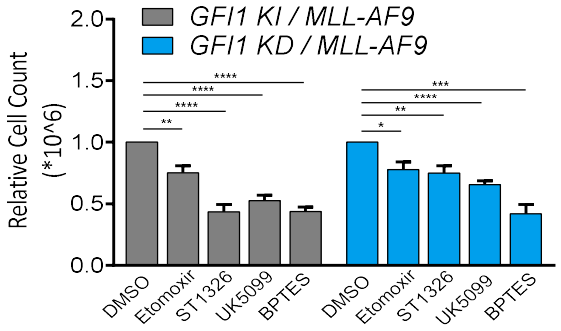


**Figure 38: Substrate oxidation stress test by cell count measurements with *in-vitro* cultured leukemic cells.**

Cell counts of *in-vitro* cultured leukemic cells after 72 hours of treatment with the substrate oxidation inhibitors. The data represents the cumulative of three individual experiments, and each experiment was performed with the leukemic cells from individual mice. The relative cell count was calculated with DMSO as a control. Average ± SEM, n=4; ****P≤0.0001, ***P=0.0002, **P≤0.0056, *P=0.0108.

### 5.4.8. *GFI1 KD* leukemic cells showed increased mitochondrial functionality

Since the *GFI1 KD* leukemic cells exhibited elevated OXPHOS, the next step was to measure the mitochondrial activity. We measured the mitochondrial membrane potential (MMP), mitochondrial mass and mitochondrial Reactive Oxygen Species (ROS) levels by flow cytometric analysis as explained in sections 4.11.6, 4.11.7 and 4.11.8. The *GFI1 KD* leukemic cells showed a significant increase in median fluorescence values (MFI) of MMP, mass and ROS levels compared to *GFI1 KI* cells (Figure 39).

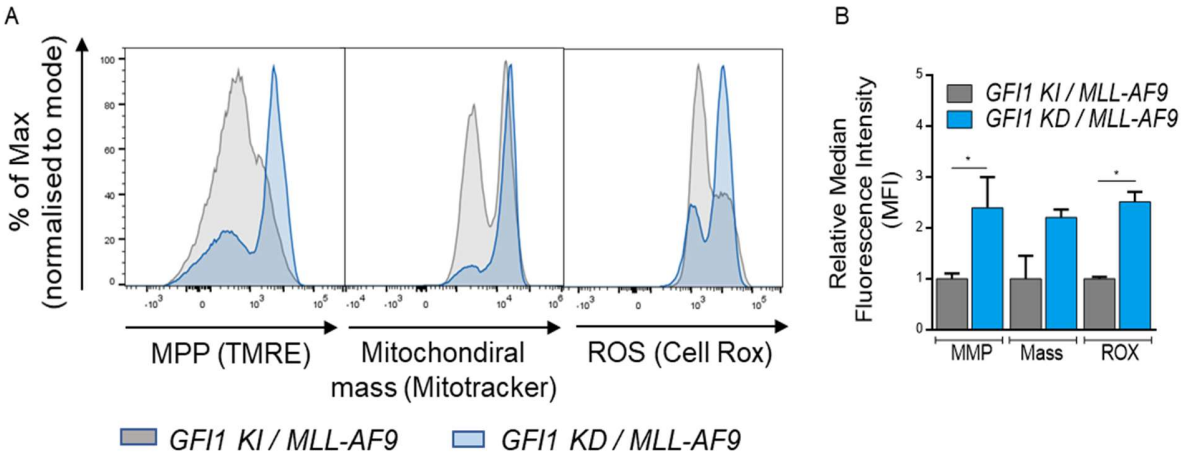


**Figure 39: Measurements of mitochondrial membrane potential, mitochondrial mass and Reactive Oxygen Species (ROS) levels from *in-vitro* leukemic cells.**

(**A**) Histogram overlay of the MMP, Mass and ROS levels data from the *GFI1 KI* and *GFI1 KD* leukemic cells (**B**) Relative median fluorescence intensity (MFI) data calculated from the flow cytometric analysis of *GFI1 KI* and *GFI1 KD* leukemic cells. The relative MFI values represent the average from at least two independent experiments. Average ± SEM, n≥2; *P≤0.0380.

### 5.5. Reduced expression of *GFI1* in human leukemic cell lines upregulated OXPHOS and mitochondrial functionality

A low expression level of *GFI1* in murine leukemic cells was found to be associated with an increased level of OXPHOS. To investigate the effect of reduced *GFI1* expression on metabolic properties, we performed metabolic experiments in human leukemic cell lines by reducing the expression levels of *GFI1*. We used the human leukemic cell line THP-1 to knock-down *GFI1*.

#### 5.5.1. Generation of *GFI1* knock-down clones in human leukemic cell lines

The shRNAs designed against the human *GFI1* coding sequence were cloned into the pRSMX-PG plasmid to generate the knock-down clones. The retrovirus was produced with the cloned construct, and the leukemic cell lines THP-1 TRBSR were transduced with the retrovirus (section 4.9). The GFP+ cells were selected by puromycin, and the cells were induced with 1µg/ml doxycycline (Sigma-Aldrich) for five days (sections 4.9.3.2 and 4.9.3.3). The generation of knock-down clones is briefly explained in section 4.9 and shown in Figure 40A.

The generated *GFI1 KD* clones in the THP-1 TRBSR cells showed a reduction in mRNA and protein levels, measured by real-time PCR (Figure 40B) and western blot (Figure 40C and D), compared to the clones with the scrambled (*SCR*) sequences.

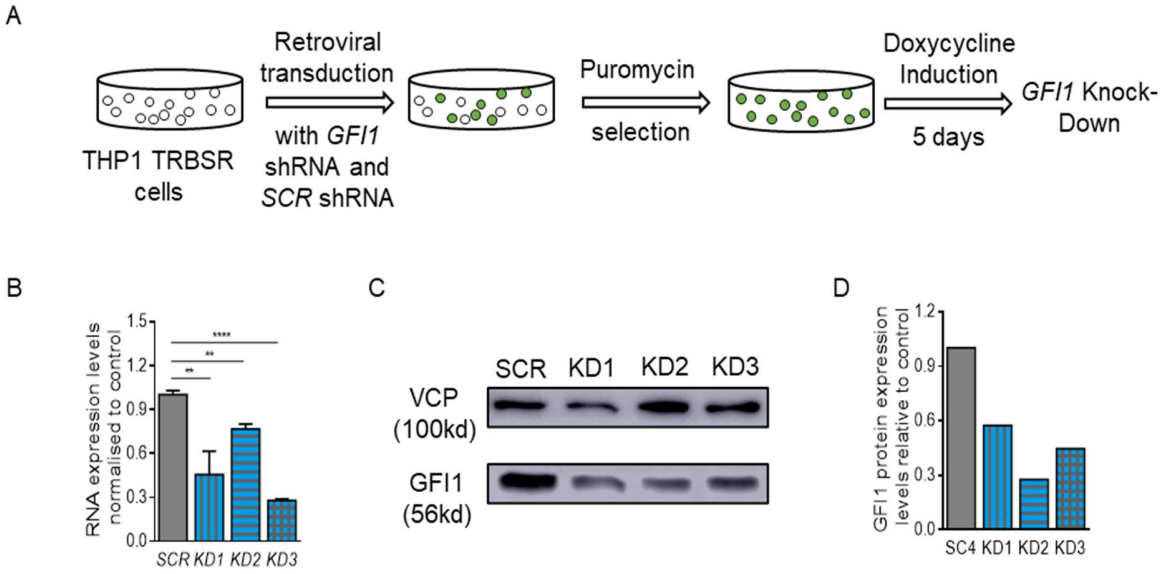


**Figure 40: Generation of induced *GFI1 KD* clones in human leukemic THP-1 cells and GFI1 expression measurements.**

(**A**) Schematic representation of retroviral transduction of human leukemic cell lines expressing TRBSR receptors with retrovirus packed with *GFI1* shRNA followed by puromycin selection and doxycycline induction. (**B**) Relative mRNA expression levels of *GFI1* normalized to *GAPDH* mRNA expression. The data was plotted from at least three biological repeats. (Average ± SEM, **P ≤0.0049; ****P < 0.0001; n ≥ 3). (**C**) Western blot displaying the GFI1 protein expression levels in knock-down clones (**D**) Relative protein quantification using ImageJ and data normalized to VCP control. *SCR*- scrambled shRNA, *KD1, KD2, KD3- GFI1* knock-down clones. The western blot data represent a single representative experiment. Three independent experiments were performed with similar results.

5.5.2. Knock-down of *GFI1* in THP-1 cells increased the rate of oxidative phosphorylation

THP-1 cells are human AML cell lines expressing the *MLL-AF9* fusion gene. Hence, we used THP-1 cells in the current study to correlate the metabolic phenotype with the experimental findings of *MLL-AF9* induced leukemic cells from mice. We employed shRNA-induced knock-down to lower *GFI1* expression in THP-1 cells (section 5.5.1). To measure the metabolic changes with the

reduced expression of *GFI1* in modified THP-1 cells, we performed the seahorse mitostress and glycostress tests with the *GFI1 KD* clones. We used the scrambled sequence (*SCR*) as an shRNA control. Seahorse Mitostress and Glycostress tests reveal upregulation of oxidative phosphorylation (Figure 41A) and glycolysis (Figure 41B) with reduced expression of *GFI1* in three THP-1 knock-down clones. A reduction in *GFI1* expression increased OCR and ECAR at the basal (Figure 41C) and maximum levels (Figure 41D) and increased the ratio of OCR to ECAR at the maximum respiratory rate (Figure 41D). This showed that reduced expression of *GFI1* in leukemic THP-1 cell lines led to similar metabolic changes in human AML cells as those we observed in *in-vitro* and *ex-vivo* murine leukemic cultures.

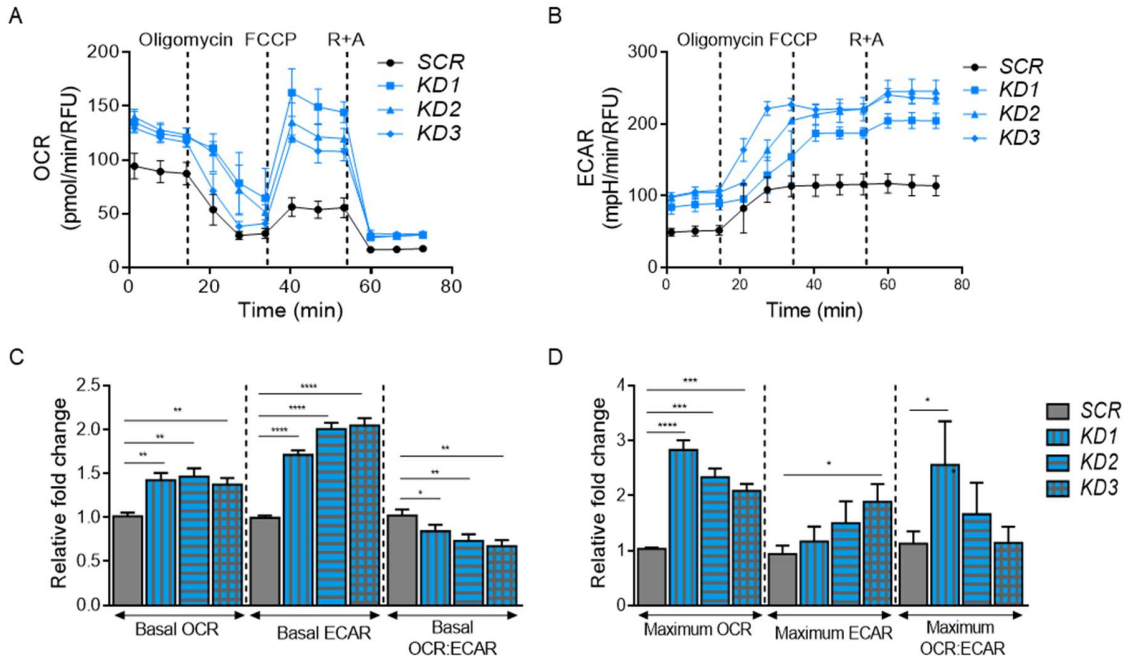


**Figure 41: Sea-horse metabolic experiments with reduced expression of *GFI1* in THP-1 cells.**

(**A**) Sea-horse, mitostress test results, showing the OCR rate with *GFI1 KD* in THP-1 cells. (**B**) Sea-horse mitostress test showing the ECAR rate with *GFI1 KD* in THP-1 cells. (**C** and **D**) Relative fold change values of OCR, ECAR and OCR to ECAR ratio at the basal and maximum respiratory rates. OCR - Oxygen Consumption rate; ECAR - Extracellular Acidification Rate: R+A - Rotenone + Antimycin A; 2-DG - 2-Deoxy Glucose. *SCR*- scrambled shRNA, *KD1, KD2, KD3*- *GFI1* knock-down shRNA clones. The data represents a single individual experiment. (Average ± SD, *P ≤ 0.0396; **P ≤ 0.0079; ***P ≤ 0.0001; ****P ≤ 0.0001; n = 3).

5.5.3. *KD* of *GFI1* in THP1 cells increased mitochondrial membrane potential (MMP)

Along with OXPHOS, we measured the mitochondrial membrane potential to measure the mitochondrial activity in THP-1 cells. The THP-1 cells were stained with TMRE, and the membrane potential was measured by flow cytometric staining, as explained in section 4.11.6. The *GFI1 KD* clones showed a significant increase in MMP compared to the scrambled sequence control, which indicates an increase in mitochondrial functionality with reduced *GFI1* expression in THP-1 cells.

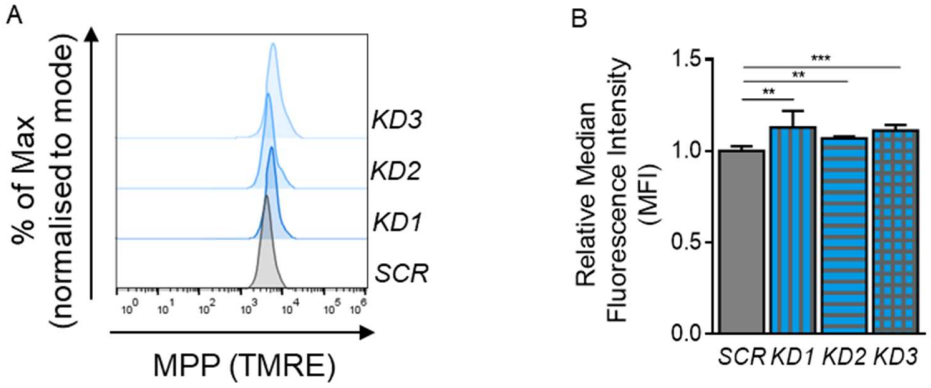


**Figure 42. The mitochondrial membrane potential of THP-1 cells within *GFI1 KD* clones.**

(**A**) Histogram overlay of MMP (TMRE staining) of THP-1 cells with *SCR* sequence and *GFI1 KD* clones. (**B**) Relative median fluorescence intensity (MFI) of TMRE staining of THP-1 *SCR* and *GFI1 KD* clones. *SCR*- scrambled shRNA, *KD1, KD2, KD3- GFI1* knock-down shRNA clones, MMP- Mitochondrial Membrane Potential. The data represent the cumulative data from multiple experiments. (Average ± SEM, **P ≤ 0.0066; ***P = 0.0001; n ≥ 3 ).

## 5.6. Reduced expression of *GFI1* in AML1-ETO9a induced AML cells lead to upregulation of OXPHOS.

As shown above, a low level of GFI1 was associated with an increased level of OXPHOS in the MLL-AF9 induced leukemic cells. To investigate whether the metabolic changes with the low *GFI1* expression levels are consistent with murine models of human leukemia and independent from one single mouse model, we used AML1-ETO9a oncofusion protein-induced leukemic cells.

5.6.1. A low level of *GFI1* in AML1-ETO9a induced leukemic cells was associated with slower growth of the cells.

To generate the leukemic cells, the lineage depleted cells were extracted from the *GFI1 KI* and *GFI1 KD* mice as explained in section 4.10.3, and the cells were transduced with the retrovirus carrying an *AML1-ETO9a* oncofusion gene (sections 4.10.4 and 4.10.5). The AML1-ETO9a fusion protein is co-expressed with a GFP reporter protein, and the GFP+ cells were FACS sorted. The sorted GFP+ cells were cultured using SCM media (Table 6), and the growth rate was measured by counting cells. The *GFI1 KD* cells expressing *AML1-ETO9a* fusion grew at a slower rate compared to the *GFI1 KI* cells.

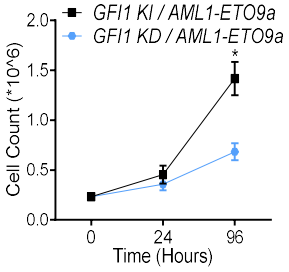


**Figure 43: The growth rate of *GFI1 KI* and *GFI1 KD* leukemic cells with *AML1-ETO9a* fusion.**

The growth curves of *GFI1 KI* and *KD* lineage deplete cells expressing an *AML1-ETO9a* oncofusion gene. The graph represents the values from three individual experiments. (Average ± SEM, *P = 0.0176; n = 3)

5.6.2. *AML1-ETO9a* induced leukemic cells with reduced expression of *GFI1* promoted high glucose consumption and lactate secretion levels

To measure the rate of glycolytic activity, we measured the amount of glucose consumed and lactate secreted by collecting the cell culture supernatant, as explained in section 4.11.1. The *GFI1 KD* leukemic cells with the retroviral expression of *AML1-ETO9a* oncofusion gene showed increased glucose consumption and a slightly increased lactate secretion compared to *GFI1 KI* cells (Figure 44).

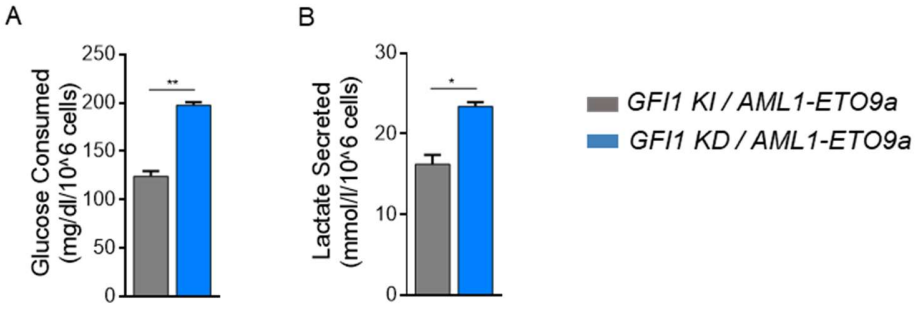


**Figure 44: Glucose consumed and lactate secretion levels from *GFI1 KI* and *KD* leukemia cells with an *AML1-ETO9a* oncofusion gene.**

Glucose consumed (**A**) and lactate secreted (**B**) measured from the cell culture supernatant of *GFI1 KI* and *KD* leukemic cells expressing an *AML1-ETO9a* oncofusion gene. The data represent the cumulative data from three independent experiments. The values were normalized to the cell counts measured while collecting the supernatant. (Average ± SEM, *P = 0.0292; **P = 0.0073; n =3).

### 5.6.3. Effect of reduced expression of *GFI1* on the metabolism of *AML1-ETO9a* induced leukemic cells

To evaluate the metabolic phenotype of *AML1-ETO9a* expressed *GFI1 KI* and *GFI1 KD* leukemic cells, we performed seahorse mitostress and glycostress tests (described in section 4.11.2) *GFI1 KD* leukemic cells expressing *AML1-ETO9a* oncofusion gene showed higher OCR values at the basal and maximum values than *GFI1 KI* cells. On the other hand, *GFI1 KD* cells had lower ECAR values compared to *GFI1 KI* cells. A high OCR to ECAR ratio was observed with reduced GFI1 expression with AML1-ETO9a fusion protein (Figure 45).

Despite the fact that *GFI1 KD* leukemic cells retrovirally expressing *AML1-ETO9a* had a lower proliferation rate (Figure 43), the metabolic phenotypes were similar to those of *GFI1 KD* leukemic cells retrovirally overexpressing *MLL-AF9*, which proliferated faster than *GFI1 KI* leukemic cells expressing *MLL-AF9* (Figure 32).

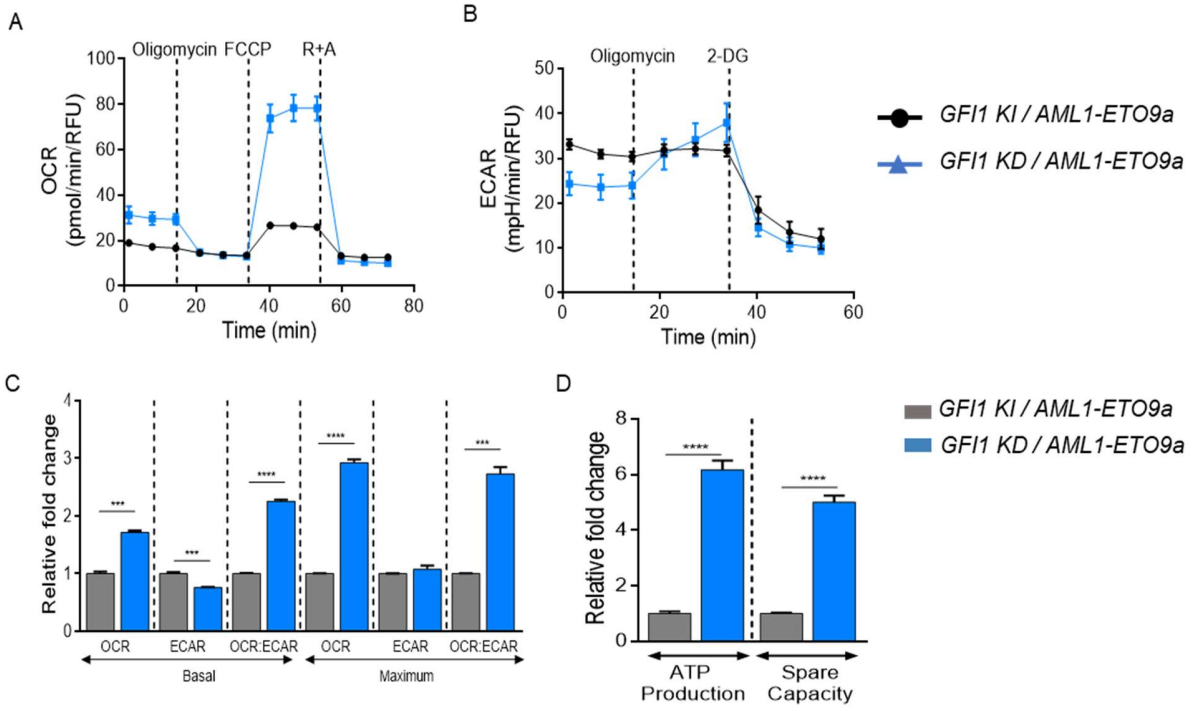


**Figure 45: Measurement of OCR and ECAR within *GFI1 KI* and *KD* leukemic cells expressing an *AML1-ETO9a* oncofusion gene.**

The OCR values were measured by mitostress (**A**), and the ECAR values were measured by the glycostress (**B**) test. (**C**) Relative fold change of OCR, ECAR and OCR to ECAR ratio at the basal and maximum levels. (**D**) Relative fold change of ATP production rate and spare respiratory capacity. The data represents a single representative experiment. (Average ± SD, ***P ≤ 0.0009; ****P ≤ 0.0001; n= 3 ).

### 5.6.4. *AML1-ETO9a* induced leukemic cells with reduced expression of *GFI1* had higher mitochondria DNA copy number

To quantify the influence of reduced expression of *GFI1* on the number of mitochondria, the mitochondrial DNA copy number was measured with reference to the nuclear DNA. The *GFI1 KD* leukemic cells expressing an *AML1-ETO9a* oncofusion gene had a higher mitochondrial DNA amount compared to leukemic *GFI1 KI* cells indicating that the number of mitochondria was increased in *GFI1 KD* leukemic cells. This was identical to the condition with *GFI1 KD* cells with *MLL-AF9* expression despite a lower rate of cell proliferation.

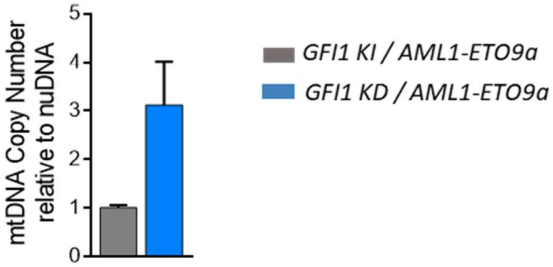


**Figure 46: Mitochondrial DNA copy number relative to the nuclear DNA calculated in *GFI1 KI* and *GFI1 KD* leukemic cells expressing an *AML1-ETO9a* fusion gene.**

5.6.5. *GFI1 KD* leukemic cells induced by *AML1-ETO9a* oncofusion gene expression exhibited a lower level of fatty acid oxidation.

To measure the dominant metabolic pathway in *GFI1 KI* and *GFI1 KD* leukemic cells with retroviral expression of *AML1-ETO9a*, the seahorse substrate oxidation stress test was performed likewise to the experiments performed with cells containing the *MLL-AF9* fusion, as described in section 4.11.4. The *GFI1 KD* leukemic cells were less sensitive to the fatty acid oxidation inhibitor Etomoxir, while they were highly sensitive to BPTES, an inhibitor of glutamine metabolism (Figure 47). This implies that similarly to cells containing the *MLL-AF9* oncofusion gene, the *GFI1 KD* leukemic cells with the *AML1-ETO9a* oncofusion gene had a low rate of fatty acid oxidation but a high rate of glutamine metabolism. The glutamine metabolism may contribute to the enhanced OXPHOS in cells with lower *GFI1* expression in *AML1-ETO9a* induced leukemic cells.

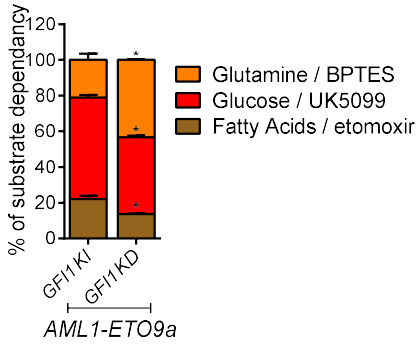


**Figure 47: OCR values of *GFI1 KI* and *KD* leukemic cells induced by the presence of an *AML1-ETO9a* oncofusion gene.**

The percentage of substrate dependency was calculated by the reduction of OCR values with the addition of inhibitor compared to empty media control. The maximum response to the inhibitors was calculated after FCCP treatment. The data represents a single representative experiment. (Average ± SD, *P ≤ 0.0429; n= 3).

### 5.7. Primary leukemic cells expressing a low level of *GFI1* were sensitive to metformin treatment

In the current study, we showed that the primary *GFI1 KD* leukemic cells had a higher rate of OXPHOS than *GFI1 KI* cells in two different murine models of human AML, which was independent of proliferation status. As described earlier, the AML patients with the physiologically low level of *GFI1* have a poor therapeutic outcome. Hence, we aimed whether the observed metabolic properties of *GFI1 KD* leukemic cells to target the leukemic cells with low levels of *GFI1* can be exploited therapeutically. In the current study, we have used drugs to interfere with the oxidative phosphorylation pathway by targeting the electron transport chain. As a potential drug, we used metformin, it is used for the treatment of patients with diabetes, and one of its properties is its ability to act as a complex I inhibitor of the electron transport chain. The detailed mechanisms of the metformin functions are explained in section 1.4.3.1.

#### 5.7.1. Metformin impeded the growth of *MLL-AF9* expressing *GFI1 KD* leukemic cells *in-vitro*

Since GFI1 is implicated in pathways dependent on oxidative phosphorylation, we examined its suitability to impede the growth of AML cells with reduced expression of *GFI1*. These cells have a higher dependency on oxidative phosphorylation and hence might be more sensitive to treatment with metformin. To measure the efficiency of metformin, we treated leukemic and non-leukemic cells with physiological (*GFI1 KI*) or reduced expression of *GFI1* (*GFI1 KD*) and cell proliferation was measured after 72 hours. The lineage depleted cells showed no change in the sensitivity towards metformin treatment between *GFI1 KI* and *GFI1 KD* cells. In contrast, metformin impeded the growth of *GFI1 KD MLL-AF9* leukemic cells *in-vitro* and *ex-vivo* more than *GFI1 KI* leukemic cells. On the other hand, the *GFI1 KD* leukemic cells with expression

of the *AML1-ETO9a* oncofuison gene did not differ in sensitivity to metformin from *GFI1 KI* cells retrovirally expressing *AML1-ETO9a* (Figure 48).

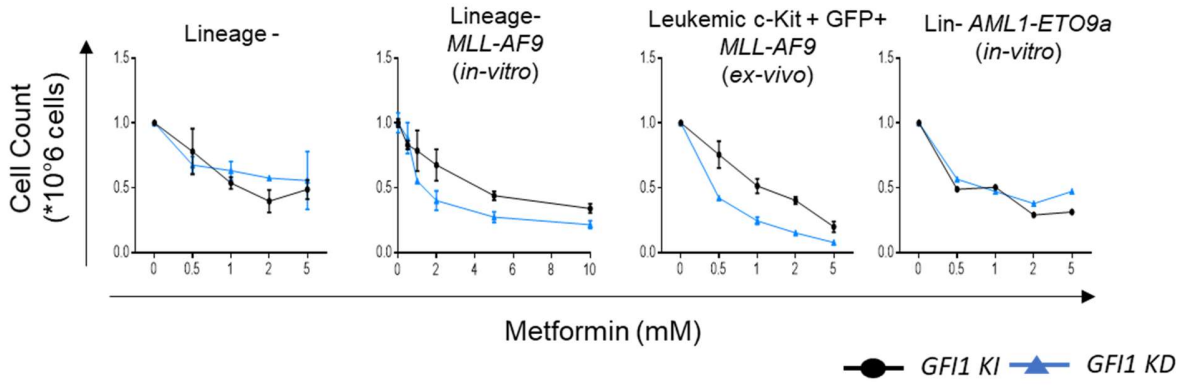


**Figure 48: Live-cell counts after metformin treatment of leukemic and non-leukemic cells.**

Live cell counts were measured after 72 hours of metformin treatment of *GFI1 KI*, and *GFI1 KD* lineage depleted cells, leukemic cells containing an *MLL-AF9* oncofusion (*in-vitro* and *ex-vivo*) and leukemic cells containing an *AML1-ETO9a* oncofusion gene (*in-vitro* culture). The data represents the cumulative values from three individual experiments. (Average ± SEM; n ≥ 3).

5.7.2. The *GFI1 KD* leukemic cells expressing *MLL-AF9* oncofusion showed high sensitivity to metformin treatment in the colony-forming assay

In addition to the liquid culture, we performed a colony-forming assay to measure if metformin can impede the colony-forming capacity of *MLL-AF9* induced leukemic cells. The *GFI1 KI* and *GFI1 KD* leukemic cells expressing MLL-AF9 fusion protein from the *in-vitro* culture were seeded in the methylcellulose media supplemented with metformin as explained in section 4.12, and the number of colonies was counted after two weeks of incubation. The *GFI1 KD* leukemic cells showed a more substantial decrease in the number of colonies than *GFI1 KI* leukemic cells after metformin treatment (Figure 49). This indicates that *GFI1 KD* leukemic were more sensitive to metformin treatment compared to *GFI1 KI* cells.

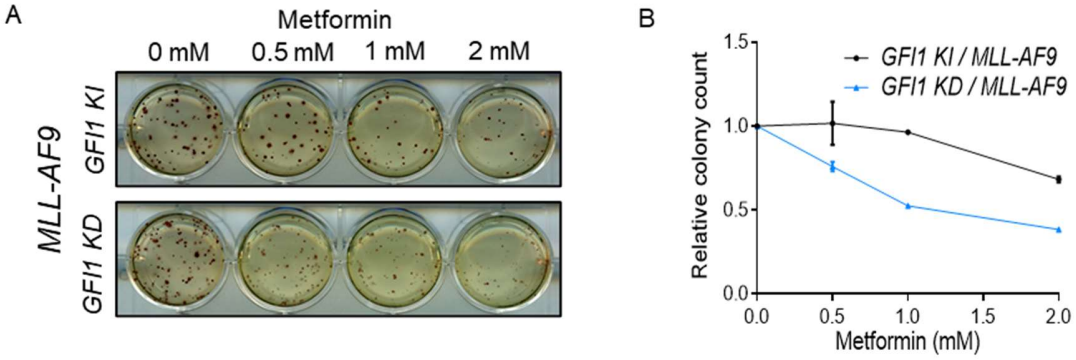


**Figure 49: Colony-forming assay with metformin treatment.**

(**A**) Images of the colonies captured after staining with p-Iodonitrotetrazolium Violet. The images represent a single representative experiment. (**B**) Relative colony counts normalized to untreated samples. The colony counts represent the cumulative of two individual experiments. (Average ± SEM; n = 2).

### 5.7.3. Metformin treatment of *GFI1 KD* leukemic cells increased glucose consumption and lactate secretion

Metformin treatment escalates the rate of glucose consumed by the cancer cells as a compensatory activation of glycolysis to enhance the bioenergetics of the cells. Consequently, lactate secretion is augmented as an end product of the upregulated glycolysis (Ben Sahra et al., 2010; Biondani & Peyron, 2018). Hence, to dissect the effect of metformin treatment, we measured the glucose consumed and lactate secreted by the cells from the culture supernatant after 72 hours of metformin treatment. The glucose consumed and lactate secreted from the culture supernatant were measured biochemically (section 4.11.1) and through mass spectrometric analysis. The mass spectrometric analysis calculated the peak-area of α-D glucose and lactate, and the values were subtracted from the empty media. The values were then normalized to the live cell counts. Metformin treatment of *MLL-AF9* expressed *GFI1 KD* leukemic cells led to higher glucose consumption and a higher lactate secretion than *GFI1 KI* leukemic cells from biochemical (Figure 50A and B) and mass- spectrometric analysis (Figure 50C and D). Since higher glucose consumption and lactate secretion indicate a higher rate of glycolysis, the metformin treatment might shift the *GFI1 KD* leukemic cells expressing *MLL-AF9* oncofusion from oxidative phosphorylation towards glycolysis.

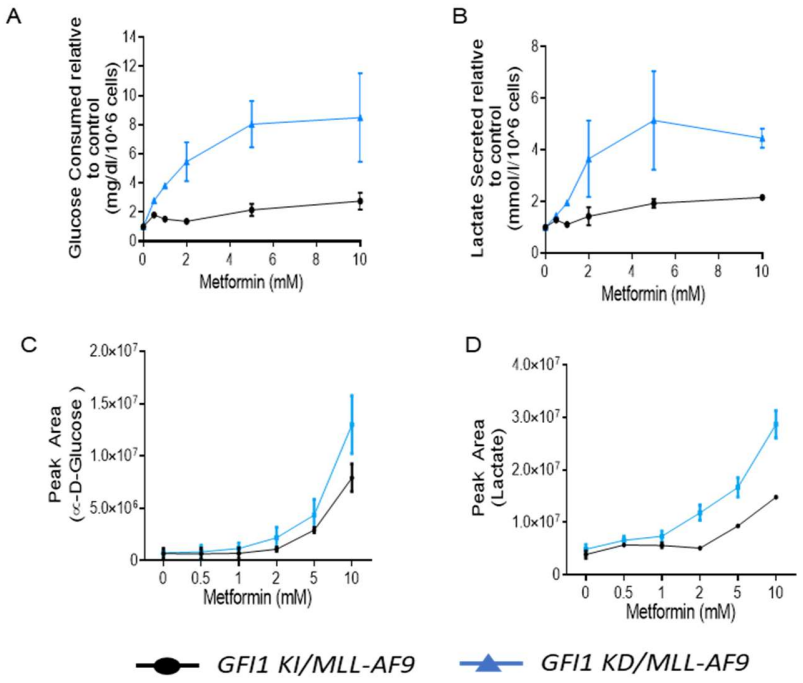


**Figure 50: Glucose consumed and lactate secretion in cells with metformin treatment.**

(**A** and **B**) Relative glucose consumed and lactate secreted were measured biochemically and calculated to the untreated control. (**C** and **D**) The relative peak area of α-D glucose and lactate was measured through mass spectrometric analysis and calculated to the untreated control. The data represents the cumulative values from multiple experiments (Average ± SEM; n = 2 ).

5.7.4. Lonidamine enhances the therapeutic efficiency of metformin with regard to *GFI1 KD* leukemic cells, expressing *MLL-AF9* oncofusion

The previous section showed that the *GFI1 KD* leukemic cells with *MLL-AF9* fusion protein consumed more glucose upon metformin treatment. Thus metformin shifted the dependency of *MLL-AF9* expressed *GFI1 KD* leukemic cells towards glycolysis for an additional energy source. We then treated the cells with Lonidamine, an inhibitor of mitochondrial bound hexokinase, which inhibits glycolysis (Nath et al., 2016). Treatment of non-leukemic and leukemic cells (with both the *MLL-AF9* and *AML1-ETO9a* fusion genes) with lonidamine alone did not give any therapeutic advantage for *GFI1 KD* cells to *GFI1 KI* cells (Figure 51A). However, the combination of metformin and lonidamine showed

the slightest increase in the metformin efficacy of *GFI1 KD* leukemic cells with an *MLL-AF9* oncofusion gene compared to *GFI1 KI* cells. In contrast, the therapeutic advantage in the combination treatment was not observed with the lineage depleted cells and as well with the leukemic cells expressing AML1-ETO9a fusion protein (Figure 51B).

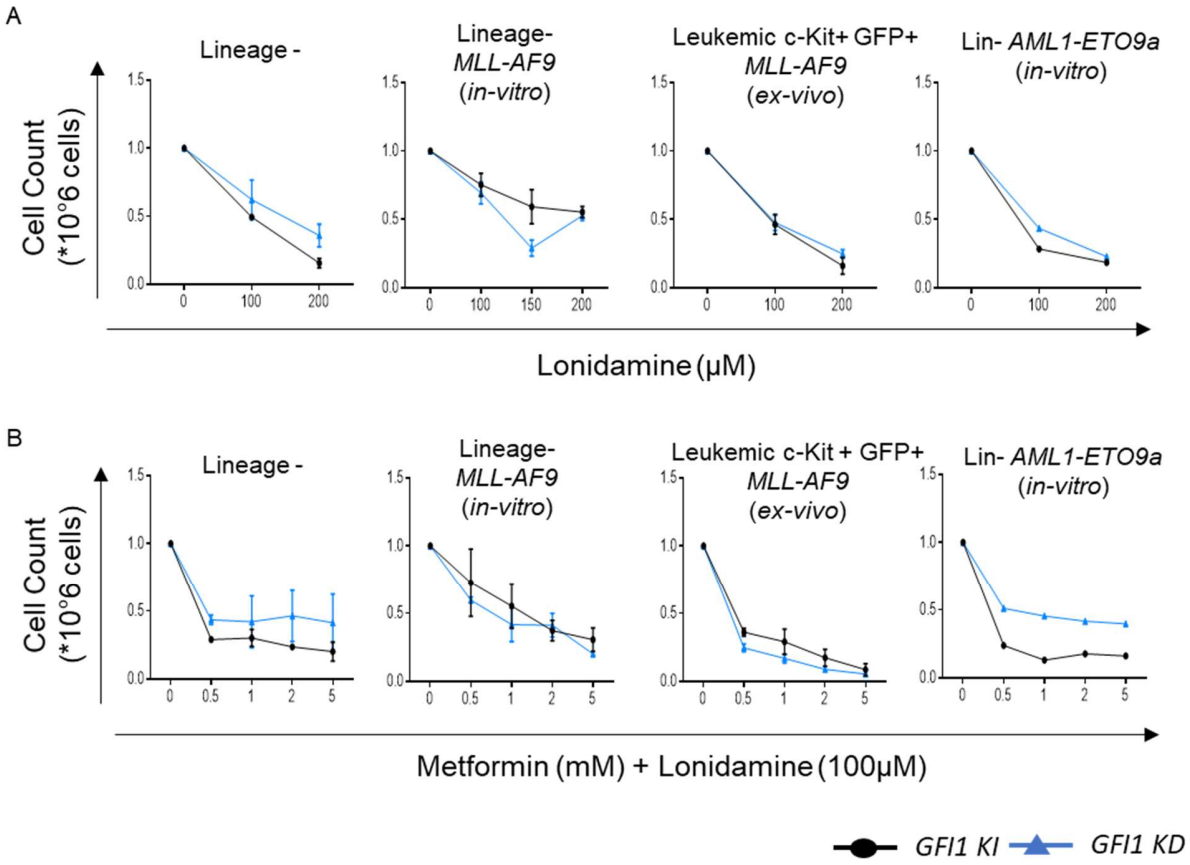


**Figure 51: Live AML cell counts after metformin and lonidamine treatment.**

(**A**) Cell counts after lonidamine treatment of lineage depleted cells, leukemic cells with an *MLL-AF9* oncofusion gene (*in-vitro* and *ex-vivo*) and leukemic cells with an *AML1-ETO9a* oncofusion gene. (**B**) Cell counts after Metformin treatment along with 100µM lonidamine treatment of lineage depleted cells, leukemic cells with *MLL-AF9* oncofusion (*in-vitro* and *ex-vivo*) and leukemic cells with *AML1-ETO9a* oncofusion. The data represent the cumulative values from more than two individual experiments (Average ± SEM; n ≥ 2).

5.7.5. Cytarabine increases the therapeutic efficiency of metformin in *MLL-AF9* expressed *GFI1 KD* leukemic cells.

AraC (cytarabine) is a therapeutic agent in AML (Lowenberg et al., 2011). It has been published that leukemic cells with a high rate of OXPHOS were

resistant to AraC treatment (Farge et al., 2017). To measure if metformin could increase the therapeutic efficiency of AraC, we treated the cells in liquid culture with gradient concentrations of metformin along with 20µM AraC and the cell counts were measured after 72 hours of treatment. *GFI1 KD* leukemic cells with *MLL-AF9* oncofusion gene from the *in-vitro* and *ex-vivo* cultures were susceptible to the combination of metformin and AraC compared to *GFI1 KI* cells. At the same time, the *GFI1 KD* non-leukemic and leukemic cells with an *AML1-ETO9a* oncofusion gene were less sensitive to the combination treatment (Figure 52).

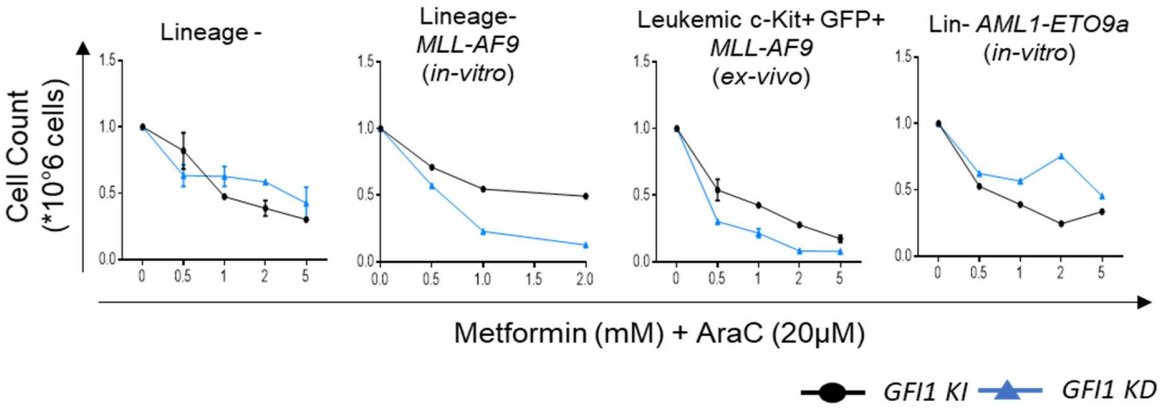


**Figure 52: Live AML cell counts after metformin and AraC combination treatment.**

Metformin and AraC combination treatment of non-leukemic lineage depleted and leukemic cells with *MLL-AF9* (*in-vitro* and *ex-vivo*) and *AML1-ETO9a* oncofusion genes. The data represents the cumulative values from more than two independent experiments (Average ± SEM; n ≥ 2).

### 5.7.6. IC50 measurements from the single and combination treatments of Metformin, Lonidamine and AraC

To measure the therapeutic efficacy of the metformin treatments alone and combination treatments with lonidamine and AraC, we measured the half-maximal inhibitory concentrations (IC50) from the measured cell counts. The IC50 values were calculated by non-linear regression analysis using the graphpad prism software. The *GFI1 KD* lineage depleted cells showed higher IC50 values than the *GFI1 KI* lineage depleted cells wither with single or combination treatments (Figure 53A). IC50 analysis from the *GFI1 KD* leukemic

cells from the *in-vitro* and *ex-vivo* cultures showed a significantly lower value than the *GFI1 KI* leukemic cells in the metformin treatment alone and combination treatments with lonidamine or AraC (Figure 53A and B).

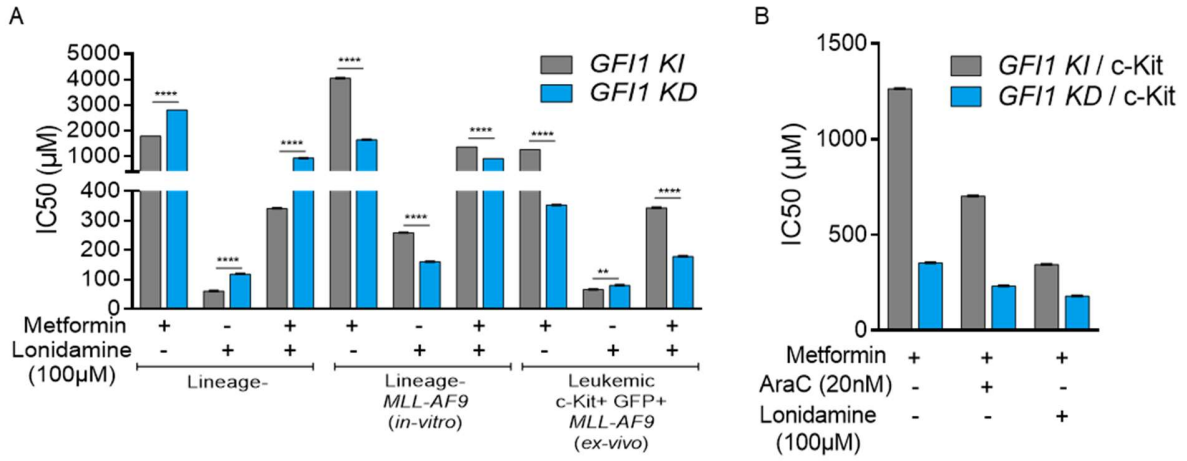


**Figure 53: The IC50 values of leukemic and non-leukemic cells with drugs treatment.**

(**A**) IC50 values of non-leukemic and leukemic cells (*in-vitro* and *ex-vivo* cultures) were calculated from the cell counts of metformin treatment alone and combined with lonidamine. (**B**) IC50 values from the cell counts of *ex-vivo* cultured leukemic cells treated with metformin and AraC or lonidamine. The data represents the cumulative values from multiple experiments (Average ± SEM; **P = 0.0060; ****P ≤ 0.0001; n ≥ 2).

### 5.8. *Foxo1* as a potential target of GFI1

The current study showed that a low level of *GFI1* is associated with high OXPHOS. Since *GFI1* is implicated in the epigenetic regulation of different pathways (Saleque et al., 2007), we first interrogated whether *GFI1* binds to the regulatory elements of genes implicated in the regulation of oxidative and glycolysis. We performed *in-silico* analysis to determine if *GFI1* regulated any intermediate genes that regulate the metabolism. We first analysed three different GFI1 CHIPseq datasets from the CODEX online database (http://codex.stemcells.cam.ac.uk/). The three datasets were generated from three hematopoietic cell types of murine origin. The cells include hematopoietic progenitor cells (Goode et al., 2016; Lie et al., 2018), Innate type-2 lymphoid cells (ILC2s) (Spooner et al., 2013) and mast cells (Moignard et al., 2013). We determined the potential targets of GFI1, which were significant in at least two

datasets. We then evaluated the RNAseq data generated from leukemic total bonemarrow cells of the serially transplanted mice (*GFI1 KI* and *GFI1 KD*). The RNAseq analysis was performed by my colleague Dr Daria Frank. Since GFI1 is a transcriptional repressor protein in the majority of the cases, we listed the genes whose RNA expression levels are significantly upregulated in *GFI1 KD* leukemic mice, measured by RNAseq analysis. In addition, we analysed the ATACseq data generated from the granulocyte-monocyte progenitor cells (GMPs) of non-leukemic *GFI1 KI* and *KD* mice. This is a crucial cell progenitor fraction since leukemic cells originate from this population. ATACseq was performed by my colleague Xiaoqing Xie. We compared the list of genes that showed an open chromatin configuration in the GMPs of *GFI1 KD* cells with the set of GFI1 targets based on CHIPseq analysis, which showed higher RNA expression levels in the *GFI1 KD* cells based on RNAseq analysis. A list of 72 genes that share similar characteristics was identified and is shown in Figure 54.

A

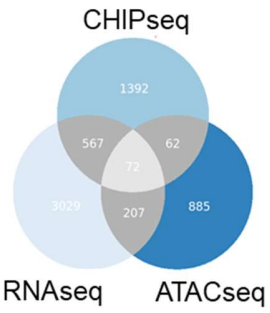


B

| | | | | | | | |
|---|---|---|---|---|---|---|---|
| Abcc4 | Atp1a1 | Emp1 | Il13ra1 | Mctp1 | Papss1 | Sgk1 | Zfp438 |
| Ablim1 | Atrnl1 | Ern1 | Irf2bp2 | Mef2a | Pde6d | Slc9a9 | Zswim6 |
| Actr3 | Atxn1 | Evi5 | Itgb2 | Mpeg1 | Plcl2 | Smyd3 | |
| Adora3 | Bcl2l11 | Foxo1 | Ldlrad3 | Mtfr2 | Plek | Sowahc | |
| Adrb2 | Camk2d | Frmd4b | Lmo4 | Nav1 | Prkcb | Sptbn1 | |
| Ahi1 | Ccdc71l | Gcnt1 | Lrrc8b | Nav2 | Ptger4 | St3gal2 | |
| Amotl1 | Cd44 | Gpr183 | Ly86 | Nbea | Ptpn2 | Tle4 | |
| Ank | Ctss | Hif1a | Man2a1 | Nceh1 | Rnf115 | Tmem65 | |
| Arhgap26 | Dlgap1 | Hivep2 | Map2k3 | Nek7 | Rxra | Tox | |
| Arhgef3 | Dock4 | Hpse | Mast4 | Osbpl5 | Samsn1 | Tpm4 | |

**Figure 54: Potential GFI1 target genes.**

(**A**) Venn diagram showing the overlap genes analysed by CHIPseq, RNAseq and ATACseq datasets. (**B**) The list of 72 genes that are common in the analysis of three datasets.

Among the list of 72 genes that were significantly enriched in *GFI1 KD* with an open chromatin configuration and potential targets of GFI1, we found *Foxo1* is compelling since *Foxo1* plays a requisite role in the metabolism of glucose and glutamine (Yadav et al., 2018). CHIPseq data sets showed peaks of GFI1

binding sites in the first exonic and intronic regions of the *Foxo1* gene, the regions enriched with promoter and enhancer sites (Figure 55A). ATACseq analysis showed a significantly more open chromatin configuration of the first intronic and exonic regions of *Foxo1* in *GFI1 KD* GMPs compared to GMPs isolated from *GFI1 KI* mice (Figure 55B).

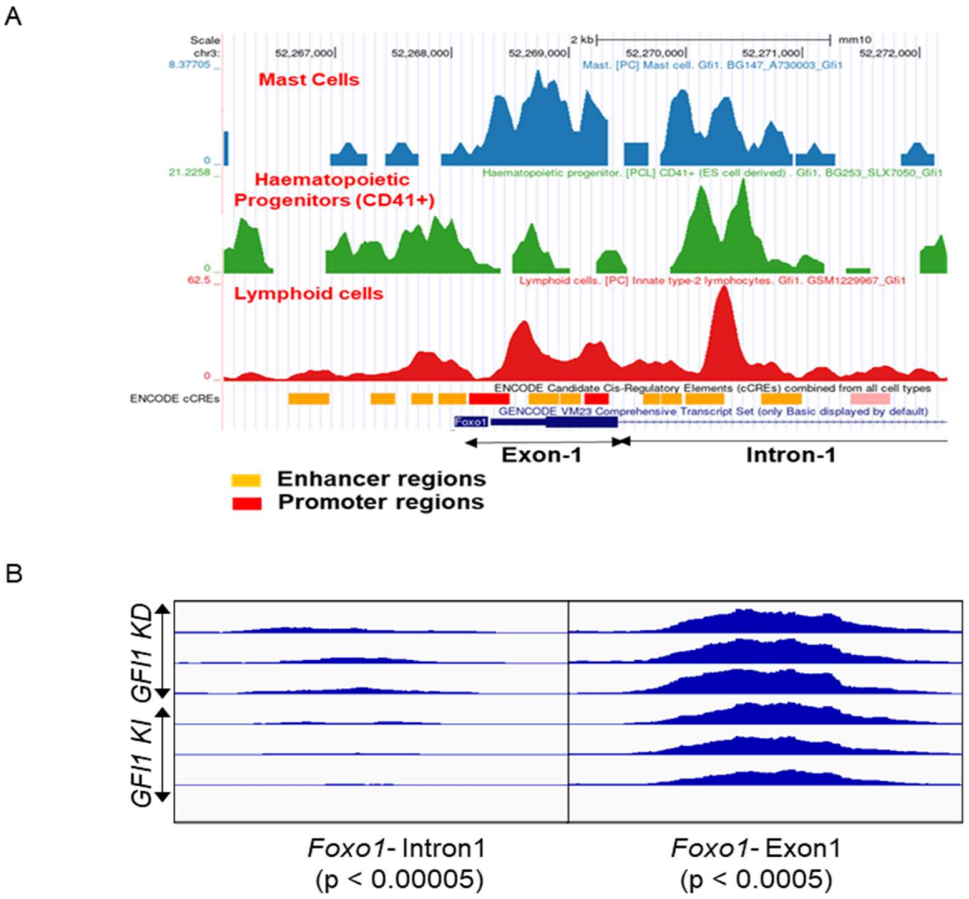


**Figure 55: CHIPseq and ATACseq peaks of *Foxo1***

(**A**) GFI1 CHIPseq data showing the peaks at the GFI1 binding regions in the promoter and enhancer regions of *Foxo1*, located in the exon-1 and intron-1 loci of the *Foxo1* gene. The peaks represent the data from three different databases. (**B**) ATACseq peaks show the open chromatin peaks of the first intronic and exonic regions of *Foxo1* of GMPs isolated from *GFI1 KI* and *GFI1 KD* mice.

### 5.9. A low level of *GFI1* expression is associated with increased expression of FOXO1 and C-MYC

To validate the *in-silico* findings, we measured the mRNA and protein expression levels of *Foxo1*/FOXO1 in the murine leukemic and non-leukemic

cells with different GFI1 expression levels. As well, we measured mRNA and protein levels of *FOXO1*/FOXO1 in human THP-1 cells with normal and reduced *GFI1* expression levels. Since *C-MYC* is one of the target genes of FOXO1 proteins that regulates metabolism (Peck et al., 2013), we measured the mRNA and protein expression levels of *c-Myc*/C-MYC in addition to *Foxo1*/FOXO1.

5.9.1. Low expression levels of *GFI1* were associated with higher *Foxo1*/*FOXO1* and *c-Myc*/*C-MYC* mRNA levels

To measure the expression levels of *Foxo1* and *c-Myc* in non-leukemic and leukemic cells, we measured mRNA expressions of *Foxo1* and *c-Myc* in lineage depleted cells and *in-vitro* cultured leukemic cells expressing *MLL-AF9* and *AML1-ETO9a* onco-fusion genes. The mRNA levels were measured by real-time PCR, as explained in section 4.4. Knock-down of *GFI1* was associated with significantly higher *Foxo1* and *c-Myc* mRNA levels in both leukemic and non-leukemic cells from mice (Figure 56A). We then measured *FOXO1 and C-MYC* mRNA levels from the *GFI1 KD* clones of THP-1 cells. A low level of *GFI1* in THP-1 cells was associated with higher mRNA levels of *FOXO1 and C-MYC* (Figure 56B).

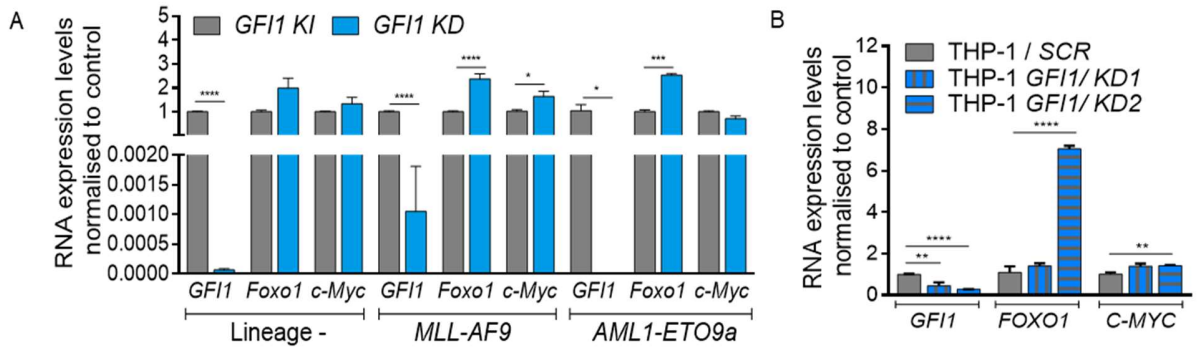


**Figure 56: *GFI1*/*GFI1*, *Foxo1*/*FOXO1* and *c-Myc*/*C-MYC* mRNA expression levels in primary cells and human leukemic THP-1 cells.**

(**A**) *GFI1*, *Foxo1 and c-Myc* mRNA expression levels in non-leukemic and leukemic *GFI1 KI* and *GFI1 KD* cells. The expression levels were normalized to *Gapdh* expression control and calculated relative to *GFI1 KI* controls. (**B**) *GFI1*, *FOXO1* and *C-MYC* mRNA expression levels in THP-1 wildtype and *GFI1 KD* clones. The expression levels were normalized to *GAPDH* expression control and calculated relative to *GFI1* wildtype controls. *SCR*- Scrambled sequence clone, *KD1* and *KD2*- *GFI1 KD* clones of THP-1. The data represents

the cumulative of more than two individual experiments. (Average ± SEM; *P = 0.0470; **P ≤ 0.0049; ***P = 0.0001; ****P ≤ 0.0001; n ≥ 2).

### 5.9.2. A low level of GFI1 upregulated FOXO1 and C-MYC protein levels

Similar to mRNA levels, we measured protein levels by western blot to see if the increased expression of FOXO1 and C-MYC was at both the transcriptional and translational levels. A low level of GFI1 was associated with elevated levels of FOXO1 and C-MYC protein levels in both the non-leukemic lineage depleted cells and leukemic cells with retroviral expression of *MLL-AF9* and *AML1-ETO9a* oncofusion genes (Figure 57A). With regard to human AML cell lines, the knock-down of *GFI1* expression in the THP-1 cells led to higher FOXO1 and C-MYC protein levels (Figure 57B).

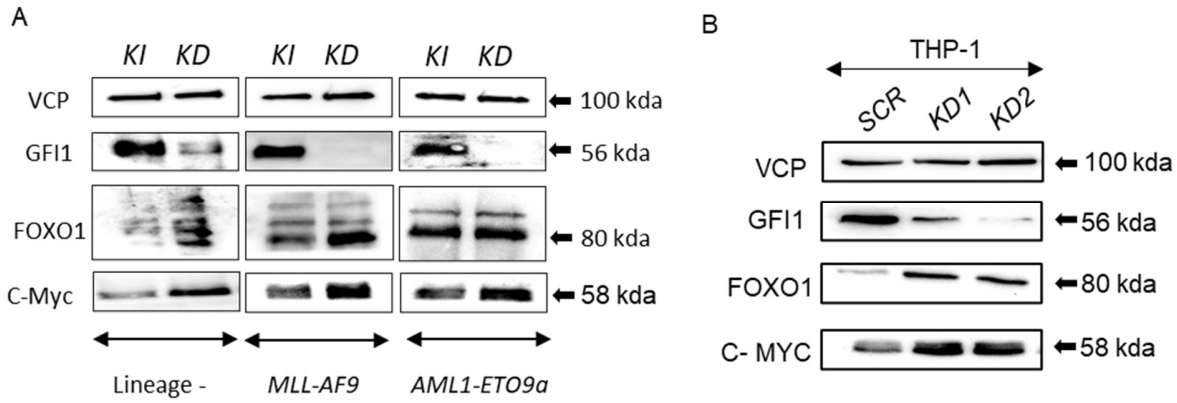


**Figure 57: Protein expression levels of GFI1, FOXO1 and C-MYC in primary cells and human leukemic THP-1 cells.**

(**A**) Western blot analysis with proteins from non-leukemic and leukemic cells from the *GFI1 KI* and *KD* mice showing VCP, GFI1, FOXO1 and C-MYC bands at 100*KD*, 56*KD*, 80*KD* and 58*KD*, respectively. (**B**) Western blot analysis of *GFI1 KI* and *KD* THP-1 cells, showing VCP. GFI1, FOXO1 and C-MYC bands at 100kd, 56kd, 80kd and 58kd, respectively. *SCR*- Scrambled sequence clone, *KD1* and *KD2*- *GFI1 KD* clones of THP-1, respectively.

# 6. Discussion

GFI1 is a transcriptional repressor protein regulating the myeloid and lymphoid lineage differentiation in healthy hematopoiesis. Additionally, it is also implicated in the pathogenesis of AML patients (van der Meer et al., 2010). *GFI1* expression levels are also a prognostic marker in the disease course of AML and MDS. A low level of *GFI1* in the AML blasts is associated with an inferior event-free survival compared to AML patients with a higher expression level of *GFI1* in their blast cells, based on cohort studies (Hönes et al., 2013). In line with this, reduced expression of *GFI1* accelerates AML development in different murine models of AML (Hones et al., 2016). Based on data from other groups and our group, we speculated that different expression levels of *GFI1* might alter metabolic pathways and serve as a novel therapeutic target.

**Increased *GFI1* expression induced differentiation and regulates metabolic changes:**

To explore the dose-dependent role of GFI1 with regard to metabolic pathways, we investigated the cellular proliferative and differentiative phenotype of human leukemic cell lines (K-562, THP-1 and KG-1) with increased *GFI1* expression. Enforced *GFI1* expression promoted the differentiation of these human leukemic cell lines and inhibited proliferation, measured by colony-forming capacity assay and live cell counts in the liquid culture (Hones et al., 2017). This is consistent with the previous reporting that ectopic expression of *Gfi1* in cells expressing BCR-ABL fusion gene repressed proliferation (Lidonnici et al., 2010). Employing a humanised AML model in mice, our lab had previously shown that increased expression of *GFI1* induced differentiation of leukemic cells towards granulocytes and was associated with a reduction in c-Kit+ cells (Hones et al., 2017). Thus to investigate the functional pathways deregulated with enhanced *GFI1* expression, we performed a microarray using K-562 cells, and the resulting gene set enrichment analysis indicated altered metabolic pathways, with a significant upregulation of the oxidative phosphorylation pathway (OXPHOS). Metabolic changes were extensively reported in various cancer types, and new therapeutic options targeting deregulated metabolic pathways are currently being developed (Pavlova &

Thompson, 2016; Sullivan, Gui, & Vander Heiden, 2016). Among the various metabolic factors, glucose, fatty acid and glutamine metabolism pathways were significantly altered in AML patients and murine models of AML (Chapuis, Poulain, Birsen, Tamburini, & Bouscary, 2019). Several drugs targeting these pathways were widely established (Chapuis et al., 2019; Stuani et al., 2019). However, the metabolic changes associated with altered expression levels of *GFI1* in AML cells were not reported. Hence, we initially investigated the metabolic changes to discern the influence of high *GFI1* expression levels. A reduction in glucose consumption, lactate secretion, lactate dehydrogenase (LDH) activity, and extracellular acidification rate (ECAR) implied that enforced expression of *GFI1* downregulated the rate of glycolysis in the human leukemic cell lines used here. On the other hand, oxidative phosphorylation was not influenced by enhanced expression of *GFI1* in the human leukemic cell lines, measured by the oxygen consumption rate (OCR). Due to a low rate of glycolysis, while no significant change in the OXPHOS with enhanced *GFI1* expression was seen, it was evident that the cells were reliant on OXPHOS rather than glycolysis for the energy source, evaluated by the OCR to ECAR ratio. OXPHOS is a series of reactions in the TCA cycle, followed by an electron transport chain leading to ATP synthesis. Identifying the significant fuel contribution to the TCA cycle and OXPHOS is pivotal in establishing potential therapeutic targets. The three prime contributors for OXPHOS include glucose, glutamine, and fatty acids (Zheng, 2012). Glutamine metabolises into alpha-ketoglutarate, thereby contributing to the TCA cycle (Altman et al., 2016). AML cells were shown to highly depend on glutamine metabolism, and therefore targeting the glutamine pathway in AML opened new therapeutic options (Emadi, 2015; Gregory et al., 2019). Fatty acids contribute to the TCA cycle by β-oxidation into acetyl-CoA, enhancing OXPHOS. Various reports showed a significant upregulation of the fatty acid oxidation in cancers and confer therapeutic resistance in AML (Stevens et al., 2020; Tabe, Konopleva, & Andreeff, 2020; Tcheng et al., 2021). The current study showed that enhanced expression of *GFI1* in human leukemic cell lines promoted fatty acid metabolism while reducing glucose and glutamine metabolism.

Nevertheless, these observations were made with the supraphysiological level of *GFI1* expression, which might have given the first insight but potentially did not represent the true biology. In addition, GFI1 was known to control proliferation, and a reduced level of proliferation might have pleiotropic effects on cell metabolism, possibly independent of GFI1. Hence these reports give a first insight, but their suitability might be limited and more work is needed.

**Reduced expression of GFI1 upregulated OXPHOS in AML:**

Tarik Möröy and his group showed previously that reduced expression of *GFI1* in the myeloid non-leukemic cells is associated with metabolic alterations compared to wild type non-malignant cells (Fraszczak et al., 2019). Here, we showed that reduced *GFI1* expression further upregulated OXPHOS, accompanied by higher mitochondrial mass, mitochondrial DNA copy number, mitochondrial membrane potential, and increased ROS levels, while there was no significant change in glycolysis in both the non-leukemic lineage depleted progenitor cells and *in-vitro* transduced *MLL-AF9* expression driven leukemic cells. The *ex-vivo* cultured primary *MLL-AF9* expression induced AML cells (c-Kit+GFP+ cells) from the serially transplanted mice with reduced expression of *GFI1* displayed a higher OXPHOS than *GFI1 KI* cells, a metabolic phenotype similar to *in-vitro* cells. *GFI1 KD* leukemic cells with an *MLL-AF9* fusion gene were associated with a higher proliferation of leukemic cells than the *GFI1 KI* leukemic cells expressing *MLL-AF9* fusion. The increased rate of OXPHOS is contrary to the Warburg effect, where the cancer cells mainly depend on glycolysis instead of OXPHOS (Hsu & Sabatini, 2008; Y. H. Wang & Scadden, 2015). Conversely, the differentiated tissues depend on OXPHOS (Vander Heiden et al., 2009).

Our current study showed that glutamine contributed to the primary fuel source for the increased OXPHOS with reduced *GFI1* expression in leukemic and non-leukemic cells and that this was associated with reduced fatty acid oxidation. Studies have shown that fatty acid oxidation plays a significant role in differentiating hematopoietic progenitors in larval Drosophila (S. K. Tiwari, Toshniwal, Mandal, & Mandal, 2020). The metabolic phenotype from primary *MLL-AF9* expression induced AML cells from mice with reduced *GFI1*

expression was consistent with the results of a *KD* of *GFI1* expression in THP-1 cells, resulting in increased OXPHOS, mitochondrial membrane potential, mitochondrial mass and mitochondrial ROS levels.

OXPHOS, electron transport chain (ETC) and ATP production contribute to excess mitochondrial ROS production in non-malignant myeloid cells and malignant AML cells (Hole, Darley, & Tonks, 2011; Khan et al., 2016; X. Li et al., 2013). Hence, increased mitochondrial ROS- associated with reduced *GFI1* expression could result from elevated OXPHOS and high ATP production capacity. The mitochondrial membrane potential (MMP) is a functional determinant of OXPHOS (Dey & Moraes, 2000). As a result, OXPHOS contributed to increased membrane potential in leukemic cells with low levels of *GFI1*.

Glutamine is a critical fuel source for the energy production of AML through the TCA cycle and OXPHOS (Goto et al., 2014). We showed that leukemic cells expressing an *MLL-AF9* fusion gene with reduced *GFI1* expression upregulated glutamine metabolism. Hence, glutamine metabolism contributed to the upregulated OXPHOS with a low level of *GFI1*. Several therapeutic options are available to target glutamine metabolism in AML (Willems et al., 2013). Furthermore, enhanced glutamine metabolism with low *GFI1* expression levels in *MLL-AF9* induced AML may help develop new therapeutic options aiming at glutamine metabolism.

**GFI1 regulated the metabolic activity through regulating *FOXO1* and *c-Myc* expression:**

We found that *Foxo1* could be a potential target of GFI1, which might partially explain the phenotypes described above. The intron-1 and exon-1 regions of the *Foxo1 gene,* comprising the promoter and enhancer sites, had a more open chromatin structure in GMPs with reduced *GFI1* expression according to the *in silico* ATACseq analysis. Additionally, these regions were also the potential binding sites for the GFI1 protein, based on the CHIPseq analysis. Analysis of RNAseq data revealed significant upregulation of *Foxo1* expression in leukemic cells with low *GFI1* expression levels. Through these analyses, we were able to identify *Foxo1* as a potential GFI1 target gene.

Gfi1b, a homolog of Gfi1, was shown to repress *Foxo1* and regulate *Rag* gene expression (Schulz et al., 2012). GFI1 was also shown to transcriptionally represses the *Foxo1* gene, which is necessary for T-cell maturation and inhibits the premature expression of genes involved in T-cell differentiation (Shi et al., 2017). In view of these previous reports showing the interactions of GFI1 and *Foxo1*, as well as our analysis, we endorse that GFI1 transcriptionally repress the *Foxo1* gene expression in non-leukemic and leukemic cells. Our lab has previously shown that *Gfi1b* deficient leukemic cells upregulated FOXO3 protein expression levels and advanced AML development (Thivakaran et al., 2018). In the current study, we postulated a comparative role for FOXO1 in the context of GFI1's influence on AML pathology.

FOXO proteins can act as tumour suppressors or oncogenic drivers, depending on the type of cells and the malignancy (Gurnari, Falconi, De Bellis, Voso, & Fabiani, 2019). FOXO1 has been found to play a dual function in AML, acting as an oncogenic mediator in AML1-ETO induced leukemogenesis (Shan Lin, Zhang, & Mulloy, 2014) and driving the AML1-ETO induced preleukemic state (S. Lin et al., 2017). Furthermore, it has a tumour suppressor role in Hodgkin's lymphoma (Xie et al., 2012) and solid tumours (Gheghiani, Shang, & Fu, 2020). FOXO proteins have diverse functions in regulating metabolism, where they negatively regulate the Warburg effect and glycolysis by inhibiting C-MYC function (Peck et al., 2013), but also suppress glutamine metabolism while promoting glutamine synthesis (van der Vos et al., 2012), suppresses fatty acid uptake, and fatty acid oxidation (Bastie et al., 2005). The *Foxo1*/*FOXO1* gene expression levels and proteins levels were validated by real-time PCR and western blot. We showed high mRNA and protein expression levels of *Foxo1*/*FOXO1* in both the non-leukemic and leukemic cells with reduced *GFI1* expression. *FOXO1*/FOXO1 expression levels similar to primary murine cells were observed with reduced *GFI1* expression in the human AML cell line, THP-1, which might explain the metabolic consistency in the phenotype in the cells expressing *MLL-AF9* oncofusion gene.

*C-MYC* is one of the target genes of FOXO proteins. It is a transcriptional factor regulating metabolism pathways. FOXO proteins repress C-MYC

function at transcriptional and translational levels (Peck et al., 2013), and FOXOs enhance the mRNA degradation of C-MYC by increasing the expression of micro-RNAs (miRNAs) (Gan et al., 2010; Kress et al., 2011). The high expression of FOXO proteins negatively regulates the protein translation and stability of C-MYC. Active FOXOs reduces the C-MYC protein stability by promoting phosphorylation (Ferber et al., 2012). FOXOs inhibit the C-MYC mediated transcription of its target genes by activating MXI1, a protein that binds to the promoter of target genes competitively with C-MYC (Delpuech et al., 2007). The findings of our real-time PCR and western blot experiments revealed that a low level of GFI1 increased C-MYC mRNA and protein levels. Furthermore, the mechanism by which both the FOXO1 and C-MYC protein levels were elevated in cells with decreased *GFI1* expression levels is indistinct. C-MYC enhances glucose and glutamine metabolism while repressing fatty acid oxidation (Dong, Tu, Liu, & Qing, 2020; Miller et al., 2012). The C-MYC mediated metabolic phenotype was in line with the observed phenotype with reduced GFI1 expression. Hence, we could extrapolate that a low expression level of *GFI1* in non-leukemic and *MLL-AF9* expression driven leukemic cells enhances OXPHOS and glutamine metabolism through FOXO1 and C-MYC (Figure 58). However, the molecular mechanisms governing GFI1, FOXO1, and C-MYC regulation must be explored further.

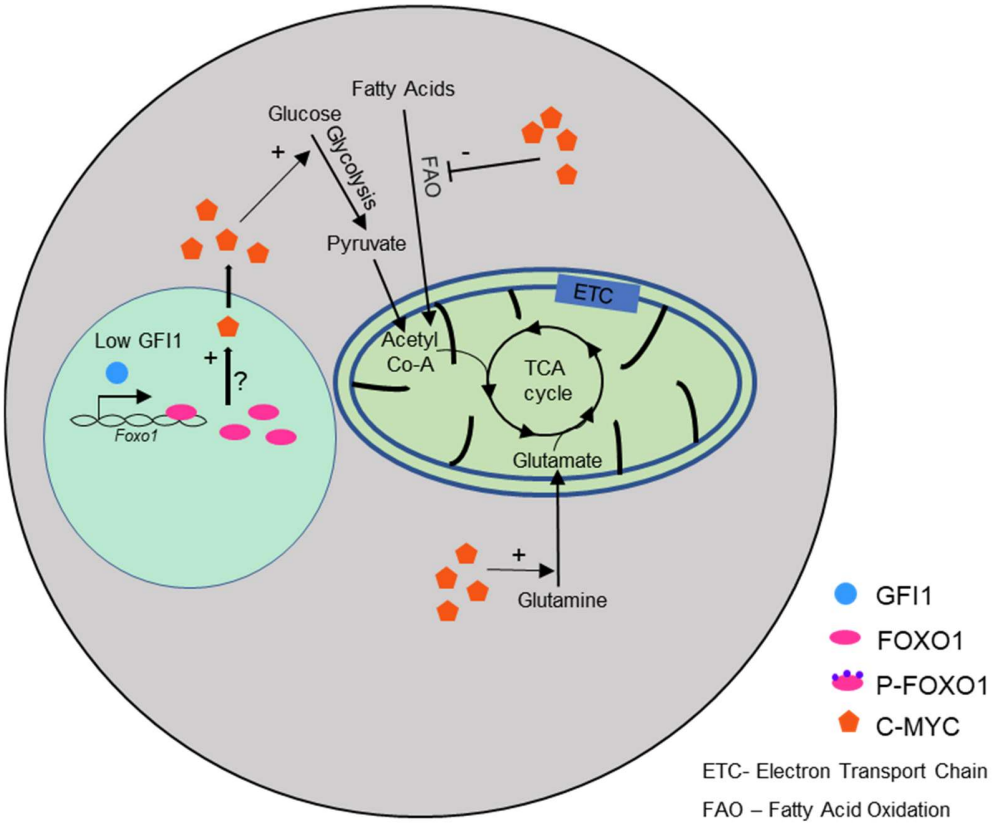


**Figure 58: Schematic representation of metabolic changes associated with low expression levels of *GFI1***

A low level of *GFI1* expression transcriptionally activated FOXO1 synthesis. High FOXO1 enhanced the expression of C-MYC through an unknown mechanism. The increased C-MYC proteins promoted glucose and glutamine metabolism while inhibiting fatty acid oxidation. ETC: Electron Transport Chain; FAO: Fatty Acid Oxidation; TCA cycle: Tricarboxylic acid cycle.

**Metformin is a therapeutic advantage for *MLL-AF9* induced leukemic cells expressing a low level of GFI1:**

With the emergent data, we showed that GFI1 has an indirect role in regulating the metabolism of AML cells by upregulating FOXO1 and C-MYC levels. We also showed that glutamine is the major contributor fuelling the increased OXPHOS. Inhibition of OXPHOS therefore, might be a treatment approach for AML cells that express a low level of *GFI1*. Drugs that target mitochondrial OXPHOS and mitochondrial translation have been used to demonstrate this approach in AML and other malignancies (Farge et al., 2017; Kuntz et al., 2017; Lagadinou et al., 2013; Sica, Bravo-San Pedro, Stoll, & Kroemer, 2020; Skrtic

et al., 2011; Tran, Lee, Park, Kim, & Park, 2016; Wen, Zhu, & Huang, 2013; Xu, Yan, Li, Qian, & Gong, 2016). Metformin, a complex I inhibitor of the electron transport chain that inhibits OXPHOS (Biondani & Peyron, 2018), was employed in this investigation. Metformin's efficacy in targeting leukemic cells with a high OXPHOS level has been previously studied (Biondani & Peyron, 2018; Scotland et al., 2010). In comparison to *GFI1 KI* cells, we effectively treated *GFI1 KD* leukemic cells expressing the *MLL-AF9* fusion gene from *in-vitro* and *ex-vivo* cultures with metformin. Metformin has also been shown to inhibit the ability of *MLL-AF9* expression induced leukemic *GFI1 KD* cells to form colonies. Appealingly, we found no disparity in metformin efficacy between *GFI1 KD* and *KI* non-leukemic lineage depleted cells

A high level of OXPHOS was observed in quiescent immature leukemic stem cells that are chemoresistant to AraC (cytarabine), and metformin treatment enhanced the antileukemic effect of AraC (Farge et al., 2017). Here, we showed that metformin enhanced the therapeutic efficiency of AraC treatment in *MLL-AF9* expression induced *GFI1 KD* leukemic cells compared to *GFI1 KI* cells. Thus, metformin might be employed as part of a therapeutic supplement regimen in *MLL-AF9* expression induced *GFI1 KD* leukemic cells to minimise AraC dose-related adverse effects.

Metformin causes enhanced glucose uptake and lactate secretion in cancer cells (Ben Sahra et al., 2010; Biondani & Peyron, 2018). Metformin treatment of *MLL-AF9* expression driven *GFI1 KD* leukemic cells resulted in high glucose consumption and lactate secretion. This implies an upregulated glycolysis with metformin treatment in *GFI1 KD* leukemic cells, induced by *MLL-AF9* expression. To inhibit the glycolysis pathway, we exploited Lonidamine, a mitochondrial bound hexokinase inhibitor (Nath et al., 2016). Treatment with lonidamine alone provided no therapeutic benefit. However, in *MLL-AF9* expression driven *GFI1 KD* leukemic cells, metformin effectiveness was improved via lonidamine therapy.

## 7. Outlook

The current doctoral thesis study investigated how differential expression of *GFI1* regulated metabolic pathways, such as glucose and glutamine metabolism, and fatty acid oxidation in non-leukemic and *MLL-AF9* expression driven AML cells. On a molecular level, we hypothesise that FOXO1 and C-MYC proteins are implicated in GFI1 mediated metabolic regulation. However, further research is essential to determine how GFI1 regulates C-MYC and FOXO1 gene and protein expressions.

FOXO1 proteins are phosphorylated, enabling them to be trafficked to the cytosol and then degraded by ubiquitination (Greer & Brunet, 2005). Phosphorylated FOXO1 proteins and the ubiquitination rate must be assessed to determine the functional state of the increased FOXO1 proteins in cells with reduced *GFI1* expression. AKT promotes the phosphorylation of FOXO proteins (Bouchard et al., 2004), while SKP2 promotes the ubiquitination of phosphorylated FOXO (pFOXO) proteins (H. Huang et al., 2005). Therefore, it would be interesting to measure the expression levels of these proteins in cells with reduced *GFI1* expression. In addition, proteins including MXI1 play a role in the negative regulation of FOXO1 and C-MYC (Delpuech et al., 2007). It would be noteworthy to look at MXI1 expression levels to determine if GFI1 has a role in regulating FOXO1 and C-MYC interactions.

To validate that GFI1 regulates metabolism through the FOXO1 and C-MYC proteins, the metabolic phenotype of cells using FOXO1 and C-MYC knock-down should be assessed in cells expressing *GFI1* at a low level. We hypothesize that knocking down FOXO1 or C-MYC proteins in cells with low GFI1 levels might reverse the metabolic phenotype. The metabolic phenotype must also be assessed by enhancing FOXO1 and/or C-MYC expression levels.

Whole-cell metabolomic profiling by mass- spectrometric analysis is underway in our lab. We were currently measuring the total metabolites' levels with reduced *GFI1* expression in leukemic and non-leukemic cells. This can provide a comprehensive perspective of all metabolic pathways affected by low GFI1 expression, and it may lead to novel treatment targets for patients with low GFI1 levels.

On a therapeutic level, we found that treating *MLL-AF9* expression induced *GFI1 KD* leukemic cells with metformin conferred a therapeutic benefit *in-vitro*. Additionally, mice transplanted with *MLL-AF9* expression driven *GFI1 KI* and *KD* leukemic cells must be treated to determine the *in-vivo* therapeutic effectiveness of metformin.

## 8. Summary

Growth factor independence 1 (GFI1) is a hematopoietic transcriptional repressor protein involved in the self-renewal and differentiation of healthy hematopoietic stem cells (HSCs) and Acute Myeloid Leukemia (AML). We have previously seen that AML patients with lower *GFI1* gene expression had a poor prognosis and a reduced survival rate.

In this study, we explored the function of GFI1 in metabolic alterations that may have an association with AML progression. As novel findings, we discovered that GFI1 regulates cellular differentiation and metabolism in a dose-dependent manner. Increased expression of *GFI1* inhibited proliferation and induced the differentiation of human leukemic cell lines, whereas reduced *GFI1* expression enhanced proliferation and colony-forming capability. Expression levels of *GFI1* regulated the most critical metabolic pathways, glycolysis and oxidative phosphorylation (OXPHOS). We found that enhanced *GFI1* expression in human leukemic cell lines deregulated glycolysis, whereas a low expression of *GFI1* in primary leukemic and non-leukemic cells from mice upregulated OXPHOPS. The observed metabolic phenotype was recapitulated in human leukemic cell lines with reduced *GFI1* expression. Hence knockdown of *GFI1* (*GFI1 KD*) altered the reliance of leukemic cells towards mitochondrial oxidative phosphorylation. We demonstrated that the elevated OXPHOS found with low expression levels of *GFI1* was associated with increased glutamine metabolism and reduced fatty acid oxidation. Reduced expression of *GFI1* upregulated the expression of *FOXO1* and *C-MYC* measured at RNA and protein levels, hinting that metabolic regulation of GFI1 is FOXO1 and C-MYC dependent. These metabolic findings intrigued us to investigate the effect of Metformin, a well established anti-diabetic drug targeting mitochondrial function. We found that *in-vitro* metformin treatment effectively targeted *GFI1-KD* murine leukemic cells co-expressing *MLL-AF9* while sparing the non-leukemic lineage depleted cell. Metformin treatment enhanced the rate of glycolysis in *MLL-AF9* induced *GFI1 KD* leukemic cells, as evaluated by enhanced glucose consumption and lactate secretion. Combining Metformin with a glycolysis inhibitor, Lonidamine improved the efficacy of metformin

treatment in *GFI1 KD* leukemic cells expressing an *MLL-AF9* oncofusion gene. Additionally, *GFI1 KD* leukemic cells harbouring an *MLL-AF9* oncofusion gene, Metformin, improved the effectiveness of the conventional treatment regimen of cytarabine.

Thus, the data provided the rationale to further exploit metabolic vulnerabilities in AML patients differentially expressing *GFI1* using an in-toxic, well-established drug to potentially eradicate leukemic cells. However, more *in-vivo* experimentation with metformin administration is required.

## 9. Summary in German

Growth factor independence 1 (GFI1) ist ein hämatopoetischer Transkriptionsrepressor, welcher eine Rolle bei der Selbsterneuerung sowie der Differenzierung gesunder hämatopoetischer Stammzellen (HSCs) und akuter myeloischer Leukämie (AML) spielt. Wir haben bereits gezeigt, dass eine geringe *GFI1*-Expression in AML-Patienten mit einer schlechten Prognose und einer geringeren Überlebensrate assoziert ist.

In der vorliegenden Studie wurde die Funktion von GFI1 innerhalb des Metabolismus untersucht. Außerdem wurde analysiert, in welchem Zusammenhang veränderte *GFI1*-Expressionen mit metabolischen Veränderungen, die mit dem Fortschreiten der AML assoziiert sind, stehen.

Wir konnten zeigen, dass GFI1 die zelluläre Differenzierung und den Metabolismus in einer dosisabhängigen Weise reguliert. Eine erhöhte Expression von *GFI1* verringerte die Proliferation und erhöhte die Differenzierung von humanen leukämischen Zelllinien. Eine verringerte *GFI1*-Expression hingegen erhöhte die Proliferation und die Fähigkeit zur Koloniebildung. Außerdem hatte das Expressionsniveau von *GFI1* einen Einfluss auf zwei wichtige Stoffwechselwege, die Glykolyse und die oxidative Phosphorylierung (OXPHOS). Wir konnten zeigen, dass eine erhöhte *GFI1*-Expression in humanen leukämischen Zelllinien die Glykolyse dereguliert. Dahingegen führte eine niedrige Expression von *GFI1* in primären murinen leukämischen und nicht leukämischen Zellen zu einer Erhöhung der OXPHOS. Die erhöhte OXPHOS konnte in humanen leukämischen Zelllinien mit niedriger *GFI1*-Expression bestätigt werden. Somit konnte gezeigt werden, dass Zellen mit niedriger *GFI1*-Expression vermehrt von der oxidativen Phosphorylierung abhängig sind. Des Weiteren ging die detektierte erhöhte OXPHOS in Zellen mit niedriger *GFI1*-Expression mit einem erhöhten Glutamin-Stoffwechsel und einer reduzierten Fettsäure-Oxidation einher. Auf molekularer Ebene führte eine niedrige *GFI1*-Expression sowohl zu einer erhöhten Geneexpression von *FOXO1* und *C-MYC* als auch zu erhöhten FOXO1 und C-MYC Proteinleveln. Diese deutet darauf hin, dass die dosisabhängige Rolle von GFI1 beim Metabolismus durch FOXO1 und C-MYC reguliert wird.

Im nächsten Schritt wurde die Wirkung von Metformin auf hämatopoetische Zellen mit unterschiedlicher *GFI1*-Expression untersucht. Metformin ist ein etabliertes Antidiabetikum, das die mitochondriale Funktion verändert. Wir konnten zeigen, dass die Behandlung einen negativen Effekt auf murine leukämische (*MLL-AF9*) Zellen mit geringer *GFI1*-Expression hatte, während Metformin keinen Effekt auf nicht leukämische Zellen hatte. Die Behandlung mit Metformin steigerte die Glykolyse in leukämischen *GFI1-KD-MLL-AF9*-Zellen , was sich in einem erhöhten Glukoseverbrauch und einer erhöhten Laktatsekretion äußerte. Die Kombination von Metformin mit einem Glykolyse-Inhibitor, Lonidamin, verbesserte die Wirksamkeit der Metformin-Behandlung in leukämischen *GFI1-KD-MLL-AF9*-Zellen zusätzlich. Darüber hinaus verbesserte Metformin ebenfalls die Wirksamkeit des Standard-Chemotherapeutikums Cytarabin auf leukämische *GFI1-KD-MLL-AF9*-Zellen.

Die vorliegende Studie liefert somit Hinweise, dass AML-Patienten, mit veränderter *GFI1*-Expression von der Behandlung mit Metformin, einem Medikament welches gut verträglich und in der Klinik etabliert ist, profitieren könnten. Allerdings sind zusätzliche *in-vivo* Experimente vonnöten, um die Metformin-Behandlung weiter zu untersuchen.

## 10. Bibliography

Adeva-Andany, M. M., Calvo-Castro, I., Fernandez-Fernandez, C., Donapetry-Garcia, C., & Pedre-Pineiro, A. M. (2017). Significance of l-carnitine for human health. *IUBMB Life, 69*(8), 578-594. doi:10.1002/iub.1646

Adhikary, S., & Eilers, M. (2005). Transcriptional regulation and transformation by Myc proteins. *Nat Rev Mol Cell Biol, 6*(8), 635-645. doi:10.1038/nrm1703

Akram, M. (2013). Mini-review on glycolysis and cancer. *J Cancer Educ, 28*(3), 454-457. doi:10.1007/s13187-013-0486-9

Altman, B. J., Stine, Z. E., & Dang, C. V. (2016). From Krebs to clinic: glutamine metabolism to cancer therapy. *Nat Rev Cancer, 16*(11), 749. doi:10.1038/nrc.2016.114

Amente, S., Zhang, J., Lavadera, M. L., Lania, L., Avvedimento, E. V., & Majello, B. (2011). Myc and PI3K/AKT signaling cooperatively repress FOXO3a-dependent PUMA and GADD45a gene expression. *Nucleic Acids Res, 39*(22), 9498-9507. doi:10.1093/nar/gkr638

Anderson, C. M., & Stahl, A. (2013). SLC27 fatty acid transport proteins. *Mol Aspects Med, 34*(2-3), 516-528. doi:10.1016/j.mam.2012.07.010

Angelescu, S., Berbec, N. M., Colita, A., Barbu, D., & Lupu, A. R. (2012). Value of multifaced approach diagnosis and classification of acute leukemias. *Maedica (Bucur), 7*(3), 254-260. Retrieved from https://www.ncbi.nlm.nih.gov/pubmed/23401730

Arber, D. A., Orazi, A., Hasserjian, R., Thiele, J., Borowitz, M. J., Le Beau, M. M., . . . Vardiman, J. W. (2016). The 2016 revision to the World Health Organization classification of myeloid neoplasms and acute leukemia. *Blood, 127*(20), 2391-2405. doi:10.1182/blood-2016-03-643544

Assi, S. A., Bonifer, C., & Cockerill, P. N. (2019). Rewiring of the Transcription Factor Network in Acute Myeloid Leukemia. *Cancer Inform, 18*, 1176935119859863. doi:10.1177/1176935119859863

Barzi, A., & Sekeres, M. A. (2010). Myelodysplastic syndromes: a practical approach to diagnosis and treatment. *Cleve Clin J Med, 77*(1), 37-44. doi:10.3949/ccjm.77a.09069

Bastie, C. C., Nahle, Z., McLoughlin, T., Esser, K., Zhang, W., Unterman, T., & Abumrad, N. A. (2005). FoxO1 stimulates fatty acid uptake and oxidation in muscle cells through CD36-dependent and -independent mechanisms. *J Biol Chem, 280*(14), 14222-14229. doi:10.1074/jbc.M413625200

Batandier, C., Guigas, B., Detaille, D., El-Mir, M. Y., Fontaine, E., Rigoulet, M., & Leverve, X. M. (2006). The ROS production induced by a reverse-electron flux at respiratory-chain complex 1 is hampered by metformin. *J Bioenerg Biomembr, 38*(1), 33-42. doi:10.1007/s10863-006-9003-8

Beauchemin, H., & Moroy, T. (2020). Multifaceted Actions of GFI1 and GFI1B in Hematopoietic Stem Cell Self-Renewal and Lineage Commitment. *Front Genet, 11*, 591099. doi:10.3389/fgene.2020.591099

Ben Sahra, I., Laurent, K., Giuliano, S., Larbret, F., Ponzio, G., Gounon, P., . . . Bost, F. (2010). Targeting cancer cell metabolism: the combination of metformin and 2-deoxyglucose induces p53-dependent apoptosis in prostate

cancer cells. *Cancer Res, 70*(6), 2465-2475. doi:10.1158/0008-5472.CAN-09-2782

Berlanga, A., Guiu-Jurado, E., Porras, J. A., & Auguet, T. (2014). Molecular pathways in non-alcoholic fatty liver disease. *Clin Exp Gastroenterol, 7*, 221-239. doi:10.2147/CEG.S62831

Bhatnagar, B., Zhao, Q., Fisher, J. L., Kohlschmidt, J., Mrózek, K., Nicolet, D., . . . Eisfeld, A.-K. (2020). Poor Treatment Outcomes of Young (<60 Years) African American Patients (Pts) Diagnosed with Acute Myeloid Leukemia (AML) (Alliance). *Blood, 136*(Supplement 1), 5-7. doi:10.1182/blood-2020-140999

Bhutia, Y. D., Babu, E., & Ganapathy, V. (2016). Re-programming tumour cell metabolism to treat cancer: no lone target for lonidamine. *Biochem J, 473*(11), 1503-1506. doi:10.1042/BCJ20160068

Bindea, G., Galon, J., & Mlecnik, B. (2013). CluePedia Cytoscape plugin: pathway insights using integrated experimental and in silico data. *Bioinformatics, 29*(5), 661-663. doi:10.1093/bioinformatics/btt019

Bindea, G., Mlecnik, B., Hackl, H., Charoentong, P., Tosolini, M., Kirilovsky, A., . . . Galon, J. (2009). ClueGO: a Cytoscape plug-in to decipher functionally grouped gene ontology and pathway annotation networks. *Bioinformatics, 25*(8), 1091-1093. doi:10.1093/bioinformatics/btp101

Biondani, G., & Peyron, J. F. (2018). Metformin, an Anti-diabetic Drug to Target Leukemia. *Front Endocrinol (Lausanne), 9*, 446. doi:10.3389/fendo.2018.00446

Bishop, J. F., Matthews, J. P., Young, G. A., Szer, J., Gillett, A., Joshua, D., . . . Juneja, S. (1996). A randomized study of high-dose cytarabine in induction in acute myeloid leukemia. *Blood, 87*(5), 1710-1717. Retrieved from https://www.ncbi.nlm.nih.gov/pubmed/8634416

Blanco, J. G., Dervieux, T., Edick, M. J., Mehta, P. K., Rubnitz, J. E., Shurtleff, S., . . . Relling, M. V. (2001). Molecular emergence of acute myeloid leukemia during treatment for acute lymphoblastic leukemia. *Proc Natl Acad Sci U S A, 98*(18), 10338-10343. doi:10.1073/pnas.181199898

Botezatu, L., Michel, L. C., Helness, A., Vadnais, C., Makishima, H., Hones, J. M., . . . Khandanpour, C. (2016). Epigenetic therapy as a novel approach for GFI136N-associated murine/human AML. *Exp Hematol, 44*(8), 713-726 e714. doi:10.1016/j.exphem.2016.05.004

Botezatu, L., Michel, L. C., Makishima, H., Schroeder, T., Germing, U., Haas, R., . . . Khandanpour, C. (2016). GFI1(36N) as a therapeutic and prognostic marker for myelodysplastic syndrome. *Exp Hematol, 44*(7), 590-595 e591. doi:10.1016/j.exphem.2016.04.001

Bouchard, C., Marquardt, J., Bras, A., Medema, R. H., & Eilers, M. (2004). Myc-induced proliferation and transformation require Akt-mediated phosphorylation of FoxO proteins. *EMBO J, 23*(14), 2830-2840. doi:10.1038/sj.emboj.7600279

Boulais, P. E., & Frenette, P. S. (2015). Making sense of hematopoietic stem cell niches. *Blood, 125*(17), 2621-2629. doi:10.1182/blood-2014-09-570192

Busiello, R. A., Savarese, S., & Lombardi, A. (2015). Mitochondrial uncoupling proteins and energy metabolism. *Front Physiol, 6*, 36. doi:10.3389/fphys.2015.00036

Byrd, J. C., Mrozek, K., Dodge, R. K., Carroll, A. J., Edwards, C. G., Arthur, D. C., . . . Leukemia Group, B. (2002). Pretreatment cytogenetic abnormalities are predictive of induction success, cumulative incidence of relapse, and overall survival in adult patients with de novo acute myeloid leukemia: results from Cancer and Leukemia Group B (CALGB 8461). *Blood, 100*(13), 4325-4336. doi:10.1182/blood-2002-03-0772

Castro, I., Sampaio-Marques, B., & Ludovico, P. (2019). Targeting Metabolic Reprogramming in Acute Myeloid Leukemia. *Cells, 8*(9). doi:10.3390/cells8090967

Chapuis, N., Poulain, L., Birsen, R., Tamburini, J., & Bouscary, D. (2019). Rationale for Targeting Deregulated Metabolic Pathways as a Therapeutic Strategy in Acute Myeloid Leukemia. *Front Oncol, 9*, 405. doi:10.3389/fonc.2019.00405

Chen, X., Burkhardt, D. B., Hartman, A. A., Hu, X., Eastman, A. E., Sun, C., . . . Guo, S. (2019). MLL-AF9 initiates transformation from fast-proliferating myeloid progenitors. *Nat Commun, 10*(1), 5767. doi:10.1038/s41467-019-13666-5

Cheng, H., Zheng, Z., & Cheng, T. (2020). New paradigms on hematopoietic stem cell differentiation. *Protein Cell, 11*(1), 34-44. doi:10.1007/s13238-019-0633-0

Cole, M. D., & Nikiforov, M. A. (2006). Transcriptional activation by the Myc oncoprotein. *Curr Top Microbiol Immunol, 302*, 33-50. doi:10.1007/3-540-32952-8_2

Currie, E., Schulze, A., Zechner, R., Walther, T. C., & Farese, R. V., Jr. (2013). Cellular fatty acid metabolism and cancer. *Cell Metab, 18*(2), 153-161. doi:10.1016/j.cmet.2013.05.017

da-Silva, W. S., Gomez-Puyou, A., de Gomez-Puyou, M. T., Moreno-Sanchez, R., De Felice, F. G., de Meis, L., . . . Galina, A. (2004). Mitochondrial bound hexokinase activity as a preventive antioxidant defense: steady-state ADP formation as a regulatory mechanism of membrane potential and reactive oxygen species generation in mitochondria. *J Biol Chem, 279*(38), 39846-39855. doi:10.1074/jbc.M403835200

Dahl, R., Iyer, S. R., Owens, K. S., Cuylear, D. D., & Simon, M. C. (2007). The transcriptional repressor GFI-1 antagonizes PU.1 activity through protein-protein interaction. *J Biol Chem, 282*(9), 6473-6483. doi:10.1074/jbc.M607613200

Dang, C. V. (2012). MYC on the path to cancer. *Cell, 149*(1), 22-35. doi:10.1016/j.cell.2012.03.003

Daver, N., Wei, A. H., Pollyea, D. A., Fathi, A. T., Vyas, P., & DiNardo, C. D. (2020). New directions for emerging therapies in acute myeloid leukemia: the next chapter. *Blood Cancer J, 10*(10), 107. doi:10.1038/s41408-020-00376-1

Davis, R. E., Ngo, V. N., Lenz, G., Tolar, P., Young, R. M., Romesser, P. B., . . . Staudt, L. M. (2010). Chronic active B-cell-receptor signalling in diffuse large B-cell lymphoma. *Nature, 463*(7277), 88-92. doi:10.1038/nature08638

de Almeida, M. J., Luchsinger, L. L., Corrigan, D. J., Williams, L. J., & Snoeck, H. W. (2017). Dye-Independent Methods Reveal Elevated Mitochondrial Mass in Hematopoietic Stem Cells. *Cell Stem Cell, 21*(6), 725-729 e724. doi:10.1016/j.stem.2017.11.002

De Kouchkovsky, I., & Abdul-Hay, M. (2016). 'Acute myeloid leukemia: a comprehensive review and 2016 update'. *Blood Cancer J, 6*(7), e441. doi:10.1038/bcj.2016.50

Delpuech, O., Griffiths, B., East, P., Essafi, A., Lam, E. W., Burgering, B., . . . Schulze, A. (2007). Induction of Mxi1-SR alpha by FOXO3a contributes to repression of Myc-dependent gene expression. *Mol Cell Biol, 27*(13), 4917-4930. doi:10.1128/MCB.01789-06

Demine, S., Renard, P., & Arnould, T. (2019). Mitochondrial Uncoupling: A Key Controller of Biological Processes in Physiology and Diseases. *Cells, 8*(8). doi:10.3390/cells8080795

Dey, R., & Moraes, C. T. (2000). Lack of oxidative phosphorylation and low mitochondrial membrane potential decrease susceptibility to apoptosis and do not modulate the protective effect of Bcl-x(L) in osteosarcoma cells. *J Biol Chem, 275*(10), 7087-7094. doi:10.1074/jbc.275.10.7087

DiNardo, C. D., Garcia-Manero, G., Pierce, S., Nazha, A., Bueso-Ramos, C., Jabbour, E., . . . Kantarjian, H. (2016). Interactions and relevance of blast percentage and treatment strategy among younger and older patients with acute myeloid leukemia (AML) and myelodysplastic syndrome (MDS). *Am J Hematol, 91*(2), 227-232. doi:10.1002/ajh.24252

Dohner, H., Estey, E. H., Amadori, S., Appelbaum, F. R., Buchner, T., Burnett, A. K., . . . European, L. (2010). Diagnosis and management of acute myeloid leukemia in adults: recommendations from an international expert panel, on behalf of the European LeukemiaNet. *Blood, 115*(3), 453-474. doi:10.1182/blood-2009-07-235358

Dombret, H., & Gardin, C. (2016). An update of current treatments for adult acute myeloid leukemia. *Blood, 127*(1), 53-61. doi:10.1182/blood-2015-08-604520

Dong, Y., Guo, C., Zhou, W., Li, W., & Zhang, L. (2021). Using a new HSPC senescence model in vitro to explore the mechanism of cellular memory in aging HSPCs. *Stem Cell Res Ther, 12*(1), 444. doi:10.1186/s13287-021-02455-x

Dong, Y., Shi, O., Zeng, Q., Lu, X., Wang, W., Li, Y., & Wang, Q. (2020). Leukemia incidence trends at the global, regional, and national level between 1990 and 2017. *Exp Hematol Oncol, 9*, 14. doi:10.1186/s40164-020-00170-6

Dong, Y., Tu, R., Liu, H., & Qing, G. (2020). Regulation of cancer cell metabolism: oncogenic MYC in the driver's seat. *Signal Transduct Target Ther, 5*(1), 124. doi:10.1038/s41392-020-00235-2

Drynan, L. F., Pannell, R., Forster, A., Chan, N. M., Cano, F., Daser, A., & Rabbitts, T. H. (2005). Mll fusions generated by Cre-loxP-mediated de novo translocations can induce lineage reassignment in tumorigenesis. *EMBO J, 24*(17), 3136-3146. doi:10.1038/sj.emboj.7600760

Eilers, M., & Eisenman, R. N. (2008). Myc's broad reach. *Genes Dev, 22*(20), 2755-2766. doi:10.1101/gad.1712408

El-Bagary, R. I., Elkady, E. F., & Ayoub, B. M. (2013). Spectrophotometric Methods for the Determination of Linagliptin in Binary Mixture with Metformin Hydrochloride and Simultaneous Determination of Linagliptin and Metformin Hydrochloride using High Performance Liquid Chromatography. *Int J Biomed Sci, 9*(1), 41-47. Retrieved from https://www.ncbi.nlm.nih.gov/pubmed/23675288

Emadi, A. (2015). Exploiting AML vulnerability: glutamine dependency. *Blood, 126*(11), 1269-1270. doi:10.1182/blood-2015-07-659508

Erdmann, T., Klener, P., Lynch, J. T., Grau, M., Vockova, P., Molinsky, J., . . . Lenz, G. (2017). Sensitivity to PI3K and AKT inhibitors is mediated by divergent molecular mechanisms in subtypes of DLBCL. *Blood, 130*(3), 310-322. doi:10.1182/blood-2016-12-758599

Estey, E., & Dohner, H. (2006). Acute myeloid leukaemia. *Lancet, 368*(9550), 1894-1907. doi:10.1016/S0140-6736(06)69780-8

Farge, T., Saland, E., de Toni, F., Aroua, N., Hosseini, M., Perry, R., . . . Sarry, J. E. (2017). Chemotherapy-Resistant Human Acute Myeloid Leukemia Cells Are Not Enriched for Leukemic Stem Cells but Require Oxidative Metabolism. *Cancer Discov, 7*(7), 716-735. doi:10.1158/2159-8290.CD-16-0441

Faruqi, A., & Tadi, P. (2021). Cytarabine. In *StatPearls*. Treasure Island (FL).

Ferber, E. C., Peck, B., Delpuech, O., Bell, G. P., East, P., & Schulze, A. (2012). FOXO3a regulates reactive oxygen metabolism by inhibiting mitochondrial gene expression. *Cell Death Differ, 19*(6), 968-979. doi:10.1038/cdd.2011.179

Fiolka, K., Hertzano, R., Vassen, L., Zeng, H., Hermesh, O., Avraham, K. B., . . . Moroy, T. (2006). Gfi1 and Gfi1b act equivalently in haematopoiesis, but have distinct, non-overlapping functions in inner ear development. *EMBO Rep, 7*(3), 326-333. doi:10.1038/sj.embor.7400618

Fraszczak, J., Vadnais, C., Rashkovan, M., Ross, J., Beauchemin, H., Chen, R., . . . Moroy, T. (2019). Reduced expression but not deficiency of GFI1 causes a fatal myeloproliferative disease in mice. *Leukemia, 33*(1), 110-121. doi:10.1038/s41375-018-0166-1

Fu, Z., & Tindall, D. J. (2008). FOXOs, cancer and regulation of apoptosis. *Oncogene, 27*(16), 2312-2319. doi:10.1038/onc.2008.24

Fuhrmann, D. C., Olesch, C., Kurrle, N., Schnutgen, F., Zukunft, S., Fleming, I., & Brune, B. (2019). Chronic Hypoxia Enhances beta-Oxidation-Dependent Electron Transport via Electron Transferring Flavoproteins. *Cells, 8*(2). doi:10.3390/cells8020172

Gan, B., Lim, C., Chu, G., Hua, S., Ding, Z., Collins, M., . . . DePinho, R. A. (2010). FoxOs enforce a progression checkpoint to constrain mTORC1-

activated renal tumorigenesis. *Cancer Cell, 18*(5), 472-484. doi:10.1016/j.ccr.2010.10.019

Ganapathy-Kanniappan, S., & Geschwind, J. F. (2013). Tumor glycolysis as a target for cancer therapy: progress and prospects. *Mol Cancer, 12*, 152. doi:10.1186/1476-4598-12-152

Gao, P., Tchernyshyov, I., Chang, T. C., Lee, Y. S., Kita, K., Ochi, T., . . . Dang, C. V. (2009). c-Myc suppression of miR-23a/b enhances mitochondrial glutaminase expression and glutamine metabolism. *Nature, 458*(7239), 762-765. doi:10.1038/nature07823

Gery, S., & Koeffler, H. P. (2007). Transcription factors in hematopoietic malignancies. *Curr Opin Genet Dev, 17*(1), 78-83. doi:10.1016/j.gde.2006.12.012

Gheghiani, L., Shang, S., & Fu, Z. (2020). Targeting the PLK1-FOXO1 pathway as a novel therapeutic approach for treating advanced prostate cancer. *Sci Rep, 10*(1), 12327. doi:10.1038/s41598-020-69338-8

Goode, D. K., Obier, N., Vijayabaskar, M. S., Lie, A. L. M., Lilly, A. J., Hannah, R., . . . Bonifer, C. (2016). Dynamic Gene Regulatory Networks Drive Hematopoietic Specification and Differentiation. *Dev Cell, 36*(5), 572-587. doi:10.1016/j.devcel.2016.01.024

Goto, M., Miwa, H., Shikami, M., Tsunekawa-Imai, N., Suganuma, K., Mizuno, S., . . . Nitta, M. (2014). Importance of glutamine metabolism in leukemia cells by energy production through TCA cycle and by redox homeostasis. *Cancer Invest, 32*(6), 241-247. doi:10.3109/07357907.2014.907419

Greenberg, P. L. (2011). Myelodysplastic syndromes: dissecting the heterogeneity. *J Clin Oncol, 29*(15), 1937-1938. doi:10.1200/JCO.2011.35.2211

Greer, E. L., & Brunet, A. (2005). FOXO transcription factors at the interface between longevity and tumor suppression. *Oncogene, 24*(50), 7410-7425. doi:10.1038/sj.onc.1209086

Gregory, M. A., Nemkov, T., Park, H. J., Zaberezhnyy, V., Gehrke, S., Adane, B., . . . DeGregori, J. (2019). Targeting Glutamine Metabolism and Redox State for Leukemia Therapy. *Clin Cancer Res, 25*(13), 4079-4090. doi:10.1158/1078-0432.CCR-18-3223

Grinberg, A. V., Hu, C. D., & Kerppola, T. K. (2004). Visualization of Myc/Max/Mad family dimers and the competition for dimerization in living cells. *Mol Cell Biol, 24*(10), 4294-4308. doi:10.1128/MCB.24.10.4294-4308.2004

Grove, C. S., & Vassiliou, G. S. (2014). Acute myeloid leukaemia: a paradigm for the clonal evolution of cancer? *Dis Model Mech, 7*(8), 941-951. doi:10.1242/dmm.015974

Gurnari, C., Falconi, G., De Bellis, E., Voso, M. T., & Fabiani, E. (2019). The Role of Forkhead Box Proteins in Acute Myeloid Leukemia. *Cancers (Basel), 11*(6). doi:10.3390/cancers11060865

Hao, X., Gu, H., Chen, C., Huang, D., Zhao, Y., Xie, L., . . . Zheng, J. (2019). Metabolic Imaging Reveals a Unique Preference of Symmetric Cell Division

and Homing of Leukemia-Initiating Cells in an Endosteal Niche. *Cell Metab, 29*(4), 950-965 e956. doi:10.1016/j.cmet.2018.11.013

Hartl, M. (2016). The Quest for Targets Executing MYC-Dependent Cell Transformation. *Front Oncol, 6*, 132. doi:10.3389/fonc.2016.00132

Held-Warmkessel, J., & Dell, D. D. (2014). Lactic acidosis in patients with cancer. *Clin J Oncol Nurs, 18*(5), 592-594. doi:10.1188/14.CJON.592-594

Heo, S. K., Noh, E. K., Kim, J. Y., Jeong, Y. K., Jo, J. C., Choi, Y., . . . Kim, H. (2017). Targeting c-KIT (CD117) by dasatinib and radotinib promotes acute myeloid leukemia cell death. *Sci Rep, 7*(1), 15278. doi:10.1038/s41598-017-15492-5

Hock, H., Hamblen, M. J., Rooke, H. M., Traver, D., Bronson, R. T., Cameron, S., & Orkin, S. H. (2003). Intrinsic requirement for zinc finger transcription factor Gfi-1 in neutrophil differentiation. *Immunity, 18*(1), 109-120. doi:10.1016/s1074-7613(02)00501-0

Hole, P. S., Darley, R. L., & Tonks, A. (2011). Do reactive oxygen species play a role in myeloid leukemias? *Blood, 117*(22), 5816-5826. doi:10.1182/blood-2011-01-326025

Hönes, J., Botezatu, L., Zeller, A., Michel, L. C., Thiede, C., Köster, R., . . . Khandanpour, C. (2013). Gfi1 As a Novel Prognostic Marker and Tumor Suppressor In Acute Myeloid Leukemia. *Blood, 122*(21), 2516-2516. doi:10.1182/blood.V122.21.2516.2516

Hones, J. M., Botezatu, L., Helness, A., Vadnais, C., Vassen, L., Robert, F., . . . Khandanpour, C. (2016). GFI1 as a novel prognostic and therapeutic factor for AML/MDS. *Leukemia, 30*(6), 1237-1245. doi:10.1038/leu.2016.11

Hones, J. M., Thivakaran, A., Botezatu, L., Patnana, P., Castro, S., Al-Matary, Y. S., . . . Khandanpour, C. (2017). Enforced GFI1 expression impedes human and murine leukemic cell growth. *Sci Rep, 7*(1), 15720. doi:10.1038/s41598-017-15866-9

Hooker, C. W., & Hurlin, P. J. (2006). Of Myc and Mnt. *J Cell Sci, 119*(Pt 2), 208-216. doi:10.1242/jcs.02815

Horman, S. R., Velu, C. S., Chaubey, A., Bourdeau, T., Zhu, J., Paul, W. E., . . . Grimes, H. L. (2009). Gfi1 integrates progenitor versus granulocytic transcriptional programming. *Blood, 113*(22), 5466-5475. doi:10.1182/blood-2008-09-179747

Hou, D., Wang, B., You, R., Wang, X., Liu, J., Zhan, W., . . . Huang, H. (2020). Stromal cells promote chemoresistance of acute myeloid leukemia cells via activation of the IL-6/STAT3/OXPHOS axis. *Ann Transl Med, 8*(21), 1346. doi:10.21037/atm-20-3191

Hsu, P. P., & Sabatini, D. M. (2008). Cancer cell metabolism: Warburg and beyond. *Cell, 134*(5), 703-707. doi:10.1016/j.cell.2008.08.021

Huang, H., Regan, K. M., Wang, F., Wang, D., Smith, D. I., van Deursen, J. M., & Tindall, D. J. (2005). Skp2 inhibits FOXO1 in tumor suppression through ubiquitin-mediated degradation. *Proc Natl Acad Sci U S A, 102*(5), 1649-1654. doi:10.1073/pnas.0406789102

Huang, J., Sengupta, R., Espejo, A. B., Lee, M. G., Dorsey, J. A., Richter, M., . . . Berger, S. L. (2007). p53 is regulated by the lysine demethylase LSD1. *Nature, 449*(7158), 105-108. doi:10.1038/nature06092

Huang, Y., Sun, G., Sun, X., Li, F., Zhao, L., Zhong, R., & Peng, Y. (2020). The Potential of Lonidamine in Combination with Chemotherapy and Physical Therapy in Cancer Treatment. *Cancers (Basel), 12*(11). doi:10.3390/cancers12113332

Huret, J. L., Minor, S. L., Dorkeld, F., Dessen, P., & Bernheim, A. (2000). Atlas of genetics and cytogenetics in oncology and haematology, an interactive database. *Nucleic Acids Res, 28*(1), 349-351. doi:10.1093/nar/28.1.349

Hwang, S. M. (2020). Classification of acute myeloid leukemia. *Blood Res, 55*(S1), S1-S4. doi:10.5045/br.2020.S001

Ikeda, H., Kanakura, Y., Tamaki, T., Kuriu, A., Kitayama, H., Ishikawa, J., . . . Griffin, J. D. (1991). Expression and functional role of the proto-oncogene c-kit in acute myeloblastic leukemia cells. *Blood, 78*(11), 2962-2968. Retrieved from https://www.ncbi.nlm.nih.gov/pubmed/1720040

Iliopoulos, D., Hirsch, H. A., & Struhl, K. (2011). Metformin decreases the dose of chemotherapy for prolonging tumor remission in mouse xenografts involving multiple cancer cell types. *Cancer Res, 71*(9), 3196-3201. doi:10.1158/0008-5472.CAN-10-3471

Jang, Y. Y., & Sharkis, S. J. (2007). A low level of reactive oxygen species selects for primitive hematopoietic stem cells that may reside in the low-oxygenic niche. *Blood, 110*(8), 3056-3063. doi:10.1182/blood-2007-05-087759

Jensen, K. S., Binderup, T., Jensen, K. T., Therkelsen, I., Borup, R., Nilsson, E., . . . Staller, P. (2011). FoxO3A promotes metabolic adaptation to hypoxia by antagonizing Myc function. *EMBO J, 30*(22), 4554-4570. doi:10.1038/emboj.2011.323

Kantarjian, H., Kadia, T., DiNardo, C., Daver, N., Borthakur, G., Jabbour, E., . . . Ravandi, F. (2021). Acute myeloid leukemia: current progress and future directions. *Blood Cancer J, 11*(2), 41. doi:10.1038/s41408-021-00425-3

Kaweme, N. M., Zhou, S., Changwe, G. J., & Zhou, F. (2020). The significant role of redox system in myeloid leukemia: from pathogenesis to therapeutic applications. *Biomark Res, 8*(1), 63. doi:10.1186/s40364-020-00242-z

Kent, W. J., Sugnet, C. W., Furey, T. S., Roskin, K. M., Pringle, T. H., Zahler, A. M., & Haussler, D. (2002). The human genome browser at UCSC. *Genome Res, 12*(6), 996-1006. doi:10.1101/gr.229102

Khan, A. U. H., Rathore, M. G., Allende-Vega, N., Vo, D. N., Belkhala, S., Orecchioni, S., . . . Villalba, M. (2016). Human Leukemic Cells performing Oxidative Phosphorylation (OXPHOS) Generate an Antioxidant Response Independently of Reactive Oxygen species (ROS) Production. *EBioMedicine, 3*, 43-53. doi:10.1016/j.ebiom.2015.11.045

Khandanpour, C., Kosan, C., Gaudreau, M. C., Duhrsen, U., Hebert, J., Zeng, H., & Moroy, T. (2011). Growth factor independence 1 protects hematopoietic stem cells against apoptosis but also prevents the

development of a myeloproliferative-like disease. *Stem Cells, 29*(2), 376-385. doi:10.1002/stem.575

Khandanpour, C., Krongold, J., Schutte, J., Bouwman, F., Vassen, L., Gaudreau, M. C., . . . Moroy, T. (2012). The human GFI136N variant induces epigenetic changes at the Hoxa9 locus and accelerates K-RAS driven myeloproliferative disorder in mice. *Blood, 120*(19), 4006-4017. doi:10.1182/blood-2011-02-334722

Khandanpour, C., & Moroy, T. (2013). Growth factor independence 1 (Gfi1) as a regulator of p53 activity and a new therapeutical target for ALL. *Oncotarget, 4*(3), 374-375. doi:10.18632/oncotarget.933

Khandanpour, C., Phelan, J. D., Vassen, L., Schutte, J., Chen, R., Horman, S. R., . . . Moroy, T. (2013). Growth factor independence 1 antagonizes a p53-induced DNA damage response pathway in lymphoblastic leukemia. *Cancer Cell, 23*(2), 200-214. doi:10.1016/j.ccr.2013.01.011

Khandanpour, C., Sharif-Askari, E., Vassen, L., Gaudreau, M. C., Zhu, J., Paul, W. E., . . . Moroy, T. (2010). Evidence that growth factor independence 1b regulates dormancy and peripheral blood mobilization of hematopoietic stem cells. *Blood, 116*(24), 5149-5161. doi:10.1182/blood-2010-04-280305

Khandanpour, C., Thiede, C., Valk, P. J., Sharif-Askari, E., Nuckel, H., Lohmann, D., . . . Moroy, T. (2010). A variant allele of Growth Factor Independence 1 (GFI1) is associated with acute myeloid leukemia. *Blood, 115*(12), 2462-2472. doi:10.1182/blood-2009-08-239822

Kleine-Kohlbrecher, D., Adhikary, S., & Eilers, M. (2006). Mechanisms of transcriptional repression by Myc. *Curr Top Microbiol Immunol, 302*, 51-62. doi:10.1007/3-540-32952-8_3

Klepin, H. D. (2016). Myelodysplastic Syndromes and Acute Myeloid Leukemia in the Elderly. *Clin Geriatr Med, 32*(1), 155-173. doi:10.1016/j.cger.2015.08.010

Kok, C. H., Watkins, D. B., Leclercq, T., D'Andrea, R. J., Hughes, T. P., & White, D. L. (2013). Low GFI1 expression in white blood cells of CP-CML patients at diagnosis is strongly associated with subsequent blastic transformation. *Leukemia, 27*(6), 1427-1430. doi:10.1038/leu.2013.47

Kress, T. R., Cannell, I. G., Brenkman, A. B., Samans, B., Gaestel, M., Roepman, P., . . . Eilers, M. (2011). The MK5/PRAK kinase and Myc form a negative feedback loop that is disrupted during colorectal tumorigenesis. *Mol Cell, 41*(4), 445-457. doi:10.1016/j.molcel.2011.01.023

Krivtsov, A. V., & Armstrong, S. A. (2007). MLL translocations, histone modifications and leukaemia stem-cell development. *Nat Rev Cancer, 7*(11), 823-833. doi:10.1038/nrc2253

Kuntz, E. M., Baquero, P., Michie, A. M., Dunn, K., Tardito, S., Holyoake, T. L., . . . Gottlieb, E. (2017). Targeting mitochondrial oxidative phosphorylation eradicates therapy-resistant chronic myeloid leukemia stem cells. *Nat Med, 23*(10), 1234-1240. doi:10.1038/nm.4399

Lagadinou, E. D., Sach, A., Callahan, K., Rossi, R. M., Neering, S. J., Minhajuddin, M., . . . Jordan, C. T. (2013). BCL-2 inhibition targets oxidative

phosphorylation and selectively eradicates quiescent human leukemia stem cells. *Cell Stem Cell, 12*(3), 329-341. doi:10.1016/j.stem.2012.12.013

Lee, S., Doddapaneni, K., Hogue, A., McGhee, L., Meyers, S., & Wu, Z. (2010). Solution structure of Gfi-1 zinc domain bound to consensus DNA. *J Mol Biol, 397*(4), 1055-1066. doi:10.1016/j.jmb.2010.02.006

Lengfelder, E., Haferlach, C., Saussele, S., Haferlach, T., Schultheis, B., Schnittger, S., . . . German, A. M. L. C. G. (2009). High dose ara-C in the treatment of newly diagnosed acute promyelocytic leukemia: long-term results of the German AMLCG. *Leukemia, 23*(12), 2248-2258. doi:10.1038/leu.2009.183

Li, H., Ji, M., Klarmann, K. D., & Keller, J. R. (2010). Repression of Id2 expression by Gfi-1 is required for B-cell and myeloid development. *Blood, 116*(7), 1060-1069. doi:10.1182/blood-2009-11-255075

Li, M., Li, X., Zhang, H., & Lu, Y. (2018). Molecular Mechanisms of Metformin for Diabetes and Cancer Treatment. *Front Physiol, 9*, 1039. doi:10.3389/fphys.2018.01039

Li, X., Fang, P., Mai, J., Choi, E. T., Wang, H., & Yang, X. F. (2013). Targeting mitochondrial reactive oxygen species as novel therapy for inflammatory diseases and cancers. *J Hematol Oncol, 6*, 19. doi:10.1186/1756-8722-6-19

Lidonnici, M. R., Audia, A., Soliera, A. R., Prisco, M., Ferrari-Amorotti, G., Waldron, T., . . . Calabretta, B. (2010). Expression of the transcriptional repressor Gfi-1 is regulated by C/EBP{alpha} and is involved in its proliferation and colony formation-inhibitory effects in p210BCR/ABL-expressing cells. *Cancer Res, 70*(20), 7949-7959. doi:10.1158/0008-5472.CAN-10-1667

Lie, A. L. M., Marinopoulou, E., Lilly, A. J., Challinor, M., Patel, R., Lancrin, C., . . . Lacaud, G. (2018). Regulation of RUNX1 dosage is crucial for efficient blood formation from hemogenic endothelium. *Development, 145*(5). doi:10.1242/dev.149419

Lin, S., Ptasinska, A., Chen, X., Shrestha, M., Assi, S. A., Chin, P. S., . . . Mulloy, J. C. (2017). A FOXO1-induced oncogenic network defines the AML1-ETO preleukemic program. *Blood, 130*(10), 1213-1222. doi:10.1182/blood-2016-11-750976

Lin, S., Zhang, J., & Mulloy, J. C. (2014). Tumor Suppressor FOXO1 Serves As a Critical Oncogenic Mediator in AML1-ETO Leukemia. *Blood, 124*(21), 264-264. doi:10.1182/blood.V124.21.264.264

Livak, K. J., & Schmittgen, T. D. (2001). Analysis of relative gene expression data using real-time quantitative PCR and the 2(-Delta Delta C(T)) Method. *Methods, 25*(4), 402-408. doi:10.1006/meth.2001.1262

Longo, N., Frigeni, M., & Pasquali, M. (2016). Carnitine transport and fatty acid oxidation. *Biochim Biophys Acta, 1863*(10), 2422-2435. doi:10.1016/j.bbamcr.2016.01.023

Love, M. I., Huber, W., & Anders, S. (2014). Moderated estimation of fold change and dispersion for RNA-seq data with DESeq2. *Genome Biol, 15*(12), 550. doi:10.1186/s13059-014-0550-8

Lowenberg, B., Pabst, T., Vellenga, E., van Putten, W., Schouten, H. C., Graux, C., . . . Swiss Group for Clinical Cancer Research Collaborative, G. (2011). Cytarabine dose for acute myeloid leukemia. *N Engl J Med, 364*(11), 1027-1036. doi:10.1056/NEJMoa1010222

Luengo, A., Gui, D. Y., & Vander Heiden, M. G. (2017). Targeting Metabolism for Cancer Therapy. *Cell Chem Biol, 24*(9), 1161-1180. doi:10.1016/j.chembiol.2017.08.028

Madiraju, A. K., Erion, D. M., Rahimi, Y., Zhang, X. M., Braddock, D. T., Albright, R. A., . . . Shulman, G. I. (2014). Metformin suppresses gluconeogenesis by inhibiting mitochondrial glycerophosphate dehydrogenase. *Nature, 510*(7506), 542-546. doi:10.1038/nature13270

Magina, K. N., Pregartner, G., Zebisch, A., Wolfler, A., Neumeister, P., Greinix, H. T., . . . Sill, H. (2017). Cytarabine dose in the consolidation treatment of AML: a systematic review and meta-analysis. *Blood, 130*(7), 946-948. doi:10.1182/blood-2017-04-777722

Marneth, A. E., Botezatu, L., Hones, J. M., Israel, J. C. L., Schutte, J., Vassen, L., . . . Khandanpour, C. (2018). GFI1 is required for RUNX1/ETO positive acute myeloid leukemia. *Haematologica, 103*(9), e395-e399. doi:10.3324/haematol.2017.180844

Mashek, D. G., & Coleman, R. A. (2006). Cellular fatty acid uptake: the contribution of metabolism. *Curr Opin Lipidol, 17*(3), 274-278. doi:10.1097/01.mol.0000226119.20307.2b

Matern, M. S., Milon, B., Lipford, E. L., McMurray, M., Ogawa, Y., Tkaczuk, A., . . . Hertzano, R. (2020). GFI1 functions to repress neuronal gene expression in the developing inner ear hair cells. *Development, 147*(17). doi:10.1242/dev.186015

Mathupala, S. P., Ko, Y. H., & Pedersen, P. L. (2006). Hexokinase II: cancer's double-edged sword acting as both facilitator and gatekeeper of malignancy when bound to mitochondria. *Oncogene, 25*(34), 4777-4786. doi:10.1038/sj.onc.1209603

Matre, P., Velez, J., Jacamo, R., Qi, Y., Su, X., Cai, T., . . . Konopleva, M. (2016). Inhibiting glutaminase in acute myeloid leukemia: metabolic dependency of selected AML subtypes. *Oncotarget, 7*(48), 79722-79735. doi:10.18632/oncotarget.12944

Medinger, M., Lengerke, C., & Passweg, J. (2016). Novel therapeutic options in Acute Myeloid Leukemia. *Leuk Res Rep, 6*, 39-49. doi:10.1016/j.lrr.2016.09.001

Melone, M. A. B., Valentino, A., Margarucci, S., Galderisi, U., Giordano, A., & Peluso, G. (2018). The carnitine system and cancer metabolic plasticity. *Cell Death Dis, 9*(2), 228. doi:10.1038/s41419-018-0313-7

Meyer, C., Hofmann, J., Burmeister, T., Groger, D., Park, T. S., Emerenciano, M., . . . Marschalek, R. (2013). The MLL recombinome of acute leukemias in 2013. *Leukemia, 27*(11), 2165-2176. doi:10.1038/leu.2013.135

Miller, D. M., Thomas, S. D., Islam, A., Muench, D., & Sedoris, K. (2012). c-Myc and cancer metabolism. *Clin Cancer Res, 18*(20), 5546-5553. doi:10.1158/1078-0432.CCR-12-0977

Milne, T. A. (2017). Mouse models of MLL leukemia: recapitulating the human disease. *Blood, 129*(16), 2217-2223. doi:10.1182/blood-2016-10-691428

Milne, T. A., Briggs, S. D., Brock, H. W., Martin, M. E., Gibbs, D., Allis, C. D., & Hess, J. L. (2002). MLL targets SET domain methyltransferase activity to Hox gene promoters. *Mol Cell, 10*(5), 1107-1117. doi:10.1016/s1097-2765(02)00741-4

Miranda, V. C., Barroso-Sousa, R., Glasberg, J., & Riechelmann, R. P. (2014). Exploring the role of metformin in anticancer treatments: a systematic review. *Drugs Today (Barc), 50*(9), 623-640. doi:10.1358/dot.2014.50.9.2229920

Mohammad, A. A. (2018). Myelodysplastic syndrome from theoretical review to clinical application view. *Oncol Rev, 12*(2), 397. doi:10.4081/oncol.2018.397

Moignard, V., Macaulay, I. C., Swiers, G., Buettner, F., Schutte, J., Calero-Nieto, F. J., . . . Gottgens, B. (2013). Characterization of transcriptional networks in blood stem and progenitor cells using high-throughput single-cell gene expression analysis. *Nat Cell Biol, 15*(4), 363-372. doi:10.1038/ncb2709

Molina, J. R., Sun, Y., Protopopova, M., Gera, S., Bandi, M., Bristow, C., . . . Marszalek, J. R. (2018). An inhibitor of oxidative phosphorylation exploits cancer vulnerability. *Nat Med, 24*(7), 1036-1046. doi:10.1038/s41591-018-0052-4

Montoya-Durango, D. E., Velu, C. S., Kazanjian, A., Rojas, M. E., Jay, C. M., Longmore, G. D., & Grimes, H. L. (2008). Ajuba functions as a histone deacetylase-dependent co-repressor for autoregulation of the growth factor-independent-1 transcription factor. *J Biol Chem, 283*(46), 32056-32065. doi:10.1074/jbc.M802320200

Mookerjee, S. A., Divakaruni, A. S., Jastroch, M., & Brand, M. D. (2010). Mitochondrial uncoupling and lifespan. *Mech Ageing Dev, 131*(7-8), 463-472. doi:10.1016/j.mad.2010.03.010

Morrish, F., Noonan, J., Perez-Olsen, C., Gafken, P. R., Fitzgibbon, M., Kelleher, J., . . . Hockenbery, D. (2010). Myc-dependent mitochondrial generation of acetyl-CoA contributes to fatty acid biosynthesis and histone acetylation during cell cycle entry. *J Biol Chem, 285*(47), 36267-36274. doi:10.1074/jbc.M110.141606

Mougiakakos, D., Jitschin, R., Braun, M., & Mackensen, A. (2014). Metabolic Reprogramming of Acute Myeloid Leukemia Blasts By Bone Marrow Stroma Cells. *Blood, 124*(21), 1585-1585. doi:10.1182/blood.V124.21.1585.1585

Mrozek, K., & Bloomfield, C. D. (2008). Clinical significance of the most common chromosome translocations in adult acute myeloid leukemia. *J Natl Cancer Inst Monogr*(39), 52-57. doi:10.1093/jncimonographs/lgn003

Mrozek, K., Heinonen, K., de la Chapelle, A., & Bloomfield, C. D. (1997). Clinical significance of cytogenetics in acute myeloid leukemia. *Semin Oncol, 24*(1), 17-31. Retrieved from https://www.ncbi.nlm.nih.gov/pubmed/9045301

Muntean, A. G., & Hess, J. L. (2012). The pathogenesis of mixed-lineage leukemia. *Annu Rev Pathol, 7*, 283-301. doi:10.1146/annurev-pathol-011811-132434

Naoe, T., & Kiyoi, H. (2013). Gene mutations of acute myeloid leukemia in the genome era. *Int J Hematol, 97*(2), 165-174. doi:10.1007/s12185-013-1257-4

Nath, K., Guo, L., Nancolas, B., Nelson, D. S., Shestov, A. A., Lee, S. C., . . . Glickson, J. D. (2016). Mechanism of antineoplastic activity of lonidamine. *Biochim Biophys Acta, 1866*(2), 151-162. doi:10.1016/j.bbcan.2016.08.001

Ngo, V. N., Davis, R. E., Lamy, L., Yu, X., Zhao, H., Lenz, G., . . . Staudt, L. M. (2006). A loss-of-function RNA interference screen for molecular targets in cancer. *Nature, 441*(7089), 106-110. doi:10.1038/nature04687

Onec, B., Okutan, H., Albayrak, M., Can, E. S., Aslan, V., Koluman, B. U., . . . Albayrak, A. (2018). Combination therapy with azacitidine, etoposide, and cytarabine in the treatment of elderly acute myeloid leukemia patients: A single center experience. *J Cancer Res Ther, 14*(5), 1105-1111. doi:10.4103/0973-1482.187369

Orkin, S. H. (2000). Diversification of haematopoietic stem cells to specific lineages. *Nat Rev Genet, 1*(1), 57-64. doi:10.1038/35049577

Orkin, S. H., & Zon, L. I. (2008). Hematopoiesis: an evolving paradigm for stem cell biology. *Cell, 132*(4), 631-644. doi:10.1016/j.cell.2008.01.025

Palanisamy, N. (2010). Chromosomal translocations in AML: detection and prognostic significance. *Cancer Treat Res, 145*, 41-58. doi:10.1007/978-0-387-69259-3_3

Panina, S. B., Pei, J., Baran, N., Konopleva, M., & Kirienko, N. V. (2020). Utilizing Synergistic Potential of Mitochondria-Targeting Drugs for Leukemia Therapy. *Front Oncol, 10*, 435. doi:10.3389/fonc.2020.00435

Patro, R., Duggal, G., Love, M. I., Irizarry, R. A., & Kingsford, C. (2017). Salmon provides fast and bias-aware quantification of transcript expression. *Nat Methods, 14*(4), 417-419. doi:10.1038/nmeth.4197

Pavlova, N. N., & Thompson, C. B. (2016). The Emerging Hallmarks of Cancer Metabolism. *Cell Metab, 23*(1), 27-47. doi:10.1016/j.cmet.2015.12.006

Peck, B., Ferber, E. C., & Schulze, A. (2013). Antagonism between FOXO and MYC Regulates Cellular Powerhouse. *Front Oncol, 3*, 96. doi:10.3389/fonc.2013.00096

Pelcovits, A., & Niroula, R. (2020). Acute Myeloid Leukemia: A Review. *R I Med J (2013), 103*(3), 38-40. Retrieved from https://www.ncbi.nlm.nih.gov/pubmed/32236160

Pernicova, I., & Korbonits, M. (2014). Metformin--mode of action and clinical implications for diabetes and cancer. *Nat Rev Endocrinol, 10*(3), 143-156. doi:10.1038/nrendo.2013.256

Peterson, L. F., Boyapati, A., Ahn, E. Y., Biggs, J. R., Okumura, A. J., Lo, M. C., . . . Zhang, D. E. (2007). Acute myeloid leukemia with the 8q22;21q22 translocation: secondary mutational events and alternative t(8;21) transcripts. *Blood, 110*(3), 799-805. doi:10.1182/blood-2006-11-019265

Phelan, J. D., Shroyer, N. F., Cook, T., Gebelein, B., & Grimes, H. L. (2010). Gfi1-cells and circuits: unraveling transcriptional networks of development

and disease. *Curr Opin Hematol, 17*(4), 300-307. doi:10.1097/MOH.0b013e32833a06f8

Pongas, G. N., Annunziata, C. M., & Staudt, L. M. (2017). PI3Kdelta inhibition causes feedback activation of PI3Kalpha in the ABC subtype of diffuse large B-cell lymphoma. *Oncotarget, 8*(47), 81794-81802. doi:10.18632/oncotarget.20864

Prieto-Bermejo, R., Romo-Gonzalez, M., Perez-Fernandez, A., Ijurko, C., & Hernandez-Hernandez, A. (2018). Reactive oxygen species in haematopoiesis: leukaemic cells take a walk on the wild side. *J Exp Clin Cancer Res, 37*(1), 125. doi:10.1186/s13046-018-0797-0

Ramos Peñafiel, C. O., Carrillo, I. O., Domínguez, J. Z., Castellanos Sinco, H. B., Fuller, E. R., Peralta, E. M., . . . Tovar, A. M. (2013). Effects Of Metformin Addition To a Standard Chemotherapy Regimen For The Treatment Of Adult Acute Lymphoblastic Leukemia. An In Vitro and In Vivo study. *Blood, 122*(21), 5024-5024. doi:10.1182/blood.V122.21.5024.5024

Randrianarison-Huetz, V., Laurent, B., Bardet, V., Blobe, G. C., Huetz, F., & Dumenil, D. (2010). Gfi-1B controls human erythroid and megakaryocytic differentiation by regulating TGF-beta signaling at the bipotent erythro-megakaryocytic progenitor stage. *Blood, 115*(14), 2784-2795. doi:10.1182/blood-2009-09-241752

Rashkovan, M., & Ferrando, A. (2019). Metabolic dependencies and vulnerabilities in leukemia. *Genes Dev, 33*(21-22), 1460-1474. doi:10.1101/gad.326470.119

Reese, N. D., & Schiller, G. J. (2013). High-dose cytarabine (HD araC) in the treatment of leukemias: a review. *Curr Hematol Malig Rep, 8*(2), 141-148. doi:10.1007/s11899-013-0156-3

Rena, G., Hardie, D. G., & Pearson, E. R. (2017). The mechanisms of action of metformin. *Diabetologia, 60*(9), 1577-1585. doi:10.1007/s00125-017-4342-z

Ricciardi, M. R., Mirabilii, S., Allegretti, M., Licchetta, R., Calarco, A., Torrisi, M. R., . . . Tafuri, A. (2015). Targeting the leukemia cell metabolism by the CPT1a inhibition: functional preclinical effects in leukemias. *Blood, 126*(16), 1925-1929. doi:10.1182/blood-2014-12-617498

Robinson, J. T., Thorvaldsdottir, H., Wenger, A. M., Zehir, A., & Mesirov, J. P. (2017). Variant Review with the Integrative Genomics Viewer. *Cancer Res, 77*(21), e31-e34. doi:10.1158/0008-5472.CAN-17-0337

Robinson, J. T., Thorvaldsdottir, H., Winckler, W., Guttman, M., Lander, E. S., Getz, G., & Mesirov, J. P. (2011). Integrative genomics viewer. *Nat Biotechnol, 29*(1), 24-26. doi:10.1038/nbt.1754

Saleque, S., Cameron, S., & Orkin, S. H. (2002). The zinc-finger proto-oncogene Gfi-1b is essential for development of the erythroid and megakaryocytic lineages. *Genes Dev, 16*(3), 301-306. doi:10.1101/gad.959102

Saleque, S., Kim, J., Rooke, H. M., & Orkin, S. H. (2007). Epigenetic regulation of hematopoietic differentiation by Gfi-1 and Gfi-1b is mediated by the

cofactors CoREST and LSD1. *Mol Cell, 27*(4), 562-572. doi:10.1016/j.molcel.2007.06.039

Salpeter, S. R., Buckley, N. S., Kahn, J. A., & Salpeter, E. E. (2008). Meta-analysis: metformin treatment in persons at risk for diabetes mellitus. *Am J Med, 121*(2), 149-157 e142. doi:10.1016/j.amjmed.2007.09.016

Samudio, I., Harmancey, R., Fiegl, M., Kantarjian, H., Konopleva, M., Korchin, B., . . . Andreeff, M. (2010). Pharmacologic inhibition of fatty acid oxidation sensitizes human leukemia cells to apoptosis induction. *J Clin Invest, 120*(1), 142-156. doi:10.1172/JCI38942

Sanchez-Castillo, M., Ruau, D., Wilkinson, A. C., Ng, F. S., Hannah, R., Diamanti, E., . . . Gottgens, B. (2015). CODEX: a next-generation sequencing experiment database for the haematopoietic and embryonic stem cell communities. *Nucleic Acids Res, 43*(Database issue), D1117-1123. doi:10.1093/nar/gku895

Saultz, J. N., & Garzon, R. (2016). Acute Myeloid Leukemia: A Concise Review. *J Clin Med, 5*(3). doi:10.3390/jcm5030033

Scatena, R., Bottoni, P., Pontoglio, A., Mastrototaro, L., & Giardina, B. (2008). Glycolytic enzyme inhibitors in cancer treatment. *Expert Opin Investig Drugs, 17*(10), 1533-1545. doi:10.1517/13543784.17.10.1533

Schieber, M., & Chandel, N. S. (2014). ROS function in redox signaling and oxidative stress. *Curr Biol, 24*(10), R453-462. doi:10.1016/j.cub.2014.03.034

Schindelin, J., Arganda-Carreras, I., Frise, E., Kaynig, V., Longair, M., Pietzsch, T., . . . Cardona, A. (2012). Fiji: an open-source platform for biological-image analysis. *Nat Methods, 9*(7), 676-682. doi:10.1038/nmeth.2019

Schulz, D., Vassen, L., Chow, K. T., McWhirter, S. M., Amin, R. H., Moroy, T., & Schlissel, M. S. (2012). Gfi1b negatively regulates Rag expression directly and via the repression of FoxO1. *J Exp Med, 209*(1), 187-199. doi:10.1084/jem.20110645

Scotland, S., Micklow, E., Wang, Z., Boutzen, H., Récher, C., Danet-Desnoyers, G., . . . Sarry, J.-E. (2010). Metformin for Therapeutic Intervention In Acute Myeloid Leukemia. *Blood, 116*(21), 4351-4351. doi:10.1182/blood.V116.21.4351.4351

Segeren, C. M., & van 't Veer, M. B. (1996). The FAB classification for acute myeloid leukaemia--is it outdated? *Neth J Med, 49*(3), 126-131. doi:10.1016/0300-2977(96)00024-1

Shanmugam, M., McBrayer, S. K., & Rosen, S. T. (2009). Targeting the Warburg effect in hematological malignancies: from PET to therapy. *Curr Opin Oncol, 21*(6), 531-536. doi:10.1097/CCO.0b013e32832f57ec

Shannon, P., Markiel, A., Ozier, O., Baliga, N. S., Wang, J. T., Ramage, D., . . . Ideker, T. (2003). Cytoscape: a software environment for integrated models of biomolecular interaction networks. *Genome Res, 13*(11), 2498-2504. doi:10.1101/gr.1239303

Shestov, A. A., Liu, X., Ser, Z., Cluntun, A. A., Hung, Y. P., Huang, L., . . . Locasale, J. W. (2014). Quantitative determinants of aerobic glycolysis

identify flux through the enzyme GAPDH as a limiting step. *Elife, 3*. doi:10.7554/eLife.03342

Shi, L. Z., Saravia, J., Zeng, H., Kalupahana, N. S., Guy, C. S., Neale, G., & Chi, H. (2017). Gfi1-Foxo1 axis controls the fidelity of effector gene expression and developmental maturation of thymocytes. *Proc Natl Acad Sci U S A, 114*(1), E67-E74. doi:10.1073/pnas.1617669114

Sica, V., Bravo-San Pedro, J. M., Stoll, G., & Kroemer, G. (2020). Oxidative phosphorylation as a potential therapeutic target for cancer therapy. *Int J Cancer, 146*(1), 10-17. doi:10.1002/ijc.32616

Sies, H., & Jones, D. P. (2020). Reactive oxygen species (ROS) as pleiotropic physiological signalling agents. *Nat Rev Mol Cell Biol, 21*(7), 363-383. doi:10.1038/s41580-020-0230-3

Skrtic, M., Sriskanthadevan, S., Jhas, B., Gebbia, M., Wang, X., Wang, Z., . . . Schimmer, A. D. (2011). Inhibition of mitochondrial translation as a therapeutic strategy for human acute myeloid leukemia. *Cancer Cell, 20*(5), 674-688. doi:10.1016/j.ccr.2011.10.015

Slovak, M. L., Kopecky, K. J., Cassileth, P. A., Harrington, D. H., Theil, K. S., Mohamed, A., . . . Appelbaum, F. R. (2000). Karyotypic analysis predicts outcome of preremission and postremission therapy in adult acute myeloid leukemia: a Southwest Oncology Group/Eastern Cooperative Oncology Group Study. *Blood, 96*(13), 4075-4083. Retrieved from https://www.ncbi.nlm.nih.gov/pubmed/11110676

Song, K., Li, M., Xu, X., Xuan, L. I., Huang, G., & Liu, Q. (2016). Resistance to chemotherapy is associated with altered glucose metabolism in acute myeloid leukemia. *Oncol Lett, 12*(1), 334-342. doi:10.3892/ol.2016.4600

Spooner, C. J., Cheng, J. X., Pujadas, E., Laslo, P., & Singh, H. (2009). A recurrent network involving the transcription factors PU.1 and Gfi1 orchestrates innate and adaptive immune cell fates. *Immunity, 31*(4), 576-586. doi:10.1016/j.immuni.2009.07.011

Spooner, C. J., Lesch, J., Yan, D., Khan, A. A., Abbas, A., Ramirez-Carrozzi, V., . . . Singh, H. (2013). Specification of type 2 innate lymphocytes by the transcriptional determinant Gfi1. *Nat Immunol, 14*(12), 1229-1236. doi:10.1038/ni.2743

Stevens, B. M., Jones, C. L., Pollyea, D. A., Culp-Hill, R., D'Alessandro, A., Winters, A., . . . Jordan, C. T. (2020). Fatty acid metabolism underlies venetoclax resistance in acute myeloid leukemia stem cells. *Nat Cancer, 1*(12), 1176-1187. doi:10.1038/s43018-020-00126-z

Stuani, L., Sabatier, M., & Sarry, J. E. (2019). Exploiting metabolic vulnerabilities for personalized therapy in acute myeloid leukemia. *BMC Biol, 17*(1), 57. doi:10.1186/s12915-019-0670-4

Sullivan, L. B., Gui, D. Y., & Vander Heiden, M. G. (2016). Altered metabolite levels in cancer: implications for tumour biology and cancer therapy. *Nat Rev Cancer, 16*(11), 680-693. doi:10.1038/nrc.2016.85

Suski, J. M., Lebiedzinska, M., Bonora, M., Pinton, P., Duszynski, J., & Wieckowski, M. R. (2012). Relation between mitochondrial membrane

potential and ROS formation. *Methods Mol Biol, 810*, 183-205. doi:10.1007/978-1-61779-382-0_12

Tabe, Y., Konopleva, M., & Andreeff, M. (2020). Fatty Acid Metabolism, Bone Marrow Adipocytes, and AML. *Front Oncol, 10*, 155. doi:10.3389/fonc.2020.00155

Takei, H., & Kobayashi, S. S. (2019). Targeting transcription factors in acute myeloid leukemia. *Int J Hematol, 109*(1), 28-34. doi:10.1007/s12185-018-2488-1

Tcheng, M., Roma, A., Ahmed, N., Smith, R. W., Jayanth, P., Minden, M. D., . . . Spagnuolo, P. A. (2021). Very long chain fatty acid metabolism is required in acute myeloid leukemia. *Blood, 137*(25), 3518-3532. doi:10.1182/blood.2020008551

TeSlaa, T., & Teitell, M. A. (2014). Techniques to monitor glycolysis. *Methods Enzymol, 542*, 91-114. doi:10.1016/B978-0-12-416618-9.00005-4

Thivakaran, A., Botezatu, L., Hones, J. M., Schutte, J., Vassen, L., Al-Matary, Y. S., . . . Khandanpour, C. (2018). Gfi1b: a key player in the genesis and maintenance of acute myeloid leukemia and myelodysplastic syndrome. *Haematologica, 103*(4), 614-625. doi:10.3324/haematol.2017.167288

Thomas, X. (2009). Chemotherapy of acute leukemia in adults. *Expert Opin Pharmacother, 10*(2), 221-237. doi:10.1517/14656560802618746

Thoms, J. A. I., Beck, D., & Pimanda, J. E. (2019). Transcriptional networks in acute myeloid leukemia. *Genes Chromosomes Cancer, 58*(12), 859-874. doi:10.1002/gcc.22794

Tiwari, M. (2012). Antimetabolites: established cancer therapy. *J Cancer Res Ther, 8*(4), 510-519. doi:10.4103/0973-1482.106526

Tiwari, S. K., Toshniwal, A. G., Mandal, S., & Mandal, L. (2020). Fatty acid beta-oxidation is required for the differentiation of larval hematopoietic progenitors in Drosophila. *Elife, 9*. doi:10.7554/eLife.53247

Tran, Q., Lee, H., Park, J., Kim, S. H., & Park, J. (2016). Targeting Cancer Metabolism - Revisiting the Warburg Effects. *Toxicol Res, 32*(3), 177-193. doi:10.5487/TR.2016.32.3.177

Turrens, J. F. (2003). Mitochondrial formation of reactive oxygen species. *J Physiol, 552*(Pt 2), 335-344. doi:10.1113/jphysiol.2003.049478

Uphoff, C. C., & Drexler, H. G. (2002). Comparative PCR analysis for detection of mycoplasma infections in continuous cell lines. *In Vitro Cell Dev Biol Anim, 38*(2), 79-85. doi:10.1290/1071-2690(2002)038<0079:CPAFDO>2.0.CO;2

Uphoff, C. C., & Drexler, H. G. (2004). Detecting Mycoplasma contamination in cell cultures by polymerase chain reaction. *Methods Mol Med, 88*, 319-326. doi:10.1385/1-59259-406-9:319

Vacanti, N. M., Divakaruni, A. S., Green, C. R., Parker, S. J., Henry, R. R., Ciaraldi, T. P., . . . Metallo, C. M. (2014). Regulation of substrate utilization by the mitochondrial pyruvate carrier. *Mol Cell, 56*(3), 425-435. doi:10.1016/j.molcel.2014.09.024

Vadnais, C., Chen, R., Fraszczak, J., Yu, Z., Boulais, J., Pinder, J., . . . Moroy, T. (2018). GFI1 facilitates efficient DNA repair by regulating PRMT1

dependent methylation of MRE11 and 53BP1. *Nat Commun, 9*(1), 1418. doi:10.1038/s41467-018-03817-5

Valverde, L. R., Matutes, E., Farahat, N., Heffernan, A., Owusu-Ankomah, K., Morilla, R., & Catovsky, D. (1996). C-kit receptor (CD117) expression in acute leukemia. *Ann Hematol, 72*(1), 11-15. doi:10.1007/BF00663010

van der Meer, L. T., Jansen, J. H., & van der Reijden, B. A. (2010). Gfi1 and Gfi1b: key regulators of hematopoiesis. *Leukemia, 24*(11), 1834-1843. doi:10.1038/leu.2010.195

van der Vos, K. E., Eliasson, P., Proikas-Cezanne, T., Vervoort, S. J., van Boxtel, R., Putker, M., . . . Coffer, P. J. (2012). Modulation of glutamine metabolism by the PI(3)K-PKB-FOXO network regulates autophagy. *Nat Cell Biol, 14*(8), 829-837. doi:10.1038/ncb2536

Van Weelderen, R. E., Klein, K., Natawidjaja, M. D., De Vries, R., & Kaspers, G. J. (2021). Outcome of pediatric acute myeloid leukemia (AML) in low- and middle-income countries: a systematic review of the literature. *Expert Rev Anticancer Ther, 21*(7), 765-780. doi:10.1080/14737140.2021.1895756

Vander Heiden, M. G., Cantley, L. C., & Thompson, C. B. (2009). Understanding the Warburg effect: the metabolic requirements of cell proliferation. *Science, 324*(5930), 1029-1033. doi:10.1126/science.1160809

Vassen, L., Fiolka, K., Mahlmann, S., & Moroy, T. (2005). Direct transcriptional repression of the genes encoding the zinc-finger proteins Gfi1b and Gfi1 by Gfi1b. *Nucleic Acids Res, 33*(3), 987-998. doi:10.1093/nar/gki243

Vassen, L., Okayama, T., & Moroy, T. (2007). Gfi1b:green fluorescent protein knock-in mice reveal a dynamic expression pattern of Gfi1b during hematopoiesis that is largely complementary to Gfi1. *Blood, 109*(6), 2356-2364. doi:10.1182/blood-2006-06-030031

Vosberg, S., & Greif, P. A. (2019). Clonal evolution of acute myeloid leukemia from diagnosis to relapse. *Genes Chromosomes Cancer, 58*(12), 839-849. doi:10.1002/gcc.22806

Wallis, D., Hamblen, M., Zhou, Y., Venken, K. J., Schumacher, A., Grimes, H. L., . . . Bellen, H. J. (2003). The zinc finger transcription factor Gfi1, implicated in lymphomagenesis, is required for inner ear hair cell differentiation and survival. *Development, 130*(1), 221-232. doi:10.1242/dev.00190

Wang, C., Curtis, J. E., Geissler, E. N., McCulloch, E. A., & Minden, M. D. (1989). The expression of the proto-oncogene C-kit in the blast cells of acute myeloblastic leukemia. *Leukemia, 3*(10), 699-702. Retrieved from https://www.ncbi.nlm.nih.gov/pubmed/2476640

Wang, Y., Zhou, Y., & Graves, D. T. (2014). FOXO transcription factors: their clinical significance and regulation. *Biomed Res Int, 2014*, 925350. doi:10.1155/2014/925350

Wang, Y. H., & Scadden, D. T. (2015). Targeting the Warburg effect for leukemia therapy: Magnitude matters. *Mol Cell Oncol, 2*(3), e981988. doi:10.4161/23723556.2014.981988

Wang, Y. W., He, S. J., Feng, X., Cheng, J., Luo, Y. T., Tian, L., & Huang, Q. (2017). Metformin: a review of its potential indications. *Drug Des Devel Ther, 11*, 2421-2429. doi:10.2147/DDDT.S141675

Wei, A. H., Strickland, S. A., Jr., Hou, J. Z., Fiedler, W., Lin, T. L., Walter, R. B., . . . Roboz, G. J. (2019). Venetoclax Combined With Low-Dose Cytarabine for Previously Untreated Patients With Acute Myeloid Leukemia: Results From a Phase Ib/II Study. *J Clin Oncol, 37*(15), 1277-1284. doi:10.1200/JCO.18.01600

Wen, S., Zhu, D., & Huang, P. (2013). Targeting cancer cell mitochondria as a therapeutic approach. *Future Med Chem, 5*(1), 53-67. doi:10.4155/fmc.12.190

Willems, L., Jacque, N., Jacquel, A., Neveux, N., Maciel, T. T., Lambert, M., . . . Bouscary, D. (2013). Inhibiting glutamine uptake represents an attractive new strategy for treating acute myeloid leukemia. *Blood, 122*(20), 3521-3532. doi:10.1182/blood-2013-03-493163

Winters, A. C., & Bernt, K. M. (2017). MLL-Rearranged Leukemias-An Update on Science and Clinical Approaches. *Front Pediatr, 5*, 4. doi:10.3389/fped.2017.00004

Wise, D. R., DeBerardinis, R. J., Mancuso, A., Sayed, N., Zhang, X. Y., Pfeiffer, H. K., . . . Thompson, C. B. (2008). Myc regulates a transcriptional program that stimulates mitochondrial glutaminolysis and leads to glutamine addiction. *Proc Natl Acad Sci U S A, 105*(48), 18782-18787. doi:10.1073/pnas.0810199105

Xiang, Y., Stine, Z. E., Xia, J., Lu, Y., O'Connor, R. S., Altman, B. J., . . . Dang, C. V. (2015). Targeted inhibition of tumor-specific glutaminase diminishes cell-autonomous tumorigenesis. *J Clin Invest, 125*(6), 2293-2306. doi:10.1172/JCI75836

Xiao, Z. D., Han, L., Lee, H., Zhuang, L., Zhang, Y., Baddour, J., . . . Gan, B. (2017). Energy stress-induced lncRNA FILNC1 represses c-Myc-mediated energy metabolism and inhibits renal tumor development. *Nat Commun, 8*(1), 783. doi:10.1038/s41467-017-00902-z

Xie, L., Ushmorov, A., Leithauser, F., Guan, H., Steidl, C., Farbinger, J., . . . Wirth, T. (2012). FOXO1 is a tumor suppressor in classical Hodgkin lymphoma. *Blood, 119*(15), 3503-3511. doi:10.1182/blood-2011-09-381905

Xu, Z., Yan, Y., Li, Z., Qian, L., & Gong, Z. (2016). The Antibiotic Drug Tigecycline: A Focus on its Promising Anticancer Properties. *Front Pharmacol, 7*, 473. doi:10.3389/fphar.2016.00473

Yadav, R. K., Chauhan, A. S., Zhuang, L., & Gan, B. (2018). FoxO transcription factors in cancer metabolism. *Semin Cancer Biol, 50*, 65-76. doi:10.1016/j.semcancer.2018.01.004

Yang, C., Ko, B., Hensley, C. T., Jiang, L., Wasti, A. T., Kim, J., . . . DeBerardinis, R. J. (2014). Glutamine oxidation maintains the TCA cycle and cell survival during impaired mitochondrial pyruvate transport. *Mol Cell, 56*(3), 414-424. doi:10.1016/j.molcel.2014.09.025

Yang, Y. L., Jaing, T. H., Chen, S. H., Liu, H. C., Hung, I. J., Lin, D. T., . . . Chang, T. T. (2021). Treatment outcomes of pediatric acute myeloid

leukemia: a retrospective analysis from 1996 to 2019 in Taiwan. *Sci Rep, 11*(1), 5893. doi:10.1038/s41598-021-85321-3

Yi, M., Li, A., Zhou, L., Chu, Q., Song, Y., & Wu, K. (2020). The global burden and attributable risk factor analysis of acute myeloid leukemia in 195 countries and territories from 1990 to 2017: estimates based on the global burden of disease study 2017. *J Hematol Oncol, 13*(1), 72. doi:10.1186/s13045-020-00908-z

Yilmaz, M., Wang, F., Loghavi, S., Bueso-Ramos, C., Gumbs, C., Little, L., . . . Ravandi, F. (2019). Late relapse in acute myeloid leukemia (AML): clonal evolution or therapy-related leukemia? *Blood Cancer J, 9*(2), 7. doi:10.1038/s41408-019-0170-3

Yucel, R., Kosan, C., Heyd, F., & Moroy, T. (2004). Gfi1:green fluorescent protein knock-in mutant reveals differential expression and autoregulation of the growth factor independence 1 (Gfi1) gene during lymphocyte development. *J Biol Chem, 279*(39), 40906-40917. doi:10.1074/jbc.M400808200

Zeisig, B. B., Milne, T., Garcia-Cuellar, M. P., Schreiner, S., Martin, M. E., Fuchs, U., . . . Slany, R. K. (2004). Hoxa9 and Meis1 are key targets for MLL-ENL-mediated cellular immortalization. *Mol Cell Biol, 24*(2), 617-628. doi:10.1128/mcb.24.2.617-628.2004

Zeller, K. I., Jegga, A. G., Aronow, B. J., O'Donnell, K. A., & Dang, C. V. (2003). An integrated database of genes responsive to the Myc oncogenic transcription factor: identification of direct genomic targets. *Genome Biol, 4*(10), R69. doi:10.1186/gb-2003-4-10-r69

Zeng, H., Yucel, R., Kosan, C., Klein-Hitpass, L., & Moroy, T. (2004). Transcription factor Gfi1 regulates self-renewal and engraftment of hematopoietic stem cells. *EMBO J, 23*(20), 4116-4125. doi:10.1038/sj.emboj.7600419

Zhang, J., Gu, Y., & Chen, B. (2019). Mechanisms of drug resistance in acute myeloid leukemia. *Onco Targets Ther, 12*, 1937-1945. doi:10.2147/OTT.S191621

Zhang, X., Yalcin, S., Lee, D. F., Yeh, T. Y., Lee, S. M., Su, J., . . . Ghaffari, S. (2011). FOXO1 is an essential regulator of pluripotency in human embryonic stem cells. *Nat Cell Biol, 13*(9), 1092-1099. doi:10.1038/ncb2293

Zhao, R. Z., Jiang, S., Zhang, L., & Yu, Z. B. (2019). Mitochondrial electron transport chain, ROS generation and uncoupling (Review). *Int J Mol Med, 44*(1), 3-15. doi:10.3892/ijmm.2019.4188

Zheng, J. (2012). Energy metabolism of cancer: Glycolysis versus oxidative phosphorylation (Review). *Oncol Lett, 4*(6), 1151-1157. doi:10.3892/ol.2012.928

Zhong, Y., Li, X., Yu, D., Li, X., Li, Y., Long, Y., . . . Suo, Z. (2015). Application of mitochondrial pyruvate carrier blocker UK5099 creates metabolic reprogram and greater stem-like properties in LnCap prostate cancer cells in vitro. *Oncotarget, 6*(35), 37758-37769. doi:10.18632/oncotarget.5386

Zhu, J., & Emerson, S. G. (2002). Hematopoietic cytokines, transcription factors and lineage commitment. *Oncogene, 21*(21), 3295-3313. doi:10.1038/sj.onc.1205318

Zorov, D. B., Juhaszova, M., & Sollott, S. J. (2014). Mitochondrial reactive oxygen species (ROS) and ROS-induced ROS release. *Physiol Rev, 94*(3), 909-950. doi:10.1152/physrev.00026.2013

Zorova, L. D., Popkov, V. A., Plotnikov, E. Y., Silachev, D. N., Pevzner, I. B., Jankauskas, S. S., . . . Zorov, D. B. (2018). Mitochondrial membrane potential. *Anal Biochem, 552*, 50-59. doi:10.1016/j.ab.2017.07.009

Zweidler-Mckay, P. A., Grimes, H. L., Flubacher, M. M., & Tsichlis, P. N. (1996). Gfi-1 encodes a nuclear zinc finger protein that binds DNA and functions as a transcriptional repressor. *Mol Cell Biol, 16*(8), 4024-4034. doi:10.1128/mcb.16.8.4024

## 11. Acknowledgements

First and foremost, I would like to express my sincere gratitude to my supervisor PD.Dr.Cyrus Khandanpour for his assistance in developing the scientific objectives and methods. Your informative remarks encouraged me to improve my thoughts and raise the quality of my work. I'd want to show my thankfulness to Dr. Cyrus Khandanpour for believing in me and assisting me throughout my PhD journey, particularly in obtaining a DAAD fellowship, without which I would not have been prepared to commence my PhD. Dr. Cyrus Khandanpour is a fantastic individual who has aided me with my personal concerns as well.

I am grateful to all of my lab companions who have supported me during my PhD and to have a fun-filled journey. Especially, I am delighted to have a wonderfully supportive friend Dr. Daria Frank, who has been there for me almost every day during the PhD and, most importantly, has helped me through the most challenging situations of my stay in Germany. Without her assistance, I could not have anticipated my stay in Germany, particularly considering the language barrier. I am also very thankful to Dr. Aniththa Thivakaran, who served as my mentor throughout the early years of my PhD and assisted me much in learning new lab skills, particularly with animal studies, owing to the new working environment and wholly new abilities. I am fortunate to have another vital companion, Dr. Yahya Almatary, who has aided me greatly in both my professional and personal lives, especially as a foreigner dealing with the new German regulations. I am thankful to my project partner Longlong Liu, who supported me with my project, and we always had good conversations. I am very thankful to my colleague Xiaoqing Xie, who was always willing to assist me during the critical experiments. I am exceedingly obliged to all my lab colleagues Dr. Subbaiah Chary Nimmagadda, Dr. Judith Schütte, Helal Noman, Sun Kaiyan, Lanying Wei with whom I have always had interesting discussions and helped in resolving key challenges. I am also thankful to all the other lab members, including Hannelore Leuschke, Dagmar Clemens, Renata Köster, Marina Suslo and also to other medical students who were part of our lab at University Hospital Essen and Münster, with whom I shared a great time and

learnt a lot. I'd also want to thank Dr.Vijay and Eloisa, as my colleagues and friends with whom I always have a great time.

I am very thankful to Prof. Dr. Ulrich Dührsen, University Hospital Essen and Prof. Dr. med. Georg Lenz, University Hospital Münster for providing the lab space and required equipment and Prof. Dr. med. Helmut Hanenberg for providing the plasmid constructs. I'm also grateful to Prof. Dr. Bertram Opalka, who offered me advice on how to compose my dissertation.

I am highly beheld to our collaboration partners Dr. Matthias Behrens, Institute for food chemistry, University of Münster and Prof. Dr. med. Luisa Klotz and Dr. Marie Liebmann, Institute of translational neurology, University Hospital Münster, with whom I have performed critical experiments of my study. I am also thankful to the collaborated working groups of Prof. Dr. med. Georg Lenz, Translational oncology and Prof. Dr. Frank Rosenbauer, institute of Molecular Tumor Biology, University Hospital Münster. I'm particularly grateful to Mr. König Thorsten and Ms. Annegret Rosemann, who gave the greatest assistance with FACS sorting.

I'm also grateful to the German Academic Exchange Service (DAAD) for providing me with a scholarship for the duration of my PhD and for assisting me in my travel to Germany DAAD.

I'd want to express my love and thankfulness to my entire family, including my father and mother, sister, niece and, most importantly, my brother-in-law, who is my greatest inspiration. Also, thank you to my paternal uncle, aunt, and grandmother for their continuous support.

I'd want to express my affection and gratitude to an incredible person and my better half, Aswini (Chinnu), for her love and unwavering support during all of my good and bad times. I'd want to thank Chaitanya, another significant person and my best friend, with whom I discuss everything and who has always been supportive.

# 12. List of Publications

## 12.1. Publications from the thesis

Hones, J. M., Thivakaran, A., Botezatu, L., **Patnana, P**., Castro, S., Al-Matary, Y. S., . . . Khandanpour, C. (2017). Enforced GFI1 expression impedes human and murine leukemic cell growth. Sci Rep, 7(1), 15720. doi:10.1038/s41598-017-15866-9.

## 12.2. Other publications

- Ahmed, H. M. M., S. C. Nimmagadda, Y. S. Al-Matary, M. Fiori, T. May, D. Frank, **P. K. Patnana**, C. Recher, C. Schliemann, J. H. Mikesch, T. Koenig, F. Rosenbauer, W. Hartmann, J. Tuckermann, U. Duhrsen, W. Lanying, M. Dugas, B. Opalka, G. Lenz and C. Khandanpour (2021). "Dexamethasone-mediated inhibition of Notch signalling blocks the interaction of leukaemia and mesenchymal stromal cells." Br J Haematol.
- Thivakaran, A., Botezatu, L., Hones, J. M., Schutte, J., Vassen, L., Al-Matary, Y. S.,**Patnana P** . . . Khandanpour, C. (2018). Gfi1b: a key player in the genesis and maintenance of acute myeloid leukemia and myelodysplastic syndrome. Haematologica, 103(4), 614-625. doi:10.3324/haematol.2017.167288
- Pandey, S. S., **Patnana, P. K**., Padhi, Y., & Chatterjee, S. (2018). Low-iron conditions induces the hypersensitive reaction and pathogenicity hrp genes expression in Xanthomonas and is involved in modulation of hypersensitive response and virulence. Environ Microbiol Rep, 10(5), 522-531. doi:10.1111/1758-2229.12650.
- Pandey, S. S., **Patnana, P. K**., Rai, R., & Chatterjee, S. (2017). Xanthoferrin, the alpha-hydroxycarboxylate-type siderophore of Xanthomonas campestris pv. campestris, is required for optimum virulence and growth inside cabbage. Mol Plant Pathol, 18(7), 949-962. doi:10.1111/mpp.12451.
- Pandey, S. S., **P. K. Patnana**, S. K. Lomada, A. Tomar and S. Chatterjee (2016). "Co-regulation of Iron Metabolism and Virulence Associated Functions by Iron and XibR, a Novel Iron Binding Transcription Factor, in the Plant Pathogen Xanthomonas." PLoS Pathog 12(11): e1006019.
- *Ratan J. Lihite, Nityanand Bolshette, Mangala Lahkar, Pabitra Kumar Gogoi,* ***Pradeep Kumar Patnana*** *(2016) "*Analysis of Prevalence and Accumulation of Mutations Associated With Imatinib Based Therapy in Chronic Myeloid Leukemia Patients" International Journal of Hematology Research, Vol 2, No 3.

## 13. Curriculum vitae

The CV is not included in this online version for reasons of data protection.

## 14. Affidavits

**Declaration:**

In accordance with § 6 (para. 2, clause g) of the Regulations Governing the Doctoral Proceedings of the Faculty of Biology for awarding the doctoral degree Dr. rer. nat., I hereby declare that I represent the field to which the topic "*The Role of GFI1 in regulating the metabolism of Acute Myeloid Leukemic cells"* is assigned in research and teaching and that I support the application of (*name of the doctoral candidate*).

Essen, date _____ _____

Apl. Prof. Dr. Cyrus Khandanpour

**Declaration:**

In accordance with § 7 (para. 2, clause d and f) of the Regulations Governing the Doctoral Proceedings of the Faculty of Biology for awarding the doctoral degree Dr. rer. nat., I hereby declare that I have written the herewith submitted dissertation independently using only the materials listed, and have cited all sources taken over verbatim or in content as such.

Essen, date _____ _____

Pradeep Kumar Patnana

**Declaration:**

In accordance with § 7 (para. 2, clause e and g) of the Regulations Governing the Doctoral Proceedings of the Faculty of Biology for awarding the doctoral degree Dr. rer. nat., I hereby declare that I have undertaken no previous attempts to attain a doctoral degree, that the current work has not been rejected by any other faculty, and that I am submitting the dissertation only in this procedure.

Essen, date _____ _____

Pradeep Kumar Patnana